JYU DISSERTATIONS 137

Anniina Kiesilä

Supramolecular Chemistry of Anion-Binding Receptors Based on Concave Macrocycles

UNIVERSITY OF JYVÄSKYLÄ
FACULTY OF MATHEMATICS
AND SCIENCE

JYU DISSERTATIONS 137

Anniina Kiesilä

Supramolecular Chemistry of Anion-Binding Receptors Based on Concave Macrocycles

Esitetään Jyväskylän yliopiston matemaattis-luonnontieteellisen tiedekunnan suostumuksella
julkisesti tarkastettavaksi yliopiston Ylistönrinteen salissa YlistöKem4
lokakuun 11. päivänä 2019 kello 12.

Academic dissertation to be publicly discussed, by permission of
the Faculty of Mathematics and Science of the University of Jyväskylä,
in Ylistönrinne, auditorium YlistöKem4, on October 11, 2019 at 12 o'clock noon.

JYVÄSKYLÄN YLIOPISTO
UNIVERSITY OF JYVÄSKYLÄ

JYVÄSKYLÄ 2019

Editors
Elina Kalenius
Department of Chemistry, University of Jyväskylä
Ville Korkiakangas
Open Science Centre, University of Jyväskylä

Permanent link to this publication: http://urn.fi/URN:ISBN:978-951-39-7855-6

ISBN 978-951-39-7855-6 (PDF)
URN:ISBN:978-951-39-7855-6
ISSN 2489-9003

ABSTRACT

Kiesilä, Anniina
Supramolecular chemistry of anion-binding receptors based on concave macrocycles
Jyväskylä: University of Jyväskylä, 2019, 68 p.
(JYU Dissertations
ISSN 2489-9003; 137)
ISBN 978-951-39-7855-6 (PDF)

This thesis describes the supramolecular chemistry of different anion-binding host molecules with a special focus on pyridine[4]arenes. The first part of the thesis gives a brief introduction to supramolecular chemistry and its special features, host-guest chemistry and self-assembly. Later on, a short review of different hosts is presented, especially focusing on those utilized in the experimental part of the thesis. In the second part of the thesis an introduction is presented to the structural analyzation techniques utilized in the experimental part. A special focus is set on ion mobility mass spectrometry, a relatively new technique for structural characterization of supramolecular complexes.

The third part presents the summary of experimental work. The binding properties of pyridinearene turned out to completely differ from previous reports in the literature. New binding features of pyridinearene were discovered, such as simultaneous *endo*- and *exo*-complex formation with neutral and anionic guests. The formation of the hexameric assembly of pyridinearene was also observed for the first time in gas phase and in solid state. In solution, the thermodynamic balance in self-assembly was revealed.

Different analyzation techniques have been utilized in the structural characterisation of pyridinearenes. Ion mobility mass spectrometry proved to be spectacular for structural characterization of the gas phase assemblies. As a new technique, its utilization for structural chemistry is demonstrated in the experimental part with several examples.

In this thesis, also the binding properties of cyclohexylhemicucurbit[8]uril and crown ether urea receptors were revealed and thoroughly studied in gas phase, solution and in solid state.

Keywords: pyridine[4]arene, supramolecular chemistry, ion mobility mass spectrometry, self-assembly, anion binding, X-ray crystallography,

Author's address

Anniina Kiesilä
Department of Chemistry
Nanoscience Center
P.O. Box 35
FI-40014 University of Jyväskylä
Finland
anniina.m.kiesila@jyu.fi

Supervisor

Adjunct Professor Elina Kalenius
Department of Chemistry
Nanoscience Center
University of Jyväskylä
Finland

Reviewers

Research Director Dr. Valérie Gabelica
Institut Européen de Chimie et Biologie
University of Bordeaux
Pessac, France

Professor Alessandro Casnati
Department of Chemistry, Life Sciences
and Sustainability
University of Parma
Parma, Italy

Opponents

Professor David V. Dearden
Department of Chemistry and Biochemistry
Brigham Young University
Provo, Utah, United States

ACKNOWLEDGEMENTS

The work presented in this thesis was carried out at the Department of Chemistry, University of Jyväskylä during the years 2015-2019. Partly the journey started already in 2014, when the learning experience to supramolecular chemistry started by work with crown ether urea receptors for my Master`s thesis. These years have been challenging, stressful, but also rewarding and full of excitement. I would not change any of it!

First and foremost, I want to thank Adjunct Professor Elina Kalenius for giving me the opportunity to work in this interesting project. I truly admire all your knowledge and expertise on mass spectrometry, thank you for sharing so big part of it! I feel grateful also for the independence I have received in my work, and for the guidance whenever needed. I also want to thank Professor Kari Rissanen for all the advices and encouragement, and also for taking me as a subunit to his wonderful research group.

Professor Alessandro Casnati and Dr. Valérie Gabelica are sincerely thanked for the pre-examination of this thesis. I feel honoured that my work has been evaluated by such distinguished scientists. I also thank Matti Nurmia for the language revision.

Doctors Filip Topić and Rakesh Puttreddy are thanked for their patience of checking my salty crystallization experiments and solving the structures of the lucky attempts. Academy research fellow Dr. Jani O. Moilanen is gratefully thanked for the collaboration and all the DFT calculations. Professor Perdita Barran, Professor Christoph A. Schalley and Dr. Anneli Kruve are thanked for the collaboration during and after my research visits to Manchester and Berlin, and for the introduction to new mass spectrometry techniques.

I would also like to thank all the colleagues and staff at the department of chemistry for creating such a nice working atmosphere. The new and former members of group Rissanen, thank you for sharing the good and bad moments at work, and especially for the awesome parties we have had together! Thank you all the friends, in and out of chemistry life, you know who you are and how much you mean to me. A very special thanks goes to Jyväskylä Muay Thai and Minh "Joji" Le for taking care of my physical (and mental) health, especially after some sport injuries. The members of local paw patrol in Kotimäki are warmly thanked for the long walks and taking my mind off from work every evening.

Last but not least, I owe my deepest gratitude to my husband Jussi and my daughter Justiina. Thank you for your endless love, support and patience. Without your encouragement this journey would have been significantly harder. I want to thank also the-one-on-the-way, for living through the stressful writing process and enabling the writing without (bad) morning sickness.

Jyväskylä 12.9.2019
Anniina Kiesilä

LIST OF ORIGINAL PUBLICATIONS

This thesis is based on the following original publications, which are referred to in the text by their Roman numerals.

I A. Kiesilä, L. Kivijärvi, N. K. Beyeh, J. O. Moilanen, M. Groessl, T. Rothe, S. Götz, F. Topić, K. Rissanen, A. Lützen and E. Kalenius. Simultaneous endo and exo complex formation of pyridine[4]arene dimers with neutral and anionic guests, *Angew. Chem. Int. Ed*. **2017**, *56*, 10942 – 10946.

II A. Kiesilä, J. O. Moilanen, A. Kruve, C. A. Schalley, P. Barran and E. Kalenius. Anion-driven encapsulation of cationic guest inside pyridine[4]arene dimers. *manuscript submitted*

III A. Kiesilä, N. K. Beyeh, J. O. Moilanen, R. Puttreddy, Sven Götz, K. Rissanen, P. Barran, A. Lützen and E. Kalenius. Thermodynamically driven self-assembly of Pyridinearene to Hexameric capsules. *Org. Biomol. Chem*. **2019,** *17*, 6980 – 6984.

IV S. Kaabel, J. Adamson, F. Topić, A. Kiesilä, E. Kalenius, M. Öeren, M. Reimund, E. Prigorchenko, A. Lõokene, H. J. Reich, K. Rissanen and R. Aav, Chiral hemicucurbit[8]uril as an anion receptor: selectivity to size, shape and charge distribution, *Chem. Sci*. **2017**, *8*, 2184 – 2190.

V T. Mäkelä, A. Kiesilä, E. Kalenius and K. Rissanen. Ion-Pair Complexation with Dibenzo[21]Crown-7 and Dibenzo[24]Crown-8 bis-Urea Receptors, *Chem. Eur. J*. **2016**, *22*, 40, 14264 – 14272.

Author`s contribution

In papers **I-III** author has synthesized the compounds used in the experimental work. She has carried out the mass spectrometric experiments, excluding ion mobility mass spectrometry experiments in **I**. She has been involved in NMR experiments and has carried out most of the crystallizations trials. The author has been actively involved in writing process and has written the first drafts of the papers. In papers **IV** and **V** the author has carried out the mass spectrometric experiments and has contributed to the writing of the original drafts. In paper **V** author has also been involved in NMR experiments and carried out part of the crystallization trials.

CONTENTS

ABBREVIATIONS

ATD	Arrival time distribution
CCS	Collision cross section
CID	Collision-induced dissociation
DFT	Density functional theory
DMSO	Dimethyl sulfoxide
DTIM	Drift tube ion mobility
DTM	Diffuse trajectory method
ESI	Electrospray ionization
ESP	Electrostatic potential
Et_2O	Diethylether
EtOH	Ethanol
D	Diffusion coefficient
DCM	Dichloromethane
DMSO	Dimethylsulfoxide
DOSY	Diffusion-ordered spectroscopy
FTICR	Fourier transform ion cyclotron resonance
IM-MS	Ion mobility mass spectrometry
IRMPD	Infrared multiphoton dissociation
K	Association constant
MALDI	Matrix assisted laser desorption ionization
MeCN	Acetonitrile
MeOH	Methanol
MS	Mass spectrometry
m/z	mass to charge ratio
NMR	Nuclear magnetic resonance spectroscopy
TBA	Tetrabutylammonium
TFA	Trifluoroacetic acid
THF	Tetrahydrofuran
TIMS	Trapped ion mobility spectrometry
TWIMS	Travelling wave ion mobility spectrometry

1 INTRODUCTION

1.1 Supramolecular chemistry

The origin of supramolecular chemistry is often ascribed to the work of Jean-Marie Lehn, Donald Cram and Charles Pedersen, who shared the Nobel Prize in 1987 for "development and use of molecules with structure-specific interactions of high selectivity". Lehn described his area of research as "chemistry beyond the molecule",[1] whereas Donald Cram referred to the same area as host-guest chemistry.[2] These descriptions of supramolecular chemistry illustrate the weak, non-covalent interactions between molecules, which can organize together to form a supramolecular complex. The concept of supramolecular chemistry reaches further in history; the first definitions date to year 1978. Emil Fischer introduced already in 1894 a lock and key-principle, which describes the basic concepts of host-guest chemistry.[3,4] The classical main areas in supramolecular chemistry are host-guest chemistry and self-assembly, but today supramolecular chemistry is understood as a much wider field. The 2016 Nobel prize was awarded to Jean-Pierre Sauvage, Bernard Feringa and Sir Fraser Stoddart for "the design and synthesis of molecular machines" based on supramolecular interactions. This type of nanochemistry is under a rapid development, for example, in constructing highly organized structures and nanomaterials. [5,6]

Even though the area of supramolecular chemistry has spread enormously, the nature of supramolecular interactions remains the same. The term "weak" does not always describe the supramolecular interactions, as they usually work cooperatively to maximize the binding strength and to stabilize the formed complex.[7,8] Yet, the key role in the non-covalent interactions, and why they are called weak, is that they are reversible. Many biological processes are based on such interactions, for example, the folding of DNA double helix and the transportation of ions through the cell membrane.[9] Therefore supramolecular chemistry is often inspired by the nature, as many supramolecular processes mimic those happening in biological context. In the next chapter the non-covalent

interactions are explained briefly and the key concepts in host-guest chemistry and self-assemby are discussed in detail.

1.1.1 Non-covalent interactions

Non-covalent interactions are forces that govern the formation of supramolecular complexes. In order to interact, the components need to have attraction towards each other, but the term non-covalent also comprehends repulsive interactions. A key feature in non-covalent nature is that the interactions are reversible, which provides the complex an ability to break and form again.

Ion-ion interactions are the strongest weak interactions; they are comparable to covalent bonds in strength, varying from 100 to 350 kJ mol^{-1}. In ionic bonds the components have electrostatic attraction towards each other as ionic bonds are formed between two ions of opposite charges, forming salts.[9]
Ion-dipole interactions are formed between an ion and a polar molecule that has a dipole. The strength of ion-dipole interaction varies between 50-200 kJ mol^{-1}. Coordination bonds are also counted as ion-dipole interactions, which makes it sometimes hard to distinguish supramolecular and molecular species from each other.[9]

Matching of two dipoles with opposing polarities towards each other can form surprisingly strong dipole-dipole interactions, usually in the range of 5-50 kJ mol^{-1}. The dipole-dipole interactions are typical, for example, in carbonyl compounds, which can align the opposing dipoles towards each other.[9] Hydrogen bonding is a type of dipole-dipole interaction where hydrogen is attached to an electronegative atom or electron withdrawing group. Hydrogen bond (HB) is generally described as a D-H $\cdots$ A system where D (donor) and A (acceptor) are electronegative atoms or electron withdrawing groups, which share the hydrogen. Typical distances between hydrogen bonded O $\cdots$ O are 2.50-2.80 Å, but significant interactions can exist also 3.0 Å apart. The angle of HB is close to linear (180°) but in weaker HB the angle can be between 100-150°. The bond strength can vary from 10 to 120 kJ mol^{-1}. Hydrogen bonding is one of the most important interactions existing in nature.[9]

Halogen bond (XB) can be described, similarly to hydrogen bonds, as an R-X $\cdots$ Y system. In this system R is a carbon, nitrogen or halogen atom where electrophilic halogen atom X (Lewis acid, XB donor) is attached. Y is a donor of electron density (Lewis base, XB acceptor). Halogen bonds strongly resemble hydrogen bonding, although their polarizability makes them more sensitive to steric hindrance. Also notable, and one key feature in halogen bond, is that they are highly linear. The angle of R-X $\cdots$ Y system is close to 180°. The strength of halogen bonds varies from 10 to 200 kJ mol^{-1}.[10,11]

π-interactions consist of cation-π, anion-π, π-π and CH-π interactions. A π system is typically an aromatic ring. Cation-π interactions are thus formed between cation and aromatic ring. The permanent quadrupole moment (Qzz) formed in electron-rich benzene rings forms negatively charged surface areas in the middle of the ring, where the cation can interact with the ring center.[12] As the

aromatic ring is electron rich, it is intuitive that it would cause repulsive interaction with anions. However, anion-π interactions are formed when an anion is interacting with an electron-deficient aromatic ring. In contrast to cation-π, the ring has several electron withdrawing groups (as in hexafluorobenzene), which creates an electron deficient center to the middle of the ring. The anion can then interact with the electron deficient center of the aromatic ring.[13,14] π-π interactions are formed between two aromatic rings, from which one is usually electron rich and the other electron deficient. Most common orientations of the two aromatic rings are face-to-face and edge-to-face. Aromatic rings cannot be stacked straight on top of each other, as it causes repulsions.[9] CH-π interactions are formed between CH groups and π systems.[15]

Van der Waal forces, also known as dispersion forces, are the weakest of intermolecular forces. They arise from polarization of electron cloud within a molecule caused by proximity of an adjacent nucleus. VdW forces are nondirectional and hence cannot be utilized for designing of specific host molecules. Although VdW forces don't seem to play a major role in the group of weak interactions, it should be still noted that their energy is proportional to their surface area. Therefore in larger molecules VdW forces do play a role. In supramolecular chemistry, VdW forces are the ones that usually govern the inclusion of a small organic compound inside cavities.[9]

Hydrophobic effect arises from exclusion of non-polar groups in aqueous solution. Water molecules prefer to interact with other polar groups and repel non-polar ones, as the non-polarity creates a "hole" without any interactions for water molecules. Therefore for example dichloromethane and water are immiscible, as the components aggregate rather than being dispersed. Hydrophobic effect can also be understood as an empirical rule "like dissolves like". The phenomenon applies to non-polar molecules in aqueous solution and also to water molecules in non-polar solvents. Therefore more generally the term solvophobic effect is preferred to describe the whole phenomenon. Hydrophobic effect can be a key feature in high binding of a guest inside a host molecule in aqueous solution. [16,17]

1.1.2 Host-guest chemistry

In host-guest chemistry, the host is typically a larger molecule that has a suitable binding site for a smaller molecule, the guest. The host can also be a larger aggregate composed of several molecules. The host can have a hole or cavity to accommodate the guest. The binding site needs to be suitable for guest binding without repulsive interactions. [9]

The background of host-guest chemistry lies in Emil Fisher`s lock-key principle that dates back to 1894.[3,4] In his theory, Fisher illustrated how in order for a substrate (key) to bind an enzyme (lock), the components need to be complementary to each other. This laid the basis for molecular recognition where the host can distinguish a certain guest from a crowd. In 1995 Daniel Koshland corrected the theory with induced fit model.[18] Whereas lock and key analogue is often seen

as rigid model where two components need to have perfect complementary geometry, the induced fit considers how the components can make significant conformational changes in order to fit each other. Nevertheless, both models describe the nature of host (lock) and guest (key).

In supramolecular systems, the complexation rarely relies just on one specific interaction. Usually the positive cooperativity has an important effect, meaning that the interactions enhance each other. In multivalent systems, cooperativity can exist in two different forms: allosteric and chelate cooperativity. The allosteric effect usually exists in hosts that can bind several guests. In the allosteric effect, the binding of one guest enhances the binding of the other.[7] Chelate effect is more important in systems that have multiple binding sites. In coordination chemistry the binding sites are referred to as teeth, and bidental ligands form more stable complexes than unidental ones. The replacement of a bidental ligand requires significantly more energy than the replacement of two unidental ligands.[17] Energetics can be expressed in terms of the Gibbs free energy change (ΔG^o) in equation (1),

$$\Delta G° = \Delta H° - T\Delta S° \quad (1)$$

where ΔH^o is the enthalpy change, T is temperature and ΔS^o is entropy change. According to equation (1) the replacement of unidental ligands with bidental ones increases the energetic factor of the reaction, as more molecules become free in solution and the entropy of the system increases.[17]

The energetic factor is important also from the perspective of host preorganisation. Macrocycles, which don't have to undergo significant conformational changes for guest binding, are highly preorganized and they benefit from the macrocyclic effect. This effect does not exist on hosts such as acyclic molecules with a long chain. This kind of host needs to change its conformation significantly, which costs energy. The entropic term becomes unfavourable when moving towards organization, decreasing the possibility of binding.[17]

For host-guest complexation the environment also plays a significant role. In solution both complex-forming components are highly solvated. The solvent is present in huge molar excess and it can compete for binding. Polar solvents can block the hydrogen bonding sites and prevent the complexation of other molecules.[9,19] However, the binding can be enhanced in polar media by utilization of an apolar binding site for an apolar guest.[19,20]

Several aspects influence the binding ability of the host. When considering complementarity, size is not all that matters and the electronic environment must meet the binding requirements. For the binding of an ionic guest, this can be illustrated with hard and soft acids and bases theory[21] that shows how hard acids bind hard bases and soft acids soft bases. In general, the binding of guests is affected by solvent effects (polarity and hydrogen bonding), degree of solvation, the effects of the counter ion, and chelate ring size, especially in the case of cationic guests.[9]

The binding of anions has been considered more challenging than binding of cations. Anions are usually larger than isoelectric cations, which means that their binding interactions are not as effective as those of cations. Anions are also sensitive to changes in pH, and might get protonated and lose their charge. Therefore anion receptors need to function in a narrow pH range. Anions also exist in a wider range of geometries, which makes the design of complementary hosts especially challenging. Solvation effects are also more crucial with anions, as they are usually highly solvated.[22]

In solution, ions are never far from their counter ions, and quite often they exist as contact ion pairs. The simple cation and anion receptors are actually dealing with ion pairs. The binding of a single ion can have a huge energetic cost, as the ions need to be first separated from each other. Therefore, the binding of an ion pair instead of single ion has an energetic benefit. When receptor binds the whole ion pair, there is no energetic cost to overcome. Also, the advantage in heteroditopic receptors over monotopic ones is that ditopic receptors usually function in a highly cooperative manner. Thus the binding of one ion (usually the cation) enhances the binding of the next ion (anion).[23] This has been demonstrated with several receptor systems that without the cation have poor affinity towards anions, but with bound cation the anion binding is remarkably increased.[24]

Neutral guest molecules are not charged and therefore relatively weak interactions need to be utilized for their binding. These interactions must be carefully designed to assist in binding.[9]

Hosts can bind a certain type of guest molecules, for example metal cations, without being selective which metal cations they bind. A receptor is called specific if it is capable of binding one guest from a crowd of other similar molecules. This is called molecular recognition. Molecular recognition has been a hot topic in supramolecular chemistry for decades and it can be utilized in several applications. For example, a sensor is a host which is capable of both molecular recognition and sensing. The binding of the guest produces in the sensor a signal that can be physically detected. The binding can cause an emission (photochemical), a current (electrochemical) or other change that can be externally detected, such as a change in the colour. [25]

Other applications for molecular recognition can be found, for example, in extraction, solubilisation, and ion transport. The next chapter describes systems, that form larger assemblies to build a suitable container for guest binding. In these systems the host is not a single receptor molecule but a self-assembled structure.

1.1.3 Self-assembly

Self-assembly refers to a process where compounds spontaneously arrange into larger assemblies and are held together by non-covalent interactions, meaning that the formation is reversible. These assemblies can form spontaneously or they can be constructed by sophisticated design.[26] The self-assembly can be utilized to build containers, such as capsules or cages, for large guest molecules. The synthetic workload can be minimized when large structures are self-assembled from small molecules. This produces economic and environmental benefits. The need and understanding of self-assembly is also recognized in nanochemistry. Self-assembly has already been exploited to build molecular machines, such as catenanes and rotaxanes.[27] The self-assembly process has also been utilized to construct very elegant nanosized hierarchies such as the star of David (figure 1b).[28,29]

The self-assembly process occurs due to the attractive and repulsive interactions. To form an ensemble, the components need to be able to move with respect to each other. Therefore self-assembly is often studied in fluid systems, but it can be detected and studied also in gas phase and solid state. Many biological systems, such as folding of proteins, RNA or DNA, are governed by hydrogen bonding. Hydrogen bonds are highly selective and directional, and therefore utilizable for self-assembly.[26] Large hydrogen bonding capsules will be discussed in detail in the following chapter. Other directional interactions, such as halogen bonding and coordination bonds of metal atoms, can also be used as building blocks in self-assembly. For example, Turunen *et al*. have demonstrated the utilization of halogen bonding to construct capsules.[30,31]

Coordination chemistry is full of examples where the assemblies can be linked and directed by the metal atoms.[32–34] For example, Fujita`s cages are one of the most ambitious constructions where extremely large cages have been designed. The cage illustrated in figure 1a is formed from 30 palladium and 60 ligand molecules and has a diameter of over 8 nanometers. The interior of this cage is large enough for complexing proteins inside its 157 000 $Å^3$ volume. The star of David, illustrated in figure 1b, was constructed from an assembly of six tris(bipyridine) ligands and six iron(II) cations forming a circular helicate. The head groups of helicates were closed in a one step reaction forming the Star of David catenane. An octameric nanospheroid in figure 1c was formed by hydrogen bonding. The void inside the capsule with 1719 $Å^3$ volume can accommodate selectively a fullerene molecule C_{70}.

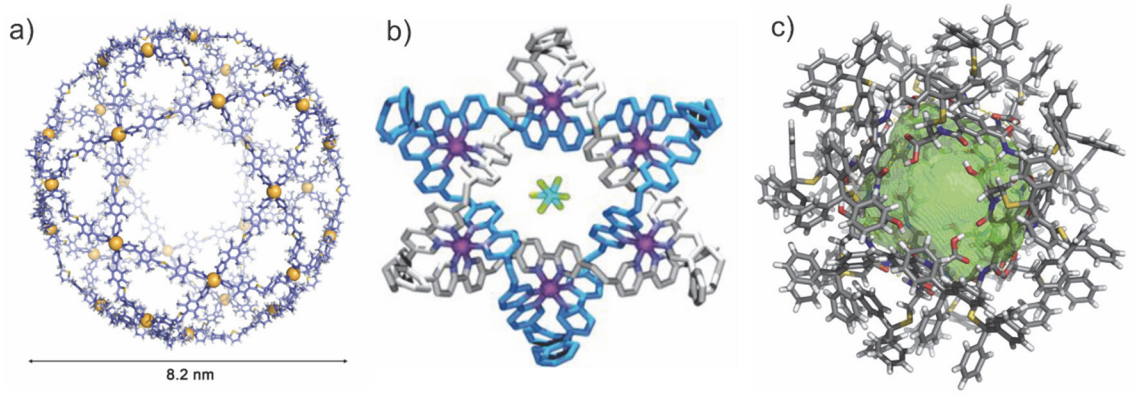

FIGURE 1. Self-assembled structures. a) Fujitas $M_{30}L_{60}$ icosidodecahedron b) star of David catenane and c) hydrogen bonded octameric nanospheroid. Figures adapted with permission a) from ref. [35] copyright © 2016 Elsevier Inc b) from ref. [28] copyright © 2014 Springer Nature and c) from ref. [36] CC BY 4.0, copyright © 2017 Springer Nature.

1.2 Supramolecular hosts

1.2.1 Resorcin[4]arenes

Resorcin[4]arenes and pyrogall[4]arenes, like the ones presented in figure 2, are traditional host molecules widely utilized in supramolecular chemistry. They belong to the class of macrocycles called calixarenes, and are typically bowl-shaped compounds. The basic scaffolds of resorcinarene and pyrogallarene are cyclic tetramers formed in a condensation reaction of resorcinol or pyrogallol with an aldehyde in acidic media.[37,38] The synthesis of the basic scaffold is fast and easy, and can be performed in large quantities. With small modifications or functionalization of the scaffold, the solubility or binding properties of the host can be changed towards more specific functions.[39] The basic scaffold can also be used as a building block to synthesize other hosts, such as cavitands or carcerands.[40–42]

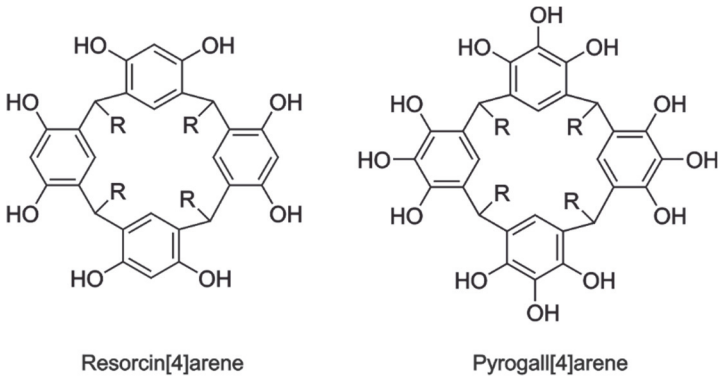

FIGURE 2. Structures of resorcin[4]arene and pyrogall[4]arene macrocycles.

Resorcinarenes and pyrogallarenes are flexible molecules, as the macrocyclic ring can adopt several different conformations shown in figure 3: crown (also known as bowl or cone) with C_{4v} symmetry, boat or pinched cone (C_{2v}), chair (C_{2h}), saddle or 1,3-alternate (D_{2d}) and diamond (C_s). The relative configurations of the methylene bridge substituents can also have different arrangements. These describe the orientation of the aldehyde units towards the resorcinol units, and are all cis (*rccc*), cis-cis-trans (*rcct*), trans-cis-trans (*rtct*) and cis-trans-trans (*rctt*).[43–45] Both resorcin- and pyrogallarenes usually exist in crown conformation, which gives the compounds its bowl shape. The conformation is rigidified by intramolecular hydrogen bonding of the hydroxyl groups at so called upper rim of the molecule. Other isomers can be isolated during the synthesis, but the synthesis favours the *rccc*-isomer as a thermodynamic product, while the others are formed as kinetic products. Esterification of the hydroxyl groups leads to other conformation due to steric effects and the loss of ability to form hydrogen bonds.[45] The lower rim on the bottom of the molecule usually consists of aliphatic alkyl chains. The elongation of the alkyl chain causes a change in solubility from polar protic to nonpolar aprotic solvents.

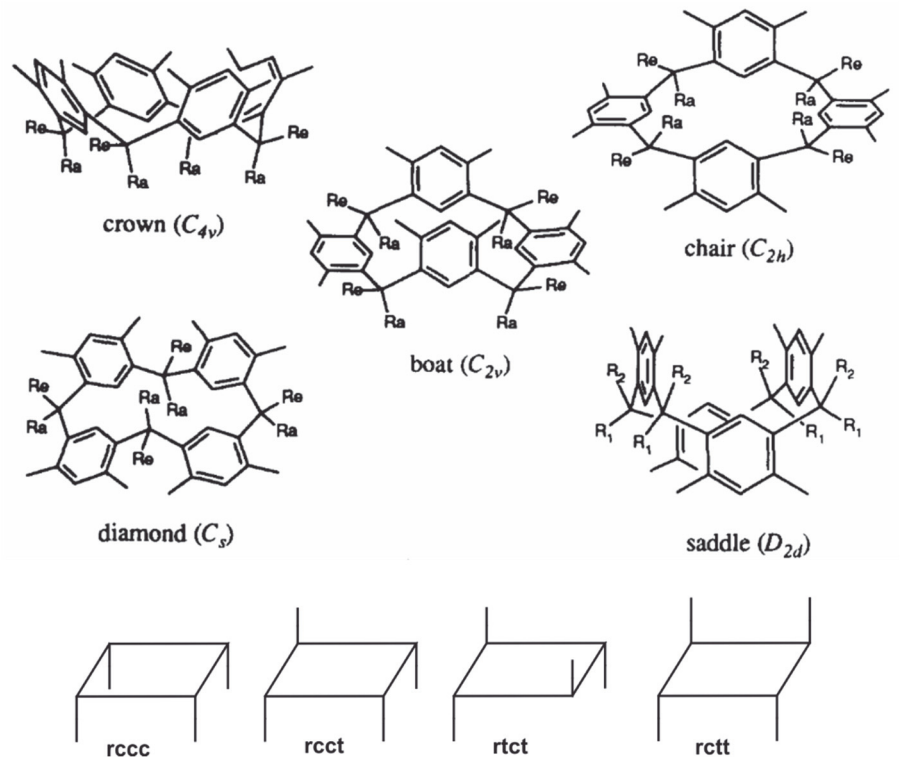

FIGURE 3. Top: Conformations of resorcinarene and their symmetry planes: crown, boat, chair, diamond and saddle. Below are presented the relative configurations, that describe the orientation of the methylene bridge substituents. Adapted with permission from ref. [38] copyright © 1996 Elsevier Ltd.

Even though the bowl shaped compound itself possesses a pocket, its cavity is rather small. The ability of hydrogen bonding at the upper rim is crucial for the formation of larger (capsular) assemblies and thus encapsulation of guests of larger size. Resorcinarenes and pyrogallarenes both form dimeric and hexameric

capsules.[46,47] While the capsules of resorcinarenes are usually solvent- or anion mediated, pyrogallarenes form capsular assemblies via direct hydrogen bonds between subunits.[47] The solvent molecules are part of the hydrogen bonding network of resorcinarenes in solid state and in solution.[46,48,49] The X-ray structures of solvent mediated resorcinarene hexamer and directly hydrogen-bonded pyrogallarene hexamer are illustrated in figure 4.

Complexation properties of dimeric and hexameric capsules of resorcinarenes and pyrogallarenes have been under intense studies over the past decades. Several reports have demonstrated their ability to encapsulate alkyl ammonium guests inside their cavities. [50–53] Neutral species and other cationic guests have also been shown to encapsulate inside the capsular assemblies.[53–56]

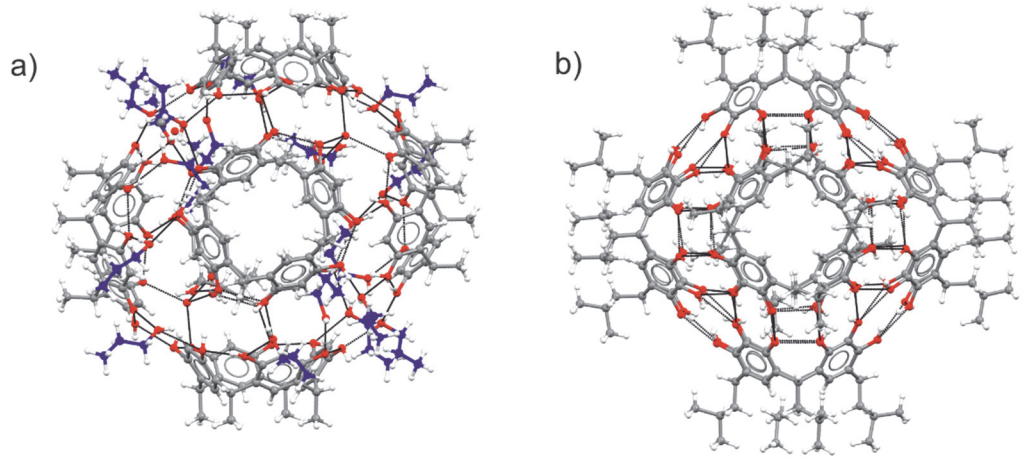

FIGURE 4. Hexameric assemblies of a) Resorcinarene (CSD ref. code: JEZPEM)[57] and b) pyrogallarene (CSD ref. code: CANQAJ).[47] The solvent molecules (propanol and water) assist in formation of hexameric capsule of resorcinarene. Propanol molecules are marked in blue. Pyrogallarene forms hexamer through direct hydrogen bonds. Hydrogen bonds are shown in black dashed lines.

Resorcinarenes and their derivatives have found most of their applications in molecular recognition, as demonstrated with various guests. The research in nanochemistry has been keen on utilization of large containers as reaction vessels for catalysis. Resorcinarenes have been found suitable for such applications and several reactions have been successfully carried out inside their hexameric assemblies. [58–61] More interesting, pyrogallarene has not shown such potential for catalysis. It is possible that water molecules in the hydrogen bonded network of resorcinearene capsules could be responsible for its catalytic activity.[59,62]

1.2.2 Pyridine[4]arenes

Pyridine[4]arenes[63] are interesting compounds, as they structurally possess clear similarities to resorcinarenes. The interesting feature in pyridinearenes is that they show completely different binding properties compared to resorcinarenes. While resorcinarenes are recognized for their cation binding properties, pyridinearenes have shown affinity towards anionic guests.[64,65]

The synthesis of pyridinearenes was presented already in 2001 by Mattay *et al.*, who prepared the compound from a condensation reaction of 2,6-dihydroxypyridine and different aldehydes in glycol monoisopropylether.[63] The required conditions in the synthesis are harsh; the reaction is refluxed at 145 °C for 10 days. Mattay studied the obtained compound and showed by X-ray analysis that the product remained in its dihydroxy-tautomer (figure 5) and cone conformation. The obtained crystal structure also showed that the host is able to form dimeric capsules via hydrogen bonding. Careful examination of the crystal structure, however, indicates that there might be misinterpretation of the tautomeric form. The C⋯O-H bond lengths in each pyridine ring should be equal in the dihydroxy form, but one is significantly shorter than the other (varying bond lengths of 1.262-1.278 Å and 1.315-1.338 Å). This indicates that the tautomeric structure is in fact hydroxy-oxo rather than dihydroxy form.

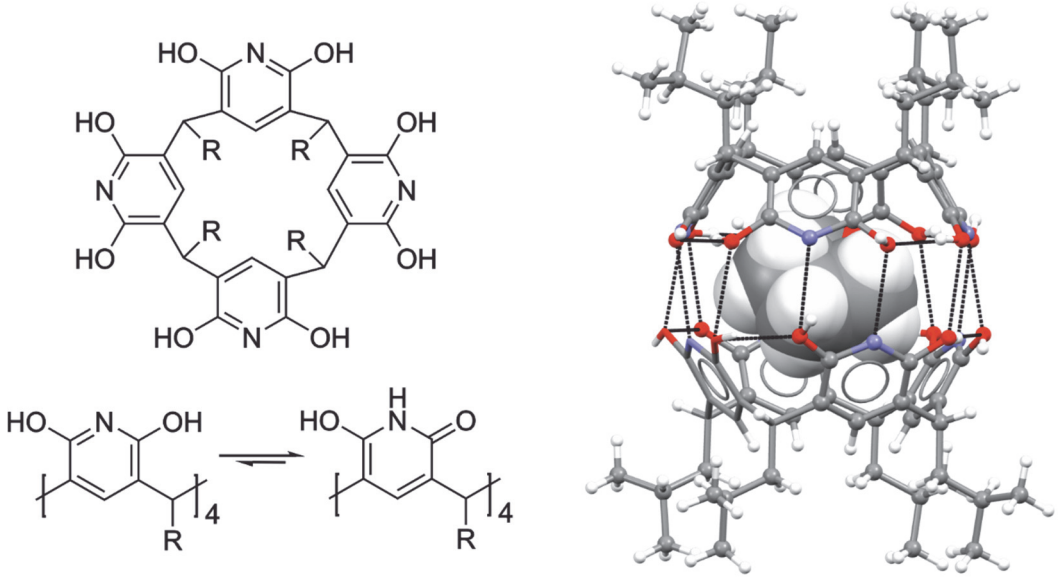

FIGURE 5. Left: Structure of pyridine[4]arene and its two possible tautomeric forms. Right: X-ray structure of dimeric pyridine[4]arene capsule, where encapsulated THF is shown in space fill model (CSD ref. code: GUKBIX).[63] Hydrogen bonds are shown in black dotted lines.

Nevertheless, Mattay`s group was interested in introducing the pyridine ring to the macrocycle, as it could mimic the pyrimidine structure of nucleobases. More interesting, studies of host-guest properties of pyridine[4]arene showed that it could encapsulate small carboxylic acids and amides inside the cavity of

the dimer. This was supported by electrospray Fourier transform ion cyclotron resonance mass spectrometry (ESI-FTICR-MS), nuclear magnetic resonance (NMR) experiments and by density functional theory (DFT) calculations.[64] In ESI-MS, the complexation was observed only for the dimer, and there seemed to be a clear preference in the size of the complex forming guests. These facts lead the authors to believe that guests are incorporated inside the cavity.[64]

The authors tried to prove the encapsulation by performing infrared multiphoton dissociation (IRMPD) experiments for the observed complexes. In IRMPD the ions are isolated and irradiated to produce fragmentation, which can yield structural information. From studied $[dimer+guest+H]^+$ ions the elimination of a neutral guest was observed at the first step, producing a $[dimer+H]^+$ ion. The hydrogen bonded capsule further breaks apart showing $[monomer+H]^+$ ion. The authors assigned this behaviour as *endo*-complexation of the guest by claiming that the $[monomer+guest+H]^+$ ion is not stable enough to be observed. They still raised the point that the guest might also be bound outside the capsule. [64]

The DFT calculated structures also supported the anion inclusion inside the dimer, as studied with different anions and ammonium cation (figure 6). The highest stabilities were observed for complexes with non-coordinating anions BF_4^- and PF_6^- which were also detected experimentally by ESI-MS.[65]

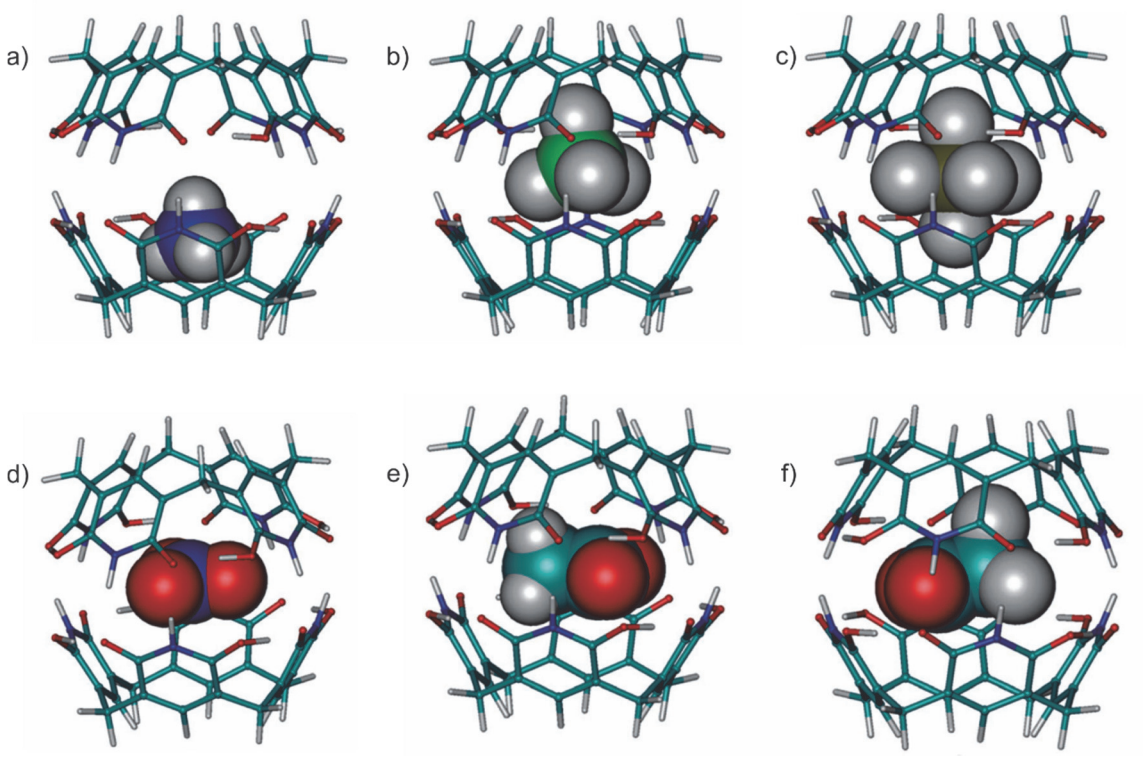

FIGURE 6. Calculated structures of a) $\mathbf{1}_2 + NH_4^+$ b) $\mathbf{1}_2 + BF_4^-$ c) $\mathbf{1}_2 + PF_6^-$ d) $\mathbf{1}_2 + NO_3^-$ e) $\mathbf{1}_2 + AcO^-$ and f) $\mathbf{1}_2 + TFA^-$. All structures showed the inclusion of the guest molecule. Adapted with permission from ref. [65] copyright © 2013 the Centre National de la Recherche Scientifique (CNRS) and The Royal Society of Chemistry

The binding properties of pyridinearene have also been studied in solution, where complexation of TFA could be demonstrated by ^{19}F NMR. In chloroform solution, pyridine[4]arene forms two species, which were first assigned as monomer and dimer.[64] Later Evan-Salem & Cohen proved by DOSY NMR that these signals corresponded to dimer and hexamer by using resorcinarenes of similar size as reference compounds.[66] In the same study, the encapsulation of chloroform molecules to pyridinearene capsules was detected.

A few studies have tried to illustrate the differences between reorcinarene and pyridinearene. First, in solution, when pyridinearene and resorcinarene are mixed to the same sample, no formation of heterodimers could be observed. This indicates that both compounds self-assemble in a self-sorting manner. In the same study it was noted that addition of TFA leads to breakage of pyridinearene capsules, while resorcinarenes capsules stay intact. [66] The host properties have also been compared by calculations and mapping the electrostatic potential (ESP) surfaces (presented in figure 7). The ESP surfaces proposed the cavity of pyridinearene to be π-acidic, while the resorcinarene cavity is π-basic. The permanent quadrupole moment, however, was slightly negative (-1.1 B) for 6-hydroxy-2-pyridone model.[67,68] In comparison, the quadrupole moment for resorcinol was -4.2 B. Therefore, it could be expected that resorcinarene is more able to bind cationic guests. The authors claim that pyridinearene could possess dual character and bind both cations and anions inside its cavity. [65]

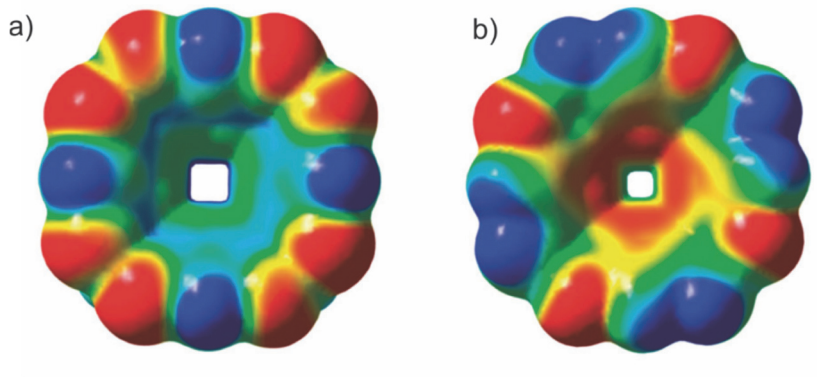

FIGURE 7. ESP surfaces for a) pyridinearene and b) resorcinarene. ESP surfaces are on the range of -30 to +30 kcal/mol. Positive regions are marked in blue and negative regions in red. Adapted with permission from ref. [65] copyright © 2013 the Centre National de la Recherche Scientifique (CNRS) and The Royal Society of Chemistry

So far only a few reports about the binding properties of pyridinearenes highlight their anion binding properties. The results are inspiring, as this type of binding does not take place in traditional resorcinarenes. In addition to anion binding, pyridinearene has been utilized in the formation of gels with aminonaphthyridine[69], in the surface of gold nanoparticles[70] and in formation of branched aggregates.[71]

1.2.3 Hemicucurbiturils

Pumpkin shaped cucurbit[n]urils,[72,73] CB[n] are cyclic macrocycles consisting of n glycoluril units, usually CB5-CB8 or CB10. Hemicucurbit[n]urils HC[n] resemble cucurbit[n]urils, but are cut in halves along the equator (see figure 8 for structures). Miyahara *et al.*,[74] who designed the synthesis of HC[n], were expecting the product to stay in cone conformation, and visualised that the carbonyl portal site could bind metal cations and the hydrophobic part organic molecules. This idea was based on the binding properties of CBs, which bind cations to its carbonyl portals while aliphatic alkyl chain resides in the hydrophobic cavity of CB.[75]

When the synthesis was successfully carried out in condensation reaction of ethyleneurea and 37 % formalin in 4 M HCl, the remaining product turned out to have remarkably different properties than expected. Single crystal analysis of the product showed the formed HC6 and HC12 to exist in their alternate conformation. The twisting is enabled by single methylene bridges between the HC[n] units, which do not rigidify the structure as do two bridges in CB[n].[74]

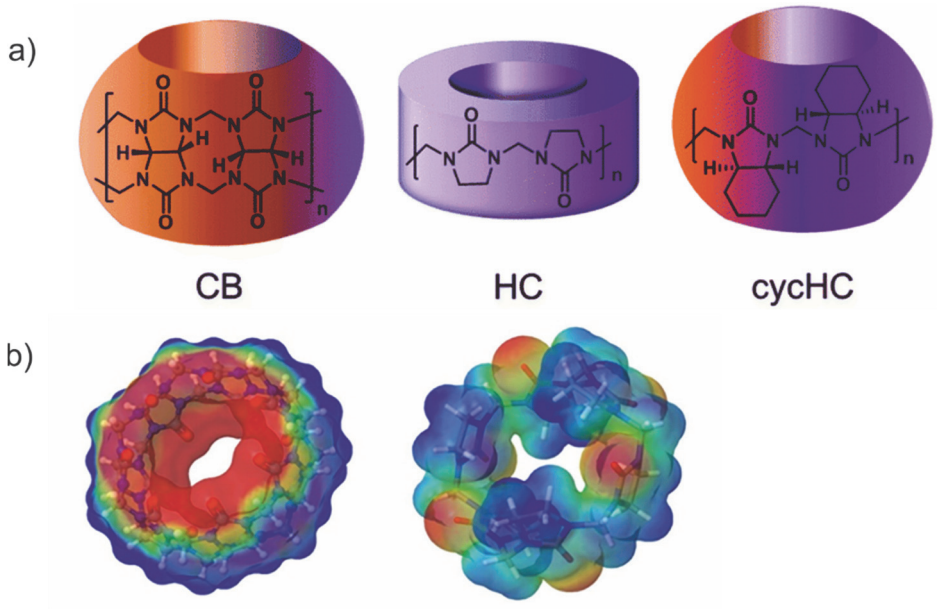

FIGURE 8. a) Structures of cucurbit[n]uril (CB), hemicucurbit[n]uril (HC) and cyclohexylhemicucurbit[n]uril (CycHC). b) ESP surfaces of CB6 and HC6 shown below CB and HC structures, respectively. Positive regions are shown in blue and negative regions in red. [76,77] Figures adapted with permission a) from ref.[77] copyright © 2015 Royal Society of Chemistry and b) from ref. [76] copyright © 2017 Elsevier B.V.

ESP surfaces in figure 8b illustrate the difference between classical CB[n] and HC[n]. CB[n] has high electron density at its carbonyl portals, illustrating the cation binding properties of the host. The inner surface of the CB cavity does not have functional groups which could participate in hydrogen-bonding, and is therefore hydrophobic and suitable for neutral guests.[75] In HC[n] the alternate conformation completely changes the binding properties. The zig-zag orientation

of the carbonyl groups scatters the electron density and leaves the inner part of the macrocycle rather electron deficient.

HC[n] have turned out to be hosts for anionic guests, usually halides.[74] Other types of hemicucurbiturils, for example cyclohexylhemicucurbit[n]urils cycHC[n],[78] have been synthesised in enantiopure form, *all*-R or *all*-S. This macrocycle resembles more of the barrel or pumpkin shaped structure of CB[n], but still holds its own properties. The polar and lipophilic regions of the molecule were shown to arrange to opposing alignments. The polar belt with urea functionalities is located in the middle of the cavity and nonpolar cyclohexyls are pointing out.[78] The cycHC6 has a suitable sized cavity for complexation of halides,[78,79] whereas larger cycHC8 can be synthesized using larger anions, for example PF_6^- or $CF_3CO_2^-$, as a suitable template.[77] It can be expected that the larger cycHC8 could act as a suitable host for other larger anionic guests as well.

The solubility of CBs vary. CB5 and CB7 have moderate solubility to water, but CB6 and CB8 are less soluble. Their solubility can be enhanced by addition of acid or alkali metal salts to the solution. The solubility of CB usually increases when a guest is incorporated inside its cavity. [20] Original hemicucurbiturils have very low solubility in aqueous solutions. [80] However, cyclohexylhemicucurbituril is fairly soluble both in aqueous media and in organic solvents. Therefore it could be more applicable for supramolecular chemistry purposes.

1.2.4 Crown ether-urea receptors

Crown ethers were discovered as a fortuitous side product by Charles Pedersen, who was later awarded a Nobel Prize for work related to these macrocycles.[81,82] Crown ethers are cyclic poly-ethers where the oxygen atoms are usually separated by two carbon atoms. The numbers in the name, for example [18]crown-6, refers to a crown ether containing 18 atoms in total, from which 6 are oxygens. The hydrophilic sites, the oxygens, point towards the interior of the macrocycle, while the hydrophobic sites of the alkyl chains point outside. Pedersen soon found out that these macrocycles possess high affinity towards alkali metal cations.[81,82] Indeed, crown ethers are capable of binding cationic guests by ion-dipole interactions through its oxygen atoms. Crown ethers can bind cations of different size, but the highest affinity is observed towards the cations with the best size fit to the cavity and therefore maximum number of interactions. For example, [18]crown-6 has the highest affinity towards potassium cation that has a perfect fit to the ring, as can be seen in figure 9. Larger cations, for example rubidium and cesium, are too large to fit inside the macrocyclic ring, and therefore [18]crown-6 forms sandwich-type complexes with larger cations where cation is bound in between two macrocycles. Cations that are small relative to the ring usually cause the crown ether to twist or wrap itself around the cation to form more interactions. The binding of a guest with good size-fit, and therefore maximum number of interactions, does not require changes in conformation and is energetically favoured.[82] Size-fit is not the only thing that explains the selectivity of crown ethers. Preorganization and complementarity, solvation and chelate

ring size are the other key issues that explain the observed selectivity.[83] Variations from crown ethers have been demonstrated by replacing oxygens with other heteroatoms, for example the nitrogen containing aza crowns and sulphur containing thia crowns.

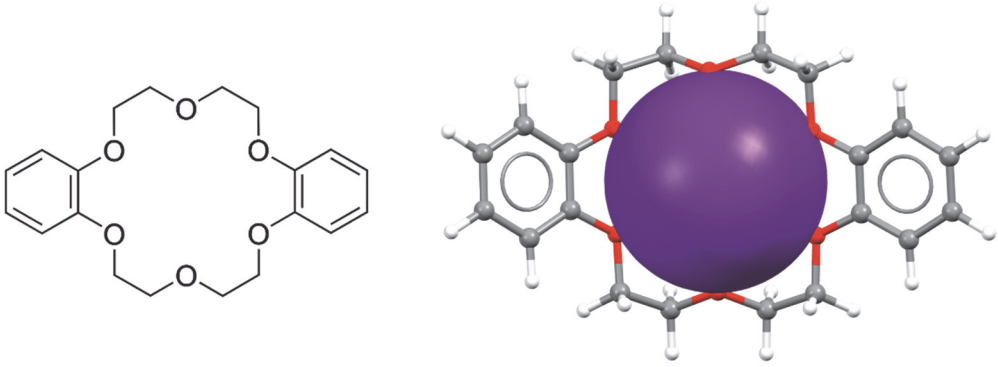

FIGURE 9. Structure of Dibenzo[18]crown-6 and X-ray structure of its complex with potassium (CSD ref. code: BEBFAP).[84] Potassium is shown in spacefill model.

Crown ethers are good in solubilizing salts in organic solvents and therefore they can act as phase transfer catalysts. The crown ethers already separate an ion pair and can transfer the reactive ion closer to the reactive center. Their use in several catalytic reactions has been demonstrated.[85] The macrocyclic ring is flexible and can flip its structure, where the oxygens point out and hydrophobic alkyl chains point in. Therefore crown ethers are soluble in lipophilic and also in aqueous solvents.[83]

Because crown ethers are well-established for their cation binding properties, they have been utilized as a part of the structure in several synthetic ditopic hosts. Reetz *et al*. published one of the earliest examples how crown ether can be utilized as a part of ditopic receptor. To a benzo[18]crown-6 was attached a Lewis-acidic boronate group where the complexation of anion could take place. As shown in figure 10a, binding of KF to the receptor was observed with the cation bound to crown ether moiety and anion to the boronate group. The receptor was found to be selective for KF, as it was formed from a mixture containing KF, KCl, KBr and KI. [86,87]

Another example of crown ethers in ditopic receptors was demonstrated by Mahoney *et al*. [88,89] They showed the transportation of alkali halides through an organic membrane by a ditopic receptor (in figure 10b). The ditopic receptor has an aza-crown ether moiety and urea functionalities. The guests are bound as a contact ion pair to the receptor. Mahoney showed that their receptor was able to transport alkali halides up to 10-fold faster than monotopic receptors.

Shukla *et al*., have demonstrated the significance of ditopic receptors for binding of different ionic species. Without the crown ether moiety a simple anion receptor based on urea-group (in figure 10c) does not bind acetate and $H_2PO_4^-$ anions in DMSO in the presence of small alkali metal cations Na^+ and K^+. When the cation is switched to larger Cs^+, the binding could be enhanced. The authors

explained the inhibition to be caused by the size and the polarizability of the cation. When Shukla utilized an almost similar receptor (in figure 10d) that included the crown ether moiety, an increase in binding was observed also in the presence of small cations which could be bound to the crown ether macrocycle.[24]

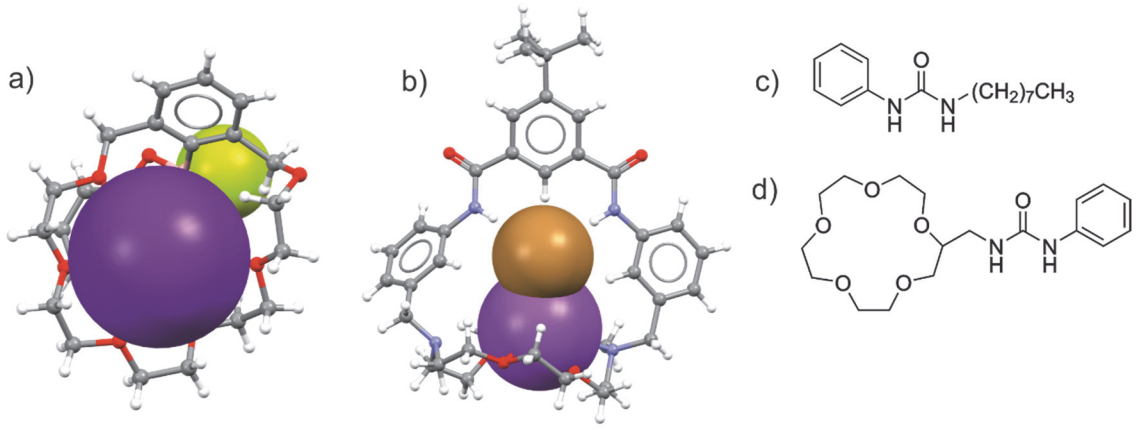

FIGURE 10. a) Ditopic receptor by Reetz shows complexation of contact ion pair KF (CSD ref. code: VOPFEL)[86] b) Ditopic receptor by Mahoney, showing complexation of KBr (CSD ref. code: IBUKEW)[88] c) urea receptor and d) ditopic receptor by Shukla,[24] who demonstrated the significance of the ditopic receptors with these examples. Guest ions are shown in space-fill model.

2 RESEARCH METHODS

Supramolecular systems and processes can be monitored in all physical states; in gas phase, in solution and in solid state. This chapter briefly describes the techniques that can be utilized to study supramolecular systems, especially focusing on the structural chemistry methods used in the experimental part of this work.

2.1 Gas phase

2.1.1 Mass spectrometry

IUPAC defines mass spectrometry as "…the study of matter through the formation of gas phase ions that are characterized using mass spectrometers by their mass, charge, structure and/or physico-chemical properties." [90] Mass spectrometry is a technique which separates ions according to their mass to charge ratio (*m/z*). In an MS spectrum, *m/z* is plotted against the relative abundance of the ions. Mass spectrometer consists of the sample inlet system, the ion source, the mass analyzer and the detector. Depending on the method, the inlet system is not always necessary, but it can be for example a chromatograph or a direct inlet. The crucial thing in mass spectrometry is that it can only detect ions, and therefore the sample needs to be ionized before analysis. Different ion sources can be utilized for this purpose. For example, electron ionization (EI), electrospray ionization (ESI) or matrix assisted laser desorption ionization (MALDI) can be utilized to ionize different analytes. The ionized sample is transferred to the mass analyzer that operates in a high vacuum. Typical analyzers are time-of-flight (TOF), quadrupole, orbitrap or Fourier transform ion cyclotron resonance (FTICR). After the analysis ions reach a detector that transfers the electric current into a mass spectrum.[91,92]

Mass spectrometry combined with a soft ionization method, such as MALDI (matrix assisted laser desorption ionization) or ESI (electrospray ionization) can be used to study supramolecular complexes in gas phase. MALDI produces mainly singly charged ions, but the samples need to be introduced from a matrix, which often causes limitations for supramolecular systems. The matrix also causes high background noise at low *m/z* (< 600), which is a problem with small analytes. On the other hand, MALDI is often utilized in proteomics and other biological applications because it can ionize large molecules and production of singly charged ions simplifies spectra of complicated mixtures. ESI can produce multiply charged ions, which enables detection of larger ions at lower *m/z* values.[91,92] ESI is more commonly utilized to study supramolecular systems as it does not require the selection of suitable matrix and is usable also at lower mass ranges. Figure 11 presents the formation of the gas phase ions in electrospray ionization. The sample is introduced from volatile solvent and transferred through a needle at a high electric potential. This causes the fluid to form a Taylor cone where ions (positive or negative) are gathered at the end of the tip. Charged droplets are ejected from the end of the tip and shrink by evaporation of the solvent assisted by the drying gas. Ions are formed at atmospheric pressure and transferred through the orifice into vacuum.[92]

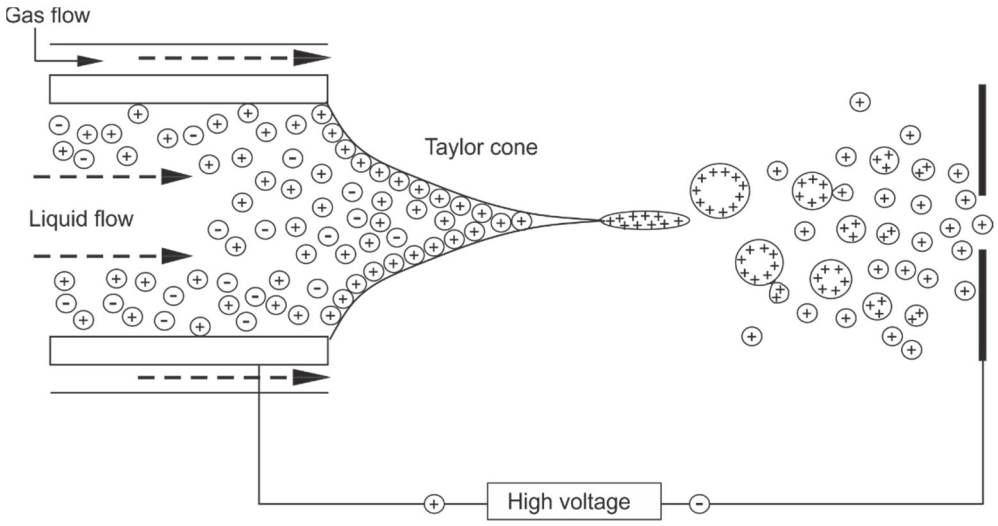

FIGURE 11. The formation of Taylor cone and gas phase ions in electrospray ionization. [92]

Even though mass spectrometry combined with a soft ionization method is an easy way to detect supramolecular complexes in gas phase, it only gives an idea that an interaction is taking place, but not of the binding site. Tandem mass spectrometry can be utilized to obtain more insight of the gas phase structure. This way selected ions can be isolated, fragmented and analysed. Tandem MS experiments can be performed in tandem-in-time or tandem-in-space methods. Tandem-in-space requires at least two mass analyzers. The first analyzer selects the precursor ions at a narrow *m/z* range. After mass selection the ions are activated, for example in a collision cell filled with gas, and the second mass analyzer analyses the fragments. In tandem-in-time method the ions are trapped, isolated,

fragmented and separated inside the same device. Only quadrupole ion trap (QIT) and FTICR instruments are capable of performing tandem-in-time experiments. The long capture time enables the use of very slow activation methods such as electron capture dissociation (ECD) or infrared multiphoton dissociation (IRMPD). [91,92]

2.1.2 Ion mobility mass spectrometry

Ion mobility (IM) [93] measures mobilities of ions through a buffer gas where the movement is caused by an electric field. Ion mobility coupled to mass spectrometer creates a hybrid technique, ion mobility mass spectrometry (IM-MS). Ion mobility is usually coupled to TOF analyser that can record spectra in a µs time scale.[93] The basic principle to measure mobilities of the ions is that the ions are released in a pulsed manner to a mobility cell where an electric field is applied. In the mobility cell ions travel through the buffer gas and the time they spend in the mobility cell is called the drift time. As the cell is filled with buffer gas, ions collide with the gas while passing through the chamber and this affects their drift times. Ions with various geometries and chemical compositions collide differently because of their different sizes and interactions between the gas and the analyte. With a known drift time, *m/z* and experimental parameters, the collision cross section (CCS) value of the analyte can be determined. CCS is thus dependent on the gas and is affected by the size, shape and chemical composition of the analyte. [94–97] CCS is not a true molecular cross section but an observable property that averages all possible orientations and interactions.[95] Yet, CCS values can be roughly compared to other measures obtained from X-ray crystallography or DOSY NMR.[94,96] The accuracy of experimental CCS values can be supported by comparing them to calculated ones. [98–102]

There are several techniques to measure ion mobility; the oldest and simplest is drift tube ion mobility (DTIM). A drift tube instrument has a linear drift cell (figure 12a) where a constant electric field is applied. The ions are released and elute through the cell while colliding with the buffer gas. Larger ions have lower mobility as they experience more collisions with the gas. Conversely, smaller ions have a higher mobility as they collide less with the gas. In a linear drift cell the CCS can be determined from the Mason-Schamp equation:

$$CCS = \frac{3}{16}\left(\frac{2\pi}{\mu k_B T}\right)^{\frac{1}{2}} \frac{ezEt_d}{LN} \qquad (2)$$

where μ is reduced mass, k_B is Boltzmann`s constant, T is the temperature, e is the charge of an electron, z is the charge of the ion, E is the magnitude of the electric field, t_d is the measured drift time, L is the length of the drift tube and N is the density of the buffer gas. [96]

In a travelling wave ion mobility (TWIM) instrument the electric field is applied through ring electrodes connected to opposite phases of radiofrequency voltages. A DC potential is added to the confining RF to create a wave potential that carries ions through the buffer gas. The smaller high-mobility ions can keep up with the waves and "surf" through the cell. Larger ions with lower mobilities need more waves to get through.[103] The determination of CCS values is more complicated with TWIMS instrument. As the electric field is not constant, the Mason-Schamp equation does not hold for TWIMS. Therefore calibrants are needed for determination of CCS values, but calibration of the TWIMS instrument is not straightforward.[97,104,105] The optimal calibrant should have similar size and same kind of interactions with the buffer gas as the analyte. Therefore supramolecular systems cannot be calibrated with commonly used peptides.

Trapped ion mobility (TIM) is the reversal of classic DTIM analyzer. In TIMS the ions are held stationary by radiofrequency voltages and an axial electric field, while the buffer gas "pushes" the ions through the cell (figure 12c). The electric field is gradually decreased so that all ions finally elute through the cell. It is noteworthy that in TIMS the larger species have highest mobility, as they are pushed the most by buffer gas, and therefore they elute out first. The smallest species have low mobility and elute last, which is reversed in DTIM and TWIM analyzers.[106–108] In TIMS, calibrants are needed to calibrate an ion`s mobility, K, which can be described in terms of drift velocity v_d, or its components length L and drift time t_d, and an electric field E as in equation (3):

$$K = \frac{v_d}{E} = \frac{L}{Et_d} \tag{3}$$

With a known mobility the CCS values can be determined from Mason-Schamp equation (2).

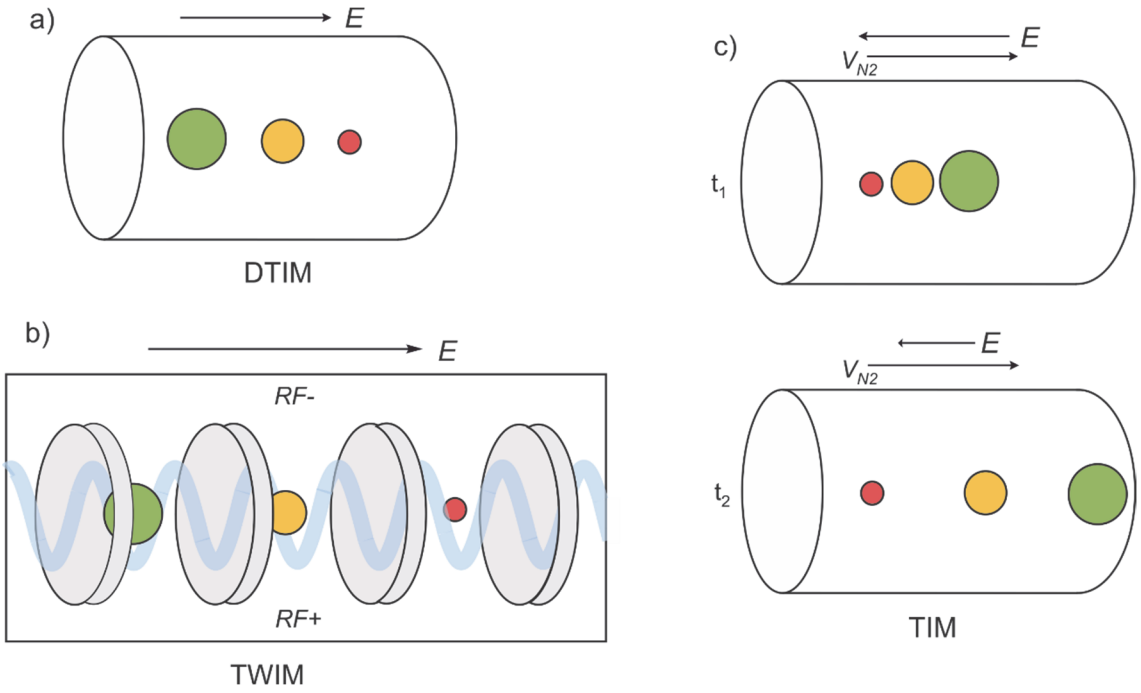

FIGURE 12. Schematic presentation of different ion mobility cells to illustrate their operation. a) In DTIM instrument the electric field is constant and separate ions based on their different mobilities while they travel through buffer gas. b) In TWIM instrument ions surf on a travelling waves applied through ring electrodes of opposing polarities. Ions with higher mobilities elute first. c) In TIM ions are trapped in an electric field at t_1. The electric field is then gradually decreased (t_2) while buffer gas pushes the ions through the mobility cell. In TIM buffer gas pushes the biggest (green) analyte the most, and therefore it elutes first. [96]

Even though the techniques to measure the mobility differ from each other, the ion mobility mass spectrometry instruments consist of similar components. An IM-MS instrument consists of an ion source (typically ESI), an ion mobility analyser (for example drift tube), and mass analyser (TOF). The instrument can contain also a mass filter (usually a quadrupole), which can be located before or after the mobility analyser. In commercial TWIMS instrument, for example, the mass filter is before ion mobility analyser, which allows the activation of the isolated ions before measuring their mobilities.[109]

2.1.2.1 IM-MS of supramolecular complexes

Ion mobility mass spectrometry is not a new technique, but the first commercial IM-MS was launched as late as 2006.[110] In chemistry the IM-MS is most often utilized in proteomics or other biological applications. For example, Stojko *et al.* studied by TWIMS the conformational changes when a ligand is bound to a peptide deformylase (PDF1B) *Arabidopsis Thaliana* protein. Changes in drift times and $^{TW}CCS_{N2}$ values were detected when inhibitor was bound to the protein (figure 13). The difference in $^{TW}CCS_{N2}$ was ~1 %, which translates to 15-22 Å^2 increase in case of the studied protein. [111]

Ion mobility can be also utilized to study metallosupramolecular complexes such as in the work of Ujma *et al*. In their work, DTIMS was demonstrated in study of three-dimensional supramolecular platinum cages. The ligands used for construction of the cages could have different relative orientations, *cis* or *trans*. The isobaric structures were in all cases easily separated according to their different drift times.[112] IM-MS can also be used to study larger complexes and their self-assembly in gas phase. This has been demonstrated by elegant structures of 2D- and 3D-stars of David.[29]

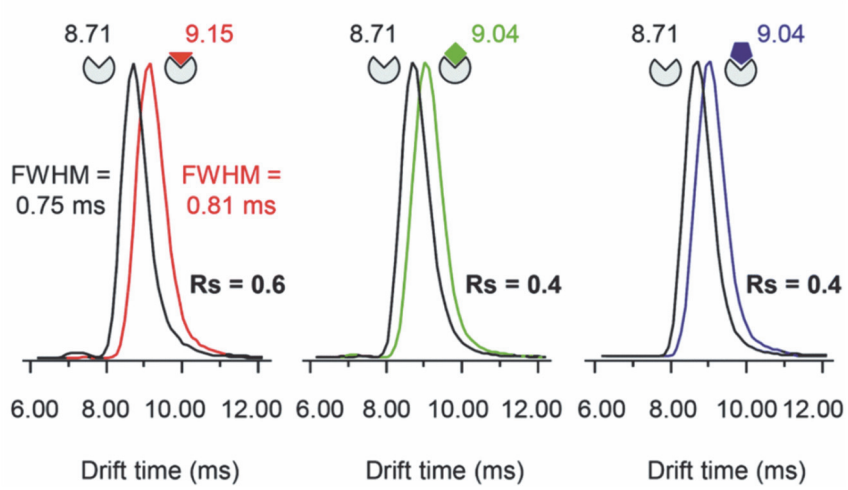

FIGURE 13. Binding of three different bacterial PDF inhibitors to peptide deformylase *A. thaliana* (PDF1B) detected by TWIMS. Adapted with permission from ref. [111], CC BY 3.0, Copyright © 2015 The Royal Society of Chemistry.

A novel ion mobility study of a supramolecular host-guest system was demonstrated by *Lee et al*. who proved by IM-MS that CB7 can perform a catalytic reaction inside its cavity. The azoalkane guest can undergo a retro-Diels-Alder reaction inside the cavity of CB7. The structure of the complex during the guest fragmentation was followed by TWIMS (see figure 14a), where the ion was activated before measuring its mobility. It could be noted that during the fragmentation the host squeezed a little bit to maximize its interactions with the remaining guest. This was observed as a small albeit notable decrease in the drift time. When the dissociation was completed, the remaining host had the same drift time as the free host.[113]

More recent ion mobility study of a supramolecular host-guest system was demonstrated by Schröder *et al*. with a pseudo[1]rotaxane (in figure 14b).[114] Rotaxanes and catenanes have been actively utilized in nanochemistry applications as molecular switches and machines.[6,27] The studied lasso-type pseudo[1]rotaxane is redox-switchable, which can exist in 3 charge states. The conformational changes are triggered by redox-stimuli. The charge states were all observable in an ESI-MS spectrum, but IM-MS showed only two drift peaks, which could be identified as threaded and non-threaded forms. In a CID experiment the increased collision energy caused unthreading of pseudo[1]rotaxane. Surprisingly, the cyclic threaded structure had larger CCS than the open non-threaded form.

This could be explained by the ability of the crown ether moiety to fold into a more compact structure, when the moiety is empty. [114]

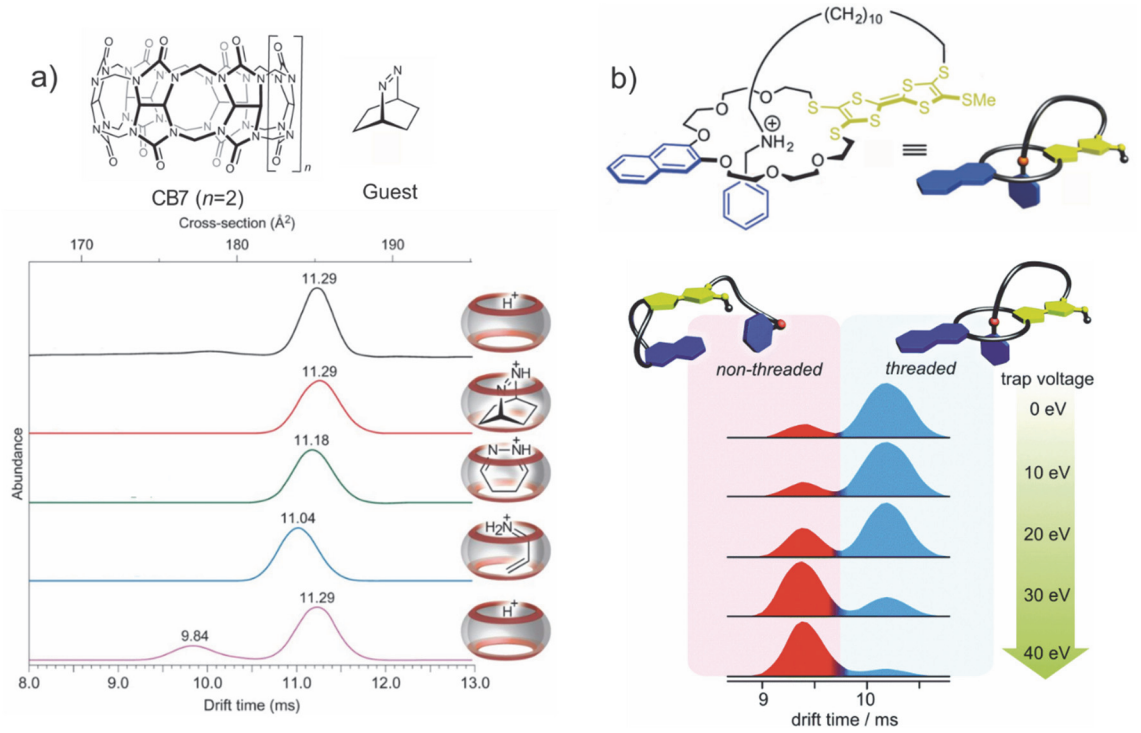

FIGURE 14. a) The fragmentation of a azoalkane guest molecule inside a CB7 could be followed by IM-MS. b) The threaded and non-threaded forms of pseudo[1]rotaxane can be separated by IM-MS. Figures adapted with permission a) from ref. [113] copyright © 2013 Springer Nature and b) from ref. [114] copyright © 2017 The Royal Society of Chemistry.

2.1.3 DFT calculations

Density functional theory, DFT, is a quantum chemical method in computational chemistry based on the physically observable electron density. In DFT functionals are used to describe the electron density that further provides all information needed to describe the wave function of many-electron systems and their properties. Many different functionals have been developed to describe electron density of many-electron systems and their performance have been thoroughly tested over the years.[115] Due to its good scalability, DFT has become one of the most popular computational approaches to model large molecular systems such as supramolecular complexes.[116,117]

Despite the popularity of DFT it has its weakness; the basic formulation of DFT, which is based on electron density, cannot describe weak dispersion forces, which are a non-local phenomenon and especially crucial in the case of supramolecules. For that reason, many methods have been developed to include dispersion correction into the framework of DFT. Some of the most utilized are DFT-D based methods where the dispersion energy is included as an add on to the

calculated DFT energy.[118,119] DFT-D3 is the newest method in the DFT-D family to describe weak dispersion forces and its good performance has been demonstrated with various supramolecular systems.[116,117]

2.2 Solution

2.2.1 NMR

Nuclear magnetic resonance (NMR) spectroscopy detects the resonances of relaxed spin states from nuclei exposed to a strong magnetic field. The NMR probe is tuned for certain nuclei (for example ^{1}H, ^{13}C, ^{19}F), and those nuclei present in the sample are observed as signals with corresponding chemical shifts in the NMR spectrum. The chemical shift of the nuclei depends on their chemical environment. When the nucleus is located close to groups that withdraw electron density, the nucleus is deshielded and the signal moves downfield in the spectrum. Vice versa, when the electronic cloud is shielding a nucleus, it moves upfield in the spectrum.[120]

In case of supramolecules, a complexation can be observed upon addition of the guest into the solution of host. In the case of complexation a shift of the signals is observed. NMR can give information of the binding, but more importantly, of the site where the binding is taking place. For example protons, which exhibit the highest shifts, also experience the greatest change in their chemical environment. The changes in the chemical shifts also indicate regioselectivity, where the binding is taking place. The strength of the binding can be determined in NMR titrations as a binding or association constant K_a that can be described in units of $dm^3\ mol^{-1}$ or M^{-1}. The higher the binding constant, the more stable is the formed complex. The scale of binding constants can vary from 10 to $10^4\ M^{-1}$. Magnitudes of K_a are usually expressed in logarithmic scale and therefore K_a should be denoted as unitless quantity.[9]

In NMR spectroscopy the stoichiometry of the supramolecular complex can be determined in solution using the method of continuous variation, also known as the Job Plot`s method. The right stoichiometry is crucial for calculation of the binding constants. In Job´s plot method, the total concentration of host and guest is kept constant, but their molar fractions are changed while the chemical shift is monitored. The Job´s Plot method has been commonly utilized but it can lead to misinterpretation if not carefully analysed. Job´s plot method works well if only one type of binding model is observed. But if several binding models are detected, the method becomes unreliable. In the latter case, other methods for determination of the possible binding models should be combined to support the analysis.[121]

2.2.1.1 DOSY NMR

Diffusion-ordered spectroscopy is used to measure diffusion and ultimately to determine diffusion coefficient D. The diffusion coefficient can be related to the size, shape and molecular weight of the diffusing particle. The hydrodynamic radius r_h can be calculated from Stokes-Einstein equation

$$D = \frac{Tk_B}{6\pi\eta r_s} \quad (4)$$

where T is the temperature, k_B the Boltzmann constant, η is the viscosity of the fluid and r_s is the radius of the diffusing species. Equation (4) is only valid for spherical species and it neglects the effects of solvation and other interactions. For many cages and capsular assemblies this equation is a reasonable approximation, as they are large enough and their diverse axes are not very different. Therefore r_s can be approximated as r_h.

DOSY NMR can be utilized to gain information of the size of diffusing species, but also of the encapsulation process. The guest molecules are a lot smaller than the host where they are encapsulated. Usually a dramatic change is observed in the diffusion coefficient of the guest when encapsulated, and their diffusion should be the same as hosts if the exchange is slow in the NMR time scale.[122]

2.3 Solid state

2.3.1 X-ray crystallography

X-ray crystallography is a technique based on X-ray diffraction, and it is used to determine the three-dimensional arrangement of atoms in a crystalline material via evaluating the electron densities within the crystal. X-ray crystallography is a powerful tool for structural analysis. It is used widely, for example to determine the structures of supramolecular complexes in solid state. It is the only method that can give a precise picture of the contents in a crystal at the atomic level. The conformation and stoichiometry are visible from the structure. Moreover, the determination of intra- and intermolecular bond lengths and angles gives detailed information of the interactions between the components. [123,124] The limitation of X-ray crystallography is that it cannot state the strength of the binding in case of a host-guest complex. Thus, this technique is often combined with other structural analysis methods. X-ray crystallography has already demonstrated its power in analysis of several supramolecular complexes throughout this thesis, for example the depicted self-assembled structures in chapter 1.1.3.

3 RESULTS AND DISCUSSION

3.1 Aim of the work

The aim of this work was to study supramolecular chemistry and binding properties of different anion binding hosts: pyridine[4]arene, cyclohexylhemicucurbit[8]uril and crown ether urea receptors. Pyridine[4]arene and cyclohexylhemicucurbit[8]uril have already shown affinity towards anionic guests,[64,65,77] but their binding properties are not fully established. Crown ether urea receptors are completely new synthetic receptors that utilize the binding of an ion pair instead of separate ions. Similar receptors have been utilized earlier in ion pair binding.[125]

Pyridine[4]arene is a relatively new host, whose supramolecular chemistry is not yet widely studied. The focus of this work is also on the self-assembly of pyridine[4]arene, as it can form capsules of different size. The earlier reports on self-assembly are contradictory about whether the most abundant assemblies are dimeric or hexameric.[64,66] So far, only one report exists on the ability of pyridine[4]arene to form hexameric aggregates in solution.[66]

The binding behaviour, characterization of the observed complexes and self-assembly have been studied by mass spectrometry, NMR spectroscopy and X-ray crystallography whenever possible. Also DFT calculations have been utilized to visualize the gas-phase structures. In this work, a special interest has been in utilization of ion mobility mass spectrometry to study the structural features of pyridinearene complexes.

3.2 Pyridine[4]arenes

3.2.1 Synthesis [I,126]

Pyridinearenes with different alkyl chains were prepared by acid-catalysed condensation reaction between 2,6-dihydroxypyridine and aldehyde. 2,6-dihydroxypyridine was dissolved in a mixture of ethanol and water where aldehyde was added. The reaction mixture was stirred under reflux for four days. The formed precipitate was filtered and washed with water, ethanol and acetone. The procedure afforded pale products with yields of 70-75 %. Via this method, isobutyl and propyl groups were introduced to the lower rim. Also ethyl was attempted, but the reaction from propanal afforded an insoluble solid. [126]

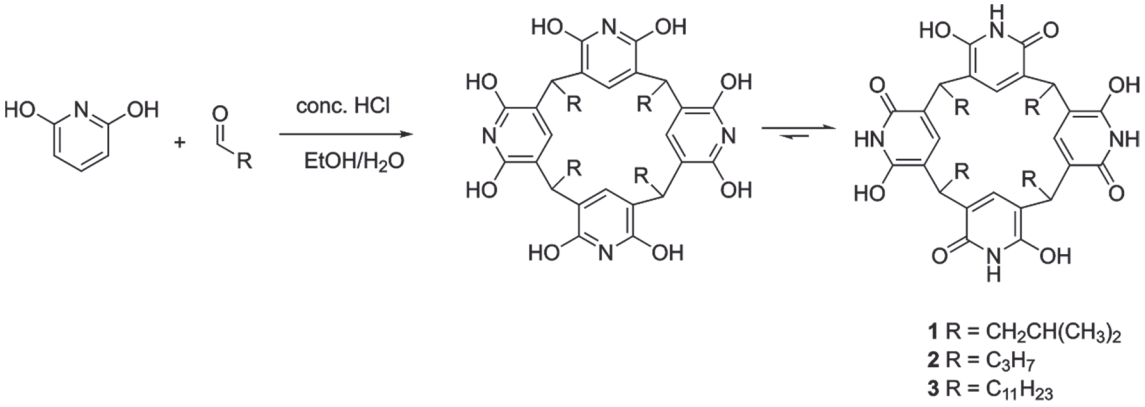

SCHEME 1. New synthesis pathway for preparation of pyridinearenes.

The first published synthesis of pyridine[4]arene [63] was carried out in isopropyl glycol, starting from 2,6-dihydroxypyridine and an aldehyde in acidic media. The reaction can be also performed by following the same reaction conditions (reflux in 145 °C for 10 days), but using 2,6-dimethoxypyridine instead of 2,6-dihydroxypyridine. [I] The advantage of this route is the lower costs of the starting materials. After 10 days the product was purified via the same procedure as in the first report. [63]

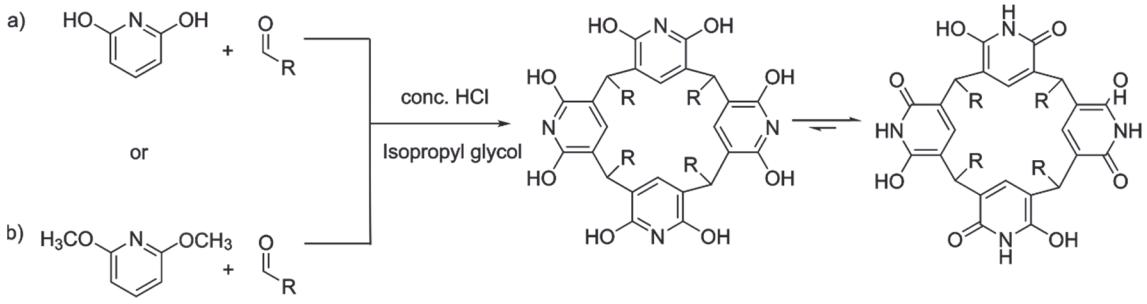

SCHEME 2. a) First published pathway for synthesis of pyridine[4]arene.[63] In b) same reaction conditions, but with cheaper starting materials, leads to formation of same product. [I]

In total, two new synthetic pathways could be demonstrated for preparation of pyridine[4]arenes. The reaction carried out in a mixture of ethanol and water affords a quicker pathway for synthesis, shortening the reaction time from 10 to 4 days. In the second pathway the benefit is economical, as cheaper starting materials can be used. The reaction time still requires 10 days for completion.

All synthesized pyridinearenes were characterized by ^{1}H NMR and ESI-MS to confirm their structure and purity. Also X-ray crystal structures were obtained with **1** and **3**, which showed the pyridinearenes to exist in their hydroxy-oxo tautomeric forms and in cone conformation.[I-III, 126] Most of the work (papers **I-III**) was conducted with pyridine[4]arene (**1**) (R = isobutyl) due to its good solubility in organic solvents. Other pyridine[4]arenes used in the experimental part were **2** (R = propyl) and **3** (R = undecyl).[126]

3.2.2 Studies of complexation properties

3.2.2.1 Anionic guests [I,126]

The affinity of pyridine[4]arene towards anionic guests was of special interest, as in earlier reports the host has shown affinity towards anions.[64,65] Therefore, the affinity of pyridine[4]arenes **1-3** towards anionic guests was screened by measuring series of profile spectra with ESI-Q-TOF mass spectrometry. For complexation experiments the following anions were used as their corresponding TBA-salts: F^-, Cl^-, Br^-, I^-, Br_3^-, CN^-, SCN^-, NO_3^-, NO_2^-, OAc^-, HSO_4^-, $H_2PO_4^-$, ClO_4^-, BF_4^-, PF_6^- and OTf^-. Complexation was observed with Cl^-, Br^-, I^-, ClO_4^-, HSO_4^-, BF_4^- and PF_6^- anions, which formed [**1**+A]$^-$ and [**1**$_2$+A]$^-$ complexes with the host (A=Anion). Also ternary complexes with solvent and anion were generally observed in the spectra as [**1**$_2$+S+A]$^-$ ions (S=solvent), depending on the solvent(s) used in sample introduction (for example MeCN or acetone). Anions I^-, BF_4^- and PF_6^- formed most intense complexes with all studied pyridine[4]arenes **1-3**. This indicates that anion complexation to all pyridinearenes is similar, as the alkyl chain (propyl, isobutyl or undecyl) did not affect on the anion binding. Therefore, later experiments were mainly done using pyridine[4]arene **1** due to its good solubility in organic solvents. The affinity of **1** towards anions was studied in competition experiments that confirmed the order in affinity as $PF_6^- > I^- > BF_4^-$.

The location of the anion in the gas phase structure was studied with collision-induced dissociation (CID). In CID experiments [**1**$_2$+A]$^-$ ions (A=Anion: PF_6^-, I^- or BF_4^-, also later on) were isolated and activated. With PF_6^- the elimination of anion was observed at the first step and only a minority of other fragments were observed with increased collision energy (see figure 15c). This indicates that the anion would be bound outside the capsule (*exo*) rather than inside the cavity (*endo*), as in CID the breakage of weakest bond is usually observed. The isolated [**1**$_2$+BF_4]$^-$ showed [**1**+BF_4]$^-$ at the first dissociation step, which could indicate *endo*-complexation. Similarly [**1**$_2$+I]$^-$ resulted to [**1**+I]$^-$ at the first dissociation step. To study the binding site of the anion, the ternary complexes with solvent and anions were also studied by CID. The cavity of the pyridinearene dimer is too small to occupy two guest molecules simultaneously and therefore one of them has to be located *exo*. The isolated [**1**$_2$+acetone+A]$^-$ showed again elimination of the anion when PF_6^- was used. [**1**$_2$+acetone+BF_4]$^-$ resulted in [**1**+BF_4]$^-$ at the first dissociation step. The CID experiments suggest that PF_6^- is bound *exo* to the pyridinearene capsule, while BF_4^- and I^- could be located *endo*. Most likely acetone is located *endo* when the anion is bound *exo*. The kinetic stabilities of the complexes were compared by calculating the $CE^{50\%}$ values, which represent the relative energy needed for the complex to dissociate to its half intensity. In the stabilities of dimeric [**1**$_2$+A]$^-$ complexes the differences were negligible. However, the monomeric [**1**+PF_6]$^-$ was found to be less stable than [**1**+BF_4]$^-$ and [**1**+I]$^-$ ions. This indicates that all studied ions show similar dissociation, but the [**1**+PF_6]$^-$ ion could not be observed due to its lower stability. In this case, it is likely that all anions are located *exo*.

To characterize the structures of the anion complexes they were further studied in IM-MS experiments. [**1**$_2$+PF_6]$^-$ and [**1**$_2$+acetone+PF_6]$^-$ ions showed longer drift times and ~8Å^2 larger $^{DT}CCS_{N2}$ values compared to [**1**$_2$-H]$^-$ and [**1**$_2$-H+acetone]$^-$ ions (see figure 15a for arrival time distributions). This confirms that acetone is located *endo* in the dimeric capsule in gas phase, while the PF_6^- anion is bound outside, *exo*. These findings show unusual complexation properties for host **1**, as similar behaviour has not been observed with resorcinarenes before. The simultaneous binding of neutral and anionic guests is a new phenomenon. Solvent adducts are common, but they are usually less abundant. A solvent inclusion in gas phase has not been reported earlier.

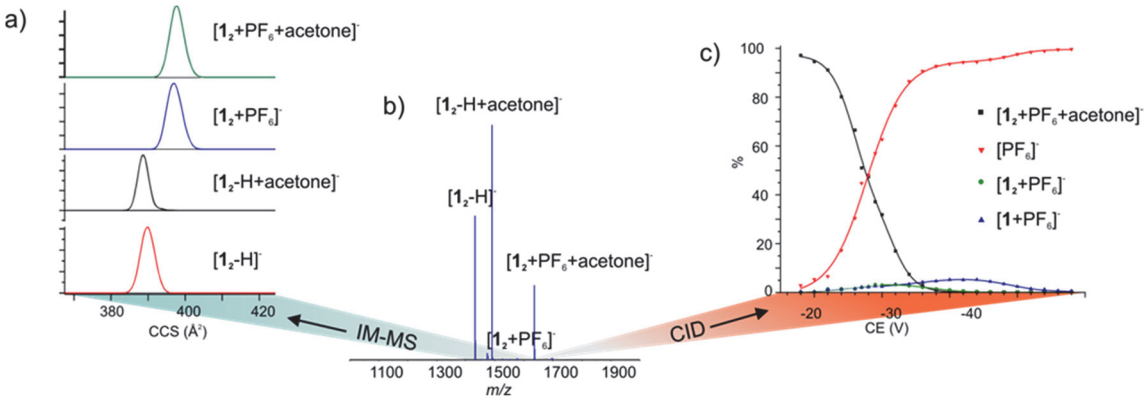

FIGURE 15. a) IMS arrival time distributions of selected ions b) (—)ESI-MS spectrum of **1** + NH_4PF_6 in acetone and c) CID of isolated [$\mathbf{1}_2$+PF_6+acetone]$^-$ complex. IM-MS experiments confirmed the *endo*-location of acetone inside the dimers cavity and *exo*-location of the PF_6^- anion. CID experiment also supports the *exo*-complexation of the anionic guest.

IM-MS experiments did not show significantly larger $^{DT}CCS_{N2}$ values for [$\mathbf{1}_2$+BF_4]$^-$, [$\mathbf{1}_2$+acetone+BF_4]$^-$ or corresponding complexes with iodide when compared to [$\mathbf{1}_2$-H]$^-$ ion. Anions BF_4^- and I^- are smaller and cannot cause as large differences in CCS values as corresponding complexes with PF_6^-. The size difference of the anions is later illustrated in observed X-ray structures in figure 17. The experimental $^{DT}CCS_{N2}$ values are 4-5 Å^2 larger also for complexes with BF_4^- and I^-, which indicates *exo*-location of these anions. CCS values and mass accuracies for the most abundant anion complexes are presented in appendix table A1. Other structural chemistry techniques have also been utilized to obtain complementary information of the binding of BF_4^- and I^- anions to **1**.

For example, in solution the complexation with anionic guests can be followed by ^{1}H and ^{19}F NMR. The ^{1}H NMR spectrum in figure 16 shows weak downfield shifts in aromatic C-H and alkyl-chain protons when PF_6^-, I^- or BF_4^- is bound to **1**. ^{19}F NMR experiments also showed small downfield shits of fluorine atoms when **1** was mixed with PF_6^- or BF_4^-. Both experiments point to the weak CH-anion interactions[127] and confirm that the anion is bound to the exterior of the pyridinearene capsule in chloroform solution. Also pyridinearene **3** with C_{11}-alkyl chains showed a 0.01 ppm downfield shift in the aromatic C-H proton with added PF_6^-.

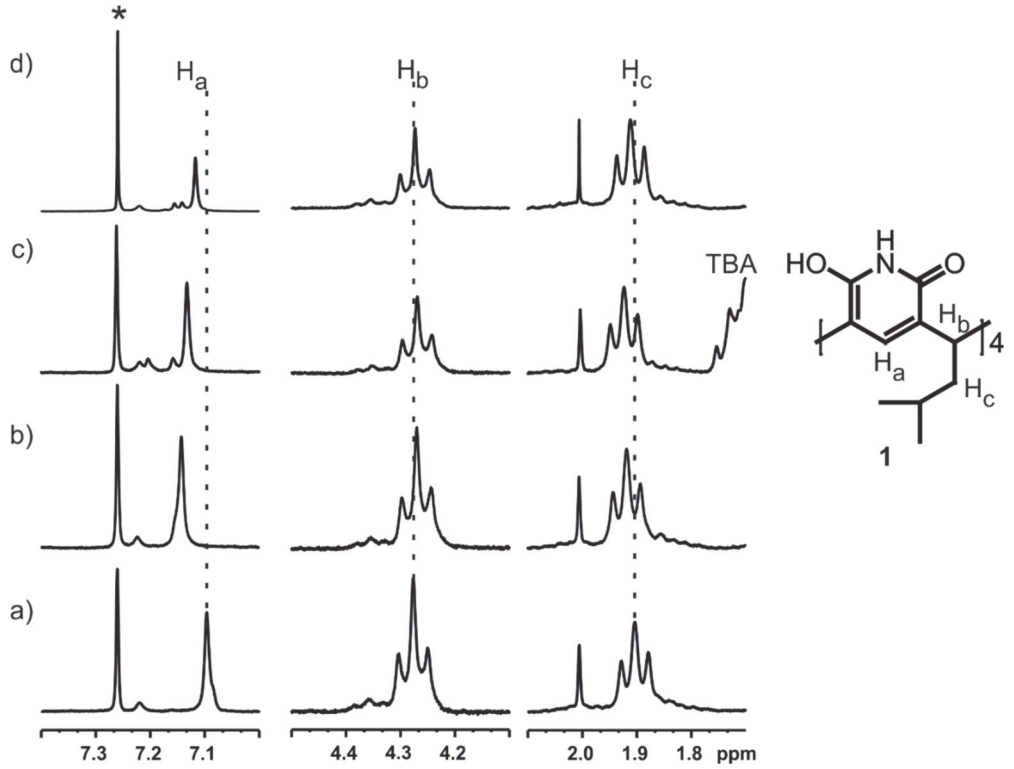

FIGURE 16. ^{1}H NMR spectra of 10 mM samples of a) **1** b) **1** + $TBABF_4$ c) **1** + TBAI and d) **1** + $TBAPF_6$ (Host:guest ratio 1:1, samples measured in $CDCl_3$ at 298K). Protons H_a and H_c show 0.01-0.05 ppm downfield shifts when the anion is bound to the lower rim of **1**.

A single crystal suitable for X-ray analysis was obtained from slow evaporation of a chloroform solution containing **1** + $TBAPF_6$. The crystal structure (Fig. 16a) showed a hydrogen-bonded dimeric structure where **1** was in its hydroxy-oxo tautomeric form. The cone conformation was stabilized by four O-H ··· O (amide) intramolecular hydrogen bonds with lengths of 2.524(5)-2.609(5) Å. The dimer was formed via N-H ··· O (amide) hydrogen bonds with lengths of 2.822(6)-3.115(8) Å. The cavity of the dimer was fully occupied with a chloroform molecule, while the PF_6^- anion was found to reside on the lower rim of **1** in the pocket formed between the isobutyl groups. Similar structure was obtained with $TBABF_4$, where BF_4^- is located on the lower rim of **1**, while a neutral guest DCM occupied the cavity of the dimer (figure 17b). The binding of BF_4^- and PF_6^- anions to **1** were found to be similar in solution and in solid state structures. Even though no X-ray structures with iodide were obtained, I^- showed similar behaviour in solution and in gas phase than other studied anions. Therefore it can be concluded that the binding mode of all anions to **1** is *exo* in gas phase, in solution and in solid state.

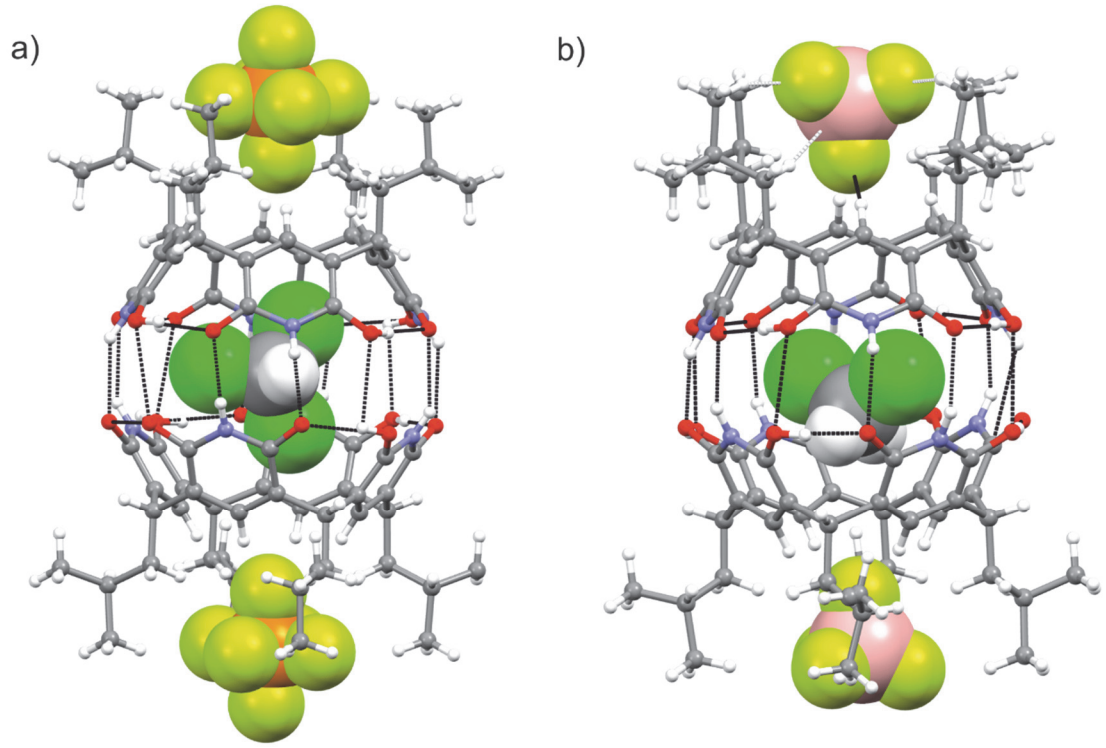

FIGURE 17. X-ray crystal structures of $\mathbf{1}_2$, showing a) the endo-complexation of $CHCl_3$ inside the dimeric capsule and *exo*-complexation of PF_6 anion between isobutyl groups. b) *endo*-complexation of DCM and *exo*-complexation of BF_4^- anion. Hydrogen bonds are shown in black dotted lines. TBA counter cations and cocrystallized solvent molecules are omitted for clarity.

DFT calculations were performed to obtain more insight into the gas phase structure of $\mathbf{1}_2$ and PF_6^- and to visualize the reasons for *exo*-complexation of the anion. Earlier studies, and especially DFT calculations, strongly indicated that anions could be *endo*-complexed to $\mathbf{1}_2$.[64,65] In the previous calculations, however, the lower rim was truncated and the solvent effects were not calculated explicitly.[65] In this study, a model was constructed from the basis of the single-crystal X-ray structure. The possible locations for PF_6^- anion, *endo* and *exo*, were analyzed. The two possible structures of simultaneous *endo*/*exo*-complexes were also compared: $[\mathbf{1}_2+\text{acetone}_{(endo)}+PF_{6(exo)}]^-$ and $[\mathbf{1}_2+PF_{6(endo)}+\text{acetone}_{(exo)}]^-$. The mapped electrostatic potential (ESP) surfaces in figure 18 showed that it is more favourable for the anion to bind outside the dimeric capsule, as the cavity is not especially well suited to bind anions. The lower rim, on the other hand, has a slightly electron-poor area that is more suitable for interacting with anions. From the two simultaneous *endo*/*exo* complexes the formation of $[\mathbf{1}_2+\text{acetone}_{(endo)}+PF_{6(exo)}]^-$ is more favourable. The DFT results support the experimental data and illustrate the reasons for *exo*-complexation. The calculations also revealed that the encapsulation of the acetone is governed by dispersion forces, and therefore neutral guests are more suitable for *endo*-complexation.

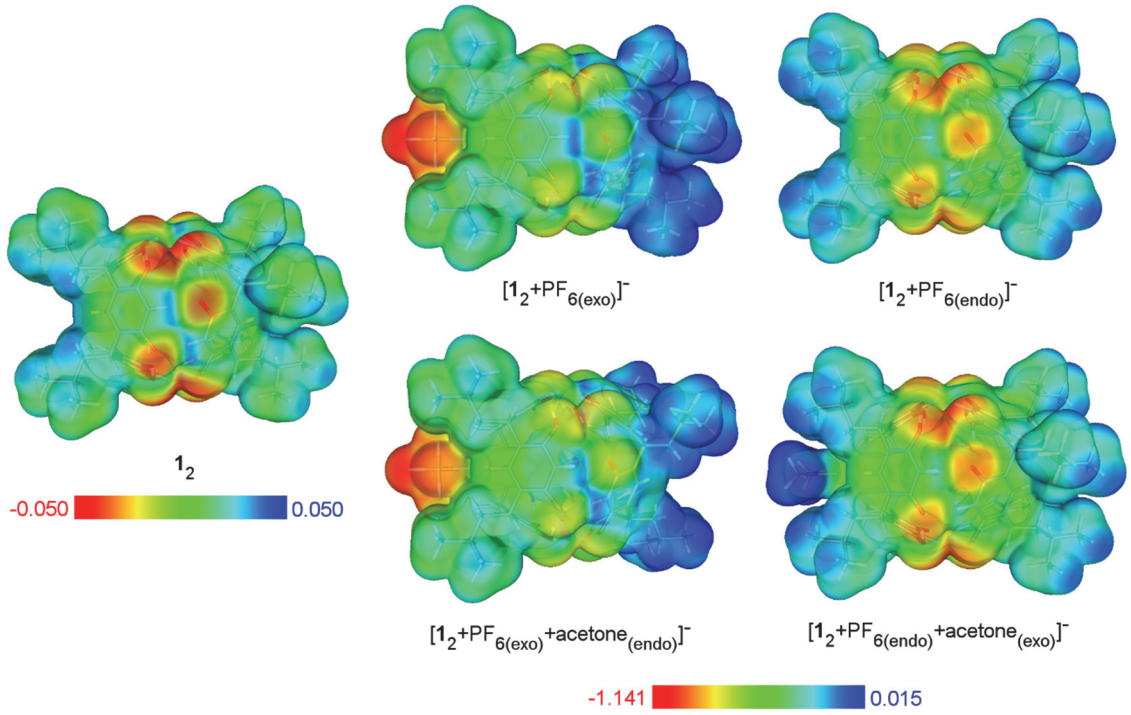

FIGURE 18. The calculated ESP surfaces for $\mathbf{1}_2$, $[\mathbf{1}_2+PF_{6(exo)}]^-$, $[\mathbf{1}_2+PF_{6(endo)}]^-$, $[\mathbf{1}_2+PF_{6(exo)}+acetone_{(endo)}]^-$ and $[\mathbf{1}_2+PF_{6(endo)}+acetone_{(exo)}]^-$.

3.2.2.2 Neutral guests [126]

As pyridinearene showed unusual *endo*-complexation of neutral guests in experiments with anions, its affinity towards neutral molecules was further studied by mass spectrometry. The study was conducted with host **1**, because the alkyl chain does not affect complexation properties inside the capsular cavity. Solvent complexes were usually observed in the mass spectrum of **1** as $[\mathbf{1}_2\text{-H+S}]^-$ ion(s), depending on the solvent(s) used in sample preparation. In all cases the solvent complexes were not the most abundant ions in the spectrum, but addition of anion enhanced their visibility by forming $[\mathbf{1}_2\text{+S+A}]^-$ ions. PF_6^- was used as the anion in these experiments due to its high affinity towards **1**.

In protic solvents H_2O and MeOH no complexation of these solvents was observed, as they resulted in the breakage of the hydrogen-bonded capsule. Both solvents also seemed to fragment the host itself. Et_2O did not form complexes with **1**, and it is probably too large to fit inside the dimeric capsule. Solvents MeCN, acetone, DCM, $CHCl_3$, THF and DMSO formed $[\mathbf{1}_2\text{-H+S}]^-$ and $[\mathbf{1}_2\text{+S+A}]^-$ complexes with **1**. The structures of these complexes were verified by DT-IMMS, which revealed that all solvents are occupying the cavity of the dimer while the anion is bound outside. This was demonstrated earlier with acetone in the previous chapter. CCS values and mass accuracies for all observed solvent complexes are presented in appendix table A2.

The affinity of **1** towards neutral guests was further studied by solvent titrations shown in figure 19, where a series of profile spectra was measured at different solvent compositions. These preliminary studies show order in affinity as MeCN < Acetone < DCM < THF << DMSO. In the experiment between THF and DMSO, no titration was performed and instead a sample was prepared in THF, where 1 µl DMSO was added (0.1% DMSO of total 1ml sample volume). Immediately after spraying the sample only complexes containing THF were observed in the spectrum. Within couple of minutes, the abundance of THF complexes diminished drastically while DMSO complex could be detected as the base peak in the spectrum (figure 20).

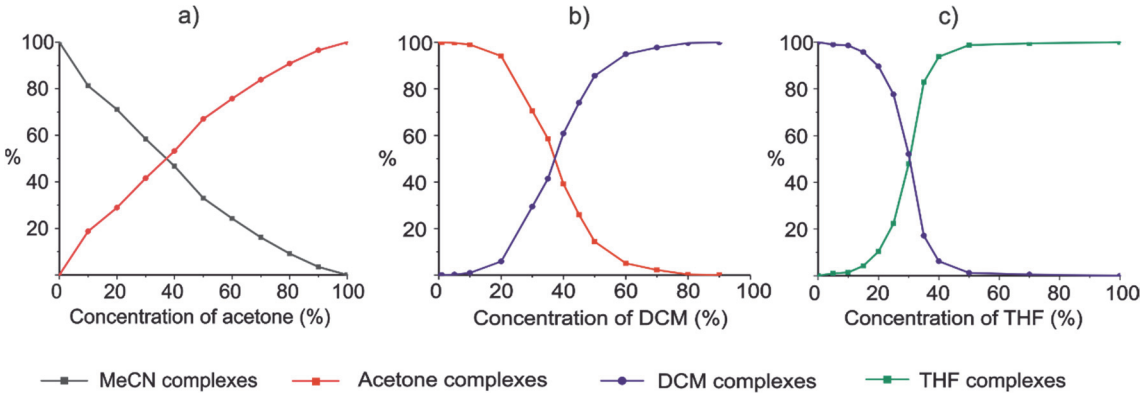

FIGURE 19. Series of titration graphs comparing the affinity of **1** towards neutral solvent molecules. Based on the experiments the affinity of **1** towards neutral guests was determined as MeCN < Acetone < DCM < THF. Percentages in y-axis present the relative intensity of the complexes.

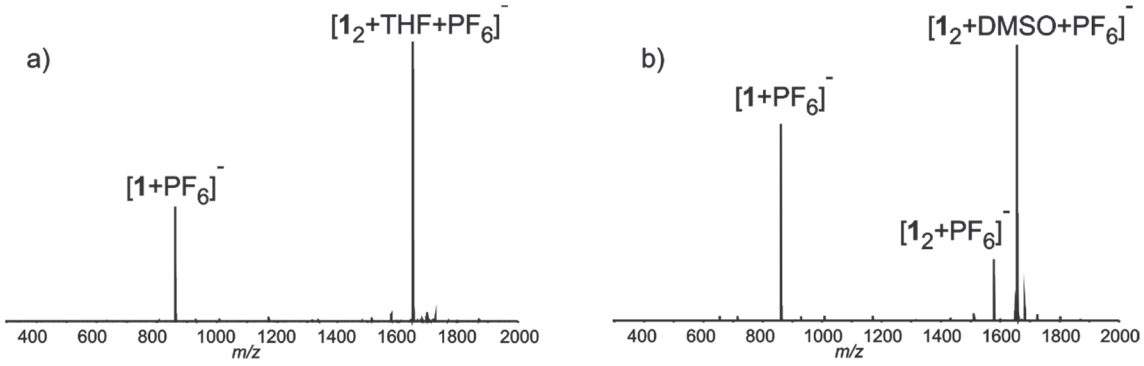

FIGURE 20. Profile spectra from a competition experiment between THF and DMSO. The amount of DMSO was 0.1% of 1ml sample volume. Spectrum a) is measured immediately after injection of the sample and b) a couple of minutes later.

X-ray structures of several dimeric capsules were obtained showing a solvent molecule occupying the cavity (see figure 21 below). X-ray structures where $CHCl_3$ or DCM was occupying the cavity of the dimer were already presented in the previous chapter. Similar structures were observed with DMSO and THF. Interestingly, in structures without *exo*-complexed anion, another solvent can host

the *exo*-binding site of the dimer. For example acetone was observed on both lower rims in *endo*-complexed THF. Chloroform was also observed to occupy the lower rim of **1**, when THF was encapsulated to the dimer. In addition to X-ray structures with **1**, two structures were obtained also with **3**. In these structures, THF or chloroform was *endo*-complexed inside the dimer. Due to bulkiness of long alkyl chain in **3**, no complexation of a second guest molecule (solvent or an anion) was observed to the lower rim in X-ray structures. The MS and NMR experiments already showed, however, the complexation of an anionic guest with **3**.

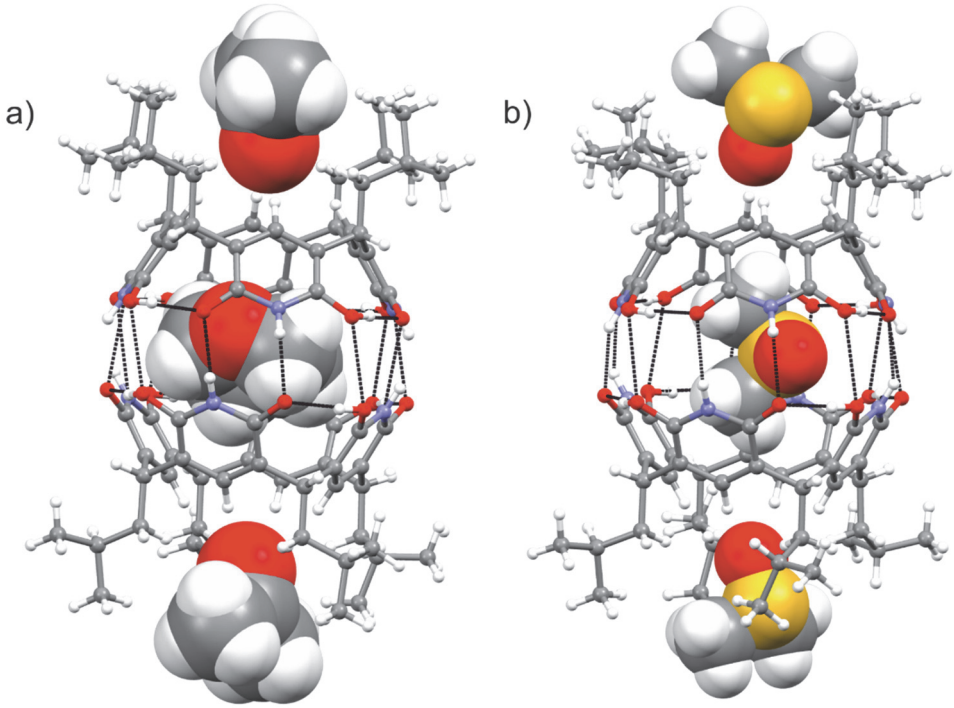

FIGURE 21. Single crystal X-ray structures of $\mathbf{1}_2$, showing *endo*-complexation of a) THF with *exo*-acetone and b) DMSO with *exo*-DMSO. Black dashed lines represent hydrogen bonds. Cocrystallized solvent molecules are omitted for clarity.

3.2.2.3 Cationic guests II

Calculated structure of $\mathbf{1}_2$ revealed in chapter 3.2.2.1 that the cavity does not possess any significant positive potential and therefore is not able to bind anions. Other studies have shown that in similar pyridine rings the π-acidic character is rather weak.[67,68] It was expected that pyridinearene could possess dual binding behaviour towards anions and cations.[65] Therefore the affinity of **1** towards cationic guests was studied with alkyl ammonium salts. Resorcinarenes are well known for their ability to bind alkyl ammonium cations inside their cavities.[51,128,129] The cavity sizes of pyridinearene and resorcinarene are roughly sim-

ilar, and the guests that bind to resorcinarene, were also utilized here. The screening of complex formation was done using chloride or bromide as counter anions, with different chain lengths and substitution degrees of alkyl ammonium cations from $MeNH_3^+$ to Pr_4N^+. Only quaternary ammonium cations Me_4N^+ and Et_4N^+ formed complexes with **1**. The complexes with Et_4N^+ were observable only in (–)ESI-MS and were therefore ruled out from later experiments. The abundance of the observed complexes with Me_4N^+ increased drastically both in (+) and (–)ESI-MS when counter anion was changed to PF_6^-, BF_4^- or I^- that were earlier observed to form *exo*-complexes with **1**. In (+)ESI the $[\mathbf{1}_2+Me_4N]^+$ could be detected as a base peak. In (–)ESI-MS in addition to $[\mathbf{1}_2-2H+Me_4N]^-$, ternary complexes with anions were also observed as $[\mathbf{1}_2-H+Me_4N+PF_6]^-$ and $[\mathbf{1}_2+Me_4N+2PF_6]^-$ ions. The structures of the observed complexes were studied with IM-MS. Ions $[\mathbf{1}_2+H]^+$, $[\mathbf{1}_2+Na]^+$ and $[\mathbf{1}_2+Me_4N]^+$ showed similar drift times, thus confirming that the Me_4N^+ cation is located inside the dimeric capsule (figure 22a). Theoretical CCS values [99,101] also support *endo*-complexation of the Me_4N^+ cation. With diffuse-trajectory method (DTM), *exo*-complexation of the cation should result in ~10 Å^2 larger $^{DTM}CCS_{N2}$ value, which is identical with $^{DTM}CCS_{N2}$ value calculated for $[\mathbf{1}_2+PF_6]^-$ ion, where PF_6^- is *exo*. Ions $[\mathbf{1}_2-H]^-$, $[\mathbf{1}_2-2H+Me_4N]^-$ and $[\mathbf{1}_2-H+acetone]^-$ also showed identical drift times. With *exo*-complexation, when PF_6^- is complexed to the lower rim of the dimer, an elongation in drift time was observed (~1-2 ms), depending on how many anions (one or two) are attached to the lower rim(s) of the dimeric capsule (figure 22b). One *exo*-complexed anion increases $^{DT}CCS_{N2}$ values by ca. 9 Å^2, and addition of a second *exo*-complexed anion results in 5-8 Å^2 larger CCS values compared to ions with one anion.

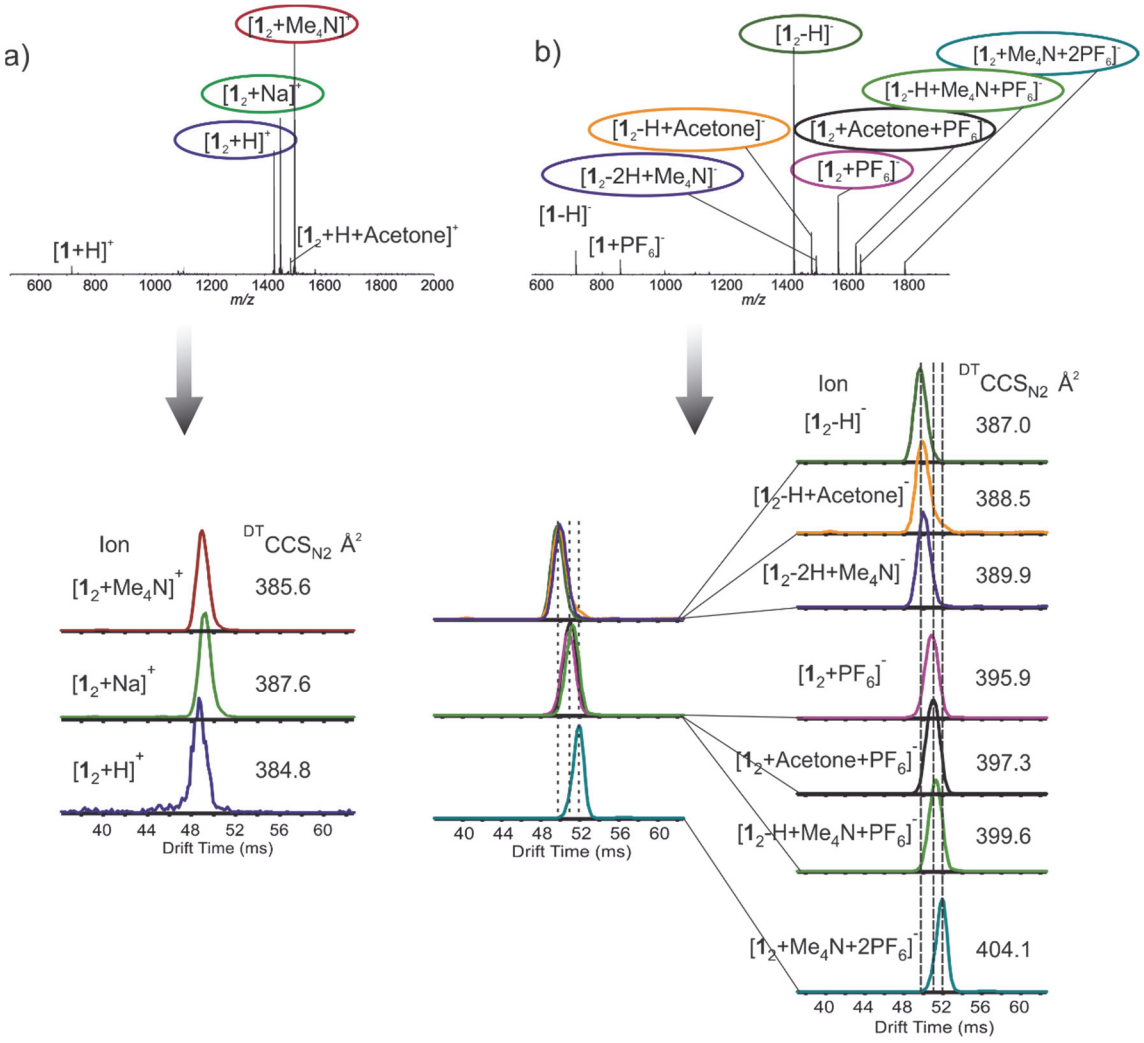

FIGURE 22. ESI-MS profile spectrum of **1**+TMAPF$_6$ and arrival time distributions of selected ions in a) (+) and b) (–) mode. In a) all the ions have roughly the same CCS and thus show that Me_4N^+ is located inside the dimeric capsule. In b) ions with *endo*-complexed guest (acetone or Me_4N^+) show the same drift times. In *exo*-complexation of PF_6^- anion longer drift times are observed.

Again, the difference between *endo*- and *exo*-located guests was clear when PF_6^- was used as a counter anion. However, with BF_4^- and I^- the difference was not that clear, as seen from CCS values in appendix table A3. Therefore, infrared multiphoton dissociation (IRMPD) was utilized to study the structures of the ternary ions. In these experiments [**1**$_2$+Me$_4$N+2A]$^-$ ions were isolated and irradiated with a CO_2 laser. At short irradiation times the main dissociation product was [**1**-2H+Me$_4$N]$^-$, which can only be produced after two eliminations of HA and cleavage of the hydrogen bonded capsule (pathway 1 in scheme 3). This type of fragmentation would be unlikely in *exo*-complexation of the cation. Also, minor fragmentation resulting in [**1**$_2$+PF$_6$]$^-$ was observed. This can occur from relocation of the anion close to the hydrogen-bonded seam during irradiation (pathway 2 in scheme 3), which results in release of an ion pair. In IM-MS experiments only one drift peak was observed for ternary complexes, which denotes that pathway 3

was not observed. As all studied ternary complexes showed similar fragmentation pathways in the experiments, it can be stated that all anions are located in the *exo*-position while the Me_4N^+ cation is bound inside the dimeric capsule.

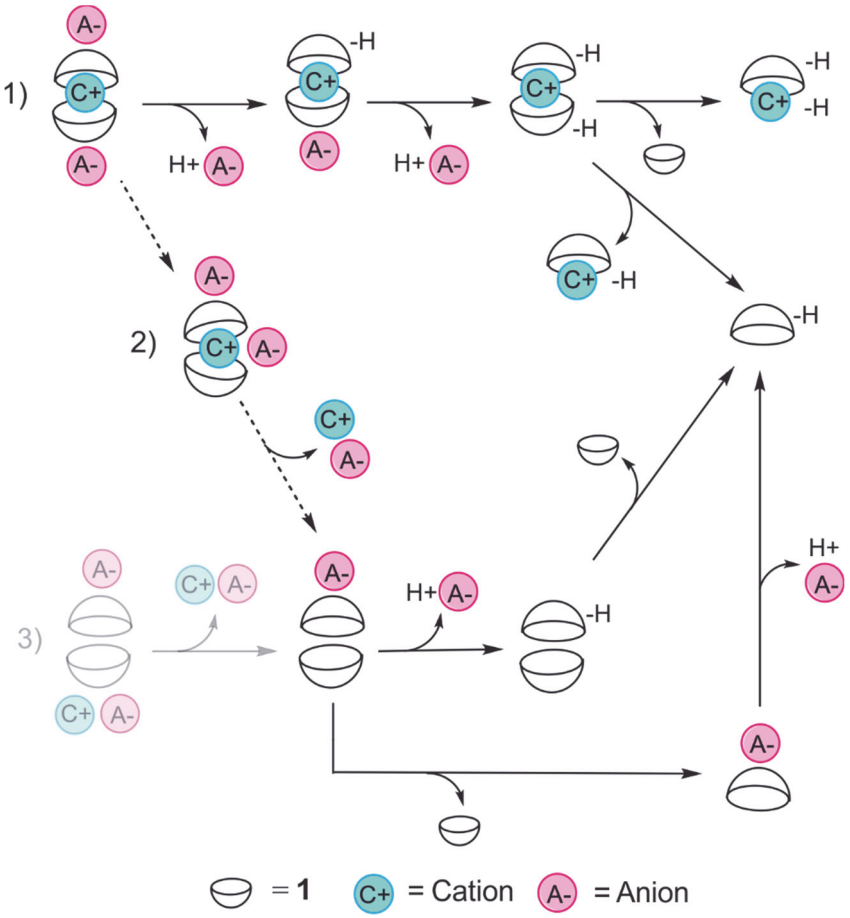

SCHEME 3. Schematic presentation of the observed fragmentation pathways in IRMPD experiments. Pathway 1) was observed as the main route.

Attempts to study the complexation of **1** with cationic guests in solution and in solid state were unsuccessful. Therefore a control experiment with isobutyl resorcinarene **4** (in figure 23) was performed. The ^1H NMR spectra in figure 23 shows a significant (0.35 ppm) upfield shift of the Me_4N^+ cation when it is bound to resorcinarene **4**. A similar experiment with **1** does not show any shift in the NMR spectrum of Me_4N^+. This shows that resorcinarene has a higher affinity towards Me_4N^+ cation, while the binding of cation to **1** is weak and could not be observed in solution. The detection of cation complexation to pyridinearene might also require special conditions present in the ESI source.

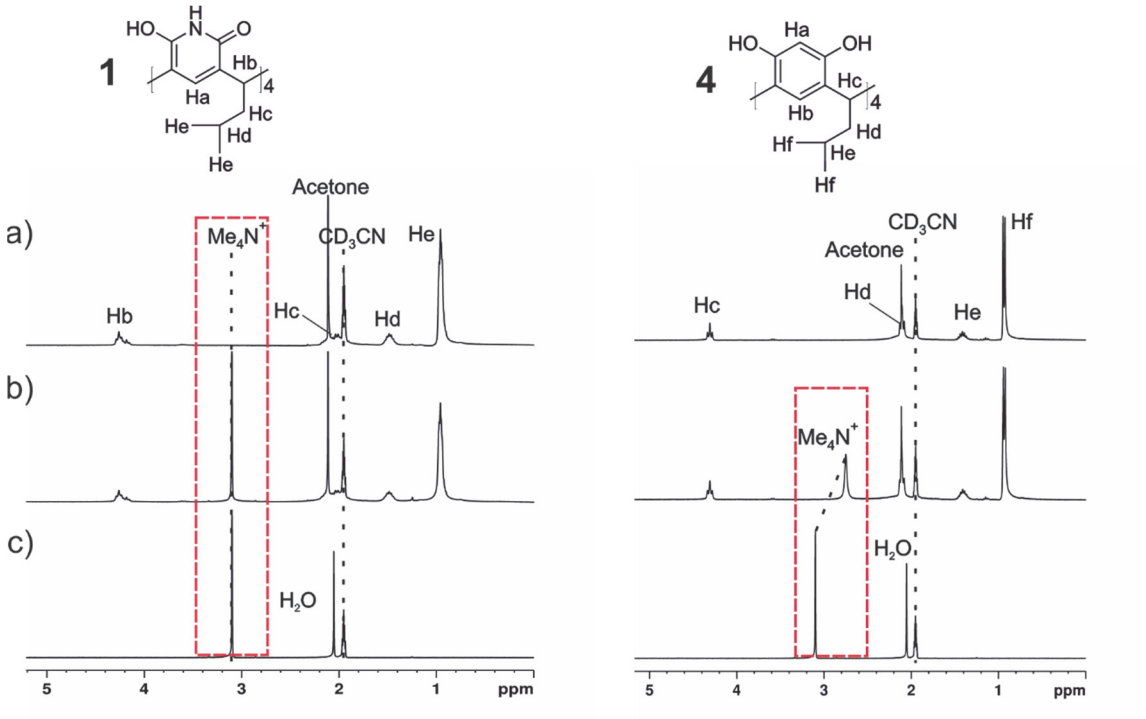

FIGURE 23. ^{1}H NMR spectra of a) host, b) host + $TMAPF_6$ and c) $TMAPF_6$. Left: spectra obtained with pyridinearene **1**, and right: spectra with resorcinearene **4**.

A mixed host experiment with pyridinearene **1**, resorcinarene **4** and $TMAPF_6$ was performed by ESI-MS to roughly compare the binding properties of the hosts. As seen from figure 24, complex formation with the cationic guest was almost exclusively observed with **4**, supporting the results from solution that **4** has higher affinity towards cations than **1**. In contrast, a ternary complex with solvent and anion was observed only with **1** in figure 24b, but not with resorcinarene. This clearly indicates that the formation of this type of ternary complexes is a feature of pyridinearene **1**, not resorcinarenes. Interestingly, the formation of heterodimers which have not been detected earlier was observed. [66] As noted earlier, the anion has a clear effect on the formation of cation complexes with pyridinearene. Therefore it is likely that the cation complexation process of pyridinearene is anion-driven.

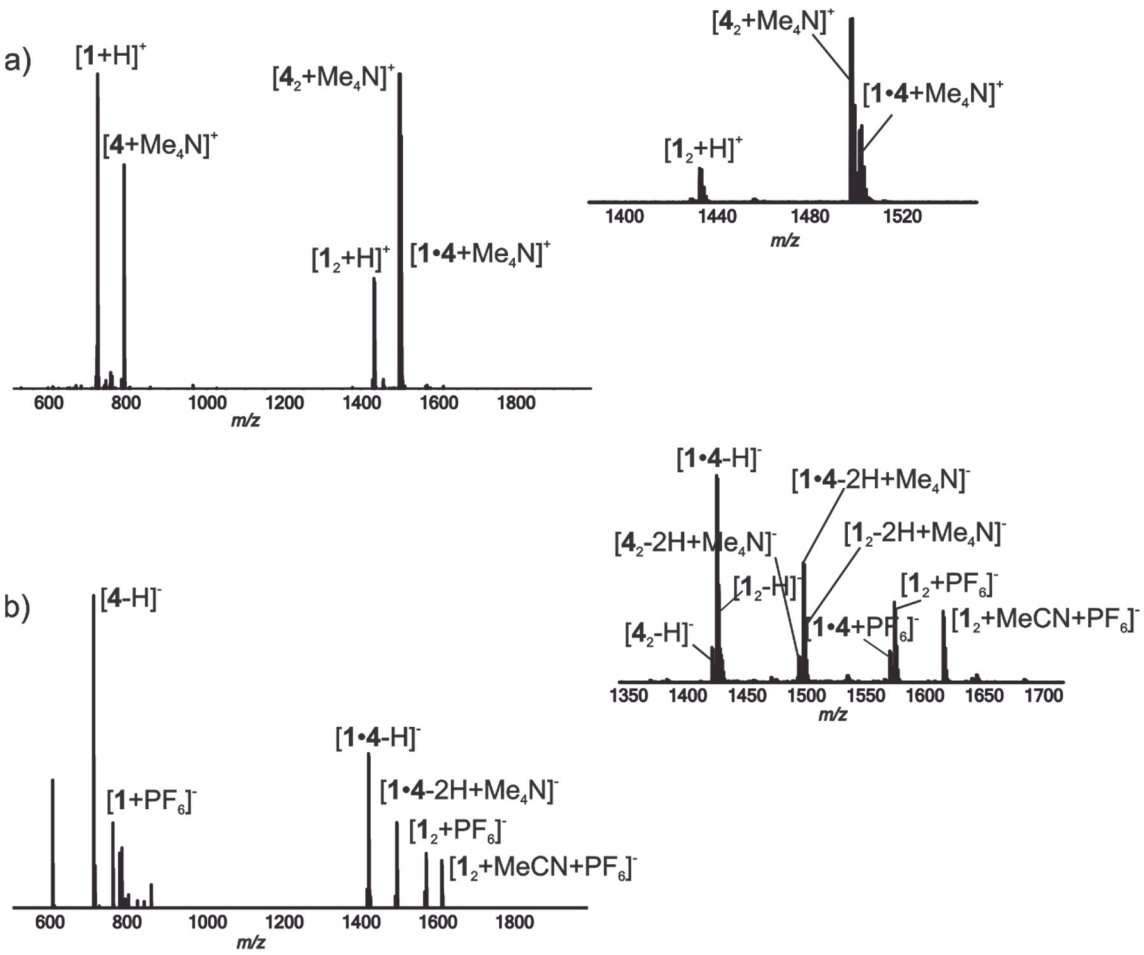

FIGURE 24. a) (+) and b) (—) ESI-MS spectra from a mixed-host experiment of **1**,**4** and $TMAPF_6$ (1:1:1 in MeCN). The cation complexes are almost exclusively observed with resorcinarene **4**. Insets show a zoom in from dimeric ions.

3.2.3 Self-assembly of pyridine[4]arenes [III]

The earlier chapters have already demonstrated that pyridinearene forms dimeric assemblies in gas phase, solution and in solid state. The self-assembly of pyridine[4]arene was chosen as one objective of this work, as only one report exists on the formation of hexameric pyridinearene capsules in solution.[66]

In (+) and (–)ESI-MS profile spectra monomer and dimeric species are generally observed as protonated/deprotonated ions and/or sodium adducts. Depending on the solvent used for sample preparation, solvent complexes are also present on both polarities as $[\mathbf{1}_2+H+S]^+$ or $[\mathbf{1}_2-H+S]^-$ ions, but usually more abundant in (–)ESI-MS. **1** ionizes more efficiently as a negatively charged ion, but in (–)ESI-MS no traces of hexamer could be observed. In (+)ESI-MS however, a peak corresponding to $[\mathbf{1}_6+Na]^+$ was observed with relatively high intensity. The aggregation is usually observed with regularity, and the lack of other species indicates that the observed hexamer could be a capsular assembly rather than a non-

specific aggregated system. In order to study the gas phase structure more closely, a cationic guest was utilized to see if it could template the formation of a hexameric assembly.

Cationic transition metal complexes have been previously used to stabilize similar hexameric complexes of resorcinarenes and pyrogallarenes in gas phase and in solution.[56,130] The cationic tris(bipyridine)ruthenium(II) (see figure 25 for structure, later referred to as **G** in the text) is complementary to the interior of their hexameric capsules and it can therefore act as a template to increase the formation of hexameric assemblies. The same cationic guest, **G**, was utilized with **1**, as the interior of formed capsules should be comparable to the size of similar capsules of resorcinarenes and pyrogallarenes. When a sample containing 60 μM **1** with 6:1 ratio of **G** was sprayed from acetone/DCM (1:1 v/v mixture), a peak corresponding to $[\mathbf{1}_6+\mathbf{G}]^{2+}$ was observed in the spectrum (Fig 24). No larger aggregates such as heptamers or octamers could be identified from the spectrum. A less intense ion $[\mathbf{1}_5+\mathbf{G}]^{2+}$ which most probably originated from dissociation of the hexamer was observed.

IM-MS experiments were further utilized to study the structure of the observed hexamer. DT-IMMS experiments showed a single well-resolved peak for $[\mathbf{1}_6+\mathbf{G}]^{2+}$ ion. When helium was used as a drift gas, a $^{DT}CCS_{He}$ value of 746.4 Å^2 was obtained. This roughly corresponds to a diameter of 3.1 nm, if the structure is assumed spherical. A calculated $^{DTM}CCS_{He}$ value of 748.2 Å^2 is well in accordance with the experimentally obtained value[99,101]. A DT-IMMS experiment in nitrogen resulted in a $^{DT}CCS_{N2}$ value of 838.7 Å^2. Theoretical $^{DTM}CCS_{N2}$ value of 928.3 Å^2 indicates slightly larger difference for experimental and theoretical value in nitrogen. Yet it is known that CCS values are typically larger when measured in nitrogen, as nitrogen is polarizable and can interact with the analyte.[97] Interactions in a theoretical model are more challenging to represent between an ion and nitrogen gas, when compared to interactions between an ion and helium. Nitrogen is a diatomic gas and causes stronger ion-dipole interactions. With multiply charged ions nitrogen also interacts stronger.[131,132] Therefore the parametrization in calculations of theoretical CCS values can result to larger errors in nitrogen.

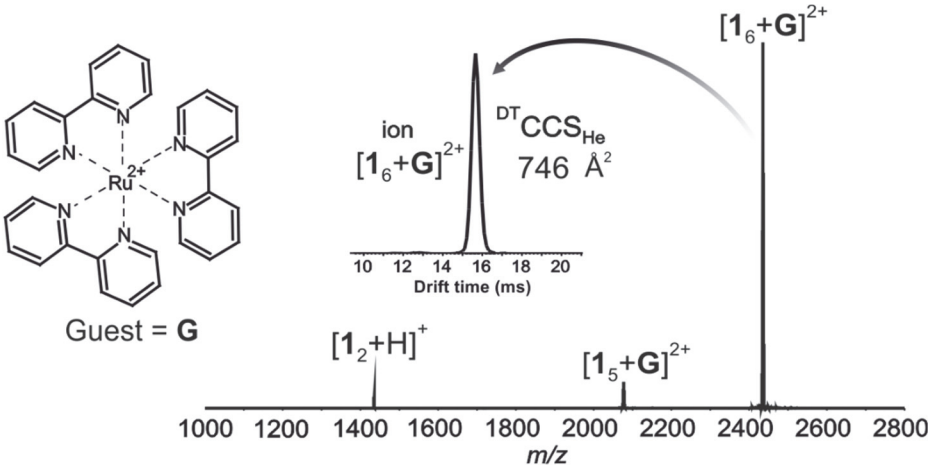

FIGURE 25. (+)ESI-MS spectrum of **1** + tris(bipyridine)ruthenium(II) **G**. Insets show the structure of **G** and the arrival time distribution for $[\mathbf{1}_6+\mathbf{G}]^{2+}$ ion.

Avram and Cohen have shown that pyridinearene **3** forms dimeric and hexameric aggregates in chloroform solution.[66] Also **1** shows two different species in ^{1}H NMR spectrum. In DOSY experiment these species had diffusion coefficients comparable to the earlier results of Cohen, and confirmed that the signals result from dimer and hexamer. In a fresh sample (figure 26a) the dimer was more abundant and the ratio between these species was 2:1 (dimer:hexamer). When the same sample was stored in the fridge and measured again after 7 days, the only signal in the spectrum was from hexamer, as proved by ^{1}H and DOSY NMR (figure 26b). Therefore it can be stated that dimer is a kinetic product while thermodynamics favours the formation of hexamer over time.

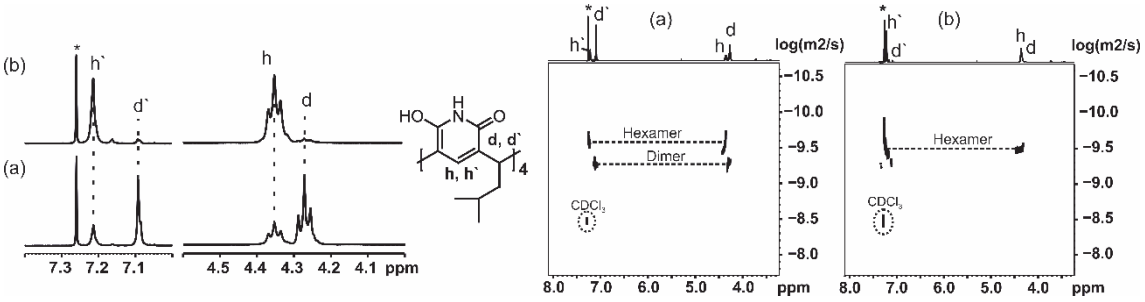

FIGURE 26. Left: ^{1}H NMR spectrum of 20 mM **1** a) within 2 hours from sample preparation and b) after 7 days from sample preparation. Right: DOSY NMR of the same sample within the same time interval. ^{1}H NMR and DOSY both show that in a) the dimeric aggregate is more abundant and in b) only the hexamer is observed.

The crystal structures of dimeric capsule $\mathbf{1}_2$ with different *endo*- and *exo*-guests have been presented in previous chapters. The $\mathbf{1}_6$ structure was obtained from slow diffusion of diisopropylether to the solution of **1** in $CHCl_3$. The X-ray structure (figure 27a) shows a hexameric assembly directly hydrogen-bonded without any incorporated solvent molecules to the hydrogen bonding network. Crystals from $\mathbf{1}_6$+**G** were not obtained due to different solubilities of **1** and **G**. Therefore DFT calculations were utilized to obtain more insight into the structure

of $[\mathbf{1}_6+\mathbf{G}]^{2+}$ (figure 27b). Optimized structures were calculated for $\mathbf{1}_2$, $\mathbf{1}_6$ and $[\mathbf{1}_6+\mathbf{G}]^{2+}$. The interaction energies suggest $[\mathbf{1}_6+\mathbf{G}]^{2+}$ to be more favourable compared to empty hexamer of $\mathbf{1}_6$ and underline the template effect in the formation of the hexameric capsule. Both complexes $\mathbf{1}_6$ and $[\mathbf{1}_6+\mathbf{G}]^{2+}$ have higher interaction energies compared to the formation of three individual dimers. This supports the results obtained by NMR that hexamer is favoured by thermodynamics while dimer is a kinetic product.

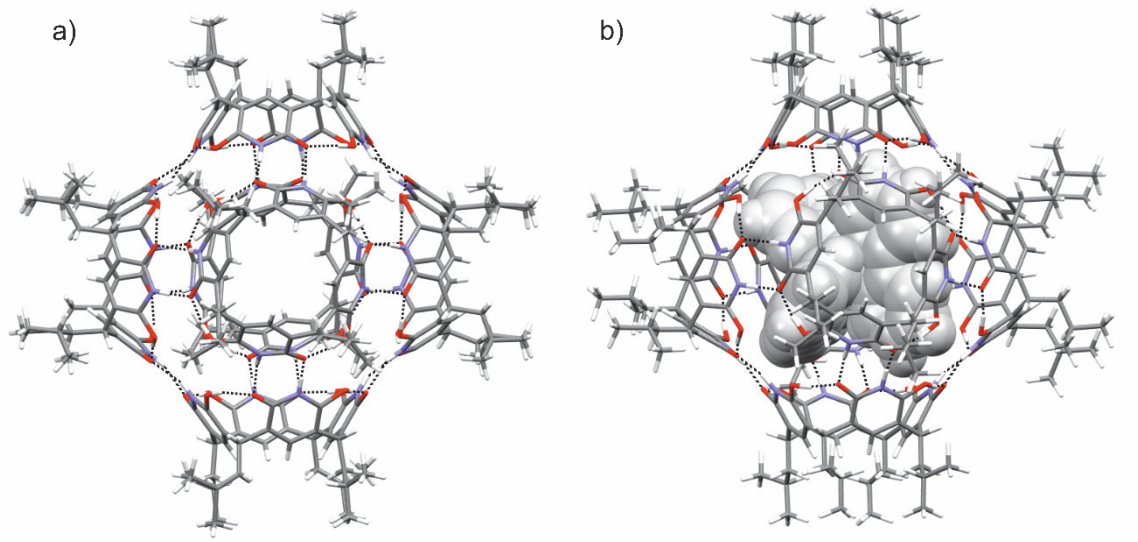

FIGURE 27. a) X-ray crystal structure of $\mathbf{1}_6$, and b) optimized structure of $[\mathbf{1}_6+\mathbf{G}]^{2+}$, guest shown in grey space fill model. Black dashed lines represent hydrogen bonds.

To compare all the structural methods, the diameters of the complexes were calculated assuming CCS to originate from spherical structure. The diameters can be roughly compared to results derived from DOSY and X-ray, as presented in table 1. The obtained results are well in line, and support the structural similarity of the species. The diameters calculated on the basis of IM-MS measurements in nitrogen result to slightly larger diameters than in helium. As discussed earlier, the obtained CCS_{N2} values are typically larger compared to CCS_{He}, due to stronger interactions between the ion and nitrogen gas. The obtained results highlight the value of IM-MS as a structural chemistry analysation technique for supramolecular complexes.

TABLE 1. Comparison of diameters (in nm) for $\mathbf{1}_2$ and $\mathbf{1}_6$ obtained from IM-MS, DOSY NMR and X-ray diffraction.

	d (IM-MS) in N_2	*d* (IM-MS) in He	*d* DOSY	*d* X-ray
Dimer	2.2	2.0	2.0	1.9
Hexamer	3.3	3.1	2.8	2.8

3.3 Hemicucurbiturils [IV]

(*all-R*)-cyclohexanohemicucurbit[8]uril in figure 28 is a chiral macrocyclic host which synthesis is templated through an anion. A large, non-coordinating anion can increase the formation of cycHC[8], while smaller anions lead to the formation of cycHC[6].[77] As anions of suitable size are necessary for the synthesis, it is likely that the host is capable of binding such guests. The smaller cycHC[6] has already been studied for its properties to bind halides inside its cavity.[79]

The anion-binding properties of cycHC[8] were screened by ESI-MS. Indeed, the formation of 1:1 complexes of host with different anions could be detected. From the most abundant complexes, the order in affinity was determined in competition experiments as follows: SbF_6^- ≈ PF_6^- >ReO_4^- > ClO_4^- > SCN^- > BF_4^- > HSO_4^- > $CF_3SO_3^-$. Other studied anions, $H_2PO_4^-$, AcO^-, F^-, Cl^-, Br^-, I^-, NO_3^- and NO_2^-, showed less abundant complexation with the host, while $AuBr_4^-$, Br_3^- and CN^- did not show any complexation.

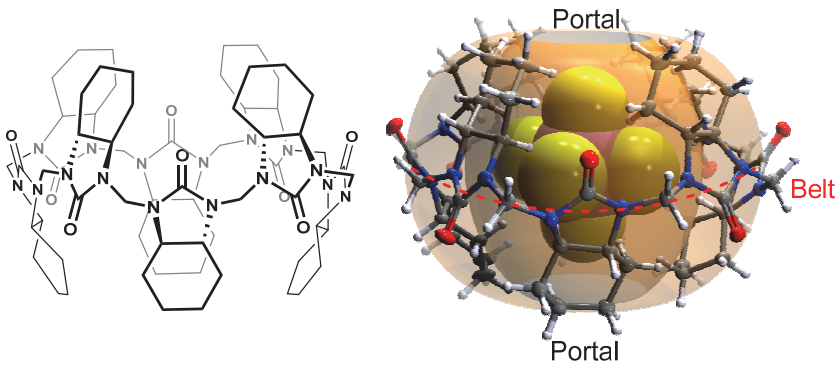

FIGURE 28. Structure of (*all-R*)cyclohexanohemicucurbit[8]uril cycHC[8] and its X-ray structure of a complex with SbF_6^- anion.

Halides, that have been observed to bind to cycHC[6] showed only weak binding to cycHC[8]. Also, the strongly solvated anions showed weak complexation with the host, while complexes with weakly solvated anions were abundant. In CID experiments the highest kinetic stability was observed for the smallest anions, whereas the complexes with larger anions were less stable. This can be seen to result from to size-fit, as smaller guests have more space to vibrate inside the cavity when they are kinetically activated. Guests with better size-fit, on the other hand, are popped out from the cavity with lower collision energy.[113]

The complexation in solution was studied in methanol-D_4 in NMR titrations and stoichiometry was analysed by Job´s plot method. Job´s method indicated 1:1 binding, which also could be observed in gas phase and later in single crystal structures. In titration experiments the strongest binding was observed with SbF_6^- anion, with K_a up to 250 000 M^{-1}. Strong binding was also observed with PF_6^- anion. Noteworthy, the binding strength of PF_6^- did not change even when the media was changed to 1:1 D_2O/MeOD environment. The K_a values are presented in table 2, with a comparison of packing coefficients.

TABLE 2. Association constants (K_a) for cycHC[8] complexes with anions. ^{1}H NMR titration experiments were performed in MeOD at 288K. Volumes of the anions and packing coefficients are shown for comparison.

Anion	Cation	V_{anion} (Å^3)	PC [a]	K_a (M^{-1})
SbF_6^-	Na^+	81.8	0.67	$(2.5 \pm 0.7) \times 10^5$
PF_6^-	TBA^+	70.6	0.57	$(2.8 \pm 0.4) \times 10^4$
PF_6^-	TBA^+	70.6	0.57	$(2.6 \pm 0.2) \times 10^4$ [b]
PF_6^-	Na^+	70.6	0.57	$(2.0 \pm 0.2) \times 10^4$
ReO_4^-	TBA^+	64.8	0.53	$(4.7 \pm 0.4) \times 10^3$
IO_4^-	Na+	64.3	0.52	$(1.8 \pm 0.2) \times 10^3$
ClO_4^-	TBA^+	54.7	0.45	$(4.7 \pm 0.2) \times 10^2$
BF_4^-	TBA^+	51.6	0.42	$(4.8 \pm 0.4) \times 10^1$
$CF_3SO_3^-$	TBA^+	82.3	0.67	$(3.9 \pm 0.5) \times 10^1$
$CF_3CO_2^-$	TBA^+	68.7	0.56	< 10

[a] PC refers to packing coefficient defined by Mecozzi and Rebek as the ratio between V_{anion} and V_{cavity}. [133] V_{anion} was determined from calculated structure and V_{cavity} from single crystal structure. [b] experiment was performed in 1:1 D_2O/MeOD.

The optimal values for packing coefficients usually follow the trend of 0.55 ± 0.09 occupancy of the cavity, as determined by Mecozzi and Rebek for the optimal guest size in solution.[133] Therefore, for the cycHC[8] cavity with volume of 123 Å^3, the optimal guests should appear in a statistical distribution around 0.68 Å^3 anion size, ranging from 57 Å^3 to 79 Å^3. However, PF_6^- anion with an optimal size, binds weaker to cycHC[8] than SbF_6^- anion that is already larger than the optimal range (PC 0.67). $CF_3SO_3^-$ anion has a similar size as SbF_6^- and roughly octahedral structure, but still it binds to host with a drastically lower affinity. This suggests that binding of cycHC[8] is also sensitive to charge distribution, not only to anion size. As a control experiment to prove this, a titration was performed with $CF_3CO_2^-$ anion that has a similar volume to PF_6^- but its charge distribution resembles the structure in $CF_3SO_3^-$. $CF_3CO_2^-$ anion can also be utilized as template to synthesize cycHC[8] host and therefore it should be optimal in size to the interior of cycHC[8]. Nevertheless, in its titration experiment in methanol no binding was observed, which also states that the charge distribution matters in binding to cycHC[8] host.

Single-crystal X-ray structures (like the one in figure 28) show that the anions are located in the middle of the cycHC[8] cavity. The orientation of the guest is strongly dependent on its size and shape. Octahedral anions SbF_6^- and PF_6^- are in fixed position and show no disorder. Tetrahedral anions BF_4^-, ClO_4^-, ReO_4^- and IO_4^- show some disorder in the structures, as these anions have more space inside the cavity. Hirschfeld surfaces[134] also suggest that smaller guests are unable to form as many interactions with the host as larger octahedral guests.

Thermodynamic parameters of the binding were determined in isothermal titration calorimetry (ITC) experiments that showed similar magnitude for binding of SbF_6^- and PF_6^- as determined in NMR titrations. Also in line, ITC showed higher affinity for cycHC[8] to bind SbF_6^- rather than PF_6^- anion. The binding of both anions was observed to be exothermal, enthalpy favoured and entropically

disfavoured. The binding of larger sized guest causes stronger host-guest interactions and is therefore favoured by enthalpy, but causes a loss in freedom and is therefore disfavoured by entropy.

All in all, the anion complexation properties of cycHC[8]host was studied in gas phase, solution and in solid state. CycHC[8] host shows almost selective binding of SbF_6^- anion over the others. Various experiments show that there is a strong dependence on the size, shape and charge distribution of the guest in binding to cycHC[8].

3.4 Crown ether-urea receptors [V]

The binding of an ion pair can significantly enhance the efficient complexation of ionic guest when the ions do not need to be separated.[135] In ion pair binding usually positive cooperativity plays its role, as binding of the first guest (usually the cation) enhances the binding of the second guest.[136,137]

The binding of an ion pair was studied with two different crown ether-urea receptors **R¹** and **R²** presented in scheme 4. Crown ethers have been utilized in vast amount of work since their discovery,[138] as crown ethers exhibit high affinity towards alkali metal cations.[82,139] The urea functional group has also been utilized in several anion receptors.[24,140,141] In this work, four urea groups have been attached to the cation binding dibenzocrown-7 (**R¹**) and dibenzocrown-8 (**R²**) macrocycles. 4-nitrophenyl groups were also attached to the heads of the urea-sidearms to increase the electron withdrawing nature of urea.[142] The crown ether macrocycle is flexible and can adopt different conformations to assist in conformational changes, which could influence on the binding, while bringing urea groups closer to each other in space.

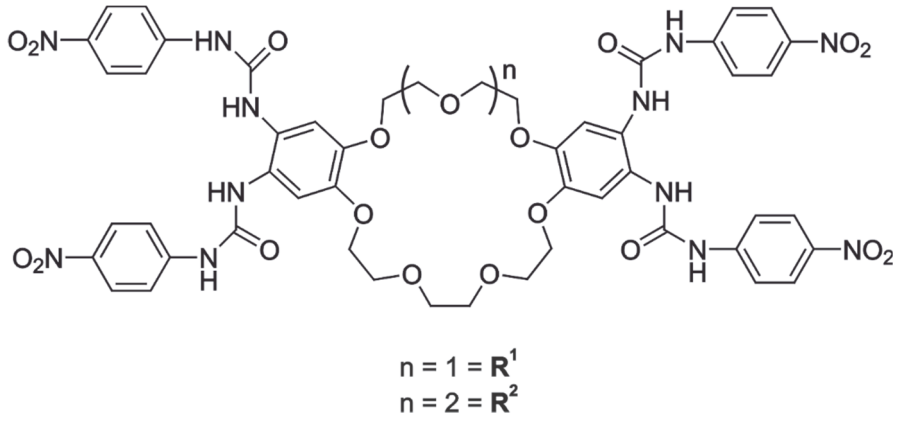

SCHEME 4. Structures of crown ether-urea receptors **R¹** and **R²**.

The ion pair binding behaviour of receptors **R¹** and **R²** was studied with RbCl, RbBr, RbI, CsCl, CsBr and CsI. Rubidium and cesium have the appropriate size fit to crown-7 and crown-8 macrocycles.[9,143] Also, urea has been demonstrated in earlier studies to have high affinity towards halides.[22,144,145] In (+)ESI-

MS mainly 1:1 cation complexes were observed with the host as [**R**+Rb]$^+$ or [**R**+Cs]$^+$, depending on the cation that was used in the experiment. In (–)ESI-MS ion pair complexes were clearly observable as [**R**+C+2A]$^-$ complexes (**R**=**R¹** or **R²**, C=cation and A=anion). In addition, [**R**+2A]$^{2-}$ complexes were abundant in the spectrum. The binding behaviour seemed to be similar with both receptors, and only the abundance of detected ion pair complex varied according to the basicity of the anion in line with Hofmeister series.[146] Both receptors showed similar affinity towards anions in competition experiments with decreasing order $Cl^- > Br^- > I^-$. Comparing the affinity of receptors towards cations, some differences could be revealed. **R¹** had clearly higher affinity towards rubidium cation. With **R²** the difference was not that clear as it showed only slight favour of the binding of cesium over rubidium. In a competition experiment between receptors it was clear that **R²** possesses higher affinity towards both RbCl and CsCl compared to **R¹**.

The gas phase structures and kinetic stabilities were further studied in CID experiments, where the ion pair complex [**R**+C+2A]$^-$ was isolated. The first dissociation step showed the elimination of an ion pair and [**R**+A]$^-$ was observed in the spectrum as a dissociation product. On the next step, the elimination of HA was observed, resulting in [**R**-H]$^-$ ion in the spectrum. The first elimination indicates that one anion is bound to the receptor as a contact ion pair rather than being hydrogen bonded. The next elimination indicates that the second anion is hydrogen bonded to the receptor, most likely to its urea moieties. Both receptors showed same kind of behaviour in dissociation. When comparing the dissociation curves in figure 29, it can be noted that both receptors form most stable complexes with RbCl and **R²** forms more stable complexes than **R¹**. However, the differences between anions were negligible.

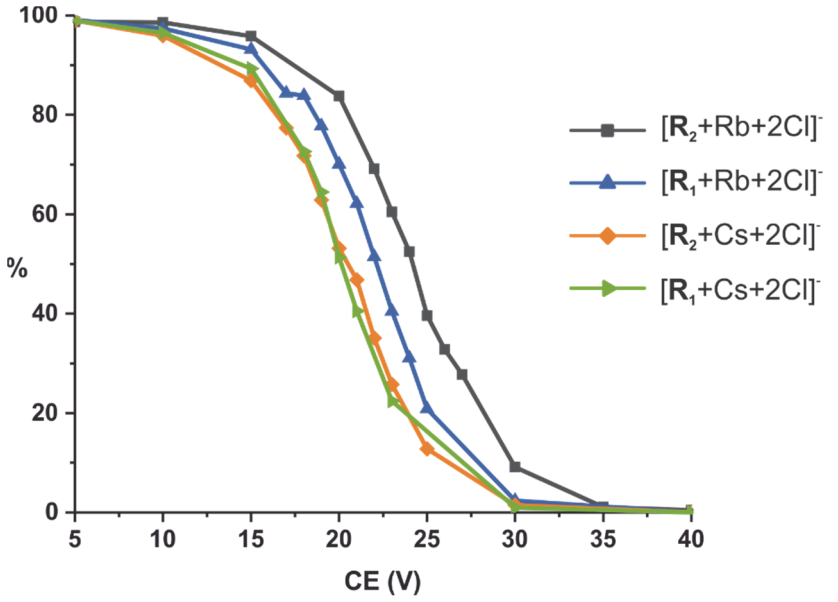

FIGURE 29. Dissociation curves for **R¹** and **R²** with RbCl and CsCl. Both receptors form more stable complexes with RbCl, and **R²** forms more stable complexes than **R¹**.

The binding behaviour of **R1** and **R2** and their Rb^+ and Cs^+ complexes was studied in a 4:1 $CDCl_3$/DMSO solution with special interest in determining the stoichiometry and strength of the binding. Job´s plot analysis has often been utilized for determination of stoichiometry, but critical evaluations of its usability have been published.[121] Therefore, more value was given to the fit of the experimental data to calculated binding constants, while Job´s plot data were seen as approximations. In titration experiments TBA-halides were used to provide the anion and alkali metals were provided as tetraphenyl borates (BPh_4). The non-interacting nature of the chosen counter ions has been demonstrated earlier with similar receptor systems.[125]

The observed chemical shifts could be followed from three different protons. When testing only the anion binding behaviour of the receptors, the largest differences in chemical shifts were observed upon addition of Cl^- anion. **R1** showed slightly higher binding of Cl^- and Br^- anions but the differences were modest. Also, the binding strengths follow the basicity of the anion. Next, the cooperative effect of the bound Rb^+ or Cs^+ cation on anion complexation properties of receptors was studied. A dramatic increase in binding was observed with all anions. Especially the binding of chloride is significantly magnified when cation is involved to the complexation in both receptors. The bound Rb^+ enhances the binding of chloride more than the bound Cs^+. This behaviour was observed with both receptors, and is perhaps surprising in the case of **R2** with a larger crown ether moiety. Yet, the larger size of cesium cation causes lower charge density and polarizability, which could explain the weaker electrostatic interaction observed between bound cation and anion. This same phenomenon was observed with all studied anions. More importantly, the binding constants show that the cation complex of **R2** has a higher affinity towards all anions. The enhancement in anion binding when the cation is bound to the receptor demonstrates well that both receptors function in a strongly cooperative manner.

Several X-ray structures were attained with **R2** and ion pairs, but only one with **R1**. All structures show that the symmetricity of the crown-8 moiety in **R2** allows it to assume a folded conformation (figure 30b). On the contrary, **R1** lacks the symmetry and has an open non-folded conformation in the solid state (figure 30a). The difference in the solid state can explain the observed results from solution and gas phase: the folded structure of **R2** is more efficient in binding.

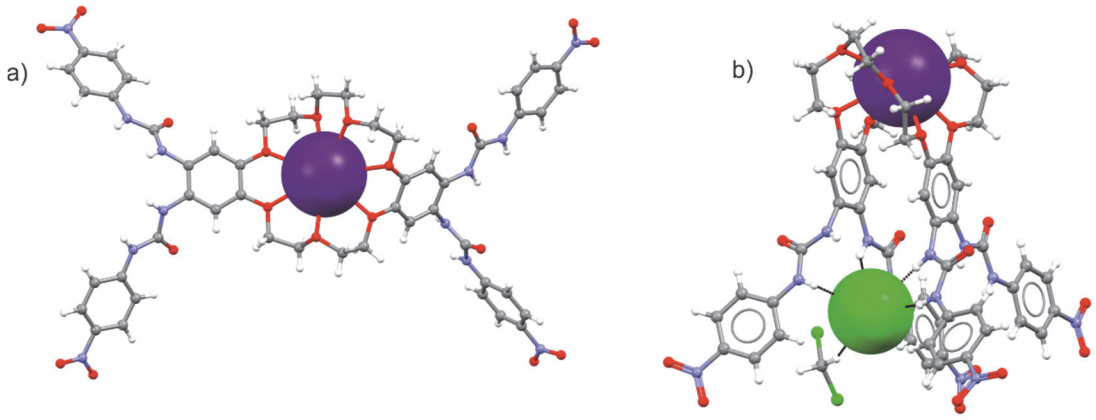

FIGURE 30. Single crystal X-ray structures of **R¹** + Rb and b) **R²**+RbCl. **R¹** has an open conformation, whereas **R²** can fold itself around the guests to maximize the interactions. The counter anion in **R¹** + Rb is CO_3^{2-}, which has been omitted for clarity. CO_3^{2-} is hydrogen bonded to urea units of two **R¹** molecules, both receptors binding one rubidium cation. Rb^+ is shown in purple space fill model and Cl^- in green, also in space fill model.

CONCLUSIONS

Before this study it was commonly thought that pyridinearenes could bind anionic guests inside their cavities, based on the studies performed by Mattay´s group.[64,65] It is now clear that the binding properties of pyridinearene are completely different, even reverse to the early assumptions as demonstrated by the encapsulation of cationic guests.[II, III] However, the pyridinearene does not seem to be very efficient cation receptor either when compared to resorcinarenes. Pyridinearene has affinity towards anions, but instead of *endo*-complexation the binding of anions takes place to their *exo*-positions.[I] Presumably, pyridinearenes possesses the highest affinity towards neutral guests, which were shown to be encapsulated to the dimer in several X-ray structures and also for the first time in gas phase structures.[I,126] The DFT calculations also support that the cavity of pyridinearene is most suited to bind neutral guests.[I]

In addition to the binding properties of pyridinearenes, new information on their self-assembly was attained. Even if it could be thought that the larger assemblies are not as easily formed as smaller ones, thermodynamics favour the formation of hexameric pyridinearene capsules over dimeric ones. The hexameric assembly of pyridinearene was also detected for the first time in gas phase and in solid state. The X-ray structures illustrated that both dimeric and hexameric capsules of pyridinearene are directly hydrogen-bonded between the subunits, without any bridging solvent molecules which are usually present in similar structures of resorcinarenes. [III]

From all the studied receptors, cycHC[8] was demonstrated to be the most promising as an anion receptor, with especially high binding shown for environmental pollutant SbF_6^-. The CycHC[8] host also showed a clear discrimination between the studied guests, as the binding was dependent on shape, size and charge distribution.[IV] A different approach to anion-binding was demonstrated by crown ether urea receptors, which are not very efficient anion receptors as their selves. However, when a cation was added as a part of the host macrocycle, a dramatic increase was observed in their anion-binding affinity. This shows that the crown ether urea receptors function in a highly cooperative manner, and they are more suited to bind a whole ion pair, not just separated ions.[V]

To conclude, this thesis describes the supramolecular chemistry and anion-binding properties of different host molecules. Especially the self-assembly of pyridinearene and its ability to form different types of capsules was under investigation. The studies have been conducted, whenever possible, in gas phase, in solution and in solid state. Ion mobility mass spectrometry, a relatively new technique, was utilized to study the structural features of pyridinearene capsules in the gas phase. Ion mobility mass spectrometry proved to be a valuable tool in structural analysis of the studied supramolecular complexes, and well comparable with other structural chemistry methods.

REFERENCES

1. J.-M Lehn, *Angew. Chem. Int. Ed. Engl.* **1988**, *27*, 89–112.
2. D. J. Cram, *Angew. Chem. Int. Ed. Engl.* **1988**, *27*, 1009–1020.
3. E. Fischer, *Berichte der Dtsch. Chem. Gesellschaft* **1894**, *27*, 2985–2993.
4. F. W. Lichtenthaler, *Angew. Chem. Int. Ed. Engl.* **1995**, *33,* 2364–2374.
5. B. L. Feringa, *Angew. Chem. Int. Ed.* **2017**, *56*, 11060–11078.
6. J. F. Sir Stoddart, *Angew. Chem. Int. Ed. Engl.* **2017**, *56,* 11094–11125.
7. C. A. Hunter & H. L. Anderson, *Angew. Chem. Int. Ed.* **2009,** *48*, 7488–7499.
8. J. D. Badjić, A. Nelson, S. J. Cantrill, W. B. Turnbull, & J. F Stoddart, *Acc. Chem. Res.* **2005**, *38,* 723–732.
9. J. W. Steed & J. L. Atwood, *Supramolecular chemistry*, 2nd ed., Wiley, Chichester, UK, **2009.**
10. G. R. Desiraju, P. S. Ho, L. Kloo, A. C. Legon, R. Marquardt, P. Metrangolo, P. Politzer, G. Resnati & K. Rissanen. *Pure Appl. Chem.* **2013**, *85,* 1711–1713.
11. P. Metrangolo, F. Meyer, T. Pilati, & G. Resnati, *Angew. Chem. Int. Ed.* **2008**, *47,* 6114–6127.
12. D. A. Dougherty, *Science* **1996**, *271*, 163–169.
13. D. Quiñonero, C. Garau, C. Rotger, A. Frontera, P. Ballester, A. Costa & P. M. Deyà, *Angew. Chem. Int. Ed.* **2002,** *41,* 3389–3392.
14. M. Göth, F. Witte, M. Quennet, P. Jungk, G. Podolan, D. Lentz, W. Hoffmann, K. Pagel, H. U. Reissig, B. Paulus & C. A. Schalley, *Chem. Eur. J.* **2018,** *24,* 12879–12889.
15. M. Nishio, *Phys. Chem. Chem. Phys*. **2011**, *13,* 13873–13900.
16. A. Marmur, *J. Am. Chem. Soc.* **2000**, *122,* 2120–2121.
17. J. W. Steed, D. R.Turner, & K. J. Wallace, *Core Concepts in Supramolecular Chemistry and Nanochemistry*, 1st Ed., John Wiley and Sons, Ltd, **2007**.
18. D. E. Koshland, *Angew. Chem. Int. Ed.* **1994**, *33,* 2375–2378.
19. D. B. Smithrud, E. M. Sanford, I. Chao, S. B. Ferguson, D. R. Carganague, J. D. Evanseck, K. N. Houk & F. Diederich, *Pure Appl. Chem.* **1990,** *62,* 2227–2236.
20. J. Murray, K. Kim, T. Ogoshi, W. Yao, & B. C. Gibb, *Chem. Soc. Rev.* **2017,** *46,* 2479–2496.
21. R. G., Pearson, *J. Am. Chem. Soc.* **1963,** *85,* 3533–3539.
22. J. L. Sessler, P. A. Gale & W.-S. Cho, *Anion Receptor Chemistry*, Royal Society of Chemistry, Cambridge, UK, **2006.**
23. A. J. McConnell & P. D. Beer, *Angew. Chem. Int. Ed.* **2012**, *51,* 5052–5061.
24. R. Shukla, T. Kida, & B. D. Smith, *Supramol. Chem.* **2000,** *2*, 3099–3102.
25. L. Fabbrizzi, & A. Poggi, *Chem. Soc. Rev.* **1995,** *24,* 197–202.
26. G. M. Whitesides, & B. Grzybowski, *Science* **2002,** *295,* 2418–2421.
27. D. Philp, & J. F. Stoddart, *Angew. Chem. Int. Ed.* **1996**, *35*, 1154–1196.
28. D. A. Leigh, R. G. Pritchard, & A. J. Stephens, *Nat. Chem.* **2014,** *6,* 978–982.
29. B. Song, Z. Zhang, K. Wang, C. H. Hsu, O. Bolarinwa, J. Wang, Y. Li, G. Q. Yin, E. Riviera, H. B. Yang, C. Liu, B. Xu & X. Li., *Angew. Chem. Int. Ed.* **2017**, *56,* 5258–5262.

30. L. Turunen, U. Warzok, R. Puttreddy, N. K. Beyeh, C. A. Schalley & K. Rissanen, *Angew. Chem. Int. Ed.* **2016**, *55,* 14033–14036.
31. L. Turunen, U. Warzok, C. A. Schalley & K. Rissanen, *Chem* **2017,** *3,* 861–869.
32. P. Jacopozzi, & E. Dalcanale, *Angew. Chem. Int. Ed.* **1997,** *36,* 613–615.
33. R. Pinalli, V. Cristini, V. Sottili, S. Geremia, M. Campagnolo, A. Caneschi & E. Dalcanale, *J. Am. Chem. Soc.* **2004,** *126,* 6516–6517.
34. S. J. Dalgarno, N. P. Power, & J. L. Atwood, *Coord. Chem. Rev.* **2008,** *252,* 825–841.
35. D. Fujita, Y. Ueda, S. Sato, H. Yokoyama, N. Mizuno, T. Kumasaka & M. Fujita, *Chem* **2016,** *1*, 91–101
36. G. Markiewicz, A. Jenczak, M. Kołodziejski, J. J. Holstein, J. K. M. Sanders, & A. R. Stefankiewicz, *Nat. Commun.* **2017,** *8,* 6–13.
37. J. B. Niederl & H. J. Vogel, *J. Am. Chem. Soc.* **1940,** *62,* 2512–2514.
38. P. Timmerman, W. Verboom, & D. N. Reinhoudt, *Tetrahedron* **1996,** *52,* 2663–2704.
39. N. K. Beyeh & K. Rissanen, *Isr. J. Chem.* **2011,** *51,* 769–780.
40. D. J. Cram, S. Karbach, H. E. Kim, C. B. Knobler, E. F. Maverick, J. L. Ericson & R. C. Helgeson, *J. Am. Chem. Soc.* **1988,** *110,* 2229–2237.
41. S. Ma, D. M. Rudkevich & J. Rebek, *J. Am. Chem. Soc.* **1998,** *120,* 4977–4981.
42. J. R. Moran, J. L. Ericson, E. Dalcanale, J. A. Bryant, & C. B. Knobler, *J. Am. Chem. Soc.* **1991,** *113,* 5707–5714.
43. H. Erdtman & S. Högberg, *Tetrahedron Lett.* **1968,** 1679–1682.
44. S. Högberg, *J. Am. Chem. Soc.* **1980,** *102,* 6046–6050.
45. A. G. S. Högberg, *J. Org. Chem.* **1980,** *45,* 4498–4500.
46. J. L. Atwood & L. R. MacGillivray, *Nature* **1997,** *389,* 469–472.
47. T. Gerkensmeier, W. Iwanek, C. Agena, R. Fröchlich, S. Kotila, C. Näther & J. Mattay, *Eur. J. Org. Chem.* **1999,** 2257–2262.
48. K. Murayama, *Chem. Commun.* **1998,** 607–608.
49. L. Avram, & Y. Cohen, *Org. Lett.* **2002,** *4,* 4365–4368.
50. T. Lippmann, H. Wilde, A. Schayer, M. Hesse & G. Mann, *Angew. Chem. Int. Ed.* **1993,** *32,* 1991–1993.
51. H. Mansikkamäki, M. Nissinen, C. A. Schalley, & K. Rissanen, *New J. Chem.* **2003,** *27,* 88–97.
52. A. Åhman, M. Luostarinen, K. Rissanen & M. Nissinen, *New J. Chem.* **2007** *31,* 169–177.
53. L. Avram, & Y. Cohen, *J. Am. Chem. Soc.* **2002,** 124, 15148–15149.
54. H. Mansikkamäki, M. Nissinen, & K. Rissanen, *Chem. Commun.* **2002,** 1902–1903.
55. L. C. Palmer, A. Shivanyuk, M. Yamanaka, & J. Rebek, *Chem. Commun.* **2005,** *5,* 857–858.
56. N. K. Beyeh, M. Kogej, A. Åhman, K. Rissanen, & C. A. Schalley, *Angew. Chem. Int. Ed.* **2006,** *45,* 5214–5218.
57. R. M. Payne & C. L. Oliver, *CrystEngComm.* **2018,** *20,* 1919–1922.
58. Q. Zhang, L. Catti & K. Tiefenbacher, *Acc. Chem. Res.* **2018,** *51,* 2107–2114.

59. Q. Zhang & K. Tiefenbacher, *J. Am. Chem. Soc.* **2013**, *135,* 16213-16219.
60. C. H. Pollok, Q. Zhang, K. Tiefenbacher & C. Merten, *ChemPhysChem* **2017,** *18,* 1987–1991.
61. C. Gaeta, C. Talotta, M. De Rosa, P. La Manna, A. Soriente & P. Neri, *Chem. Eur. J.* **2019,** *25,* 4899–4913.
62. Q. Zhang, L. Catti, V. R. I. Kaila & K. Tiefenbacher, *Chem. Sci.* **2017,** *8,* 1653–1657.
63. T. Gerkensmeier, J. Mattay & C. Näther, *Chem. Eur. J.* **2001**, 7 (2), 465–474.
64. M. C. Letzel, B. Decker, A. B. Rozhenko, W. W. Schoeller & J. Mattay, *J. Am. Chem. Soc.* **2004,** *126,* 9669–9674.
65. A. B. Rozhenko, W. W. Schoeller, M. C. Letzel, B. Decker & J. Mattay, *New J. Chem.* **2013,** *37,* 356–365.
66. T. Evan-Salem & Y. Cohen, *Chem. Eur. J.* **2007,** *13,* 7659–7663.
67. B. L. Schottel, H. T. Chifotides & K. R. Dunbar, *Chem. Soc. Rev.* **2008,** *37,* 68–83.
68. R. E. Dawson, A. Hennig, D. P. Weimann, D. Emery, V. Ravikumar, J. Montenegro, T. Takeuchi, S. Gabutti, M. Mayor, J. Mareda, C. A. Schalley & S. Matile, *Nat. Chem.* **2010,** *2,* 533–538.
69. T. Gerkensmeier, B. Decker, M. Schwertfeger, W. Buchheim & J. Mattay, *Eur. J. Org. Chem.* **2002,** 2120–2125.
70. B. Kim, R. Balasubramanian, W. Perez-Segarra, A. Wei, B. Decker & J. Mattay, *Supramol. Chem.* **2005,** *17,* 173–180.
71. T. Witte, B. Decker, J. Mattay & K. Huber, *J. Am. Chem. Soc.* **2004,** *126,* 9276–9282.
72. K. I. Assaf & W. M. Nau, *Chem. Soc. Rev.* **2015,** *44,* 394–418.
73. J. Lagona, P. Mukhopadhyay, S. Chakrabarti & L. Isaacs, *Angew. Chemie Int. Ed.* **2005,** *44,* 4844–4870.
74. Y. Miyahara, K. Goto, M. Oka & T. Inazu, *Angew. Chem. Int. Ed.* **2004,** *43,* 5019–5022.
75. C. Márquez, R. R. Hudgins & W. M. Nau, *J. Am. Chem. Soc.* **2004,** *126,* 5806–5816.
76. T. F. G. G. Cova, S. C. C. Nunes, A. J. M. Valente, T. M. V. D. Pinho e Melo & A. A. C. C. Pais, *J. Mol. Liq.* **2017,** *242,* 640–652.
77. E. Prigorchenko, M. Öeren, S. Kaabel, M. Fomitšenko, I. Reile, I. Järving, T. Tamm, F. Topić, K. Rissanen & R. Aav, *Chem. Commun.* **2015,** *51,* 10921–10924.
78. R. Aav, E. Shmatova, I. Reile, M. Borissova, F. Topić & K. Rissanen, *Org. Lett.* **2013,** *15,* 3786–3789.
79. M. Öeren, E. Shmatova, T. Tamm & R. Aav, *Phys. Chem. Chem. Phys.* **2014,** *16,* 19198.
80. N. N. Andersen, M. Lisbjerg, K. Eriksen & M. Pittelkow, *Isr. J. Chem.* **2018,** *58,* 435–448.
81. C. J. Pedersen, *J. Am. Chem. Soc.* **1967,** *89,* 2495–2496.
82. C. J. Pedersen, *J. Incl. Phenom. Mol. Recognit. Chem.* **1992,** *12,* 7–10.
83. J. W. Steed, *Coord. Chem. Rev.* **2001,** *215,* 171–221.

84. R. Hilgenfeld & W. A Saenger, *Angew. Chem. Int. Ed.* **1981,** *242,* 1045–1046.
85. C. Yoo, H. M. Dodge & A. J. M. Miller, *Chem. Commun.* **2019,** *55,* 5047–5059.
86. M. T. Reetz, C. M. Niemeyer & K. Harms, *Angew. Chem. Int. Ed.* **1991,** *30,* 1472–1474.
87. M. T. Reetz, C. M. Niemeyer & K. Harms, *Angew. Chem. Int. Ed.* **1991,** *30,* 1474–1476.
88. J. M. Mahoney, G. U. Nawaratna, A. M. Beatty, P. J. Duggan, & B. D. Smith, *Inorg. Chem.* **2004,** *43,* 5902–5907.
89. J. M. Mahoney, A. M. Beatty, & B. D. Smith, *Inorg. Chem.* **2004,** *43,* 7617–7621.
90. K. K. Murray, R. K. Boyd, M. E. Eberlin, G. J. Langley, L. Li & Y. Naito, *Pure Appl. Chem.* **2013,** *85,* 1515–1609.
91. K. Downard, *Mass spectrometry: A foundation course*, Royal Society of Chemistry, **2004**.
92. D. M. Desiderio, N. M. Nibbering & A. Kraj, *Mass spectrometry : instrumentation, interpretation, and applications*. John Wiley & Sons, Inc., **2009**.
93. C. Lapthorn, F. Pullen, & B. Z. Chowdhry, *Mass Spectrom. Rev.* **2013,** *32,* 43–71.
94. E. Jurneczko & P. E. Barran, *Analyst* **2011,** *136,* 20–28.
95. J. C. May, C. B. Morris & J. A. Mclean, *Anal. Chem.* **2017,** *89*, 1032-1044.
96. E. Kalenius, M. Groessl & K. Rissanen, *Nat. Rev. Chem.* **2019,** *3,* 4–14.
97. V. Gabelica & E. Marklund, *Curr. Opin. Chem. Biol.* **2018,** *42,* 51–59.
98. T. Wyttenbach, C. Bleiholder & M. T. Bowers, *Anal. Chem.* **2013,** *85,* 2191–2199.
99. C. Larriba & C. J. Hogan, *J. Phys. Chem. A* **2013,** *117,* 3887–3901.
100. T. Wyttenbach, C. Bleiholder, S. E. Anderson & M. T. Bowers, *Mol. Phys.* **2015,** *113,* 2344–2349.
101. C. Larriba & C. J. Hogan, *J. Comput. Phys.* **2013,** *251,* 344–363.
102. A. A. Shvartsburg & M. F. Jarrold, *Chem. Phys. Lett.* **1996**, *261,* 86–91.
103. K. Giles, J. P. Williams & I. Campuzano, *Rapid Commun. Mass Spectrom.* **2011** *25,* 1559–1566.
104. J. C. May & J. A. Mclean, *Int. J. Ion Mobil. Spectrom.* **2003**, *16,* 85–94.
105. K. M. Hines, J. C. May, J. A. McLean & L. Xu, *Anal. Chem.* **2016**, *88,* 7329–7336.
106. K. Michelmann, J. A. Silveira, M. E. Ridgeway & M. A. Park, *J. Am. Soc. Mass Spectrom.* **2014**, *26,* 14–24.
107. J. A. Silveira, K. Michelmann, M. E. Ridgeway & M. A. Park, *J. Am. Soc. Mass Spectrom.* **2016**, *27,* 585–595.
108. M. E. Ridgeway, M. Lubeck, J. Jordens, M. Mann, & M. A. Park, *Int. J. Mass. Spectrom.* **2018**, *425*, 22–35.
109. J. C. May & J. A. McLean, *Anal. Chem.* **2015**, *87,* 1422–1436.
110. K. Giles, S. D. Pringle, K. R. Worthington, D. Little, J. L. Wildgoose & R. H. Bateman, *Rapid Commun. Mass Spectrom.* **2004**, *18,* 2401–2414.
111. J. Stojko, S. Fieulaine, S. Petiot-Bécard, A. Van Dorsselaer, T. Meinnel, C. Giglione and S. Cianférani, *Analyst* **2015**, *140,* 7234–7245.

112. J. Ujma, M. De Cecco, O. Chepelin, H. Levene, C. Moffat, S. J. Pike, P. J. Lusby & P. E. Barran, *Chem. Commun.* **2012**, *48,* 4423–4425.
113. T.-C. Lee, E. Kalenius, A. I. Lazar, K. I. Assaf, N. Kuhnert, C. H. Grün, J. Jänis, O. A. Scherman & W. M. Nau, *Nat. Chem.* **2013**, *5,* 376–82.
114. H. V. Schröder, J. M. Wollschläger & C. A. Schalley, *Chem. Commun.* **2017**, *53,* 9218–9221.
115. W. Koch & M. C. Holthausen, *A Chemist's Guide to Density Functional Theory*. WILEY-VCH Verlag GmbH, **2001**.
116. S. Grimme, *Chem. Eur. J.* **2012,** *18,* 9955–9964.
117. J. Antony, R. Sure & S. Grimme, *Chem. Commun.* **2015,** *51,* 1764–1774.
118. S. Grimme, *J. Comput. Chem.* **2004,** *25,* 1463–1473.
119. S. Grimme, J. Antony, S. Ehrlich & H. Krieg, *J. Chem. Phys.* **2010**, *132*, 154104.
120. J. H. Simpson, *Organic structure determination using 2-D NMR spectroscopy*. Academic Press, **2012**.
121. P. Thordarson, *Chem. Soc. Rev.* **2011**, *40,* 1305–1323.
122. L. Avram & Y. Cohen, *Chem. Soc. Rev.* **2015,** *44,* 586–602.
123. W. Massa, *Crystal Structure Determination*, Springer, **2000**.
124. K. Rissanen, *Chem. Soc. Rev.* **2017,** *46,* 2638–2648.
125. T. Mäkelä, E. Kalenius & K. Rissanen, *Inorg. Chem.* **2015,** *54,* 9154–9165.
126. A. Kiesilä, J. O. Moilanen, F. Topić, S. Götz, K. Rissanen, A. Lützen & E. Kalenius. *Unpublished results*.
127. F. Tancini, R. M. Yebeutchou, L. Pirondini, R. De Zorzi, S. Geremia, Oren A. Scherman & E. Dalcanale, *Chem. Eur. J.* **2010,** *16,* 14313–14321.
128. K. Murayama, *Chem. Commun.* **1998,** 607–608.
129. M. Mäkinen, P. Vainiotalo, M. Nissinen & K. Rissanen, *J. Am. Soc. Mass Spectrom.* **2003,** *14,* 143–151.
130. G. Bianchini, A. Scarso, G. La Sorella & G. Strukul, *Chem. Commun.* **2012,** *48,* 12082–12084.
131. K. J. Laszlo & M. F. Bush, *J. Phys. Chem. A* **2017**, *121,* 7768–7777.
132. D. Canzani, K. J. Laszlo & M. F. Bush, *J. Phys. Chem. A* **2018**, *122*, 5625–5634.
133. S. Mecozzi & J. Rebek, *Chem. Eur. J.* **1998,** *4,* 1016–1022.
134. M. A. Spackman & D. Jayatilaka, *CrystEngComm.* **2009,** *11,* 19–32.
135. M. D. Lankshear, I. Dudley, K. M. Chan, A. R. Cowley, S. M. Santos, V. Felix & P. D. Beer, *Chem. Eur. J.* **2008,** *14,* 2248–2263.
136. P. D. Beer & S. W. Dent, *Chem. Commun.* **1998,** 825–826.
137. J. Romański, B. Trzaskowski & P. Piątek, *Dalt. Trans.* **2013,** *42,* 15271–15274.
138. G. W. Gokel, W. M. Leevy & M. E. Weber, *Chem. Rev.* **2004,** *104,* 2723–2750.
139. C. J. Pedersen, *J. Am. Chem. Soc.* **1967,** *89,* 2495–2496.
140. O. Jurček, H. Valkenier, R. Puttreddy, M. Novak, H. A. Sparkles, R. Marek, K. Rissanen & A. P. Davis, *Chem. Eur. J.* **2018,** *24,* 8178–8185.
141. P. A. Gale, *Chem. Soc. Rev.* **2010,** *39,* 3746–3771.
142. S. Camiolo, P. A. Gale, M. B. Hursthouse & M. E. Light, *Org. Biomol. Chem.* **2003**, *1*, 741–744.
143. J. C. Bryan, R. A. Sachleben, J. M. Lavis & M. C. Davis, *Inorg. Chem.* **2002,** 37, 2749–2755.

144. P. A. Gale, N. Busschaert, C. J. E. Haynes, L. E. Karagiannidis & I. L. Kirby, *Chem. Soc. Rev.* **2014,** *43,* 205–41.
145. A. Pramanik, D. R. Powell, B. M. Wong & A. Hossain, *Inorg. Chem.* **2012,** *51,* 4274–4284.
146. Y. Zhang & P. S. Cremer, *Curr. Opin. Chem. Biol.* **2006,** *10,* 658–663.

APPENDIX

TABLE A1. Obtained $^{DT}CCS_{N2}$ values and mass accuracies for **1** and its complexes with most abundant anions.

m/z	ion	Δ*m/z* (mDa)	$^{DT}CCS_{N2}$ (Å^2)
1431	[**1**$_2$+H]$^-$	2.15	384.3 ± 0.32
1489	[**1**$_2$-H+Acetone]$^-$	1.72	387.7 ± 0.41
1519	[**1**$_2$+BF_4]$^-$	1.2	388.7 ± 0.59
1559	[**1**$_2$+I]$^-$	- 0.25	389.3 ± 0.54
1577	[**1**$_2$+PF_6]$^-$	-0.14	394.0 ± 0.32
1577	[**1**$_2$+Acetone+BF_4]$^-$	1.76	390.4 ± 0.54
1617	[**1**$_2$+Acetone+I]$^-$	0.72	391.2 ± 0.52
1635	[**1**$_2$+Acetone+PF_6]$^-$	- 0.08	395.0 ± 0.34

TABLE A2. Obtained $^{DT}CCS_{N2}$ values and mass accuracies for **1** and its complexes with different solvents.

m/z	ion	Δ*m/z* (mDa)	$^{DT}CCS_{N2}$ (Å^2)
715	[**1**-H]$^-$	0.94	269.2 ± 0.27
861	[**1**+PF_6]$^-$	0.84	273.7 ± 0.22
1431	[**1**$_2$+H]$^-$	2.15	384.3 ± 0.32
1472	[**1**$_2$-H+MeCN]$^-$	2.2	387.0 ± 0.97
1489	[**1**$_2$-H+Acetone]$^-$	1.72	387.7 ± 0.41
1503	[**1**$_2$-H+THF]$^-$	-2.23	387.9 ± 0.26
1509	[**1**$_2$-H+DMSO]$^-$	-1.71	387.4 ± 0.56
1515	[**1**$_2$-H+DCM]$^-$	0.91	387.1 ± 0.72
1577	[**1**$_2$+PF_6]$^-$	-0.14	394.0 ± 0.32
1618	[**1**$_2$+MeCN+PF_6]$^-$	- 0.1	393.8 ± 0.33
1635	[**1**$_2$+Acetone+PF_6]$^-$	- 0.08	395.0 ± 0.34
1649	[**1**$_2$+THF+PF_6]$^-$	-1.63	394.0 ± 0.61
1655	[**1**$_2$+DMSO+PF_6]$^-$	-2.61	393.6 ± 0.5
1661	[**1**$_2$+DCM+PF_6]$^-$	-0.29	393.9 ± 0.39
1695	[**1**$_2$+$CHCl_3$+PF_6]$^-$	1.84	394.9 ± 0.50

TABLE A3. Observed ions, their $^{DT}CCS_{N2}$ values and mass accuracies for **1** and its complexes with Me_4N^+ salts. Theoretical $^{DTM}CCS_{N2}$ values shown for ions: $[1_2+Me_4N_{endo}]^+$, $[1_2+PF_{6exo}]^-$, $[1_2+Acetone_{endo}+PF_{6exo}]^-$. *Obtained theoretical $^{DTM}CCS_{N2}$ value for $[1_2+Me_4N_{exo1}]^+$ and $[1_2+Me_4N_{exo2}]^+$ are 415.6 Å² and 429.2 Å², respectively.

m/z	ion	Δ*m/z* (mDa)	experimental $^{DT}CCS_{N2}$ (Å²)	theoretical $^{DTM}CCS_{N2}$ (Å²)
717	$[1+H]^+$	0.39	268.9 ± 0.24	
739	$[1+Na]^+$	1.08	276.8 ± 0.25	
1433	$[1_2+H]^+$	-0.39	384.8 ± 0.41	
1455	$[1_2+Na]^+$	-0.65	387.6 ± 0.36	
1506	$[1_2+Me_4N]^+$	0.06	385.6 ± 0.40	405.7 *
715	$[1-H]^-$	-0.06	270.9 ± 0.32	
788	$[1-2H+Me_4N]^-$	-0.41	278.6 ± 0.22	
803	$[1+BF_4]^-$	-2.92	269.8 ± 0.26	
843	$[1+I]^-$	-2.86	271.6 ± 0.32	
861	$[1+PF_6]^-$	-0.46	275.2 ± 0.35	
1431	$[1_2-H]^-$	-0.45	387.0 ± 0.44	
1489	$[1_2-H+Acetone]^-$	2.42	388.5 ± 0.47	
1504	$[1_2-2H+Me_4N]^-$	1.8	389.9 ± 0.41	
1519	$[1_2+BF_4]^-$	-1.5	389.9 ± 0.43	
1559	$[1_2+I]^-$	-2.25	390.6 ± 0.51	
1577	$[1_2+PF_6]^-$	0.36	395.9 ± 0.50	415.4
1577	$[1_2+Acetone+BF_4]^-$	-2.34	391.4 ± 0.43	
1617	$[1_2+Acetone+I]^-$	-2.38	392.2 ± 0.50	
1635	$[1_2+Acetone+PF_6]^-$	0.42	397.3 ± 0.49	421.5
1592	$[1_2-H+Me_4N+BF_4]^-$	-0.35	393.6 ± 0.46	
1632	$[1_2-H+Me_4N+I]^-$	-2.00	394.0 ± 0.56	
1650	$[1_2-H+Me_4N+PF_6]^-$	0.41	399.6 ± 0.49	
1680	$[1_2+Me_4N+2BF_4]^-$	-2.21	393.0 ± 0.47	
1760	$[1_2+Me_4N+2I]^-$	-2.50	394.1 ± 0.51	
1796	$[1_2+Me_4N+2PF_6]^-$	0.51	404.1 ± 0.52	

ORIGINAL PAPERS

I

SIMULTANEOUS *ENDO* AND *EXO* COMPLEX FORMATION OF PYRIDINE[4]ARENE DIMERS WITH NEUTRAL AND ANIONIC GUESTS

by

Anniina Kiesilä, Lauri Kivijärvi, Ngong Kodiah Beyeh, Jani O. Moilanen, Michael Groessl, Tatiana Rothe, Sven Götz, Filip Topić, Kari Rissanen, Arne Lützen & Elina Kalenius.

Angewandte Chemie International Edition, **2017**, *57*, 10942-10946.

https://doi.org/10.1002/anie.201704054

A Journal of the Gesellschaft Deutscher Chemiker

Angewandte International Edition Chemie

GDCh

www.angewandte.org

Accepted Article

Title: Simultaneous Endo- and Exo-Complex Formation of Pyridine[4]arene Dimer with Neutral and Anionic Guests

Authors: Anniina Kiesilä, Lauri Kivijärvi, Ngong Kodiah Beyeh, Jani Moilanen, Michael Groessl, Filip Topic, Tatiana Rothe, Sven Götz, Kari Rissanen, Arne Lützen, and Elina Kalenius

To be cited as: *Angew. Chem. Int. Ed.* 10.1002/anie.201704054
Angew. Chem. 10.1002/ange.201704054

Link to VoR: http://dx.doi.org/10.1002/anie.201704054
http://dx.doi.org/10.1002/ange.201704054

WILEY-VCH

10.1002/anie.201704054

WILEY-VCH

COMMUNICATION

Simultaneous *Endo*- and *Exo*-Complex Formation of Pyridine[4]arene Dimer with Neutral and Anionic Guests

A. Kiesilä,[a] L. Kivijärvi,[a] N.K. Beyeh,[b] J. O. Moilanen,[a] M. Groessl,[c] T. Rothe,[d] S. Götz,[d] F. Topić,[a] K. Rissanen,[a] A. Lützen,[d]* and E. Kalenius[a]*

Abstract: Complex formation between hexafluorophosphate (PF_6^-) and tetraisobutyl-octahydroxypyridine[4]arene (**1**) has been thoroughly studied in gas phase (ESI-QTOF-MS, IM-MS, DFT calculations), solid state (X-ray crystallography) and in chloroform solution (^{1}H, ^{19}F and DOSY NMR). In all states of matter, simultaneous *endo*-complexation of solvent molecules and *exo*-complexation of PF_6^- anion within pyridine[4]arene dimer was observed. While similar ternary complex formation is often observed in solid state, this is a unique example of such behaviour in the gas phase that has never been observed so far.

Resorcinarenes, their derivatives, and their dimeric and hexameric assemblies have found numerous applications in molecular recognition as binding motifs for neutral molecules and cations but also for anions.[1] Over the years, however, there have been contradicting reports on the actual binding site for anionic guests: Dimeric capsules, for example, bind separated ion pairs by encapsulating the cation in the cavity of the dimeric capsule with the anion bound at the lower rim via alkyl- and aryl-CH-anion interactions as evidenced by X-ray diffraction analysis.[2] Likewise, a monomeric cavitand was found to bind ion pairs in a similar fashion in solution, with the anion located at the lower rim between the alkyl chains.[3] Such an arrangement was somewhat counterintuitive, especially regarding our previous work on anion binding with functionalized cavitands in the gas phase where computational studies suggested binding of the anions at the upper rim via CH-anion hydrogen bonding involving the H atoms of the acetal bridges.[4] Nevertheless, this study clearly revealed that anion binding is significantly enhanced by functionalizing the cavitand with electron-withdrawing groups. Therefore, the corresponding pyridine[4]arenes[5] derived from the condensation of 2,6-dihydroxypyridine[6] and aldehydes seemed even more promising for this purpose. They are even more electron deficient and present a unique array of hydrogen bond donor and acceptor functions fixing these molecules in cone conformation. Pioneering work by Mattay already suggested octahydroxypyridine[4]arenes to have affinity towards anions.[7] Rozhenko's theoretical studies on octahydroxypyridine[4]arene, without lower rim alkyl chains, strongly supported the encapsulation of anionic guests inside the dimer, located in the middle of the cavity close to the hydrogen bonded seam of the dimer. The computational studies showed that anions like tetrafluoroborate and hexafluorophosphate are optimally sized for encapsulation inside the dimer.[8] Moreover, the complexation of carboxylates was experimentally observed, but the mass spectrometric investigation also suggested that the guest could actually be located outside the cavity, with the IRMPD experiments showing the elimination of the guest as the first dissociation step.[7]

Therefore, we decided to thoroughly re-investigate the anion binding behaviour of these interesting but least studied members of the family of resorcinarenes, choosing tetraisobutyl-octahydroxy-pyridine[4]arene (**1**, Scheme 1) to study its binding behavior towards hexafluorophosphate (PF_6^-) in solution (NMR), the solid state (X-ray crystallography), and the gas phase (ESI-MS, IM-MS, DFT calculations) as a first example.

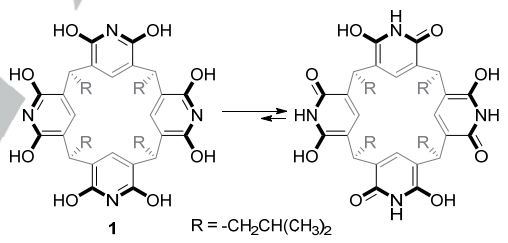

Scheme 1. Tautomerism of tetraisobutyloctahydroxypyridine[4]arene **1** (only one of the two possible enantiomers of the pyridone tautomer is shown).

Cohen earlier showed by ^{1}H DOSY NMR that the tetraundecyloctahydroxypyridine[4]arene forms an equilibrium of dimeric and hexameric aggregates in chloroform solution.[9] The ^{1}H NMR spectra of 10 mM solution of **1** in chloroform clearly show the formation of dimeric capsule-like aggregates, indicated by the signals at 7.10, 4.28 and 1.90 ppm (Figure 1), which can be assigned to the dimeric species by DOSY NMR. These signals give a diffusion coefficient of $0.411 \cdot 10^{-5}$ cm^2s^{-1} which is comparable with the $0.37 \cdot 10^{-5}$ cm^2s^{-1} value measured for tetraundecyloctahydroxypyridine[4]arene dimer by Cohen.[9]

Interestingly, the ^{1}H NMR spectra measured of equimolar solutions of **1** and $TBAPF_6$ in chloroform (Figure 1) show significant, albeit small downfield shifts for the signals of the Ar-H protons H_a and the CH_2 protons H_c at the lower rim of the pyridinearene, in accordance with the observations of Diederich and Dalcanale[3] and resulting from weak CH-anion interactions between the PF_6^- anion and the dimer of **1**. This is a strong

[a] University of Jyväskylä, Department of Chemistry, Nanoscience Center, P.O. Box 35, FI-40014 University of Jyvaskyla, Finland. E-mail: elina.o.kalenius@jyu.fi
[b] Aalto University, School of Science, Department of Applied Physics, Puumiehenkuja 2, FI-02150 Espoo, Finland
[c] TOFWERK, Uttigenstr. 22, 3600 Thun, Switzerland.
[d] University of Bonn. Kekulé-Institute of Organic Chemistry and Biochemistry, Gerhard-Domagk-Str. 1, D-53121 Bonn, Germany. E-mail: arne.luetzen@uni-bonn.de

Supporting information for this article is given via a link at the end of the document.

10.1002/anie.201704054
WILEY-VCH

COMMUNICATION

indication that the anion is bound on the exterior of the dimeric capsule, and not inside the cavity as suggested by the previous reports.

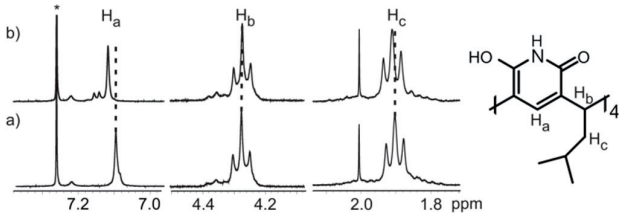

Figure 1. Selected regions of ^{1}H NMR spectra (10 mM, $CDCl_3$, 298 K) of a) **1** and b) **1** + $TBAPF_6$ (1:1). Shift was observed in H_a (0.02 ppm) and smaller shift in H_c (0.01 ppm). $CDCl_3$ marked with an asterisk.

Additional proof for such *exo*-interactions came from the comparison of the ^{19}F NMR spectra of the $TBAPF_6$ and **1**+$TBAPF_6$ samples. Significant downfield shift of the fluorine atoms signals (Figure 2) was observed upon binding of hexafluorophosphate.[10] The fact that only a single set of downfield shifted signals of the guests is observed suggests a fast exchange and/or tumbling motion of the almost spherical anion within its binding pocket on the NMR time scale. While the *endo*-complexation would be expected to result in the shielding of the guests and an upfield shift of the guest signals a downfield shift, however, agrees very well with weak CH-anion interactions, again strongly supporting *exo*-complexation of the anion with **1**.

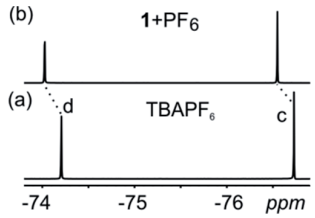

Figure 2. Selected regions of the ^{19}F NMR spectra (20 mM, $CDCl_3$, 298 K) observed from: a) $TBAPF_6$ and b) **1**+$TBAPF_6$ (1:1).

Single crystals of the **1**+$TBAPF_6$ complex were obtained from a chloroform solution of **1** and 3 eq. $TBAPF_6$, by slow evaporation at around 4 °C. The crystal structure (Figure 3) shows **1** in the pyridone tautomeric form (see Table S1). Its cone conformation is stabilized by four intramolecular (hydroxyl)O−H···O(amide) hydrogen bonds with lengths of 2.524(5), 2.553(5), 2.571(6) and 2.609(5) Å, unidirectionally oriented along the upper rim in a clockwise manner. Similarly, the isobutyl groups are aligned unidirectionally along the lower rim with the methane CH groups in an anticlockwise arrangement. Next, two molecules of **1** form a dimeric capsule sustained by eight N−H···O(amide) hydrogen bonds, with the lengths of symmetrically independent hydrogen bonds of 2.822(6), 2.872(6), 3.108(6) and 3.115(8) Å. The latter two hydrogen bonds are elongated due to bifurcation, as both the NH donors and O(amide) acceptors are also engaged in hydrogen bonding with the neighbouring capsule (3.018(6) and 3.040(5) Å long, Figure S1 in SI). Instead of PF_6^- anion, we found the dimer cavity fully occupied by a $CHCl_3$ molecule.[11] On the other hand, the PF_6^- anion was found to reside on the lower rim of **1**, in a slightly asymmetric tilted orientation within the pocket formed by the four isobutyl groups. To the best of our knowledge this is the first solid state structure of a pyridinearene host-guest complex and such a motif of simultaneous *endo*-binding of a solvent molecule and *exo*-binding of an anion has never been observed for any other resorcinarene system. The apical fluorine atom of PF_6^- forms short contacts with the four lower rim aromatic CH protons, with respective C−H···F hydrogen bond lengths of 3.445(8), 3.516(8), 3.566(7) and 3.616(7) Å, as well as with the isobutyl groups. Equatorial fluorine atoms further form a number of C−H···F hydrogen bonds with the isobutyl groups. The PF_6^- anion is further surrounded by two $CHCl_3$ molecules and the tetrabutyl ammonium (TBA^+) cation, also forming a number of C−H···F hydrogen bonds (Figure S2 in SI).

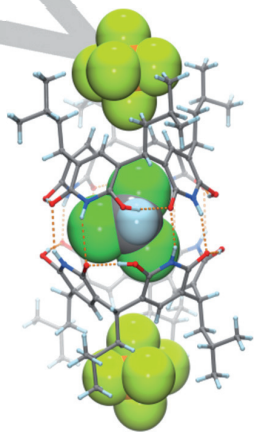

Figure 3. Crystal structure of [**1**$_2$+2$PF_{6(exo)}$+$CHCl_{3(endo)}$]$^{2-}$. *Endo*-complexed $CHCl_3$ and *exo*-complexed PF_6^- are shown in space-filling model. Hydrogen bonds are shown as dashed orange lines. TBA^+ cations and co-crystallized $CHCl_3$ solvent molecules are omitted for clarity.

The spontaneous self-assembly of **1** into dimeric ions was also clearly observed in ESI-MS spectra. In addition to the deprotonated ion [**1**$_2$−H]$^-$ at *m/z* 1432 and anion complex [**1**$_2$+PF_6]$^-$ at *m/z* 1578, abundant formation of solvent adduct [**1**$_2$−H+S]$^-$ (S = solvent, e.g. acetone, acetonitrile or CH_2Cl_2, depending on sample solvent) and ternary complex [**1**$_2$+PF_6+S]$^-$ were clearly detected (Figure 4).[10] Even though the formation of solvent adducts or even inclusion of solvent molecules is relatively common in condensed phase where the solvent often fills the void space, this phenomenon is extremely surprising and novel in gas phase and has – to the best of our knowledge – never been described in any anion- or cation-binding study with resorcinarenes before. It is important to note that the monomer region of the mass spectra did not show any peaks corresponding to solvent adducts such as [**1**-H+S]$^-$ or [**1**+PF_6+S]$^-$, implying that the phenomenon is indeed a feature of the dimer via inclusion, and not adduct formation.

10.1002/anie.201704054
WILEY-VCH

COMMUNICATION

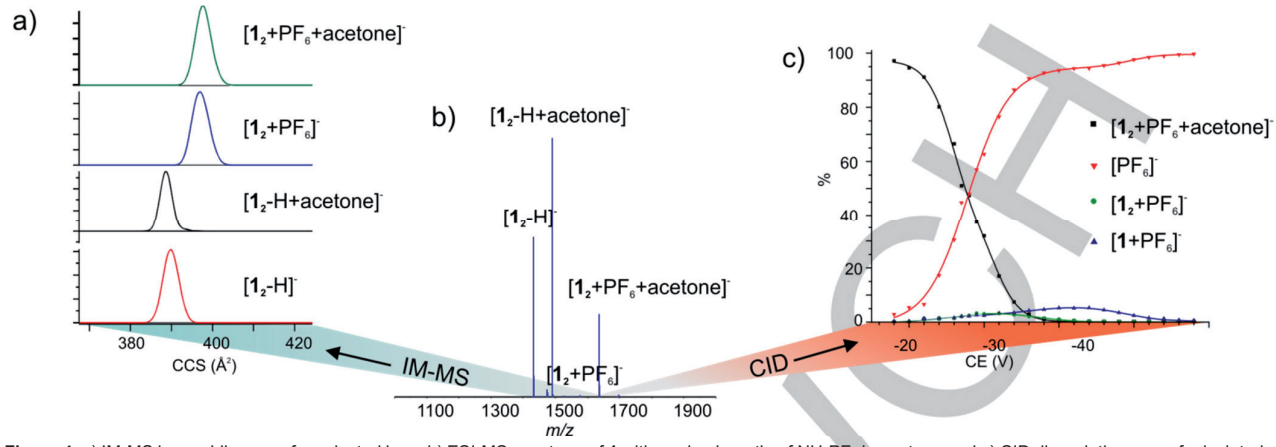

Figure 4. a) IM-MS ion mobilograms for selected ions, b) ESI-MS spectrum of **1** with equimolar ratio of NH_4PF_6 in acetone and c) CID dissociation curve for isolated ion $[\mathbf{1}_2+PF_6+acetone]^-$.

When ternary complex, $[\mathbf{1}_2+PF_6+acetone]^-$, was isolated in gas phase and activated in collision-induced dissociation (CID) experiment, PF_6^- anion was eliminated in the initial dissociation step. CID is an ergodic activation technique and due to energy randomization the weakest bond or interaction is generally broken first. Elimination of the anion as the initial dissociation step, implies to weak and *exo*-complexation of PF_6^- with pyridinearene **1**, since only small amounts of other dissociation products were observed. In the case of *endo*-complexed PF_6^- and *exo*-complexed solvent, elimination of solvent or pyridinearene monomer would be expected as the first step. Definitive proof for the *exo*-complexation of anion in the gas phase was obtained by drift tube ion-mobility mass spectrometry (DTIM-MS) experiments.[12,13] IM-MS is still rarely utilized tool in supramolecular chemistry despite its benefits in the detection of host-guest complexes and the analysis of conformers and structural features.[14] As the drift tube of the IM-MS instrument is operated at atmospheric pressure, it allows high resolution separations and therefore accurate determination of collision cross section (CCS) values[15] without the need for cumbersome calibration, which often severely complicates the analysis when the more common TW-IM-MS (travelling-wave ion-mobility MS) is used. The ion mobilograms (Figure 4a) show very similar but clearly larger $^{DT}CCS_{N2}$ values for ions $[\mathbf{1}_2+PF_6+acetone]^-$ and $[\mathbf{1}_2+PF_6]^-$ compared to ions $[\mathbf{1}_2-H]^-$ and $[\mathbf{1}_2-H+acetone]^-$. In terms of collision cross sections (CCS), the PF_6^- complexes are ~8 Å^2 larger compared to the deprotonated dimer (Table 1).

Table 1. Experimental $^{DT}CCS_{N2}$ values and comparison of approximated diameters (nm) obtained by IM-MS, ^{1}H DOSY NMR and X-ray diffraction.

Ion	*m/z*	$^{DT}CCS_{N2}$ (Å^2)	IM-MS[a] *d* (nm)	DOSY *d* (nm)	X-ray *d* (nm)
$[\mathbf{1}-H]^-$	715	264.5			
$[\mathbf{1}_2-H]^-$	1432	389.8	2.2		
$[\mathbf{1}_2+acetone-H]^-$	1490	388.6	2.2		
$[\mathbf{1}_2+PF_6]^-$	1578	396.9	2.3	2.0[b]	1.9[b]
$[\mathbf{1}_2+PF_6+acetone]^-$	1636	397.6	2.3		

[a] Diameters calculated on basis of CCS by assuming a spherical conformation.
[b] Diameters for ^{1}H DOSY NMR and X-ray diffraction apply generally to dimers.

Therefore, it is reasonable to conclude that, also in the gas phase, the dimers of **1** contain *endo*-complexed solvent and *exo*-complexed anion and can thus be denoted as $[\mathbf{1}_2+PF_{6(exo)}+acetone_{(endo)}]^-$. Assuming the spherical shape for dimer of **1**, the obtained CCS values can be roughly compared with the hydrodynamic radii from the ^{1}H DOSY NMR and the crystal structure (Table 1). Each of the methods results in very similar diameters (1.9 to 2.3 nm), demonstrating structural similarity of dimers in solid state, gas phase, and solution and also highlighting the potential of IM-MS technique for structural chemistry purposes of host-guest systems.

To further analyse the gas phase structures of the observed ternary complexes, we performed density functional theory (DFT) calculations for the dimer and its inclusion complexes *in vacuo* at the RI-PBEPBE/def2-TZVP and RI-PBEPBE/def2-TZVP-D3 levels of theory.[16-18] As mentioned above, previous computational studies suggested the encapsulation of PF_6^- within the octahydroxypyridine[4]arene capsule.[8] However, the lower rim alkyl chains were truncated and the solvent molecules were not modelled explicitly in this earlier study, with the solvent effects included using the COSMO-model only. Therefore, both the *endo*- and *exo*-complexes of PF_6^- with and without acetone were re-examined by simulating the complete structures.

Optimized structures of the inclusion complexes are in good agreement with solid state structures, with the *exo*-complexed PF_6^- showing several F···H interactions with the lower rim alkyl chains of **1**, in $[\mathbf{1}+PF_{6(exo)}]^-$, $[\mathbf{1}_2+PF_{6(exo)}]^-$, and $[\mathbf{1}_2+PF_{6(exo)}+acetone_{(endo)}]^-$ (Table S3 and Figure S4).

The calculated interaction energies, given in Table 2, reveal that the *exo*-complexation of PF_6^- is favoured over the *endo*-complexation in all studied systems, except in $[\mathbf{1}_2+PF_6]^-$, when the dispersion correction is applied. The dispersion-corrected calculation predicts the interaction energy for $[\mathbf{1}_2+PF_{6(endo)}]^-$ to be ~10 kJmol^{-1} more favourable compared to the one for $[\mathbf{1}_2+PF_{6(exo)}]^-$. However, this is reversed in case of the ternary complexes, where the $[\mathbf{1}_2+PF_{6(exo)}+acetone_{(endo)}]^-$ is significantly more favoured (by >20 kJmol-1) compared to $[\mathbf{1}_2+PF_{6(endo)}+acetone_{(exo)}]^-$. Interestingly, the dispersion-corrected

10.1002/anie.201704054
WILEY-VCH

interaction energies are much higher (40-120 kJmol^{-1}) than the non-corrected energies underlining the important role of dispersion forces in the formation of the inclusion complexes at hand.

Table 2. Calculated interaction energies for **1** and complexes at the RI-PBEPBE/def2-TZVP (E_{int}) and RI-PBEPBE/def2-TZVP-D3 (E_{int-D3}) levels of theory.

Compound	ΔE_{int} (kJ mol^{-1})	ΔE_{int-D3} (kJ mol^{-1})
[**1**+$PF_{6(exo)}$]$^-$ [a]	−122.49	−161.27
[**1**+$PF_{6(endo)}$]$^-$ [a]	−56.84	−100.59
[$\mathbf{1}_2$+$PF_{6(exo)}$]$^-$ [b]	−116.90	−155.55
[$\mathbf{1}_2$+$PF_{6(endo)}$]$^-$ [b]	−85.85	−165.88
[$\mathbf{1}_2$+$PF_{6(exo)}$+acetone$_{(endo)}$]$^-$ [c]	−117.03	−239.3
[$\mathbf{1}_2$+$PF_{6(endo)}$+acetone$_{(exo)}$]$^-$ [c]	−105.70	−217.56

[a] $\Delta E_{int} = E_{complex} - (E_{PF6} + E_1)$, [b] $\Delta E_{int} = E_{complex} - (E_{PF6} + E_1)$, [c] $\Delta E_{int} = E_{complex} - (E_{PF6} + E_1 + E_{acetone})$

To visualize the reason for the *exo*-complexation of PF_6^- we mapped the electrostatic potential (ESP) surfaces of the $\mathbf{1}_2$ dimer and its complexes with acetone and/or PF_6^- (Figure 5). The cavity of the dimer itself does not show any significant positive partial potential. Instead, the seam of hydrogen bonds is clearly polarized and contains electron-rich surfaces implying poor affinity of the cavity towards anions. In contrast to the cavity, however, the lower rim alkyl chains show an electron-poor area that is more suitable for anion binding. The computational data not only supports the experimental finding that the *exo*-complexation of PF_6^- is more favourable than the *endo*-complexation but it also indicates that the guest encapsulation is largely governed by dispersion forces, making the solvent molecules better guests for the *endo*-complexation.

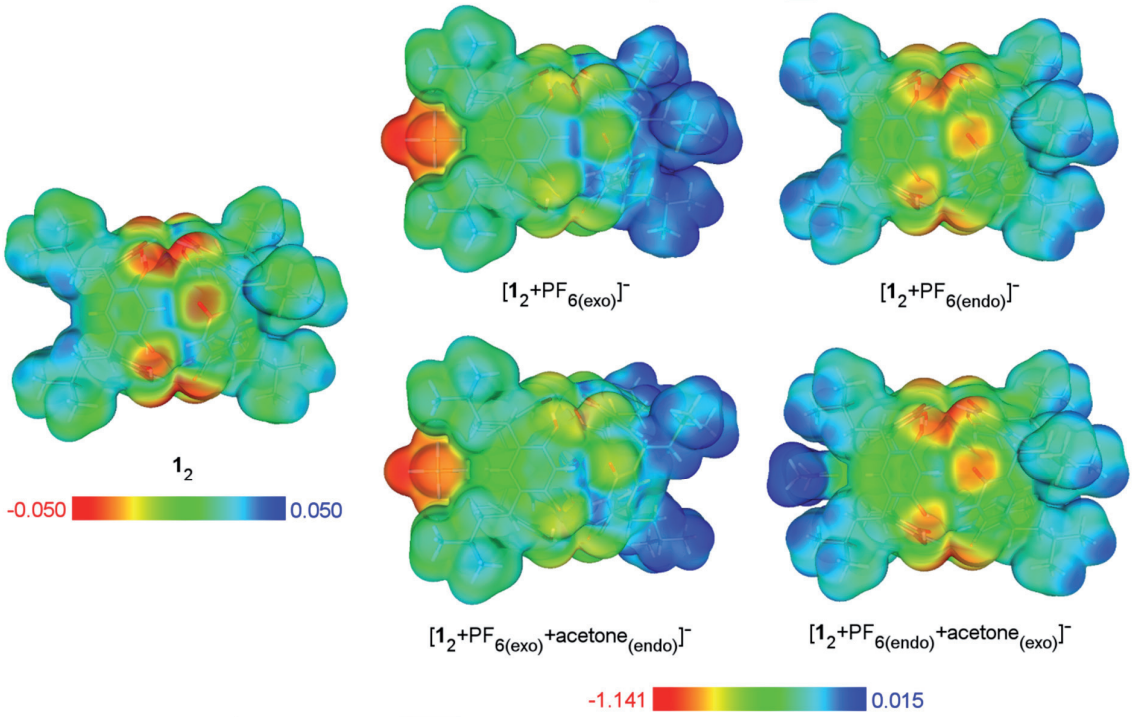

Figure 5. Calculated RI-PBEPBE/def2-TZVP electrostatic potentials for pyridinearene dimer (−0.050 – 0.050 au) and for complexes with PF_6^- and acetone (−1.414 – (−0.015) au) mapped on the isosurface of the total electron density (0.003 au). Top row: [$\mathbf{1}_2$], [$\mathbf{1}_2$+$PF_{6(exo)}$]$^-$, [$\mathbf{1}_2$+$PF_{6(endo)}$]$^-$, bottom row: [$\mathbf{1}_2$+$PF_{6(exo)}$+acetone$_{endo}$]$^-$, [$\mathbf{1}_2$+$PF_{6(endo)}$+acetone$_{exo}$]$^-$.

In conclusion, we have unambiguously shown the anion complexation by an *exo*-binding site of pyridine[4]arene **1** through CH-anion interactions in gas phase, solid state, and in solution. This is rationalized by the computed electrostatic potential surfaces which, in contradiction to previous reports, show partial positive potential located between the lower rim alkyl chains, not in cavity. In contrast to earlier assumptions, it is clear that the pyridine[4]arene cavity is not particularly well suited to anion binding. Instead, efficient *endo*-complexation of neutral molecules by dispersion interactions and formation of ternary complexes is detected. Even though the anion binding (*exo*-)site is similar in pyridine[4]arenes and classical resorcinarenes, the binding mode in pyridine[4]arene dimer deviates from that of the latter and is unpresented. Whereas resorcinarenes complex separated ion pairs (cations in cavity and anions at lower rim), the pyridine[4]arene complexes neutral molecules within the cavity and anion on lower rim. Although common in the solid state, similar ternary complex formation has not been previously observed in any gas phase studies of resorcinarenes. This study also shows the importance of utilising novel techniques and

10.1002/anie.201704054

approaches, such as IM-MS to study the structural chemistry of host-guest complexes in gas phase. Preliminary results,[10,11] concerning binding of other anions in variety of other solvents indicate that this binding motif is a unique feature of the pyridinearenes but it is not limited to the combination of the PF_6^- anion and chloroform or acetone but is more general in terms of both the anion, the solvent and the pyridinearene lower rim alkyl chains. We are currently investigating the potential of pyridinearenes in host-guest chemistry in more detail and these results will reported in due course.

Experimental Section

Experimental details for synthesis, NMR, mass spectrometry, DFT calculations and X-ray crystallography are presented in supporting material.

Acknowledgements

The Academy of Finland (K.R. proj. nos. 263256, 265328 and 292746, E.K.: nos. 284562 and 278743) and the University of Jyväskylä are gratefully acknowledged for financial support.

Keywords: pyridinearenes • resorcinarenes • molecular recognition • anion binding • ion mobility mass spectrometry

[1] a) H.-J. Schneider, U. Schneider, *J. Incl. Phenom. Mol. Recogn. Chem.* **1994**, *19*, 67-83; b) P. Timmerman, W. Verboom, D. N. Reinhoudt, *Tetrahedron*, **1996**, *52*, 2663-2704; L. C. Palmer, J. Rebek, Jr., *Org. Biomol. Chem.* **2004**, *2*, 3051-3059; d) S. M. Biros, J. Rebek, Jr., *Chem. Soc. Rev.* **2009**, *36*, 93-104; e) N. Li, R. G. Harrison, J. D. Lamb, *J. Incl. Phen. Macrocycl. Chem.* **2014**, *78*, 39-60; f) K. Kobayashi, M. Yamanaka, *Chem. Soc. Rev.* **2015**, *44*, 449-466.

[2] a) A. Shivanyuk, K. Rissanen, E. Kolehmainen, *Chem. Commun.* **2000**, 1107-1108; b) H. Mansikkamäki, M. Nissinen, K. Rissanen, *Chem. Commun.* **2002**, 1902-1903; c) H. Mansikkamäki, M. Nissinen, C. A. Schalley, K. Rissanen, *New J. Chem.* **2003**, *27*, 88-97; d) E. Biavardi, M. Favazza, A. Motta, I. L. Fragalà, C. Massera, L. Prodi, M. Montalti, M. Melegari, G. G. Condorelli, E. Dalcanale, *J. Am. Chem. Soc.* **2009**, *131*, 7447-7455.

[3] F. Tancini, T. Gottschalk, W. B. Schweizer, F. Diederich, E. Dalcanale, *Chem. Eur.* J. **2010**, *16*, 7813-7819.

[4] S. S. Zhu, H. Staats, K. Brandhorst, J. Grunenberg, F. Gruppi, E. Dalcanale, A.Lützen, K. Rissanen, C. A. Schalley, *Angew. Chem.* **2008**, *120*, 800-804; *Angew. Chem. Int. Ed.* **2008**, *47*, 788-792.

[5] T. Gerkensmeier, J. Mattay, C. Näther, *Chem. Eur. J.* **2001**, *7*, 465-474.

[6] Please note, that it is actually more efficient to use 2,6-dimethoxypyridine instead of 2,6-dihydroxypyridine for the synthesis of pyridine[4]arenes. For more details see SI.

[7] M. C. Letzel, B. Decker, A. B. Rozhenko, W. W. Schoeller, J. Mattay, *J. Am. Chem. Soc.* **2004**, *126*, 9669-9674.

[8] A. B. Rozhenko, W. W. Schoeller, M. C. Letzel, B. Decker, J. Mattay, *New J. Chem.* **2013**, *37*, 356-365.

[9] T. Evan-Salem, Y. Cohen, *Chem. Eur. J.* **2007**, *13*, 7659-7663.

[10] Preliminary studies show that a similar *exo*-binding is also found with other anions like BF_4^- and I^- as revealed by NMR and mass spectrometry.

[11] Preliminary studies show that a similar encapsulation of solvent molecules is also found with other solvents like THF and CH_2Cl_2 as revealed by XRD-analysis and mass spectrometry.

[12] F. Lanucara, S. W. Holma, C. J. Gray, C. E. Eyers, *Nat. Chem.* **2014**, *6*, 281-294.

[13] C. Lapthorn, F. Pullen, B. Z. Chowbury, *Mass Spec. Rev.* **2013**, *32*, 43-71.

[14] a) T.-C. Lee, E. Kalenius, A. I. Lazar, K. I. Assaf, N. Kuhnert, C.H. Grün, J. Jänis, O.A. Scherman, W.M. Nau, *Nat. Chem.,* **2013**, *5*, 376-382; b) P. Bonakdarzadeh, F. Topic, E. Kalenius, S. Bhowmik, M. Groessl, R. Knochenmuss, S. Sato and K. Rissanen, *Inorg. Chem.* **2015**, *54*, 6055−6061; c) O. Jurček, P. Bonakdarzadeh, E. Kalenius, J. M. Linnanto, M. Groessl, R. Knochenmuss, R. Puttreddy, J. Ihalainen, K. Rissanen, *Angew. Chem.* **2015**, *54*, 15462-15467; d) E. S. Baker, J. E. Bushnell, S. R. Wecksler, M. D. Lim, M. J. Manard, N. F. Depuis, P. C. Ford, M. T. Bowers, *J. Am. Chem. Soc.* **2005**, *127*, 18222-18228; e) X. Li, Y.-T. Chan, M. Casiano-Maldano, J. Yu, G. A. Carri, G. R. Newkome, C. Wesdemiotis, *Anal. Chem.* **2011**, *83*, 6667-6674; f) J. Ujma, M. De Cecco, O. Chepelin, H. Levene, C. Moffat, S. J. Pike. P. J. Lusby, P. E. Barran, *Chem. Commun.* **2012**, *48*, 4423-4425; g) P. J. Robbins, A. J. Surman, J. Thiel, D.-L. Long, L. Cronin, *Chem. Commun.* **2013**, *49*, 1909-1911.

[15] J. C. May, C. B. Morris, J. A. McLean, *Anal. Chem.* **2017**, *89,* 1032−1044.

[16] (a) P.A.M. Dirac, Proc. Royal Soc. A, **1929**, *123*, 714-733 (b) J.C. Slater, *Phys. Rev.* **1951**, *81*, 385-390. (c) J.P. Perdew, Y. Wang, *Phys. Rev. B*, **1992**, *45*, 13244-13249. (d) J.P. Perdew, K. Burke, M. Ernzerhof, *Phys. Rev. Lett.* **1996**, *77*, 3865-3868

[17] (a) K. Eichkorn, O. Treutler, H. Öhm, M. Häser, R. Ahlrichs, *Chem. Phys. Lett.* **1995**, *242*, 652–660 (erratum, **1995**, *242*, 283-290). (b) K. Eichkorn, F. Weigend, O. Treutler, R. Ahlrichs, *Theor. Chem. Acc.* **1997**, *97*, 119-124.

[18] S. Grimme, J. Antony, S. Ehrlich, H. Krieg, *J. Chem. Phys.* **2010**, *132*, 154104-154104.

II

ANION-DRIVEN ENCAPSULATION OF CATIONIC GUEST INSIDE PYRIDINE[4]ARENE DIMERS

by

A. Kiesilä, J. O. Moilanen, A. Kruve, C. A. Schalley, P. Barran & E. Kalenius.

Submitted manuscript

Anion-driven encapsulation of cationic guests inside pyridine[4]arene dimers

Anniina Kiesilä[1], Jani O. Moilanen[*1], Anneli Kruve[2], Christoph A. Schalley[2], Perdita Barran[3] and Elina Kalenius[*1]

Address: [1]Department of Chemistry, Nanoscience Center, University of Jyväskylä, P.O. Box 35, University of Jyväskylä, Finland [2]Institut für Chemie und Biochemie, Freie Universität Berlin, Takustrasse 3, 14195 Berlin, Germany [3]Michael Barber Centre for Collaborative Mass Spectrometry, Manchester Institute of Biotechnology, School of Chemistry, The University of Manchester, Princess Street, Manchester, UK

Email: Elina Kalenius – elina.o.kalenius@jyu.fi

* Corresponding author

Abstract

Pyridine[4]arenes have previously been considered as anion binding hosts due to the electron-poor nature of the pyridine ring. Herein, we demonstrate the encapsulation of Me_4N^+ cations inside a dimeric hydrogen-bonded pyridine[4]arene capsule, which contradicts with earlier assumptions. The complexation of a cationic guest inside the pyridine[4]arene dimer has been detected and studied by multiple gas-phase techniques, ESI-QTOF-MS, IRMPD, and DT-IMMS experiments, as well as DFT calculations. The comparison of classical resorcinarenes with pyridinearenes by MS and NMR experiments reveals clear differences in their host-guest chemistry and implies that cation encapsulation in pyridine[4]arene is an anion-driven process.

Keywords

pyridinearenes; resorcinarenes; ion mobility mass spectrometry; DFT calculations; cation binding

Introduction

Resorcinarenes and their derivatives are known for the molecular recognition properties of their self-assembled dimeric and hexameric capsules, which can encapsulate cationic and neutral guests [1-3]. Pyridine[4]arenes [4] are analogous macrocycles to resorcin[4]arenes. Whereas resorcinarenes are cyclic tetramers of resorcinol, pyridinearenes are formed from 2,6-dihydroxypyridine (see Scheme 1). Although the synthesis of pyridine[4]arenes dates back to 2001 [4], their host-guest chemistry is still much less explored. Both macrocycles are concave and are known to form capsular assemblies via intermolecular hydrogen bonding [5,6]. Pyridine is significantly less electron-rich than benzene. Consequently, pyridinearene capsules were originally assumed to encapsulate anionic guests inside their cavity due to a π-acidic character of the aromatic walls [7,8]. Mattey et. al. detected 1:1 complex formation with PF_6^- and BF_4^- by mass spectrometry, however without ion mobility mass spectrometry, the location of anion could not be verified and the anions were assumed to interact with the pyridinearene cavity. Inclusion complexes of anions within pyridinearene dimer were also theoretically studied by DFT calculations, but using truncated pyridinearene dimer model [8]. However, previous studies have also shown that the π-acidic character of pyridine rings such as 2-oxo-6-oxypyridine is rather weak [9,10]. Thus, pyridine[4]arenes may be expected to show a dual binding behaviour towards anions and cations [8]. In addition to anion complexes also 2:1

complex formation with neutral carboxylic acids and amides have been previously detected by ESI-MS [7]. Very recently, with the help of ion mobility mass spectrometry, we showed that pyridine[4]arenes favour encapsulation of neutral molecules over anionic species and anions are in fact complexed in an *exo* position (exclusion complexation) between the lower-rim alkyl chains [11]. A PF_6^- anion was bound to the lower rim of the pyridine[4]arene dimer via CH-anion and CH-F interactions, while the neutral guest was hosted inside the dimer. Calculated electrostatic potential (ESP) surfaces revealed that the cavity does not possess any significant partial positive potential on the surface of the cavity, except on the N-H hydrogen atoms. They are, however, on tangential positions along capsules surface, and therefore do not significantly contribute to anion binding [8]. More recently, we were also able to demonstrate, that cationic transition metal complexes can template the formation of pyridinearene hexameric capsules in gas phase [6].

Here, we report our novel findings on the ability of dimeric tetra-isobutyl-pyridine[4]arene (compound **1** in Scheme 1) to encapsulate cationic guests. Despite of the obvious structural similarities between the dimeric resorcin[4]arene and pyridine[4]arene capsules, we highlight here unique host-guest properties of pyridinearene capsules. In marked contrast to the corresponding resorcin[4]arene capsules, cation binding is clearly feasible, when anions bind in an *exo* site and support cation encapsulation by "through-wall" electrostatic interactions.

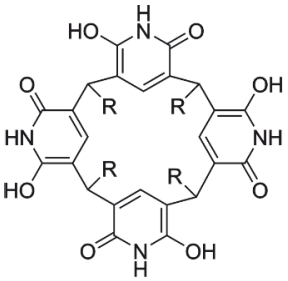

R=$CH_2CH(CH_3)_2$

1

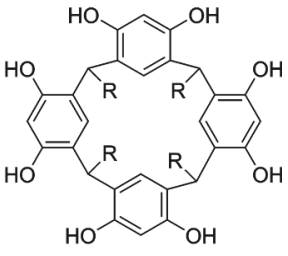

R=$CH_2CH(CH_3)_2$

2

Scheme 1: Structures of tetra-isobutylpyridine[4]arene (**1**) and tetra-isobutylresorcin[4]arene (**2**).

Results and Discussion

We have previously shown that tetra-isobutyl-pyridine[4]arene forms hydrogen-bonded dimers with eight intermolecular N-H···O(amide) hydrogen bonds in the solid state, in solution and in the gas phase [11]. Resorcinarene capsules of similar size are well-known for their ability to encapsulate small alkyl ammonium cations inside the dimer, especially quaternary ammonium cations [12-14]. As the cavity sizes of both pyridinearene and resorcinarene dimers are comparable, alkyl ammonium cations were chosen as the guests for complexation studies with ESI-Q-TOF mass spectrometry. Complex formation was tested with the following series of cationic guests: $MeNH_3^+$, $Me_2NH_2^+$, Me_3NH^+, Me_4N^+, $EtNH_3^+$, $Et_2NH_2^+$, Et_4N^+ and Pr_4N^+, which were used as the corresponding Cl^- or Br^- salts. None of the cations $MeNH_3^+$, $Me_2NH_2^+$, Me_3NH^+, $EtNH_3^+$, $Et_2NH_2^+$ or Pr_4N^+ formed complexes with **1** and $\mathbf{1}_2$ neither using electrospray ionization (ESI) in the positive nor the negative mode. Pr_4N^+ is certainly too large to fit inside the dimeric capsule, whereas the other non-complexing cations are protic and – as rather strong hydrogen bond donors – may interfere with intermolecular hydrogen bonds of the dimer. Smaller quaternary cations Me_4N^+ and Et_4N^+ were observed to form 1:1 and 2:1 host-guest complexes. With Me_4N^+, $[\mathbf{1}_2+Me_4N]^+$ was observed in the positive mode, and ions $[\mathbf{1}\text{-}2H+Me_4N]^-$ and $[\mathbf{1}_2\text{-}2H+Me_4N]^-$ in the negative mode (Figure 1). Complexation of Et_4N^+ was observed only in (–)ESI-MS as $[\mathbf{1}\text{-}2H+Et_4N]^-$ and $[\mathbf{1}_2\text{-}2H+Et_4N]^-$ ions. With the chloride and bromide salts, the abundance of cation complexes was modest, but it significantly increased, in both the positive and negative modes, when the counterion was

changed to PF_6^-, BF_4^- or I^-, which have previously been observed to form *exo* complexes with pyridinearenes [8]. In addition, ternary ion pair complexes such as $[\mathbf{1}_2+Me_4N+2A]^-$ and $[\mathbf{1}_2-H+Me_4N+A]^-$ (A = anion, i.e. PF_6^-, BF_4^-, or I^-) were detected in the negative mode.

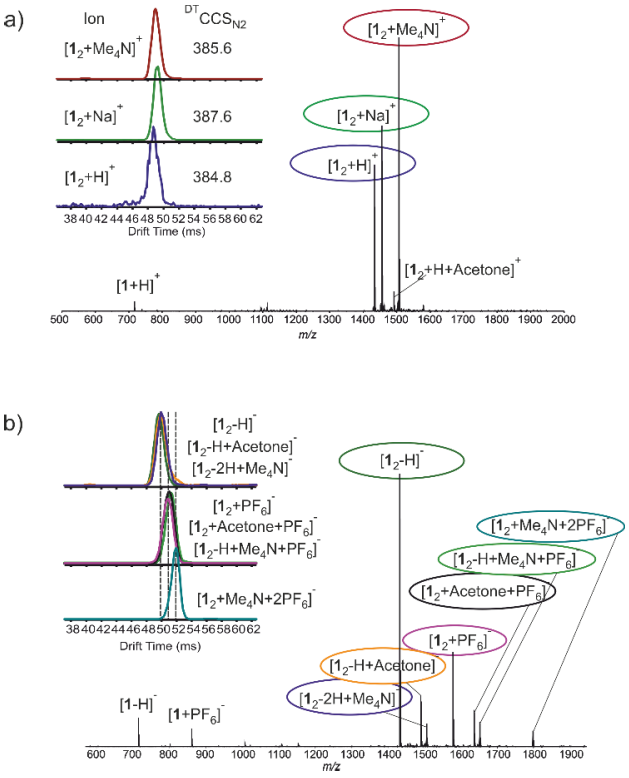

Figure 1: Spectra of **1** + Me_4NPF_6 1:3 in acetone in a) (+) ESI-MS and b) (–)ESI-MS. Insets showing arrival time distributions for selected ions. Same drift times demonstrate same structural diameters and CCS values for these ions. Separate ATDs for ions in Figure 1b are shown in ESI material (Figure S2). *m/z* values, mass accuracies and CCS values are listed in table S1.

The location (*endo* or *exo*) of the cation is of structural interest and of especial importance to understand the supramolecular chemistry of pyridinearenes. Interestingly, ternary complexes of $\mathbf{1}_2$ containing both cation and solvent are not observed in either of the ESI-MS modes, even though in earlier studies such complexes were observed with solvent and anion [11]. This points to an *endo*

location of the cation. Ion mobility mass spectrometry (IM-MS) is a powerful tool to study structural features such as the *endo*/*exo*-complexation of supramolecular complexes [11,15-18]. Drift tube ion mobility-mass spectrometry (DT-IMMS) enables the determination of structure-related collision cross section (CCS) values without complicated calibration. As depicted in Figure 1, DT-IMMS revealed that drift times for the ions $[\mathbf{1}_2+H]^+$, $[\mathbf{1}_2+Me_4N]^+$ and $[\mathbf{1}_2+Na]^+$ are very similar. In fact, the obtained $^{DT}CCS_{N2}$ [19] value for $[\mathbf{1}_2+Me_4N]^+$ (385.6 ± 0.40 Å^2) is, within the error, the same as for $[\mathbf{1}_2+H]^+$ (384.8 ± 0.41 Å^2) and smaller than $[\mathbf{1}_2+Na]^+$ complex, thus indicating inclusion. This clearly indicates that the Me_4N^+ complex of $\mathbf{1}_2$ has the same rotation averaged diameter as the protonated dimer and thus the cation is encapsulated inside the cavity. Calculated [20,21] theoretical $^{DTM}CCS_{N2}$ [22] values indicate that an *exo*-complexation of the cation should result in a ca. 10 Å^2 larger CCS (415.6 Å^2 vs. 405.7 Å^2) value as compared to the *endo*-complex. Ions $[\mathbf{1}_2-H]^-$ ($^{DT}CCS_{N2}$ = 387.0 ± 0.44 Å^2) and $[\mathbf{1}_2-2H+Me_4N]^-$ ($^{DT}CCS_{N2}$ = 389.9 ± 0.41 Å^2) also exhibit effectively the same $^{DT}CCS_{N2}$ values and show similar drift times (Figures 1 and S2, Table S1) in their arrival time distributions (ATDs). Ions $[\mathbf{1}_2+PF_6]^-$ and $[\mathbf{1}_2-H+Me_4N+PF_6]^-$ that presumably carry one *exo*-complexed anion result in ca. 9 Å^2 larger $^{DT}CCS_{N2}$ values of 395.9 ± 0.50 Å^2 and 399.6 ± 0.49 Å^2. For $[\mathbf{1}_2+Me_4N+2PF_6]^-$ with two attached counter ions, the $^{DT}CCS_{N2}$ value is even larger (5-8 Å^2 larger compared to ions with one anion). This clearly demonstrates the anions to be located in the outer periphery, while the cation is encapsulated inside the dimer.

The difference in *endo/exo* complexation is clear in IM-MS, when the larger PF_6^- anion is used in the experiment. For complexes with smaller anions BF_4^- and I^- the structural conclusions are more difficult to draw based only on CCS values, as the difference between the *endo* and *exo* complexes is smaller. To obtain complementary information, the ternary complex ions $[\mathbf{1}_2+Me_4N+2A]^-$ (A = PF_6^-, BF_4^-,

I^-) were further investigated by infrared multiphoton dissociation (IRMPD). IRMPD is an MS/MS technique, which can be utilized to study the fragmentation of supramolecular complexes [23]. In these experiments, the [**1**$_2$+Me_4N+2A]$^-$ ions were mass-selected and irradiated for 20 to 250 ms with a laser power of 95 % of 25 W. At short irradiation times, the main dissociation product was [**1**$_2$+Me_4N-2H]$^-$, which is produced after elimination of two molecules of HA (HA = H^+A^-, Schematic presentation of dissociation in Figure S4). This ion further dissociates to a neutral monomer and to [**1**-2H+Me_4N]$^-$ ion, which can only result from two HA eliminations and dissociation of the H-bonded capsule. Elimination of two HA molecules and formation of [**1**+Me_4N-2H]$^-$ would be unexpected from a complex with *exo*-complexed cation. Minor fragments resulting from a direct elimination of an ion pair are observed and [**1**$_2$+A]$^-$ appears in spectra. This likely results from a relocation of the anion to a position close to the hydrogen-bonded seam of the dimer, which is then partially opened to release the ion pair (pathway 2 in Figure S4). As all studied ternary complexes behaved similarly in the experiments, it can be stated that Me_4N^+ is located inside the cavity, while the PF_6^-, BF_4^- and I^- anions reside in the *exo*-binding site.

The binding efficiency of pyridine[4]arene towards the Me_4N^+ cation was compared to that of resorcin[4]arene, which is known to bind small cations with high affinity. **1**, **2** and Me_4NPF_6 were mixed in 1:1:1 ratio and measured by ESI-QTOF-MS. As seen in Figure 2, the resorcin[4]arene dimer [**2**$_2$+Me_4N]$^+$ was detected as the base peak in the positive mode, while [**1**$_2$+Me_4N]$^+$ was hardly observed. In addition to the pure dimers, the formation of the heterodimer [**1**•**2**+Me_4N]$^+$ was also observed. In the negative mode, heterodimers [**1**•**2**-H]$^-$ and [**1**•**2**-2H+Me_4N]$^-$ were observed with higher intensity than the corresponding homodimeric capsules of **1** or **2** (Figure S1). This is surprising due to differences in H-bonding geometry between dimers of **1** or **2**.

Previously in case of hexameric capsules heterohexamers of pyridinearene and resorcinarene were not observed [5]. The PF_6^- anion was observed to be bound to the pyridine[4]arene dimer in [**1**$_2$+PF_6]$^-$ and the heterodimer [**1**•**2**+PF_6]$^-$, but interestingly the abundance of [**1**•**2**+PF_6]$^-$ was half of [**1**$_2$+PF_6]$^-$, and PF_6^- complexes with **2** or **2**$_2$ had even lower abundance. This clearly shows that the anion has a higher affinity to pyridinearene than to resorcinarene. Inclusion complexation of solvent was also only detected with the pyridinearene homodimer (for example as the [**1**$_2$+MeCN+PF_6]$^-$ ion). This mixed host experiment shows the resorcin[4]arene affinity towards Me_4N^+ to be higher than that of pyridine[4]arene. Also, the lack of anion and/or solvent complex formation with **2** or **2**$_2$ in gas phase indicates that this binding feature is unique to pyridinearenes and it does not take place with resorcinarene. The high abundance of ternary ion pair complexes with pyridinearene, but not with resorcinarene indicates that the cation complexation process to pyridinearene is anion driven at least to some extent. The reduced electron-density in the pyridine rings is compensated by favourable "through-wall" electrostatic interactions between the *exo*-anion(s) and the *endo*-cation.

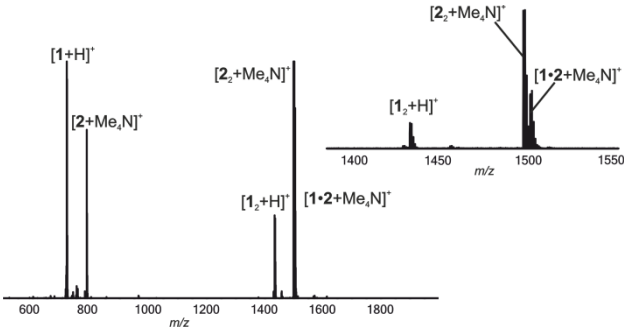

Figure 2: (+)ESI-MS profile spectrum of the mixture of **1**, **2** and $TMAPF_6$ in acetonitrile (20 μM, 1:1:1). Inset shows a zoom in for region showing dimeric ions.

In solution, by ^{1}H NMR, complexation of Me_4N^+ cation was observed with **2**, but not with **1** (Figures S5-S6). In a sample of 10 mM **2** and Me_4NPF_6 (1:3 ratio in

$CDCl_3/CD_3CN$ 4:3 v:v mixture) a 0.35 ppm upfield shift was observed in Me_4N^+ signal. In a sample of **1** and Me_4NPF_6 no shift is observed. This clearly indicates that also in solution **1** does not possess similar affinity towards Me_4N^+ cation as **2**. Also, all our attempts to obtain solid-state single crystal structure of **1** with cationic guest were unsuccessful. It is possible that observation of complexes require special conditions present in ESI source.

To obtain more detailed insight into the observed gas phase structures, DFT calculations were carried out for **1**, $\mathbf{1}_{OH}$, $\mathbf{1}_2$, $[\mathbf{1}_2+Me_4N_{endo}]^+$, $[\mathbf{1}_2+Me_4N_{exo1}]^+$, $[\mathbf{1}_2+Me_4N_{exo2}]^+$, $[\mathbf{1}_2+Me_4N_{endo}+I_{endo}]$, $[\mathbf{1}_2+Me_4N_{endo}+I_{exo}]$, $[\mathbf{1}_2+Me_4N_{endo}+2I_{exo}]^-$, $[\mathbf{1}_2+I_{exo}]^+$, and $[\mathbf{1}_2+2I_{exo}]^+$ (Figure S7) without (PBE0/def2-TZVP) and with (PBE0-D3/def2-TZVP) dispersion correction because in the gas phase dispersion plays an important role in the formation of supramolecular complexes [24-30]. Conformational analysis was first performed for both tautomers of monomer to ensure that further calculations were carried out for the most stable tautomer. The conformational analysis revealed that the pyridone tautomer (**1**) is ~150 kJ/mol lower in energy than the dihydroxyl tautomer ($\mathbf{1}_{OH}$). The geometry optimizations showed that the geometry of $[\mathbf{1}_2+Me_4N_{endo}]^+$ is similar without and with dispersion correction (hydrogen bond lengths are listed in Table S2). This is expected, because the standard hybrid functionals are able to describe strong hydrogen bonds such as NH···O and OH···O in a reasonable manner [31,32]. Due to the encapsulated guest molecule, the $[\mathbf{1}_2+Me_4N_{endo}]^+$ complex has slightly longer NH···O and OH···O bonds than empty $\mathbf{1}_2$. The addition of I^- anion(s) at the lower rim(s) of $[\mathbf{1}_2+Me_4N_{endo}]^+$ has hardly any influence on the length of NH···O and OH···O bonds as exemplified by the hydrogen bond lengths of $[\mathbf{1}_2+Me_4N_{endo}+I_{exo}]$ and $[\mathbf{1}_2+Me_4N_{endo}+2I_{exo}]^-$. The same trend is also observed for cation-free complexes ($[\mathbf{1}_2+I_{exo}]^-$ and $[\mathbf{1}_2+2I_{exo}]^{2-}$) if their NH···O and OH···O bond lengths are compared to those in $\mathbf{1}_2$.

Calculations were also carried out for complexes, where *exo* binding of cation was considered. The geometry optimization yields two different geometries, $[\mathbf{1}_2+Me_4N_{exo1}]^+$ and $[\mathbf{1}_2+Me_4N_{exo2}]^+$ (Figure S7). In $[\mathbf{1}_2+Me_4N_{exo1}]^+$, the Me_4N^+ cation interacts with lower rim isobutyl groups only when the dispersion interaction is included in calculations, whereas at the PBE0/def2-TZVP level $[\mathbf{1}_2+Me_4N_{exo1}]^+$ is not a stable minimum on the potential energy surface and results in additional *exo* complex, namely $[\mathbf{1}_2+Me_4N_{exo2}]^+$, in which Me_4N^+ cation resides in proximity to the seam of hydrogen bonds. The NH···O and OH···O bond distances for $[\mathbf{1}_2+Me_4N_{exo1}]^+$ are almost identical with $\mathbf{1}_2$ indicating that the coordination of the Me_4N^+ cation at the lower rim has only a minor effect on the hydrogen bond network of $\mathbf{1}_2$. To verify complexation of separate ion pair, the geometry optimization was carried out also for $[\mathbf{1}_2+Me_4N_{endo}+I_{endo}]$, which showed that the cavity of $\mathbf{1}_2$ is too small for the simultaneous complexation of anionic and cationic guests, resulting in a partial rupture of the hydrogen-bonding seam and ~100 kJ/mol weaker interaction energy compared to $[\mathbf{1}_2+Me_4N_{endo}+I_{exo}]$, (Figure S7 and Table S2).

To illustrate the unsuitability of lower rim for binding cationic guests, we mapped the ESP surfaces for **1**, $\mathbf{1}_2$, $[\mathbf{1}_2+Me_4N_{endo}]^+$, $[\mathbf{1}_2+Me_4N_{exo1}]^+$, and $[\mathbf{1}_2+Me_4N_{exo2}]^+$. Although the ESP surface of **1** show some π-acidic character for the cavity, as depicted in Figure 3, the electron-poor areas of $\mathbf{1}_2$, $[\mathbf{1}_2+Me_4N_{endo}]^+$, $[\mathbf{1}_2+Me_4N_{exo1}]^+$, and $[\mathbf{1}_2+Me_4N_{exo2}]^+$ (See also Figures S9-S10) are more concentrated on the lower rim isobutyl groups than on the seam of the hydrogen bonds that actually contains electron-rich oxygen atoms that can interact with Me_4N^+ cation through ion-dipole interactions. In the gas phase and in the absence of the dispersion force, the positively charged Me_4N^+ cation, therefore, prefer interaction with the electron-rich oxygen atoms of hydrogen bond network to the positively charged lower rim isobutyl group.

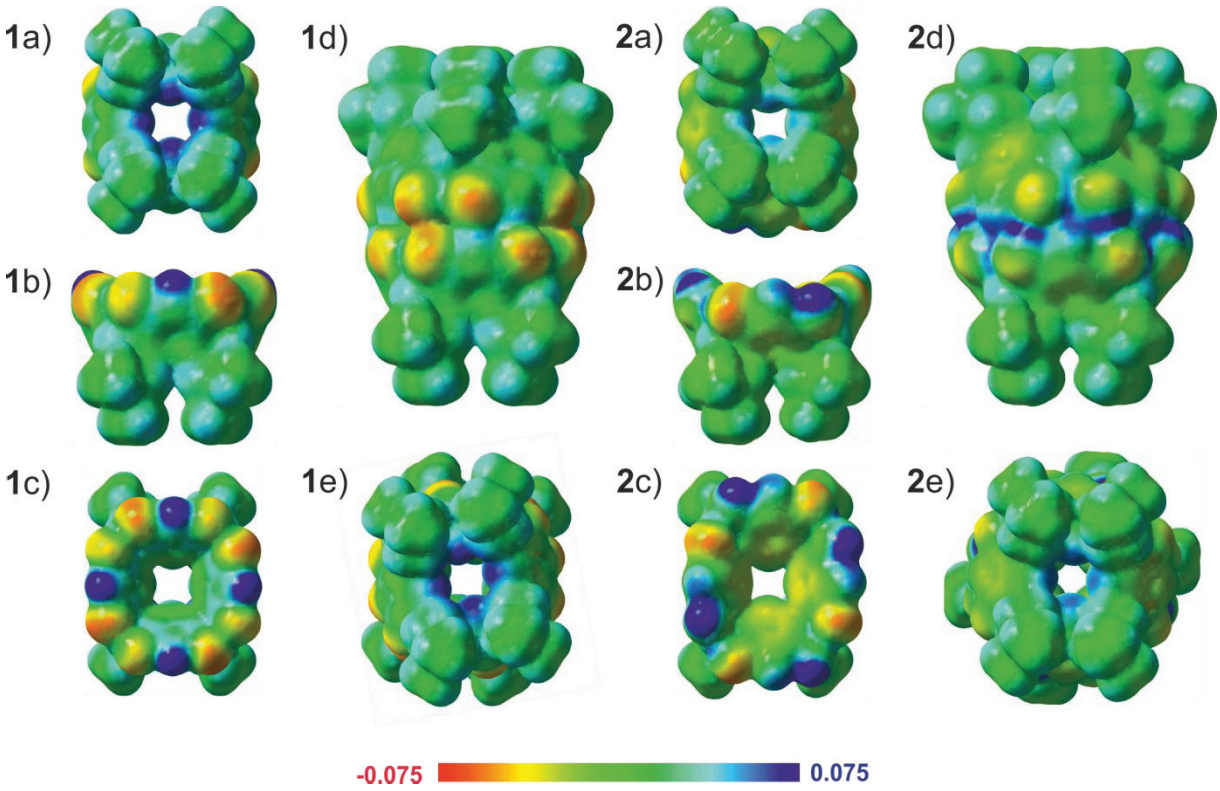

Figure 3: Calculated ESP surfaces (in au) superimposed on the total electron density (0.004 au) for **1** and **2:** a) monomer, bottom view b) monomer, side view c) monomer, top view, d) dimer, side view and e) dimer, bottom view. Red, blue and green surfaces indicate negative, positive and neutral ESP, respectively.

The calculated interaction energies are listed in Table S2. When the dispersion correction and/or the counterion(s) are taken into account, the energy analysis supports the findings obtained from ESI-MS studies, geometry optimizations and ESP surfaces: The Me_4N^+ cation is most likely bound inside in the cavity of $\mathbf{1}_2$. It is also important to note that the calculated dispersion-corrected interaction energy of $[\mathbf{1}_2+Me_4N_{exo1}]^+$ (-37 kJ/mol) is roughly two fifth of the interaction energy of $[\mathbf{1}_2+Me_4N_{exo2}]^+$ (-98 kJ/mol) because there is no favourable ion-dipole interaction between $\mathbf{1}_2$ and Me_4N^+ in $[\mathbf{1}_2+Me_4N_{exo1}]^+$. Even though the encapsulation of the Me_4N^+ cation is a favourable process already even without anions, the calculated

interaction energies show that the complexation of cationic guest can be enhanced by the additional *exo*-complexation of anions to the lower rims. The interaction energies of [**1**$_2$+Me_4N_{endo}], [**1**$_2$+Me_4N_{endo}+I_{exo}], and [**1**$_2$+Me_4N_{endo} +2I_{exo}]$^-$, increases from -152 kJ/mol to -342 kJ/mol, and -521 kJ/mol, respectively, when the amount of I^- anions is increased in the complex. Moreover, the calculated interaction energies illustrate well that the dispersion interaction has considerable influence on the interaction energies of [**1**$_2$+Me_4N_{endo}]$^+$ (-126.4 kJ/mol), [**1**$_2$+Me_4N_{exo1}]$^+$ (-37.5 kJ/mol), [**1**$_2$+Me_4N_{exo2}]$^+$ (-23.2 kJ/mol), [**1**$_2$+Me_4N_{endo}+I_{exo}] (-130.5 kJ/mol), and [**1**$_2$+Me_4N_{endo}+2I_{exo}]$^-$ (-133.7 kJ/mol), although their geometries are similar at both levels of theory. This means that pyridinearene dimers and their complexes are already sufficiently large supramolecular systems in which the omnipresent dispersion interaction can add up to a substantial force due to multiple interaction sites.

Calculations were also carried out for **2**, **2**$_2$, [**2**$_2$+Me_4N_{endo}]$^+$, [**2**$_2$+I_{exo}]$^+$, and [**2**$_2$+2I_{exo}]$^+$, at the PBE0-D3/def2-TZVP level of theory (Fiure S8) to explain the observed difference between **1** and **2** in experimental ESI-MS studies. If the interaction energies of [**2**$_2$+Me_4N_{endo}]$^+$ (-220 kJ/mol) and [**1**$_2$+Me_4N_{endo}]$^+$ (-152 kJ/mol) are compared it is evident that **2**$_2$ is better host for Me_4N^+ cation than **1**$_2$.On the other hand, when comparing the interaction energies of complexes [**2**$_2$+I_{exo}]$^+$ (-149 kJ/mol), [**2**$_2$+2I_{exo}]$^+$ (-170 kJ/mol), [**1**$_2$+I_{exo}]$^+$ (-175 kJ/mol), and [**1**$_2$+2I_{exo}]$^+$ (-223 kJ/mol), it can be stated that **1**$_2$ has stronger affinity towards anions than **2**$_2$. These results are fully in line with the MS studies and calculated ESP surfaces. By comparing the calculated ESP surfaces of **1** and **2** in Figure 3, it is a clear that the π-basic character of the cavity is more pronounced in **2** than **1**. The investigation of ESP surfaces of **1**, **1**$_2$, **2**, and **2**$_2$ also reveal that the lower rims of pyridine[4]arenes **1** and **1**$_2$ are more electron deficient than **2** and **2**$_2$, explaining the weaker affinity of **2** and **2**$_2$ towards anions.

Moreover, if only the calculated interaction energies of anionic complexes $[\mathbf{2}_2+I_{exo}]^+$ (-149 kJ/mol), $[\mathbf{2}_2+2I_{exo}]^+$ (-170 kJ/mol), $[\mathbf{1}_2+I_{exo}]^+$ (-175 kJ/mol), and $[\mathbf{1}_2+2I_{exo}]^+$ (-223 kJ/mol) are compared, it can be concluded that $\mathbf{1}_2$ has stronger affinity towards anions than $\mathbf{2}_2$.

Conclusion

In conclusion, we have shown that the pyridine[4]arene dimer, which until recently was considered to be an anion receptor, can bind also cationic guests. The Me_4N^+ cation was observed to bind to the pyridine[4]arene dimer, and all mass spectrometric data and theoretical calculations show undoubtedly that the cation is located inside the cavity of the dimer in gas phase. It is an interesting fact, that the binding properties of pyridine[4]arene differ from earlier reports [7,8]. However, cation binding to pyridinearene is clearly not as strong as with resorcin[4]arene, which is known for its excellent cation receptor properties. A comparison of these two macrocyclic hosts reveals significant differences in their binding properties. Pyridine[4]arene appears to have better affinity towards neutral guests and has also higher affinity to complex anions at the *exo*-binding sites at the lower rim, whereas resorcin[4]arene clearly has a higher affinity towards cations. However, the pyridinearene's ability to form *exo*-complexes with anions can assist its ability to bind cations in endo-position.

Experimental

The compound **1** and **2** have been prepared according to the reported procedures [11,33,34]. Salts were commercially available (From Aldrich, Fluka and TCI) and used as received.

Mass spectrometric experiments have been performed with ABSciex QSTAR Elite ESI-Q-TOF mass spectrometer. Ion Mobility mass spectrometry experiments were conducted with Waters Synapt G2 equipped with a linear drift cell and Agilent 6560 Ion mobility Q-TOF mass spectrometers. All CCS values were obtained using nitrogen as a drift gas and stepped field methods. IRMPD experiments were performed with Ionspec QFT-7 ESI-FT-ICR with a 7 T superconducting magnet. Samples for all mass spectrometric experiments were prepared with 10 or 20 μM concentration and 1:3 host:guest ratio in acetone. Theoretical CCS values were calculated using IMoS [20,21].

NMR experiments were performed with Bruker Avance III HD 300 NMR Spectrometer. Samples were prepared with 10 mM concentration and 1:3 host:guest ratio in $CDCl_3/CD_3CN$ (4:3, v:v) mixture.

DFT calculations were performed by Spartan' 16 and Gaussian 09 (D01) software packages.

More detailed information of the experiments and parametrization can be found from supporting information.

Supporting Information

Supporting Information File 1:

File Name: SI_Pyridinearenes_manuscript_BJOC_Kalenius

File Format: PDF

Title: Experimental details and supplementary information

Acknowledgements

We wish to thank The Academy of Finland (projects 284562, 278743 and 312514 to E.K. and 285855 to J.O.M.), the University of Jyväskylä and the Deutsche Forschungsgemeinschaft (Core Facility BioSupraMol) for financial support. J.O.M wishes to acknowledge CSC – IT Center for Science, Finland, and Prof. Heikki M. Tuononen for computational resources. A. Kruve is grateful for a postdoctoral fellowship from the Alexander von Humboldt Foundation. Prof. Magdalena Zimnicka is gratefully acknowledged for her assistance and helpful discussions regarding the determination of theoretical CCS values.

ORCID® iDs

Anniina Kiesilä - https://orcid.org/0000-0002-2952-2377

Jani O. Moilanen - https://orcid.org/0000-0002-2096-593X

Anneli Kruve - https://orcid.org/0000-0001-9725-3351

Christoph A. Schalley - https://orcid.org/0000-0002-8634-3578

Perdita Barran - https://orcid.org/0000-0002-7720-586X

Elina Kalenius - https://orcid.org/0000-0001-8038-1314

References

1. Timmerman, P.; Verboom, W.; Reinhoudt, D. N. *Tetrahedron* **1996**, *52*, 2663–2704.

2. Avram, L.; Cohen, Y. *J. Am. Chem. Soc*. **2002**, *124*, 15148–15149.

3. Palmer, L. C.; Shivanyuk, A.; Yamanaka, M.; Rebek, J. Jr. *Chem. Commun*. **2005**, *0*, 857–858.

4. Gerkensmeier, T.; Mattay, J.; Näther, C. *Chem. Eur. J*. **2001**, *7*, 465–474.

5. Evan-Salem, T.; Cohen, Y. *Chem. Eur. J.* **2007**, *13*, 7659–7663.

6. Kiesilä, A.; Beyeh, N. K.; Moilanen, J. O.; Puttreddy, R.; Götz, S.; Rissanen, K.; Barran, P.; Lützen, A.; E. Kalenius. *Org. Biomol. Chem.* **2019**, *17*, 6980–6984.

7. Letzel, M. C.; Decker, B.; Rozhenko, A. B.; Schoeller, W. W.; Mattay, J. *J. Am. Chem. Soc*. **2004**, *126*, 9669–9674.

8. Rozhenko, A. B.; Schoeller, W. W.; Letzel, M. C.; Decker, B.; Mattay, J. *New J. Chem*. **2013**, *37*, 356–365.

9. Schottel, B. L.; Chifotides, H. T.; Dunbar, K. R. *Chem. Soc. Rev*. **2008**, *37*, 68–83.

10. Dawson, R. E.; Hennig, A.; Weimann, D. P.; Emery, D.; Ravikumar, V.; Montenegro, J.; Takeuchi, T.; Gabutti, S.; Mayor, M.; Mareda, J.; Schalley, C. A.; Matile, S. *Nat. Chem*. **2010**, *2*, 533–538.

11. Kiesilä, A.; Kivijärvi, L.; Beyeh, N. K.; Moilanen, J. O.; Groessl, M.; Rothe, T.; Götz, S.; Topić, F.; Rissanen K.; Lützen, A.; Kalenius, E. *Angew. Chem. Int. Ed*. **2017**, *56*, 10942–10946.

12. Murayama, K.; Aoki, K. *Chem. Commun*. **1998**, *0*, 607–608.

13. Mansikkamäki, H.; Nissinen, M.; Schalley, C. A.; Rissanen. K. *New J. Chem*. **2003**, *27*, 88–97.

14. Mäkinen, M.; Vainiotalo, P.; Nissinen, M.; Rissanen, K. *J. Am. Soc. Mass Spectrom*. **2003**, *14*, 143–151.

15. Kalenius, E.; Groessl, M.; Rissanen, K. *Nat. Rev. Chem*. **2019**, *3*, 4-14.

16. Lee, T-C.; Kalenius, E.; Lazar, A. I.; Assaf, K. I.; Kuhnert, N.; Grün, C. H.; Jänis, J.; Scherman, O. A.; Nau, W. M. *Nat. Chem*. **2013**, *5*, 376–382.

17. Dearden, D. V.; Ferrell, T. A.; Asplund, M. C.; Zilch, L. W.; Julian, R. R.; Jarrold. M. F. *J. Phys. Chem. A* **2009**, *113*, 989–997.

18. Jurček, O.; Bonakdarzadeh, P.; Kalenius, E.; Linnanto, J. M.; Groessl, M.; Knochenmuss, R.; Ihalainen, J. A.; Rissanen, K. *Angew. Chem. Int. Ed*. **2015**, *54*, 15462–15467.

19. $^{DT}CCS_{N2}$ states for CCS values obtained using drift tube instrument with nitrogen gas, nomenclature recommended in Gabelica V. *et al*., *Mass Spectrom. Rev*. **2019**, *38*, 291-320.

20. Larriba, C.; Hogan C. J. Jr., *J. Comput. Phys*. **2013**, *251*, 344-363.

21. Larriba, C.; Hogan C. J. Jr. *J. Phys. Chem. A* **2013**, *117*, 3887-3901.

22. $^{DTM}CCS_{N2}$ states for CCS values obtained using diffuse trajectory method with nitrogen gas.

23. Beyeh, N. K.; Kogej, M.; Åhman, A.; Rissanen, K.; Schalley, C. A. *Angew. Chem. Int. Ed*. **2006**, *45*, 5214–5218.

24. Ernzerhof, M.; Scuseria, G. E. *J. Chem. Phys.* **1999**, *110*, 5029–5036.

25. Adamo, C.; Barone, V. *J. Chem. Phys.* **1999**, *110*, 6158–6170.

26. Weigend, F.; Ahlrichs, R. *Phys. Chem. Chem. Phys.* **2005**, *7*, 3297–3305.

27. Grimme, S.; Antony, J.; Ehrlich, S.; Krieg, H. *J. Chem. Phys.* **2010**, *132*, 154104.

28. Grimme, S.; Ehrlich, S.; Goerigk, L. *J. Comput. Chem.* **2011**, *32*, 1456–1465.

29. Hermann, J.; DiStasio, R. A.; Tkatchenko, A. *Chem. Rev.* **2017**, *117*, 4714–4758.

30. Ambrosetti, A.; Alfè, D.; Distasio, R. A.; Tkatchenko, A. *J. Phys. Chem. Lett.* **2014**, *5*, 849–855.

31. Rao, L.; Ke, H.; Fu, G.; Xu, X.; Yan, Y. *J. Chem. Theory Comput.* **2009**, *5*, 86–96.

32. Ireta, J.; Neugebauer, J.; Scheffler, M. *J. Phys. Chem. A* **2004**, *108*, 5692–5698.

33. Högberg, A.G.S. *J. Org. Chem*. **1980**, *45*, 4498-4500.

34. Tunstad, L. M.; Tucker, J. A.; Dalcanale, E.; Weiser, J.; Bryant, J. A.; Sherman, J. C.; Helgeson, R. C.; Knobler, C. B.; Cram, D. J. *J. Org. Chem*. **1989**, *54*, 1305–1312.

III

THERMODYNAMICALLY DRIVEN SELF-ASSEMBLY OF PYRIDINEARENE TO HEXAMERIC CAPSULES

by

A. Kiesilä, N. K. Beyeh, J. O. Moilanen, R. Puttreddy, Sven Götz, K. Rissanen, P. Barran, A. Lützen & E. Kalenius.

Organic and Biomolecular Chemistry, **2019,** *17*, 6980 – 6984

Organic & Biomolecular Chemistry

COMMUNICATION

View Article Online
View Journal

Cite this: DOI: 10.1039/c9ob01383k

Received 19th June 2019,
Accepted 1st July 2019

DOI: 10.1039/c9ob01383k

rsc.li/obc

Thermodynamically driven self-assembly of pyridinearene to hexameric capsules†

Anniina Kiesilä,[a] Ngong Kodiah Beyeh,[b] Jani O. Moilanen,[a] Rakesh Puttreddy,[a] Sven Götz,[c] Kari Rissanen,[a] Perdita Barran,[d] Arne Lützen[c] and Elina Kalenius *[a]

Pyridinearene macrocycles have previously shown unique host–guest properties in their capsular dimers including *endo* complexation of neutral molecules and *exo* complexation of anions. Here, we demonstrate for the first time the formation of hydrogen bonded hexamer of tetraisobutyl-octahydroxypyridinearene in all three states of matter – gas phase, solution and solid-state. Cationic tris(bipyridine)ruthenium(II) template was found to stabilize the hexamer in gas phase, whereas solvent molecules do this in condensed phases. In solution, the capsular hexamer was found to be the thermodynamically favoured self-assembly product and transition from dimer to hexamer occurred in course of time. The crystal structure of hexamer revealed 24 N–H···O direct intermolecular hydrogen bonds between the six pyridinearene macrocycles without any bridging solvent molecules. Hydrogen bond patterns correlate well with DFT computed structures. Thus, all structural chemistry methods (IM-MS, DOSY NMR, DFT, X-ray crystallography) support the same structure of the hexameric capsule that has a diameter of *ca.* 3 nm and volume of 1160 Å^3.

Introduction

Capsular supramolecular structures are tempting species, as they enable encapsulation of guest molecules and their voids may act as confined spaces suitable for nanocatalysis.[1] Resorcinarenes and pyrogallarenes (see Scheme 1), have been long known for their capability to spontaneously self-assemble into large hexameric capsules.[2] Interestingly, the hydrogen bonding network in resorcinarene hexamers typically involve bridging solvent molecules, which might even be responsible for their unique catalytic activity.[4] Both resorcinarenes and pyrogallarenes have demonstrated their ability to encapsulate various guest molecules in the voids of their capsular dimeric and hexameric assemblies.[2,3]

Pyridinearene[5] (**1** in Scheme 1) is closely related to resorcinarene and pyrogallarene. Despite their obvious structural similarities, pyridinearenes display different binding properties due to amide–iminol tautomerism and electronic properties arising from the pyridine ring.[6] From the two tautomeric forms, dihydroxy and hydroxy-oxo, only the latter has been observed in crystal structures.[6] Recently, conformational analysis for the tautomers also revealed that the hydroxy-oxo

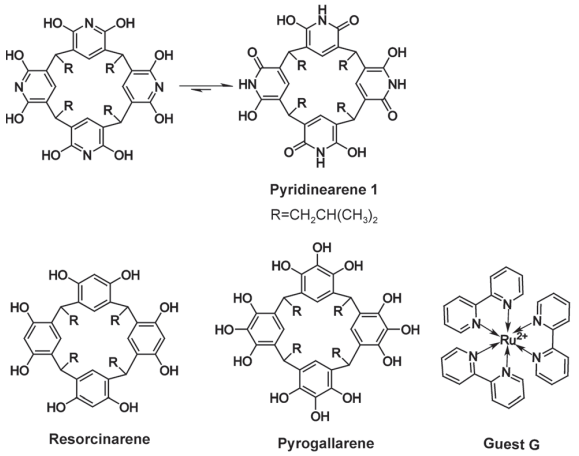

Scheme 1 Structures of tetraisobutyl-pyridinearene **1**, tris(bipyridine) ruthenium(II) guest (**G**), resorcinarene and pyrogallarene. For pyridinearene two tautomeric forms are shown, but equilibrium is greatly favoring hydroxy-oxo tautomer.

[a]*Department of Chemistry, Nanoscience Center, P. O. Box 35, FI-40014 University of Jyväskylä, Finland. E-mail: Elina.o.kalenius@jyu.fi*
[b]*Oakland University, Department of Chemistry, 146 Library Drive, Rochester, Michigan, 48309-4479, USA*
[c]*University of Bonn, Kekulé-Institute of Organic Chemistry and Biochemistry, A, D-53121 Bonn, Germany*
[d]*Michael Barber Centre for Collaborative Mass Spectrometry, Manchester Institute of Biotechnology, School of Chemistry, The University of Manchester, Princess Street, Manchester, UK*

†Electronic supplementary information (ESI) available: Mass spectrometry, NMR, X-Ray crystallography and DFT calculations. CCDC 1899745. For ESI and crystallographic data in CIF or other electronic format see DOI: 10.1039/c9ob01383k

tautomer (Scheme 1) is ~150 kJ mol^{-1} lower in energy than the dihydroxy tautomer.[7]

The cavity of pyridinearene was earlier considered electron deficient and suitable to bind anionic guests.[8,9] Recently, instead of encapsulation of anions, the pyridinearene dimers were shown to actually favour encapsulation of neutral guests of matching size, and hence maximizing dispersion interactions. In fact, pyridinearenes bind anions, but outside the cavity, in *exo* position between the lower rim alkyl chains *via* CH···anion interactions.[6] Although the cavity of pyridinearenes is most suitable for neutral guests, also anion-driven encapsulation of cations inside the pyridinearene dimers was recently demonstrated.[7]

In one of the earliest reports concerning the self-assembly of pyridinearene, two species were observed in chloroform solution which were initially erroneously assigned as a mixture of monomers and dimeric assemblies.[9] Cohen *et al.* later proved these as dimeric and hexameric species using diffusion ordered (DOSY) NMR spectroscopy experiments.[10] In here, we report a detailed study of pyridinearene hexamer formation and structure in solution (NMR, DOSY NMR), in solid-state (X-ray crystallography) and in the gas phase (IM-MS, ESI-QTOF MS, DFT calculations).

Results and discussion

In the gas phase, by ESI-QTOF mass spectrometry, **1** typically ionizes well through deprotonation or anion complex formation (with PF_6^-, BF_4^- or I^-). Despite many attempts, no traces of hexamer was detected in the negative mode. Similar hexameric capsules based on resorcinarene or pyrogallarene molecules have been earlier detected on positive mode by using a spherical and cationic transition metal complexes[11] as the stabilizing templates.[3] We, therefore, chose tris(bipyridine) ruthenium(II) (see Scheme 1, guest **G**) as a suitable complementary template. The cavity size for pyridinearene assemblies are roughly comparable to the size of corresponding assemblies of resorcinarenes and pyrogallarenes, but the affinity of pyridinearene towards cationic guests is lower. Nevertheless, when a sample of **1** (60 μM) with **G** (1 : 6) was sprayed from an acetone/dichloromethane (1 : 1 v/v) mixture, a host–guest hexameric assembly $[\mathbf{1}_6 + \mathbf{G}]^{2+}$ was detected in the mass spectrum (Fig. 1). In addition, a pentameric host–guest $[\mathbf{1}_5 + \mathbf{G}]^{2+}$ and a dimeric $[\mathbf{1}_2 + \mathrm{H}]^+$ complexes were also observed, but the hexameric assembly was clearly the dominating ion in the spectrum (Fig. 1). Ion $[\mathbf{1}_5 + \mathbf{G}]^{2+}$ likely originates from the hexamer through fragmentation. Assemblies larger than the hexamer, namely heptamers or octamers were not observed. The abundance of hexameric ion and lack of other aggregates in the spectrum suggest that hexamer could be a hydrogen bonded capsule rather than an unspecific aggregated system or a polymer.‡

To get actual proof whether the studied system is really a capsular assembly, ion mobility mass spectrometry (IM-MS) was utilized to acquire ion mobility arrival time distribution (ATD) and to determine the structure related collision cross

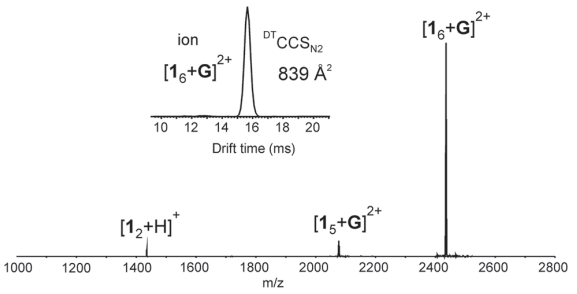

Fig. 1 (+)ESI-MS spectrum of **1** (60 μM) and tris(bipyridine)ruthenium(II) (**G**) with 6 : 1 ratio measured from acetone/DCM mixture. Inset showing IMS arrival time distribution (ATD) for $[\mathbf{1}_6 + \mathbf{G}]^{2+}$ ion.

section (CCS) value for the hexamer. IM-MS has already demonstrated its power in structural analysis of different supramolecular systems.[12] In the ATD only a single well-resolved peak was observed. This implies that the corresponding $[\mathbf{1}_6 + \mathbf{G}]^{2+}$ ion has a relatively rigid well-defined structure. When a drift tube ion mobility (DT-IMMS) instrument employing helium as a drift gas was used, an experimental $^{DT}CCS_{He}$ value of 746.4 Å^2 was obtained.§ If a spherical structure is assumed, this corresponds roughly to a diameter of 3.1 nm for the assembly. The theoretical $^{DTM}CCS_{He}$ was calculated on basis of the DFT calculated structure by using diffuse trajectory method and yielded a $^{DTM}CCS_{He}$ of 748.2 Å^2,[13]¶ which is in good agreement with the experimental value. When more polarizable nitrogen was used as a drift gas, the $^{DT}CCS_{N2}$ value was determined as 838.7 Å^2.‖ This roughly corresponds to a sphere with a diameter of 3.3 nm. The theoretical $^{DTM}CCS_{N2}$ of 928.3 Å^2 for the $[\mathbf{1}_6 + \mathbf{G}]^{2+}$ ion indicate slightly bigger difference between experimental and theoretical values when N_2 is used as a drift gas. In general, these CCS values are in good agreement with dimensions reported earlier for hexameric capsules of pyrogallarenes and resorcinarenes,[14,15] and thus, verify that the gas phase structure is indeed a capsular hexameric assembly.

The self-assembly of **1** was further studied in solution by ^{1}H and DOSY NMR (in $CDCl_3$ at 298 K). In a 20 mM solution of **1**, two different species were observed in ^{1}H NMR spectra shortly after preparing the sample (Fig. 2a): one causing signals at 4.28 and 7.10 ppm (d/d′), and another (h/h′) with signals at 4.36 and 7.22 ppm. The ratio of these two (d : h) was 2 : 1. The diffusion coefficient determined for assembly d was 0.411×10^{-5} cm^2 s^{-1}, and 0.287×10^{-5} cm^2 s^{-1} for assembly h. These values are in accordance with earlier results from Cohen,[10] and confirm that the signal sets d/d′ and h/h′ correspond to the dimer and the hexamer of **1**. These values are in the expected range when compared with the diffusion coefficients of the corresponding assemblies of resorcinarene and pyrogallarene, which were used as internal standards. Assuming spherical shapes of these assemblies this translates into diameters of 2.0 nm for the dimer and 2.8 nm for the hexamer using the Stokes–Einstein equation (see ESI†). These

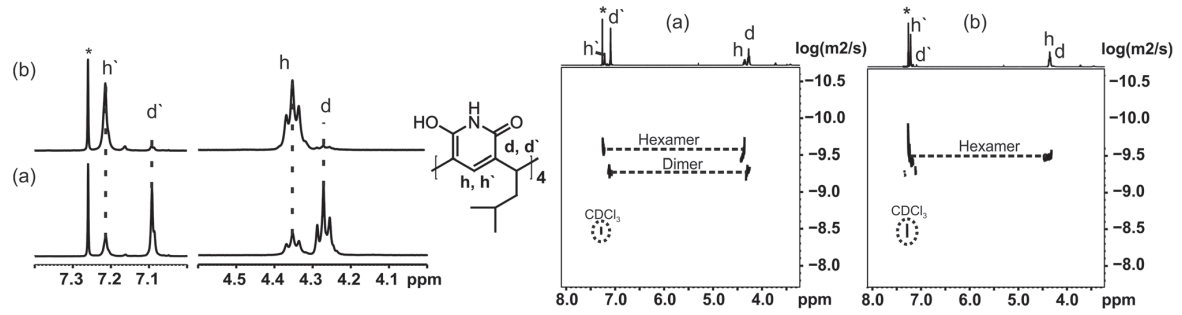

Fig. 2 Left: ^{1}H NMR of **1** (20 mM in $CDCl_3$) (a) measured within 2 hours after sample preparation and (b) same sample after 7 days from sample preparation. Right: DOSY NMR of the same sample (a) measured within 2 hours form sample preparation and (b) after 7 days from sample preparation. Signals d and d′ correspond to the dimeric assembly and signals h and h′ to the hexameric assembly.

values are also well in line with the observed gas phase structures and determined CCS values. The DOSY NMR experiment in Fig. 2a was measured within 2 hours after sample preparation and shows the dimeric assembly as more abundant (2 : 1). The same NMR sample was stored and re-measured after seven days showing that the intensity of the signals for the dimer diminished dramatically, while at the same time signals for the hexamer increased and were now dominating (ratio d : h 1 : 10). This can also be seen in DOSY NMR, where only the signal of hexamer is observed after 7 days from sample preparation (Fig. 2b). This shows that pyridinearene forms indeed both dimeric and hexameric capsules in solution but the dimeric capsule is obviously only the kinetically favoured product while the hexameric capsule is the thermodynamic product, which abundance increases over time.

Single crystals suitable for X-ray diffraction analysis were obtained by slow vapour diffusion of diisopropyl ether into the solution of **1** in chloroform. Block shaped crystals were formed and the hexamer structure ($\mathbf{1}_6$) in the solid-state could be confirmed by X-ray crystallography (Fig. 3a). The asymmetric unit contains three crystallographically independent molecules of **1**, and the resultant self-assembled hexameric structure contains 24 O–H···O and 24 N–H···O hydrogen bonds. As a result of hydroxy-oxo tautomer form, the 6-hydroxyl position in 6-hydroxy-2(1*H*)-pyridone units manifest four O–H···O circular intramolecular hydrogen bonds to give **1** bowl-like C_{4v} conformation. The intermolecular N–H···O hydrogen bonding between the pyridone units in $\mathbf{1}_6$ provides a compact internal cavity with volume of 1160 Å^3. This is smaller than corresponding hexameric capsules based on resorcinarenes and

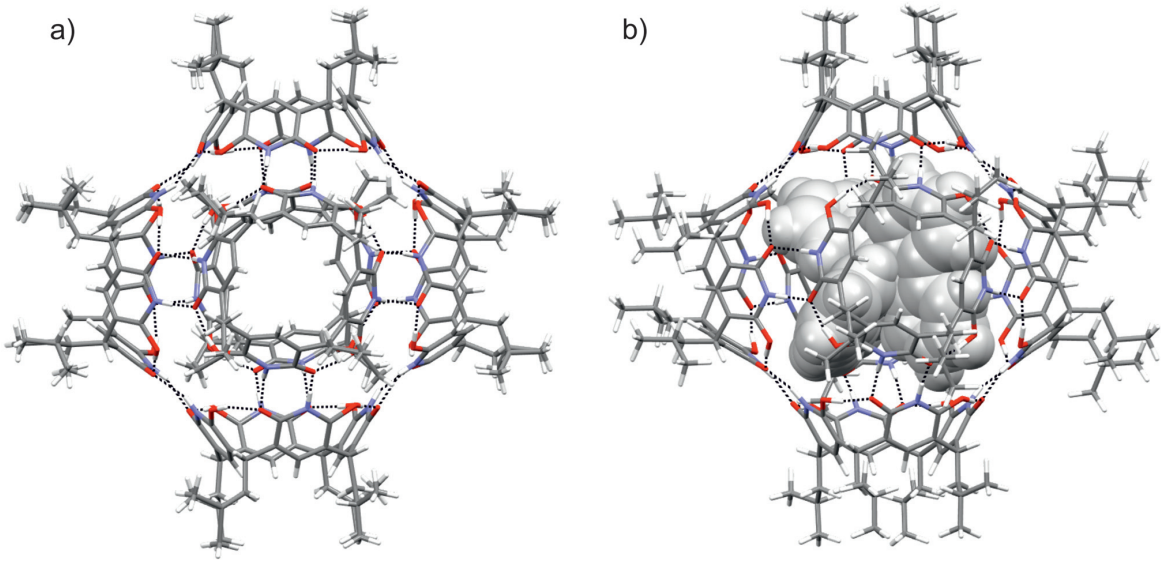

Fig. 3 X-Ray crystal structure of $\mathbf{1}_6$ and (b) optimized structure of $[\mathbf{1}_6 + \mathbf{G}]^{2+}$ at the RI-PBE-D3/def2-SVP level of theory in capped stick model. Tris (bipyridine)-ruthenium(II) (**G**) is shown in grey CPK model in (b). Black dashed lines represent hydrogen bonds. Color code: H = white, C = grey, N = blue, O = red.

pyrogallarenes (volumes >1200 Å^3, see ESI Fig. S4†).[14,15] The DOSY derived hydrodynamic radii (2.80 nm) agrees well with the calculated value obtained from the X-ray crystal structure (2.82 nm). Of special note, the hydroxy-oxo tautomerism renders **1** a rigid cavity and definite directionality for hydrogen bonding. Robust C_{4v} cavities are seamed together with direct N–H···O intermolecular hydrogen bonding to produce solvent-free hexamer $\mathbf{1}_6$. Solvent-free hydrogen bonding is also observed in the solid-state pyrogallarene hexamer structures.[14] In the resorcinarene hexamers, due to flexible C_{4v} cavities and steric reasons solvent molecules typically assist in capsule formation *via* intermolecular hydrogen bonding interactions, found between two resorcinarene units.[15] Although chloroform is essential to obtain a stable $\mathbf{1}_6$ single-crystals its passive role in hydrogen bonding could be observed in the 3-D crystal lattice. The features of pyridinearene lead to unique and complementary alignment of the individual monomers in order to maximize the number of intermolecular hydrogen bonds. In the case of the resorcinarenes, this requires incorporation of solvent molecules as part of the intermolecular hydrogen bond network. Consequently, this causes the differences in the void size for three different hexamers.

Unfortunately, all our attempts to obtain single crystals from $[\mathbf{1}_6 + \mathbf{G}]^{2+}$ were unsuccessful. Therefore, we decided to carry out the computational analysis for studied systems at the RI-PBE-D3/def2-SVP//RI-PBE-D3/def2-TZVP level of theory in order to investigate the gas phase structure of $\mathbf{1}_6$ and $[\mathbf{1}_6 + \mathbf{G}]^{2+}$ and to evaluate their interaction energies in detail.[16–24]

The optimized structures and hydrogen bonding patterns of $\mathbf{1}_6$ and $[\mathbf{1}_6 + \mathbf{G}]^{2+}$ are illustrated in Fig. 3b (see also ESI†). Within $\mathbf{1}_6$ and $[\mathbf{1}_6 + \mathbf{G}]^{2+}$, each monomer interacts with four neighbouring monomers through intermolecular N–H···O bonds whose distances vary from 1.703 to 1.716 Å and from 1.657 to 1.699 Å for $\mathbf{1}_6$ and $[\mathbf{1}_6 + \mathbf{G}]^{2+}$, respectively (Table 1). Interestingly, as compared to the dimeric capsule, $\mathbf{1}_2$, the N–H···O bonds are slightly shorter in the hexamer. The total number of N–H···O bonds in one hexamer unit is 24. Furthermore, the seam of hydrogen bonds, consisting of four intramolecular O–H···O bonds, of each monomer **1**, is retained during hexamer formation. However, small changes are observed in the O–H···O bonds of **1**, $\mathbf{1}_2$, $\mathbf{1}_6$ and $[\mathbf{1}_6 + \mathbf{G}]^{2+}$ if compared with each other: the H-bonds are slightly longer in the hexamers and the dimers than in the monomer. The elongation of the O–H···O bonds in the hexamers and dimers most likely arises from the small changes in electron density distribution around/on the oxygen atoms that function as a hydrogen bond acceptors in both, N–H···O and O–H···O, bonds in the hexamers and the dimers. Some electron density is therefore transferred from O–H···O bonds to N–H···O bonds upon the formation of dimers and hexamers. In the monomer, however, these acceptors oxygen atoms participates only in the formation of O–H···O bonds.

Due to the multiple intermolecular N–H···O bonds, 24 in total, the interaction energies of $\mathbf{1}_6$ and $[\mathbf{1}_6 + \mathbf{G}]^{2+}$ are very high −717 kJ mol^{-1} and −1205 kJ mol^{-1}, respectively (Table 1). These energy numbers suggest that the $[\mathbf{1}_6 + \mathbf{G}]^{2+}$ is ∼500 kJ mol^{-1} more stable than empty hexamer $\mathbf{1}_6$ and underline the significance of template effect.[3] If the interaction energies of $\mathbf{1}_6$ and $[\mathbf{1}_6 + \mathbf{G}]^{2+}$ are compared to the interaction energies of 3 individual dimers $\mathbf{1}_2$ (3 × −197 kJ mol^{-1} = −590 kJ mol^{-1}), it is clear that the formation of hexamer is more favourable than the formation of 3 individual dimers from six monomers. Although this very simplified gas phase model does not take into account all forces acting in the solution state, it not only supports the result obtained from MS studies, but is also in agreement with the NMR data: the hexamer $\mathbf{1}_6$ is thermodynamically more stable than the dimer $\mathbf{1}_2$ in gas phase and solution state.

Table 1 Calculated O–H···O and N–H···O distances and interaction energies at the RI-PBE-D3/def2-SVP level of theory. RI-PBE-D3/def2-SVP//RI-PBE-D3/def2-TZVP single-point energies in parenthesis

Compound	O–H···O [Å]	N–H···O [Å]	E_{int} [kJ mol^{-1}]
1	1.425–1.432	—	—
$\mathbf{1}_2$	1.519–1.525	1.800–1.821	−280 (−197)[a]
$\mathbf{1}_6$	1.554–1.560	1.703–1.716	−942 (−717)[b]
$[\mathbf{1}_6 + \mathbf{G}]^{2+}$	1.528–1.563	1.657–1.699	−1517 (−1205)[c]

[a] $E_{int} = E_{dimer} - 2 \times E_{monomer}$. [b] $E_{hexamer} - 6 \times E_{monomer}$. [c] $E_{complex} - (6 \times E_{monomer} + E_{guest})$.

Conclusions

To conclude, the pyridinearene hexamers were structurally characterized in all three states of matter, and hence, for the first time in gas-phase and solid-state. X-ray structure shows that the hexameric assembly is formed *via* directly linked, intermolecular hydrogen bonds without bridging solvent molecules, which are usually required in the solid-state structures of closely related resorcinarenes. This makes hexamer more compact and decreases the size of empty windows between monomer units, which is a significant feature when applications, especially related to catalysis in confined space, are considered. In chloroform solution the hexamer was found to be the thermodynamically favoured product compared to the corresponding kinetically favoured dimer. All analytical techniques used result in a structure with a diameter of ∼3 nm, and support the structural similarity of the pyridinearene hexamer in gas phase, solution and in solid state. As such, it is slightly more compact than the related hexamers of resorcinarenes and pyrogallarenes due to the different intermolecular hydrogen bonding network that implies to unique mutual alignment of the monomers in these assemblies. Interestingly, the use of a cationic, structurally complementary template increased the gas phase stability of the hexamer substantially, which could be rationalized by sophisticated DFT calculations.

Having established the structural properties of these large hydrogen-bonded capsules now paves the avenue to explore its host–guest binding properties arising from its different and unique interactions and geometric features compared to the other similar assemblies.

Conflicts of interest

There are no conflicts to declare.

Acknowledgements

The authors acknowledge the Academy of Finland for the funding (JOM: 285855, 315829, 320015, RP: 298817, EK: 284562, 278743 and 312514) as well as Prof. H. M. Tuononen, University of Jyväskylä, CSC-IT Center for Science in Finland, and the Finnish Grid and Cloud Infrastructure (persistent identifierurn:nbn:fi:research-infras-2016072533) for providing computational resources. NKB gratefully acknowledge the financial support from Oakland University, MI, USA.

Notes and references

‡Please note, that the template **G** is not necessary to observe the hexameric assembly in (+)ESI-MS. Without templating guest hexamer can be observed as $[\mathbf{1}_6 + Na]^+$ even in low (20 μM) concentration, but with relatively lower abundancy (see Fig. S1†).

§ $^{DT}CCS_{He}$ states for CCS values obtained using drift tube instrument with helium gas, nomenclature recommended in V. Gabelica *et al.*[25]

¶ $^{DTM}CCS_{He}$ states for CCS values obtained using diffuse trajectory method with helium gas.

‖According to Mason–Schamp equation, different gases result in different drift times, and thus to different CCS values. For more detailed explanation see V. Gabelica and E. Marklund.[26]

1 D. Fiedler, D. H. Leung, R. G. Bergman and K. N. Raymond, *Acc. Chem. Res.*, 2005, **38**, 349; M. D. Pluth, R. G. Bergman and K. N. Raymond, *Acc. Chem. Res.*, 2009, **42**, 1650; L. Catti, Q. Zhang and K. Tiefenbacher, *Chem. – Eur. J.*, 2016, **22**, 9060.

2 M. Yamanaka, A. Shivanyuk and J. Rebek, *J. Am. Chem. Soc.*, 2004, **126**, 2939; L. Avram and Y. Cohen, *J. Am. Chem. Soc.*, 2002, **124**, 15148; L. MacGillivray and J. Atwood, *Nature*, 1997, **389**, 469.

3 N. K. Beyeh, M. Kogej, A. Åhman, K. Rissanen and C. A. Schalley, *Angew. Chem., Int. Ed.*, 2006, **45**, 5214.

4 Q. Zhang, L. Catti and K. Tiefenbacher, *Acc. Chem. Res.*, 2018, **51**, 2107.

5 T. Gerkensmeier, J. Mattay and C. Näther, *Chem. – Eur. J.*, 2001, **7**, 465.

6 A. Kiesilä, L. Kivijärvi, N. K. Beyeh, J. O. Moilanen, M. Groessl, T. Rothe, S. Götz, F. Topić, K. Rissanen, A. Lützen and E. Kalenius, *Angew. Chem., Int. Ed.*, 2017, **56**, 10942.

7 A. Kiesilä, J. O. Moilanen, A. Kruve, C. A. Schalley, P. Barran and E. Kalenius, Unpublished results.

8 A. B. Rozhenko, W. W. Schoeller, M. C. Letzel, B. Decker and J. Mattay, *New J. Chem.*, 2013, **37**, 356.

9 M. C. Letzel, B. Decker, A. B. Rozhenko, W. W. Schoeller and J. Mattay, *J. Am. Chem. Soc.*, 2004, **126**, 9669.

10 T. Evan-Salem and Y. Cohen, *Chem. – Eur. J.*, 2007, **13**, 7659.

11 G. Bianchini, A. Scarso, G. La Sorella and G. Strukul, *Chem. Commun.*, 2012, **48**, 12082–12084.

12 E. Kalenius, M. Groessl and K. Rissanen, *Nat. Chem. Rev.*, 2019, **3**, 4.

13 C. Larriba and C. J. Hogan, Jr., *J. Comput. Phys.*, 2013, **251**, 344; C. Larriba and C. J. Hogan Jr., *J. Phys. Chem. A*, 2013, **117**, 3887.

14 T. Gerkensmeier, W. Iwanek, C. Agena, R. Fröhlich, S. Kotila, C. Näther and J. Mattay, *Eur. J. Org. Chem.*, 1999, 2257.

15 R. M. Payne and C. L. Oliver, *CrystEngComm*, 2018, **20**, 1919.

16 K. Eichkorn, O. Treutler, H. Öhm, M. Häser and R. Ahlrichs, *Chem. Phys. Lett.*, 1995, **242**, 652.

17 K. Eichkorn, F. Weigend, O. Treutler and R. Ahlrichs, *Theor. Chem. Acc.*, 1997, **97**, 119.

18 K. Eichkorn, O. Treutler, H. Öhm, M. Häser and R. Ahlrichs, *Chem. Phys. Lett.*, 1995, **240**, 283.

19 J. P. Perdew and Y. Wang, *Phys. Rev. B: Condens. Matter Mater. Phys.*, 1992, **45**, 13244.

20 J. J. Perdew, K. Burke and M. Ernzerhof, *Phys. Rev. Lett.*, 1996, **77**, 3865.

21 S. Grimme, J. Antony, S. Ehrlich and H. Krieg, *J. Chem. Phys.*, 2010, **132**, 154104.

22 S. Grimme, S. Ehrlich and L. Goerigk, *J. Comput. Chem.*, 2011, **32**, 1456.

23 D. Andrae, U. Haeussermann, M. Dolg, H. Stoll and H. Preuss, *Theor. Chim. Acta*, 1990, **77**, 123.

24 F. Weigend and R. Ahlrichs, *Phys. Chem. Chem. Phys.*, 2005, **7**, 3297.

25 V. Gabelica, *et al.*, *Mass Spectrom. Rev.*, 2019, DOI: 10.1002/mas.21585.

26 V. Gabelica and E. Marklund, *Curr. Opin. Chem. Biol.*, 2018, **42**, 51.

IV

CHIRAL HEMICUCURBIT[8]URIL AS AN ANION RECEPTOR: SELECTIVITY TO SIZE, SHAPE AND CHARGE DISTRIBUTION

by

S. Kaabel, J. Adamson, F. Topić, A. Kiesilä, E. Kalenius, M. Öeren, M. Reimund, E. Prigorchenko, A. Lõokene, H. J. Reich, K. Rissanen & R. Aav

Chemical Science, **2017**, *8*, 2184 – 2190

Chemical Science

EDGE ARTICLE

View Article Online
View Journal | View Issue

Cite this: *Chem. Sci.*, 2017, **8**, 2184

Chiral hemicucurbit[8]uril as an anion receptor: selectivity to size, shape and charge distribution†

Sandra Kaabel,[ab] Jasper Adamson,[c] Filip Topić,[b] Anniina Kiesilä,[b] Elina Kalenius,[b] Mario Öeren,[a] Mart Reimund,[a] Elena Prigorchenko,[a] Aivar Lõokene,[a] Hans J. Reich,[d] Kari Rissanen*[b] and Riina Aav*[a]

Received 16th November 2016
Accepted 29th November 2016

DOI: 10.1039/c6sc05058a

www.rsc.org/chemicalscience

A novel eight-membered macrocycle of the hemicucurbit[*n*]uril family, chiral (*all-R*)-cyclohexanohemicucurbit[8]uril (**cycHC[8]**)‡ binds anions in a purely protic solvent with remarkable selectivity. The **cycHC[8]** portals open and close to fully encapsulate anions in a 1 : 1 ratio, resembling a molecular Pac-Man™. Comprehensive gas, solution and solid phase studies prove that the binding is governed by the size, shape and charge distribution of the bound anion. Gas phase studies show an order of SbF_6^- ≈ PF_6^- > ReO_4^- > ClO_4^- > SCN^- > BF_4^- > HSO_4^- > $CF_3SO_3^-$ for anion complexation strength. An extensive crystallographic study reveals the preferred orientations of the anions within the octahedral cavity of **cycHC[8]** and highlights the importance of the size- and shape-matching between the anion and the receptor cavity. The solution studies show the strongest binding of the ideally fitting SbF_6^- anion, with an association constant of 2.5 × 10^5 M^{-1} in pure methanol. The symmetric, receptor cavity-matching charge distribution of the anions results in drastically stronger binding than in the case of anions with asymmetric charge distribution. Isothermal titration calorimetry (ITC) reveals the complexation to be exothermic and enthalpy-driven. The DFT calculations and VT-NMR studies confirmed that the complexation proceeds through a pre-complex formation while the exchange of methanol solvent with the anion is the rate-limiting step. The octameric **cycHC[8]** offers a unique example of template-controlled design of an electroneutral host for binding large anions in a competitive polar solvent.

Introduction

The importance of ion recognition and transport in biological systems is well established, bringing about the quest for synthetic receptors capable of binding ions in physiological conditions. The syntheses of crown ethers,[1] cryptands[2] and cucurbiturils[3] among others have contributed to the rich history of cation recognition whereas development of anion receptors effective in protic solvents remains challenging.[4–7] Anion sensing motifs based on cationic species are usually effective in a narrow range of pH, plagued by low binding selectivity and counteranion competition for the binding site. Neutral anion receptors relying on hydrogen or halogen bonding are often affected by strong competition from the protic solvent with host–guest interactions having to disrupt the solvation shell of the anion.[8,9]

Exemplary studies on anion binding by cyclic hexapeptides show that introducing a confined cavity to the structure of the receptor significantly increases the anion binding ability, as abundant 2 : 1 host–guest complexes were observed with halides and SO_4^{2-} where the anion was enclosed in the cavity formed by two cyclopeptide units.[10,11] This led to the design of sandwich-like bis(cyclopeptide) receptors that reached association constants of up to 10^6 M^{-1} for binding SO_4^{2-} in a water–methanol mixture.[12,13] Employing a hydrophobic pocket for anion binding in water has been illustrated by the Gibb's octa-acid cavitand,[14] where the binding of partially hydrated anions yielded association constants up to 10^3 M^{-1} at pH 11.5. Likewise, the size-dependent complexation of dodecaborate dianions within the hydrophobic cavity of γ-cyclodextrin was studied by Nau and co-workers, with the strongest association in the case of $B_{12}Br_{12}^{2-}$ (K_a = 9.6 × 10^5 M^{-1}).[15]

Cucurbituril family members have been explored as ion receptors due to their well-defined hydrophobic cavity.[16,17]

[a]*Department of Chemistry, Tallinn University of Technology, Akadeemia tee 15, 12618 Tallinn, Estonia. E-mail: riina.aav@ttu.ee*

[b]*University of Jyvaskyla, Department of Chemistry, Nanoscience Center, P.O. Box. 35, FI-40014 Jyvaskyla, Finland. E-mail: kari.t.rissanen@jyu.fi*

[c]*National Institute of Chemical Physics and Biophysics, Akadeemia tee 23, 12618 Tallinn, Estonia*

[d]*Department of Chemistry, University of Wisconsin, Madison, WI 53706, USA*

† Electronic supplementary information (ESI) available: MS, NMR, dynamic NMR and computational details and a DFT-based video of complexation. CCDC 1514736–1514741, 1521388. For ESI and crystallographic data in CIF or other electronic format see DOI: 10.1039/c6sc05058a

‡ The name cyclohexylhemicucurbituril, previously used for these macrocycles, is changed in accordance with the IUPAC nomenclature for fused cycles, as the cyclohexane substituents are fused with the parent hemicucurbituril.

Hemicucurbiturils,[18] cyclohexanohemicucurbit[6]urils,[19] bambus[6]urils[20] and biotin[6]urils[21–23] have been shown to bind anions within their electron-deficient (*i.e.* partially positively charged) hydrophobic cavities. Presently, bambus[6]urils hold the record for the strongest anion binding ($K_a = 5.5 \times 10^7\ M^{-1}$) by a neutral host in exclusively protic solvent.[24] Based on the crystal structures of six-membered hemicucurbiturils, bambus[6]uril[25–28] and biotin[6]uril[21] complexes the central cavities readily accommodate halide anions. Larger anions have been shown to prefer the formation of 1 : 2 host : guest complexes with double-cone-shaped bambus[6]urils,[29,30] with the anions bound away from the centre of the cavity.

We have previously demonstrated the synthesis of the first 8-membered hemicucurbituril, (*all-R*)-cyclohexanohemicucurbit[8]uril (**cycHC[8]**), by an approach using anion-templating.[31] Given that larger anions such as PF_6^- and $CF_3CO_2^-$ were observed to act as effective templates, we decided to investigate the binding of other larger inorganic anions by **cycHC[8]**. Such anions are for example used in ionic liquids[32] (BF_4^-, PF_6^-, SbF_6^-, $CF_3SO_3^-$) and as oxidizing agents[33] (ClO_4^-, IO_4^-). On the other hand, they are considered as environmental pollutants.[33,34] Binding of these anions in protic media is important from a biological and environmental point of view.

Results and discussion

The chiral host molecule (*all-R*)-cyclohexanohemicucurbit[8]uril[31,35] (**cycHC[8]**) fully encapsulates certain anions forming 1 : 1 complexes (Fig. 1) with high selectivity and binding affinities of up to $2.5 \times 10^5\ M^{-1}$ in methanol.

The scope of anionic guests that form complexes with **cycHC[8]** was determined by mass spectrometry (see ESI†). Only 1 : 1 complexes were observed in ESI-MS spectra and abundant complexes were observed with $SbF_6^- \approx PF_6^- > ReO_4^- > ClO_4^- > SCN^- > BF_4^- > HSO_4^- > CF_3SO_3^-$, ranked by decreasing affinity for **cycHC[8]**. The anions $H_2PO_4^-$, AcO^-, Br^-, Cl^-, I^-, F^-, NO_3^- and NO_2^- showed only weak complexation, while no complexes were formed with $AuBr_4^-$, Br_3^- and CN^-. The order of affinity was ascertained through competition experiments, performed on three-component mixtures of the host with two competing anions in 1 : 1 : 1 molar ratio (ESI Fig. S2 and S3†). Halide anions (13 to 35 Å^3 in volume[36]), while readily forming complexes with 6-membered hemicucurbiturils,[37–41] appear to have very low affinity towards **cycHC[8]**, presumably due to a mismatch in size with the cavity of **cycHC[8]**. As expected, the affinity towards more heavily solvated anions was found to be lower than for weakly solvated ones. On the other hand, tetrahedral and octahedral anions falling into the volume range of 50 to 80 Å^3 form stronger complexes with **cycHC[8]**, presumably due to a better size fit. This is also in good agreement with Rebek's rule suggesting a packing coefficient (PC)[42] of 0.55 ± 0.09 for optimal fit in the **cycHC[8]** cavity with a volume of 123 Å^3.[31] The MS/MS collision-induced dissociation (CID) experiments (Fig. S4†) on isolated complexes revealed the most efficient dissociation (lowest kinetic stability) for the host–guest complexes with highest PCs (>0.55). This results from the sensitive interplay of the attractive and repulsive forces between the anion and the cavity walls, and the lack of void space. More importantly, it also indicates the full encapsulation of the anions in the complexes in the gas phase. The same phenomenon has been studied in detail with cucurbiturils and azoalkanes,[43] but is reported here for the first time with anionic complexes.

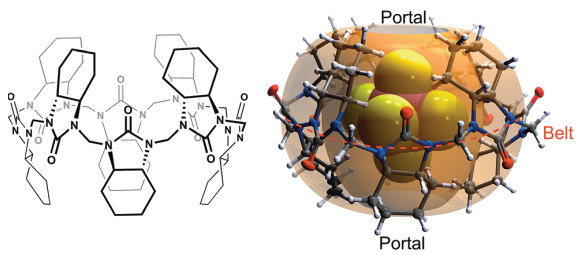

Fig. 1 Molecular structure of (*all-R*)-cyclohexanohemicucurbit[8]uril, cycHC[8] (left), and the X-ray structure of an inclusion complex with SbF_6^- (right).

The crystal structures of the host–guest complexes, obtained by single crystal X-ray diffraction, demonstrate unambiguously the 1 : 1 stoichiometry of the anion inclusion complexes in the solid state (Fig. 2). Single crystals of the complexes were obtained from solutions of **cycHC[8]** in methanol with the guest added as a tetrabutylammonium (TBA) or tetrabutyl-phosphonium (TBP) salt. The TBA or TBP cations and a number of solvent molecules fill the space between the capsule-like moieties, affording isostructural crystals regardless of the guest anion used. The guest anions are situated at the center of the **cycHC[8]** cavity, in a manner depending on their size and shape. The octahedral anions SbF_6^- and PF_6^- are locked in a fixed position showing no disorder. Four fluorine atoms of SbF_6^-/PF_6^- lying on the equatorial plane of the macrocycle point to the four corners of its square-shaped belt, while the two remaining fluorines point to the opposite portals (Fig. 2a and b). The Hirshfeld surface[44] plotted for the encapsulated octahedral anion SbF_6^- indicates that the host–guest C–H···F interactions are responsible for the fixed orientation of these guests (ESI Fig. S6†). The shortest C–H···F distances are found between the four equatorial fluorine atoms and the axial 2*ax* protons in each corner of the macrocyclic cavity (Fig. 3B and Table S3†). In contrast to the octahedral anions, the tetrahedral anions BF_4^-, ClO_4^-, ReO_4^- and IO_4^- have more space inside the cavity (Fig. 2c–f) and show disorder in the crystal. As the host cavity is symmetric and therefore offers a number of equal interaction sites, several orientations of the tetrahedral anions are equally favored. The Hirshfeld surface of encapsulated IO_4^- (Fig. S7†), together with the close contact analysis of other tetrahedral anions (Tables S5–S8†) reveals that these anions can only form a limited number of interactions with the host cavity wall in a given orientation. Smaller anions like BF_4^- and ClO_4^- can form even fewer host–guest interactions simultaneously. The large $CF_3SO_3^-$ anion has two orientations (Fig. 2g and Table S9†). Given that **cycHC[8]** preserves its conformation almost fully regardless of the guest anion encapsulated, its cavity can be considered as an octahedrally shaped void, which

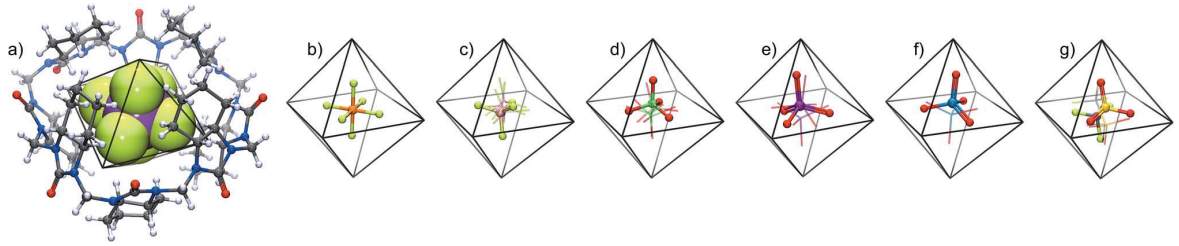

Fig. 2 The crystal structures of 1 : 1 host–guest complexes of (a) SbF_6^-, (b) PF_6^-, (c) BF_4^-, (d) ClO_4^-, (e) IO_4^-, (f) ReO_4^- and (g) $CF_3SO_3^-$ anions in the **cycHC[8]** cavity. Minor disorder components are shown as a wireframe model. The host in (b–f) is represented by an octahedron depicting the cavity of **cycHC[8]**.

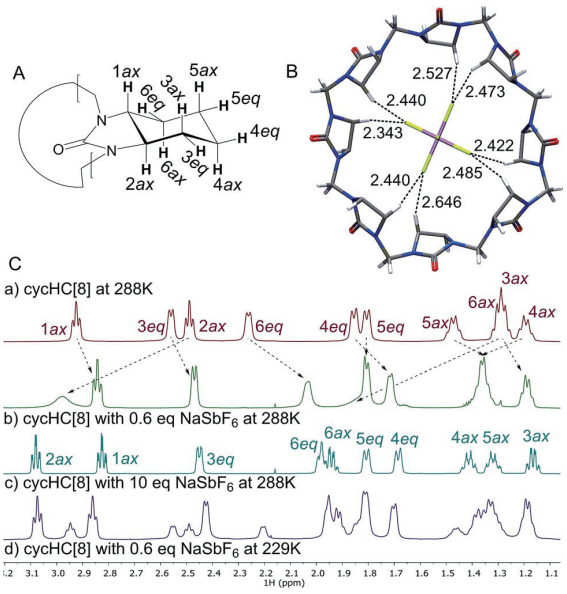

Fig. 3 (A) Labelling of **cycHC[8]** protons, (B) C–H···F distances between the host proton 2*ax* and SbF_6^- from the X-ray structure; all $(CH_2)_4$ groups are omitted for clarity, (C) ^{1}H NMR in MeOD of (a) free **cycHC[8]**, (b) **cycHC[8]** with 0.6 eq. of $NaSbF_6$ at 288 K (c) **cycHC[8]** with 10 eq. of $NaSbF_6$ at 288 K; (d) SbF_6^-@**cycHC[8]** and free **cycHC[8]** formed from **cycHC[8]** with 0.6 eq. of $NaSbF_6$ at 229 K.

encapsulates guests in a manner depending on their shape, volume and complementarity of the interactions.

Next, we examined anion complexation with **cycHC[8]** in solution using ^{1}H NMR spectroscopy. The complex with SbF_6^- showed the largest complexation-induced chemical shift changes (downfield shifts of 0.52, 0.23 and 0.64 ppm for 2*ax*, 4*ax* and 6*ax*, respectively). The signals for 2*ax*, 4*ax* and 6*ax* in the complex with SbF_6^- also showed significant signal broadening at room temperature, indicating a slow guest exchange rate for SbF_6^-. The guest exchange slows down at low temperature resulting in the signals of SbF_6^-@**cycHC[8]** and excess free **cycHC[8]** being separate (Fig. 3C(d)).

The Job plot analysis confirmed 1 : 1 stoichiometry of binding for all studied guests in methanol (ESI†), as also observed by crystallography in the solid state and by mass spectrometry in the gas phase. Association constants were determined by NMR titrations (Table 1), simultaneously following three **cycHC[8]** proton signals 1*ax*, 2*ax* and 3*eq* (Fig. 3A). The association constant for SbF_6^- was, due to the broadening of the 2*ax* signal, determined only from the 1*ax* and 3*eq* proton signals. The range of association constants varied over five orders of magnitude, strongly dependent on the size and shape of the guest. The poor water solubility of **cycHC[8]** prevented measurements in pure water, but no significant decrease in binding strength was observed when pure methanol was changed to a 1 : 1 methanol/water mixture (Table 1, rows 2–3).

For tetrahedral and octahedral anions, the affinity to the host grows exponentially with the increasing size of the guest, ranging from 48 M^{-1} for the smallest tested anion BF_4^- to 250 000 M^{-1} for the largest tested octahedral anion SbF_6^- (Table 1 and Fig. 4). The anion size dependency for anion binding has also been discussed by Sindelar and co-workers for a bambus[6]uril host in chloroform,[24] with the highest selectivity towards ClO_4^-. Given the double-cone shape of the dodecabenzylbambus[6]uril host and the restricted diameter of

Table 1 Association constants K_a for **cycHC[8]** inclusion complexes with anions, measured in MeOD at 288 K by ^{1}H NMR titration experiments. Volumes of the anions (V_{anion}) and their packing coefficients (PC)[a]

Anion	Cation	V_{anion} (Å^3)	PC	K_a (M^{-1})
SbF_6^-	Na^+	81.8	0.67	$(2.5 \pm 0.7) \times 10^5$
PF_6^-	Bu_4N^+	70.6	0.57	$(2.8 \pm 0.4) \times 10^4$
PF_6^{-b}	Bu_4N^+	70.6	0.57	$(2.6 \pm 0.2) \times 10^4$
PF_6^-	Na^+	70.6	0.57	$(2.0 \pm 0.2) \times 10^4$
ReO_4^-	Bu_4N^+	64.8	0.53	$(4.7 \pm 0.4) \times 10^3$
IO_4^-	Na^+	64.3	0.52	$(1.8 \pm 0.2) \times 10^3$
ClO_4^-	Bu_4N^+	54.7	0.45	$(4.7 \pm 0.2) \times 10^2$
BF_4^-	Bu_4N^+	51.6	0.42	$(4.8 \pm 0.4) \times 10$
$CF_3SO_3^-$	Bu_4N^+	82.3	0.67	$(3.9 \pm 0.5) \times 10$
$CF_3CO_2^-$	Bu_4N^+	68.7	0.56	<10

[a] Anion volume is based on optimized anion geometries (BP86-D/def2-TZVPD) and calculated using a triangulated sphere model (based on CSD default atomic radii) through the Olex2 program package.[45] PC is defined as the ratio between the V_{anion} to V_{cavity}(host).[42] V_{cavity}(**cycHC[8]**) = 123.0 Å^3 is measured from the crystal structure of **cycHC[8]**.[31] [b] ^{1}H NMR in 1 : 1 MeOD/D_2O.

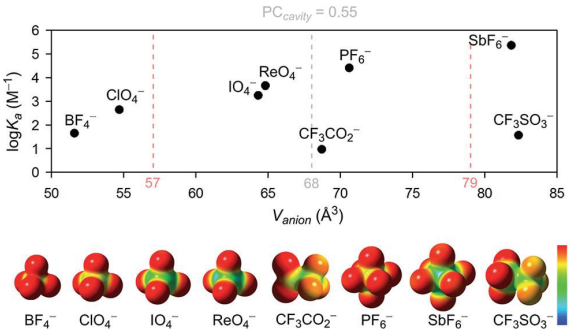

Fig. 4 The association constant dependency on the anion size and the electrostatic surface potential of the studied anions. Surface potential calculated using Gaussian 09,[46] visualized using GaussView5,[47] red to blue surface color range spans from −0.2 to 0.2. Pale red dashed lines represent the 68 ± 11 Å^3 anion volume range (PC = 0.55 ± 0.09).

the central cavity of 6-membered hemicucurbiturils, it seems that anions larger than perchlorate are bound away from the center of the bambus[6]uril macrocycle, inside the cone-shaped pockets formed by the extending substituents.[25,30] With **cycHC[8]**, a single binding site is suggested by the crystal structures, with the anion in each case fully encapsulated in the center of the cavity. The selectivity of this 8-membered host is therefore determined by the parameters of its central cavity. Based on the crystal structures, the correlation between the binding strength and the size of the anion can arguably be ascribed to the number of host–guest interactions an anion can form simultaneously. Thus smaller anions BF_4^- and ClO_4^-, which are able to form only one or two C–H···anion interactions in a given orientation, are bound with considerably lower affinities.

Surprisingly, however, the association constant for the binding of roughly octahedral $CF_3SO_3^-$ is dramatically lower compared to the similarly sized octahedral guest SbF_6^-, regardless of the several interactions between the host and the encapsulated $CF_3SO_3^-$ apparent in the crystal structure (Table S9†). Given the inherent symmetry of **cycHC[8]**, one can argue that the binding might be stronger with anions having the charge equally distributed over the surface. To assess whether the low binding affinity of $CF_3SO_3^-$ is caused by the asymmetric charge distribution, a control experiment was conducted with $CF_3CO_2^-$, similar in volume to PF_6^-, but with a charge distribution resembling that in $CF_3SO_3^-$. The fact that $CF_3CO_2^-$, which effectively templates the synthesis of **cycHC[8]** (in acetonitrile) and has been shown by diffusion NMR to bind to **cycHC[8]** in chloroform,[31] does not bind to **cycHC[8]** in methanol (K_a < 10), indicates that the binding of anions to **cycHC[8]** in methanol is sensitive to charge distribution around the anion.

According to the range of optimal packing coefficients, 0.55 ± 0.09, the association constants within the tested group of tetrahedral and octahedral anions with roughly spherical charge distribution should follow a statistical distribution around the optimal guest fit at PC = 0.55. For **cycHC[8]**, with a cavity volume 123.0 Å^3, the optimal guest volume should therefore centre in the range of 68 ± 11 Å^3 (Fig. 4). However, the strongest association was in fact observed for SbF_6^- (V_{anion} = 81.8 Å^3), suggesting a shift from the optimal PC to higher values which might be due to the stabilizing effect of host–guest interactions with tighter-fitting guests like SbF_6^- or the conformational flexibility of the macrocycle itself.

Next, isothermal titration calorimetry (ITC) was used to determine thermodynamic parameters for the complexes of **cycHC[8]** with SbF_6^- and PF_6^- in methanol. The raw thermogram and the binding isotherm for SbF_6^- are presented in Fig. 5 with the calculated parameters given in Table 2. The K_a values obtained by ITC were comparable with those obtained by NMR spectroscopy. Similarly to NMR, ITC showed higher affinity of **cycHC[8]** for SbF_6^- than PF_6^-, with binding being exothermal, enthalpy driven and entropically disfavored for both. Comparing the two anions revealed that the binding of SbF_6^- was accompanied by a greater change in both enthalpy and entropy. This is in line with tighter binding of the larger SbF_6^- anion, giving rise to a stronger host–guest interaction (enthalpic term) but also a greater loss in degrees of freedom (entropic term). Generally, the thermodynamic profile of **cycHC[8]** binding resembles the behavior of other hemicucurbiturils.[37]

The complexation kinetics of normal cucurbiturils has been thoroughly[48–56] studied and the exchange of neutral guests has been shown to proceed through a single step,[55,56] while the complexation of cationic guests proceeds through a number of intermediates.[50–54] To the best of our knowledge, the kinetics of anion binding by hemicucurbiturils has not been previously studied. A particularly interesting aspect of the **cycHC[8]** behavior is the conformational dynamics of guest encapsulation. Given the bulkiness of the encapsulated guests (Fig. 1), the conformation of the host clearly has to change considerably for the guest to pass through the narrow portals of **cycHC[8]**. The

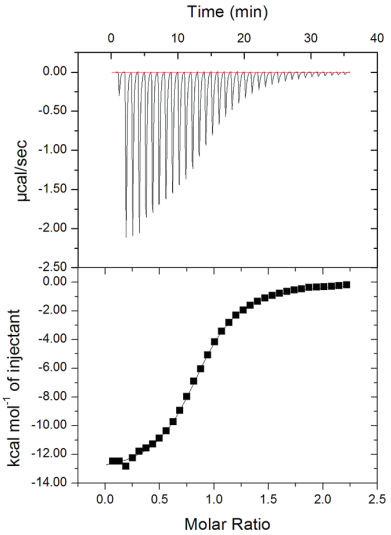

Fig. 5 Raw thermogram (above) for SbF_6^- titration with cycHC[8] and the binding isotherm (below) from the integrated thermogram fit using the one-site model.

Table 2 Thermodynamic and kinetic parameters for the complexation with **cycHC[8]** at 298 K, all energies given in kJ mol^{-1}

	ITC titration			ΔG°			VT-NMR			
							Activation parameters for complex formation			Association rate constant[a]
Guest	K_a (M^{-1})	ΔH°	$T\Delta S^\circ$	ITC titration	NMR titration	DFT calc.	$\Delta H^\ddagger$	$T\Delta S^\ddagger$	$\Delta G^\ddagger$	$k \times 10^3$ s^{-1}
$NaSbF_6$	$(1.02 \pm 0.03) \times 10^5$	-56.2 ± 0.3	-27.7	-28.5	-30.8	—	38.6	-13.4	51.9	2.6
$NaPF_6$	$(1.29 \pm 0.04) \times 10^4$	-43.8 ± 0.2	-20.4	-23.4	-24.5	-22	42.1	-5.5	47.5	17.5

[a] Determined at 291 K.

flexibility of the host is seemingly crucial to the encapsulation and, likewise, to the ejection of the guests, and the reaction pathway of host–guest complex formation was therefore studied computationally. Density functional theory (DFT) calculations were used to model the complexation of **cycHC[8]** with PF_6^- utilizing COSMO solvation model for methanol.[57,58]

By positioning up to four methanol molecules inside the cavity of **cycHC[8]** we found that, at temperatures above 100 K, a single molecule of methanol is preferably accommodated within the cavity, close to its center. As the association constants derived from NMR titration with sodium and tetrabutylammonium PF_6^- salts were very similar, cation influence was assumed to be negligible and was not studied. Modelling the exchange of methanol in MeOH@**cycHC[8]** with PF_6^- showed the initial formation of a pre-complex with PF_6^- at the portal of **cycHC[8]** (MeOH@**cycHC[8]** + PF_6^-; Fig. 6). Next, through a transition state involving the dissociation of a hydrogen bond between methanol and **cycHC[8]**, the inclusion complex PF_6^-@**cycHC[8]** is formed (the complexation reaction pathway is visualized in a video, ESI†). The DFT-derived Gibbs free energy difference indicates that the methanol-solvated cycHC[8] is 22 kJ mol^{-1} higher in energy compared to its inclusion complex with PF_6^-, which is in good agreement with the experimental ΔG values calculated from equilibrium constants obtained by NMR and ITC analyses (Table 2).

Additional experimental insight into the kinetics of the complexation and the reaction pathway was gained by variable temperature NMR (VT-NMR) studies of SbF_6^- and PF_6^-, using a 2 : 1 host-to-guest ratio (Fig. 7). The complexation reaction order was determined by dilution experiments near the coalescence temperature (241 K and 253 K for SbF_6^- and PF_6^-, respectively).

Reaction rates remained constant upon dilution, indicating that the complexation process follows first order kinetics, characteristic for a unimolecular reaction. This suggests that the overall complexation reaction occurs *via* a low-energy pre-complex. Moreover, the complexation reaction rate constants for both SbF_6^- and PF_6^- (Table 2) were determined, allowing us to derive the activation parameters (Table 2) using the Eyring equation (for details, see ESI†). As expected, the complexation rate constant was an order of magnitude higher for PF_6^- than for the larger SbF_6^-, also in good agreement with our initial solution studies by NMR. The entropy of activation of the complexation is negative for both anions, as expected for the host and guest forming one host–guest complex. Other entropic contributions that play a role in the host–guest formation reaction are the entropic penalty of orientation of the guest within the macrocycle and the desolvation of the cavity of the host and the collapse of the methanol cluster around the chaotropic guests.

Both the computational and kinetic studies propose the existence of pre-complexes, although the computations suggest them to be higher in energy than the precursors, whereas the VT-NMR results require this pre-complex to be more stable than

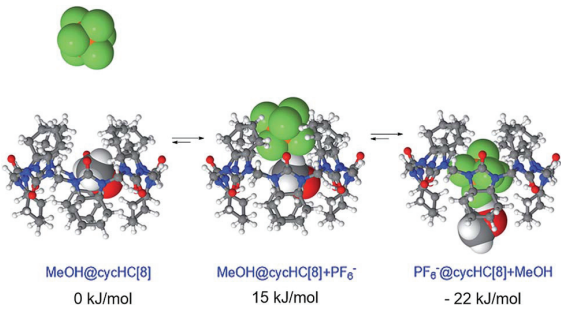

Fig. 6 Minimum energy geometries of **cycHC[8]** complexes with PF_6^- in MeOH and the associated relative Gibbs free energy values.

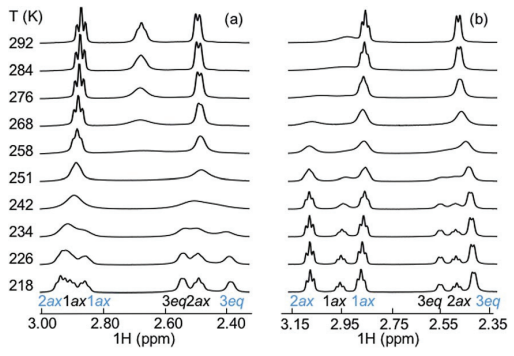

Fig. 7 Evolution of proton resonances in the variable temperature NMR study (a) for PF_6^- and (b) for SbF_6^-. The **cycHC[8]** and guest concentrations were 2.6 mM and 1.5 mM in MeOD solution, respectively. At 218 K, the hydrogen signals labelled with blue arise from the host–guest complex and black ones from the free host.

the starting components. This reflects a complicated complexation reaction pathway that includes several steps. We propose that either the anion pre-complex formation or the reorganization of the methanol solvation shell around anions and the macrocycle play an important role, which merits further investigation.

Conclusions

The inherently chiral (*all-R*)-cyclohexanohemicucurbit[8]uril, **cycHC[8]**, is the first example of an octameric macrocycle of the hemicucurbituril family acting as a neutral host that fully encapsulates anions as 1 : 1 complexes in gas, solution and solid state. The binding affinity strongly depends on the size, shape and charge distribution of the anion. Crystallographic studies show the importance of the shape fit between the **cycHC[8]** cavity and the anion guest, with the octahedral guests bound in a perfectly ordered manner, while the tetrahedral guests exhibited various degrees of disorder. Moreover, due to the unique size and shape of **cycHC[8]**, the large, octahedrally shaped SbF_6^- was found to be the most tightly bound guest, closely followed by PF_6^-. On the other hand, binding of the similarly sized $CF_3SO_3^-$ and $CF_3CO_2^-$ was around four orders of magnitude weaker, which could be ascribed to their asymmetric charge distribution limiting the number of hydrogen bonds that can be formed simultaneously. The complexation was found to proceed through the formation of a pre-complex, accompanied by the ejection of a solvent molecule from the **cycHC[8]** cavity and involving a large movement of the portals during the encapsulation.

This work, besides being the first comprehensive anion-binding study on an eight-membered hemicucurbituril-type macrocycle, also demonstrates the unique anion binding properties of a macrocyclic host easily accessible through a simple templated synthetic protocol.[31] Moreover, it proposes a pathway to and encourages the preparation of new hemicucurbiturils for anion binding and transport, catalysis in confined space and other supramolecular applications.

Author contribution

The manuscript was written through contributions of all authors.

Acknowledgements

This research was supported by the Academy of Finland (KR: grants 263256, 265328 and 292746, EK: grants 284562 and 278743), the Estonian Ministry of Education and Research through Grants IUT19-32, IUT19-9, IUT23-7 and PUT692, TUT grant No. B25, the ESF DoRa, and the EU European Regional Development Fund through the Center of Excellence in Molecular Cell Engineering projects 3.2.0101.08-0017 and TK134. Computations were performed on the HPC cluster at TUT, which is part of the ETAIS project. FT acknowledges the support from NGS-NANO through a Ph.D. fellowship. The authors would like to thank Marina Kudrjašova and Mari-Liis Kasemets for assistance with NMR, Ly Pärnaste with ITC, Toomas Kaevand with computations and Lauri Kivijärvi with MS experiments.

Notes and references

1 C. J. Pedersen, *Angew. Chem.*, 1988, **100**, 1053; *Angew. Chem., Int. Ed. Engl.*, 1988, **27**, 1021.
2 J.-M. Lehn, *Angew. Chem.*, 1988, **100**, 91; *Angew. Chem., Int. Ed. Engl.*, 1988, **27**, 89.
3 W. A. Freeman, W. L. Mock and N. Y. Shih, *J. Am. Chem. Soc.*, 1981, **103**, 7367.
4 M. J. Langton, C. J. Serpell and P. D. Beer, *Angew. Chem., Int. Ed.*, 2016, **55**, 1974.
5 P. A. Gale and C. Caltagirone, *Chem. Soc. Rev.*, 2015, **44**, 4212.
6 N. H. Evans and P. D. Beer, *Angew. Chem., Int. Ed.*, 2014, **53**, 11716.
7 J. L. Sessler, P. A. Gale and W.-S. Cho, *Anion Receptor Chemistry*, ed. J. F. Stoddart, Royal Society of Chemistry, Cambridge, 2006.
8 P. A. Gale, E. N. W. Howe and X. Wu, *Chem*, 2016, **1**, 351.
9 S. Kubik, *Chem. Soc. Rev.*, 2010, **39**, 3648.
10 S. Kubik, R. Goddard, R. Kirchner, D. Nolting and J. Seidel, *Angew. Chem., Int. Ed.*, 2001, **40**, 2648.
11 S. Kubik and R. Goddard, *Proc. Natl. Acad. Sci. U. S. A.*, 2002, **99**, 5127.
12 S. Kubik, R. Kirchner, D. Nolting and J. Seidel, *J. Am. Chem. Soc.*, 2002, **124**, 12752.
13 F. Sommer and S. Kubik, *Org. Biomol. Chem.*, 2014, **12**, 8851.
14 P. Sokkalingam, J. Shraberg, S. W. Rick and B. C. Gibb, *J. Am. Chem. Soc.*, 2016, **138**, 48.
15 K. I. Assaf, M. S. Ural, F. Pan, T. Georgiev, S. Simova, K. Rissanen, D. Gabel and W. M. Nau, *Angew. Chem., Int. Ed.*, 2015, **54**, 6852.
16 E. Masson, X. Ling, R. Joseph, L. Kyeremeh-Mensah and X. Lu, *RSC Adv.*, 2012, **2**, 1213.
17 S. J. Barrow, S. Kasera, M. J. Rowland, J. Del Barrio and O. A. Scherman, *Chem. Rev.*, 2015, **115**, 12320.
18 Y. Miyahara, K. Goto, M. Oka and T. Inazu, *Angew. Chem., Int. Ed.*, 2004, **43**, 5019.
19 R. Aav, E. Shmatova, I. Reile, M. Borissova, F. Topić and K. Rissanen, *Org. Lett.*, 2013, **15**, 3786.
20 J. Svec, M. Necas and V. Sindelar, *Angew. Chem., Int. Ed.*, 2010, **49**, 2378.
21 M. Lisbjerg, B. M. Jessen, B. Rasmussen, B. Nielsen, A. Ø. Madsen and M. Pittelkow, *Chem. Sci.*, 2014, **5**, 2647.
22 M. Lisbjerg, B. E. Nielsen, B. O. Milhøj, S. P. A. Sauer and M. Pittelkow, *Org. Biomol. Chem.*, 2015, **13**, 369.
23 M. Lisbjerg, H. Valkenier, B. M. Jessen, H. Al-Kerdi, A. P. Davis and M. Pittelkow, *J. Am. Chem. Soc.*, 2015, **137**, 4948.
24 M. A. Yawer, V. Havel and V. Sindelar, *Angew. Chem., Int. Ed.*, 2015, **54**, 276.
25 V. Havel, J. Svec, M. Wimmerova, M. Dusek, M. Pojarova and V. Sindelar, *Org. Lett.*, 2011, **13**, 4000.
26 J. Svec, M. Dusek, K. Fejfarova, P. Stacko, P. Klan, A. E. Kaifer, W. Li, E. Hudeckova and V. Sindelar, *Chem.–Eur. J.*, 2011, **17**, 5605.

27 J. Rivollier, P. Thuéry and M.-P. Heck, *Org. Lett.*, 2013, **15**, 480.
28 M. Singh, E. Solel, E. Keinan and O. Reany, *Chem.–Eur. J.*, 2015, **21**, 536.
29 T. Fiala and V. Sindelar, *Supramol. Chem.*, 2016, **28**, 810.
30 V. Havel, V. Sindelar, M. Necas and A. E. Kaifer, *Chem. Commun.*, 2014, **50**, 1372.
31 E. Prigorchenko, M. Öeren, S. Kaabel, M. Fomitšenko, I. Reile, I. Järving, T. Tamm, F. Topić, K. Rissanen and R. Aav, *Chem. Commun.*, 2015, **51**, 10921.
32 H. Olivier-Bourbigou, L. Magna and D. Morvan, *Appl. Catal., A*, 2010, **373**, 1.
33 E. T. Urbansky, *Biorem. J.*, 1998, **2**, 81.
34 R. F. M. Frade and C. A. M. Afonso, *Hum. Exp. Toxicol.*, 2010, **29**, 1038.
35 M. Fomitšenko, E. Shmatova, M. Öeren, I. Järving and R. Aav, *Supramol. Chem.*, 2014, **26**, 698.
36 Anion volumes in this report are calculated using a triangulated sphere model (based on CSD default atomic radii) through Olex2 program package. Ref. 42.
37 H.-J. Buschmann, E. Cleva and E. Schollmeyer, *Inorg. Chem. Commun.*, 2005, **8**, 125.
38 H.-J. Buschmann, A. Zielesny and E. J. Schollmeyer, *J. Inclusion Phenom. Macrocyclic Chem.*, 2006, **54**, 181.
39 M. Sundararajan, R. V. Solomon, S. K. Ghosh and P. Venuvanalingam, *RSC Adv.*, 2011, **1**, 1333.
40 H.-J. Buschmann and A. Zielesny, *Comput. Theor. Chem.*, 2013, **1022**, 14.
41 M. Öeren, E. Shmatova, T. Tamm and R. Aav, *Phys. Chem. Chem. Phys.*, 2014, **16**, 19198.
42 S. Mecozzi and J. Rebek, *Chem.–Eur. J.*, 1998, **4**, 1016.
43 T.-C. Lee, E. Kalenius, A. I. Lazar, K. I. Assaf, N. Kuhnert, C. H. Grün, J. Jänis, O. A. Scherman and W. M. Nau, *Nat. Chem.*, 2013, **5**, 376.
44 M. A. Spackman and D. Jayatilaka, *CrystEngComm*, 2009, **11**, 19.
45 O. V. Dolomanov, L. J. Bourhis, R. J. Gildea, J. A. K. Howard and H.-J. Puschmann, *J. Appl. Crystallogr.*, 2009, **42**, 339.
46 M. J. Frisch, G. W. Trucks, H. B. Schlegel, G. E. Scuseria, M. A. Robb, J. R. Cheeseman, G. Scalmani, V. Barone, B. Mennucci, G. A. Petersson, H. Nakatsuji, M. Caricato, X. Li, H. P. Hratchian, A. F. Izmaylov, J. Bloino, G. Zheng, J. L. Sonnenberg, M. Hada, M. Ehara, K. Toyota, R. Fukuda, J. Hasegawa, M. Ishida, T. Nakajima, Y. Honda, O. Kitao, H. Nakai, T. Vreven, J. A. Montgomery Jr, J. E. Peralta, F. Ogliaro, M. Bearpark, J. J. Heyd, E. Brothers, K. N. Kudin, V. N. Staroverov, R. Kobayashi, J. Normand, K. Raghavachari, A. Rendell, J. C. Burant, S. S. Iyengar, J. Tomasi, M. Cossi, N. Rega, J. M. Millam, M. Klene, J. E. Knox, J. B. Cross, V. Bakken, C. Adamo, J. Jaramillo, R. Gomperts, R. E. Stratmann, O. Yazyev, A. J. Austin, R. Cammi, C. Pomelli, J. W. Ochterski, R. L. Martin, K. Morokuma, V. G. Zakrzewski, G. A. Voth, P. Salvador, J. J. Dannenberg, S. Dapprich, A. D. Daniels, Ö. Farkas, J. B. Foresman, J. V. Ortiz, J. Cioslowski and D. J. Fox, *Gaussian 09, Revision E.01*, Gaussian, Inc., Wallingford CT, 2009.
47 R. Dennington, T. Keith and J. Millam, *GaussView, Version 5*, Semichem Inc., Shawnee Mission, KS, 2009.
48 W. L. Mock and N.-Y. Shih, *J. Org. Chem.*, 1986, **51**, 4440.
49 W. L. Mock and N.-Y. Shih, *J. Am. Chem. Soc.*, 1989, **111**, 2697.
50 R. Hoffmann, W. Knoche, C. Fenn and H.-J. Buschmann, *J. Chem. Soc., Faraday Trans.*, 1994, **90**, 1507.
51 C. Márquez and W. M. Nau, *Angew. Chem., Int. Ed.*, 2001, **40**, 3155.
52 C. Márquez, R. R. Hudgins and W. M. Nau, *J. Am. Chem. Soc.*, 2004, **126**, 5806.
53 X. Ling, E. L. Samuel, D. L. Patchell and E. Masson, *Org. Lett.*, 2010, **12**, 2730.
54 H. Tang, D. Fuentealba, Y. H. Ko, N. Selvapalam, K. Kim and C. Bohne, *J. Am. Chem. Soc.*, 2011, **133**, 20623.
55 J.-S. Yu, F.-G. Wu, L.-F. Tao, J.-J. Luo and Z.-W. Yu, *Phys. Chem. Chem. Phys.*, 2011, **13**, 3638.
56 Z. Miskolczy and L. Biczók, *J. Phys. Chem. B*, 2014, **118**, 2499.
57 TURBOMOLE V6.5 2013, a development of University of Karlsruhe and Forschungszentrum Karlsruhe GmbH, 1989-2007, TURBOMOLE GmbH, since 2007, available from http://www.turbomole.com.
58 A. Klamt and G. Schüürmann, *J. Chem. Soc., Perkin Trans. 2*, 1993, 799.

V

ION-PAIR COMPLEXATION WITH DIBENZO[21]CROWN-7 AND DIBENZO[24]CROWN-8 BIS-UREA RECEPTORS

by

T. Mäkelä, A. Kiesilä, E. Kalenius & K. Rissanen

Chemistry - A European Journal, **2016**, *22*, 40, 14264 – 14272

https://doi.org/10.1002/chem.201602362

Ion Pair Complexation with Dibenzo-21-Crown-7 and Dibenzo-24-Crown-8 bis-Urea Receptors

Toni Mäkelä,[a] Anniina Kiesilä,[a] Elina Kalenius[a] and Kari Rissanen[a]*

Abstract: Synthesis and ion pair complexation properties of novel ditopic bis-urea receptors based on dibenzo-21-crown-7 (**R¹**) and dibenzo-24-crown-8 (**R²**) scaffolds have been studied in solid-state, solution, and gas-phase. In 4:1 $CDCl_3$/DMSO-d_6 solution both receptors show clear positive heterotropic cooperativity toward halide anions when complexed with Rb^+ or Cs^+, with the halide affinity increasing in order $I^- < Br^- < Cl^-$. In solution the rubidium complexes with both receptors have higher halide affinities compared to the cesium complexes. However, Rb^+ and Cs^+ complexes of **R²** show stronger affinity toward all the studied anions compared to the corresponding cation complexes of **R¹**. Similar selectivity between the receptors toward the studied ion pairs was observed also in the gas-phase by competition experiments with mass spectrometry. Total eight crystal structures with different rubidium and cesium halides and oxyanions were obtained in addition to the crystal structure of **R²·BaCl₂**. The selectivity observed in solution and in the gas-phase is explainable by the conformational differences observed in the crystal structures of ion pair complexes with **R¹** and **R²**. In the solid-state, **R¹** has an open conformation due to the asymmetric crown ether scaffold, whereas **R²** has a compact folded conformation. Computational studies of ion pair complexes of **R²** show that the interaction energies of the complexes increase in the order CsI < CsBr < CsCl < RbCl, supporting the selectivity observed in solution and gas-phase.

Introduction

Ion pair receptors are defined as molecules having binding site for both the cation and the anion, built by using generally well-characterized binding units for each species. The ion pairs can be bound to the receptor in three different modes: 1) as contact ion pairs, 2) as solvent separated ion pairs, or 3) as receptor-separated ion pairs.[1] Ditopic receptors generally have stronger affinity for both ions due to the positive cooperative effects resulting from electrostatic interactions between the co-bound ions and conformational changes induced by the guest inclusion, although also negative cooperativity can exist in binding both guests.[2,3] Nevertheless, ion pair recognition has attracted a growing interest in supramolecular chemistry and anion/cation recognition. Utilizing ion pair receptors in various applications such as salt solubilisation[4,5] and extraction,[6,7] membrane transport,[8-12] catalysis,[13] sensing,[14-16] and logic gates[17,18] offers a strong motive to further develop these systems. In spite of the intriguing features of the ion pair receptors, still surprisingly limited amount of different systems have been developed, possibly because of the more difficult synthesis of the receptors with several binding sites and the more complicated ion pairing equilibriums in the systems under investigation.[1,2]Since the groundbreaking discovery of crown ethers by Charles Pedersen in 1967,[19,20] a huge amount of work has been published using these macrocycles as cation receptors.[21] In addition to utilize them in cation recognition, crown ethers have also been used as the core unit in many ditopic receptors. Especially the work of Reetz,[22] Smith,[23,24] Reinhoudt,[25] Barboiu,[26] Beer,[27,28] Sessler,[29,30], Romanski,[31] and Jurkschat[32] and their co-workers demonstrate how different crown ethers can be further functionalized to build more complex receptor systems. A frequently observed feature in these receptors is the turn-on effect, where one guest, generally the cation, enhances remarkably the binding of the second guest.[30,33-37] However, this simple cooperativity effect is not thoroughly understood and only recently very detailed investigations on the factors influencing the cooperativity have been presented.[38,39] In addition to the simple ion pair receptors with binding sites for a single cation and anion, recently more complicated multitopic receptors have also been reported.[39-44] The limited amount of published work on these types of receptors underpins the challenges for studying and characterizing the intuitively complicated behaviour of these systems.

Recently we have studied the ion pair recognition of benzo-15-crown-5 (B15C5) and benzo-18-crown-6 (B18C6) based bis-urea receptors[45,46] and also the ion pair binding of B15C5 and B18C6 based uranyl salophen receptors in the solid-state.[47] Comprehensive studies of the bis-urea receptors in the solid-state have revealed general characteristics of how these types of molecules behave depending on the nature of the ion pairs, and how the crown ether size affects to the ion pair recognition modes. In addition, solution studies in fairly competitive 4:1 $CDCl_3$/DMSO media manifest strong positive heterotropic cooperativity in halide anion binding with the positively charged alkali metal complexes of these receptors.

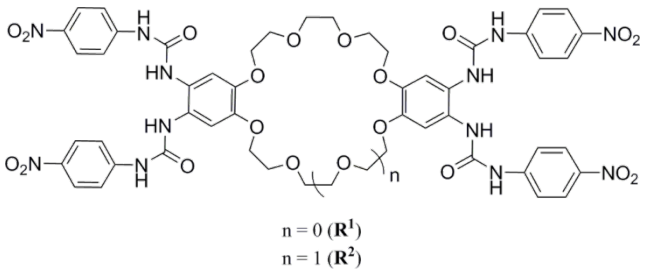

Figure 1. Receptors **R¹** and **R²** used in this study.

[a] M. Sc. T. Mäkelä, M. Sc. A. Kiesilä, Dr. E. Kalenius, Acad. Prof. K. Rissanen
University of Jyvaskyla, Department of Chemistry, Nanoscience Center, P.O. Box 35, FI-40014 University of Jyvaskyla, Finland
E-mail: kari.t.rissanen@jyu.fi

Supporting information for this article is given via a link at the end of the document.((Please delete this text if not appropriate))

Utilization of larger crown ethers with two aromatic rings in the crown ether scaffold makes it possible to modify the ditopic bis-urea receptors even further. Especially intriguing is the possibility of having larger number of urea-groups in the dibenzo-crown ether scaffold, and to take advantage of the larger crown ether size for recognition of larger alkali metals. Therefore, we have synthesized two novel crown ether based receptors with four urea functionalized arms, **R¹** and **R²**, based on dibenzo-21-crown-7 (DB21C7) and dibenzo-24-crown-8 (DB24C8) molecules, respectively (see Figure 1/Scheme 1). The 4-nitrophenyl substituent of the urea-group is known to enhance the anion binding due to strong electron-withdrawing nature of the nitro-group, resulting in increased acidity of the urea-hydrogens, and the stronger hydrogen bonding interactions that follow.[48] Herein, we present the ion pair recognition studies in the solid-state by single-crystal X-ray crystallography, in solution by ^{1}H NMR studies, in gas-phase by mass spectrometry, complemented by computational studies to gain insight about the energetics of the ion pair complexation.

Results and Discussion

The receptors **R¹** and **R²** were synthesized with methods described previously.[45,46] Commercially available starting materials **1** and **2** were nitrated by a two-phase reaction in chloroform and nitric acid/sulfuric acid mixture (Scheme 1). The tetra-nitro products **3** and **4** were obtained in 70 % and 69 % yields, respectively. Tetra-amine compounds **5** and **6** (from **3** and **4**) were synthesized in CH_3CN by reduction of nitro-groups with hydrazine monohydrate under anaerobic conditions in argon atmosphere using 10 % palladium on activated charcoal as catalyst. The yield for **5** was > 98 %, and **6** was obtained with 76 % yield, possibly due to the precipitation of the product during the filtration of the reaction mixture (see Supporting Information). The amines were used in the next step without further purification due to the instability of the products in the presence of oxygen. Condensation reaction with 4-nitrophenylisocyanate (**7**) with vacuum-dried **5** and **6** under argon atmosphere in CH_2Cl_2/DMF mixture gave the desired products **R¹** and **R²**. The products precipitated out from the solution as red solids with 61 % and 64 % yields, respectively. Products **3**, **4**, **R¹**, and **R²** were characterized by ^{1}H, ^{13}C NMR, and ESI-MS. Single-crystal X-ray structures of **3** and **4** were obtained, and the existence of **R¹** and **R²** was proven by single-crystal X-ray structures of their ion pair complexes. The tetra-amines **5** and **6** were characterized by ^{1}H NMR.

The solution-state behaviour of **R¹** and **R²** and their Rb and Cs complexes toward halide anions (chloride, bromide, and iodide) was studied in 4:1 $CDCl_3$/DMSO solution with ^{1}H NMR titrations using alkali metal tetraphenylborates ($MBPh_4$, M = Rb and Cs) as cation source and the tetrabutylammonium halides (TBAX, X = Cl, Br, and I) as the anion source. The non-interacting nature of the counter-ions (BPh_4^- and TBA^+) has been shown before with similar receptor.[46] DMSO was used to solubilize the receptors and to

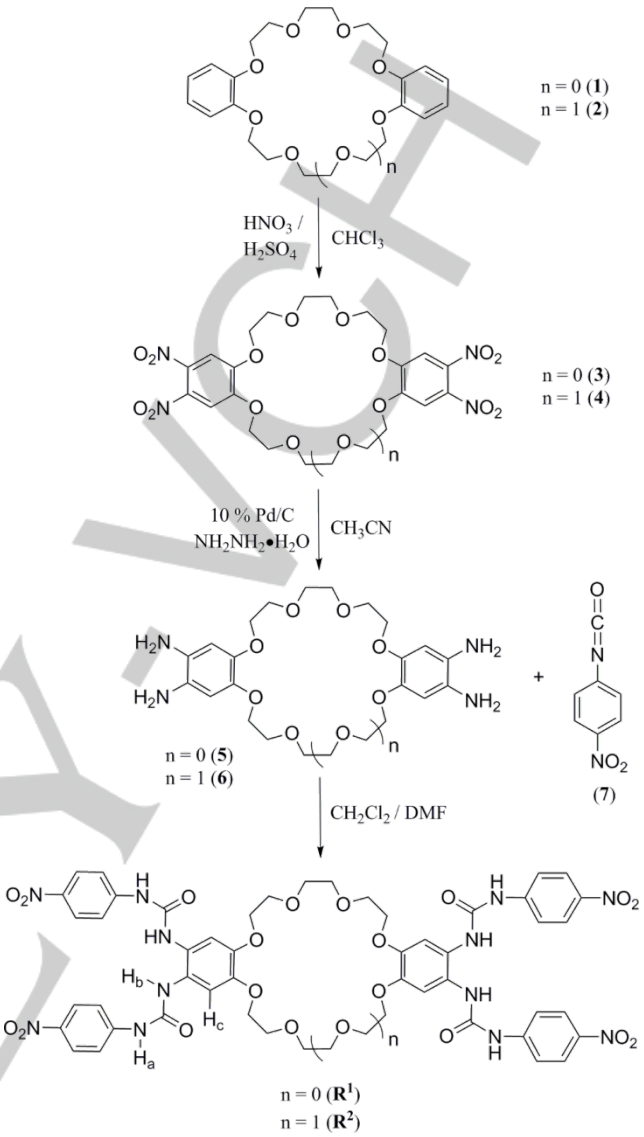

Scheme 1. The synthesis of receptors **R¹** and **R²**. The protons H_a, H_b, and H_c followed in solution studies are presented in the structure of **R¹** and **R²**.

create more competitive media for anion binding studies. The calculated host and guest concentrations, and the binding induced chemical shifts were used in HypNMR2008 program,[49] utilizing global analysis,[50] and using H_a, H_b, and H_c proton signals (see Scheme 1) to calculate the binding constants (*K*). The use of Job's plot analysis in estimating the binding stoichiometries of supramolecular systems has been critically evaluated recently by Thordarsson[50] and Jurczak[51]. Therefore results from Job's plot analysis were treated with caution and more weight was given to the fitting between the observed and calculated chemical shifts in the binding constant calculations.

The halide binding strength of **R¹** and **R²** was studied with ^{1}H NMR titrations in 4:1 $CDCl_3$/DMSO at 303 K. The similar anion binding behaviour was observed for **R¹** and **R²**, as can be seen from the plotted chemical shift differences and the total

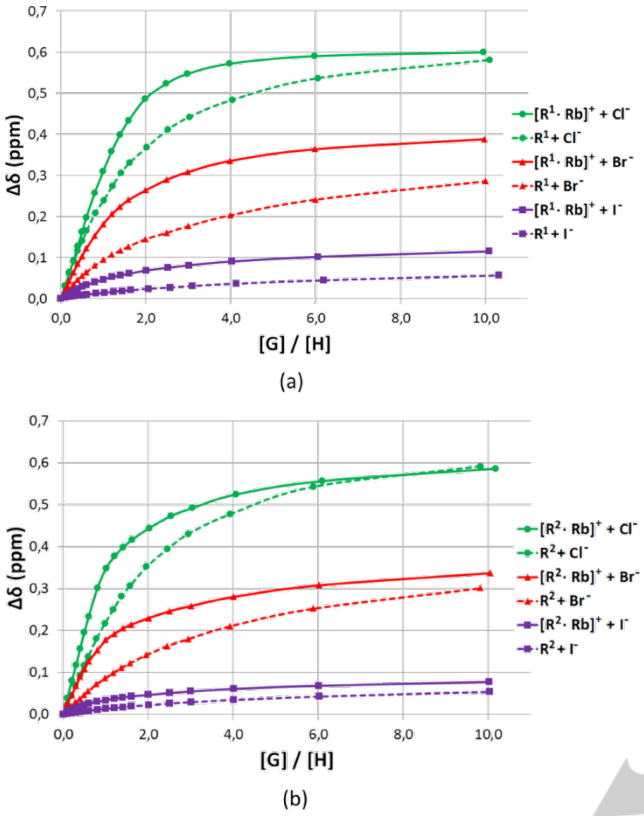

Figure 2. (a) The chemical shift differences observed with (a) **R¹** (dashed line) and [**R¹**·Rb]⁺ (solid line), (b) **R²** (dashed line) and [**R²**·Rb]⁺ (solid line) upon stepwise addition of chloride (green), bromide (red), and iodide (purple).

chemical shift changes (Δδ(Cl⁻) ≈ 0.59 ppm, Δδ(Br⁻) ≈ 0.30 ppm, Δδ(I⁻) ≈ 0.05 ppm) observed upon stepwise addition of the studied halides up to 10 equiv (Figure 2). The binding induced chemical shifts were used to calculate the binding constants with 1:1 binding model (see the Job's plot analysis, Figure S22, S24) for all the anions with good fit between the observed and calculated chemical shifts (Figure S26-S31). The 1:1 binding constants for chloride and bromide are slightly higher for **R¹**, and on the contrary the binding constant for iodide is slightly higher for **R²**. However, the binding constants follow the basicity of the halides, and are in fairly close agreement to the previously obtained binding constants with similar receptors.[45,46] The obtained binding constants are presented in Table 1.

Table 1. Binding constants (K_{xy})[a] obtained with 1:1 binding model for **R¹** and **R²** with halide anions (X = Cl⁻, Br⁻, and I⁻) in 4:1 $CDCl_3$/DMSO-d_6 at 303 K.

		R¹	**R²**
Cl⁻	K_{11}	354 ± 6	258 ± 6
Br⁻	K_{11}	163 ± 7	124 ± 2
I⁻	K_{11}	71 ± 4	83 ± 3

[a] K_{xy}, where x = host, y = guest stoichiometry.

The effect of the alkali metal complexation with **R¹** and **R²** on the halide affinity was studied with ^{1}H NMR titrations in 4:1 $CDCl_3$/DMSO. To study the anion binding affinity of rubidium and cesium complexes of **R¹** and **R²**, the receptors with equimolar amount of $RbBPh_4$ or $CsBPh_4$ were titrated with the corresponding tetrabutylammonium halide. As can be seen from the observed chemical shift differences in Figure 2, the cation complexation has a clear effect on the anion binding behaviour of **R¹** and **R²**, resulting in larger anion induced chemical shifts compared to **R¹** and **R²** alone. The binding constants for chloride binding with rubidium and cesium complexes of **R¹** and **R²** were calculated using 1:1 + 1:2 binding model (see Job's plot analysis, Figure S23 and S25). The chosen binding model gave a very good fit between the observed and calculated chemical shifts and resulted in very high 1:1 binding constants K_{11} = 77965 M^{-1} for [**R¹**·Rb]⁺ + Cl⁻, and K_{11} = 95521 M^{-1} for [**R²**·Rb]⁺ + Cl⁻ complexations (Figure S32 and S38, respectively). The stepwise constants for 1:2 complexations were noticeably smaller (K_{12} = 1318 M^{-1} for [**R¹**·Rb]⁺ + 2Cl⁻, and K_{12} = 275 M^{-1} for [**R²**·Rb]⁺ + 2Cl⁻), indicating that the 1:1 complex is the main component with small chloride concentrations (< 1 equiv, see Figure S32d and S38d). Similar behaviour was observed also for cesium complexes and the binding constants were calculated using the same binding stoichiometry. However, the obtained 1:1 binding constants were lower for cesium complexes of **R¹** and **R²** (Table 2, Figure S35 and S41). This might stem from the larger size, and lower charge density and polarizability of cesium, resulting in weaker electrostatic interactions between the cation and the anion. Interestingly, the observed chemical shifts for [**R²**·Rb]⁺ complex upon chloride addition are reminiscent of behaviour of a dimeric potassium complex of benzo-15-crown-5 based bis-urea receptor.[45] In the solid-state this dimeric assembly (and its ion pair binding behaviour) is structurally very similar to **R²** (see later in the text). Thus, there is a strong structure-function relationship as observed in the similar solution behaviour between two different systems having resembling ion pair binding characteristics in the solid-state.

When bromide binding with rubidium and cesium complexes of **R¹** and **R²** was studied with ^{1}H NMR titrations, a different behaviour between the receptors emerged. The titration data of [**R¹**·Rb]⁺ and [**R¹**·Cs]⁺ with bromide was successfully modelled with 1:1 + 2:1 binding model with a very good fit between the observed and calculated chemical shifts. The obtained 1:1 binding constants for [**R¹**·Rb]⁺ and [**R¹**·Cs]⁺ were K_{11} = 965 and K_{11} = 688 M^{-1}, respectively, being clearly larger than for **R¹** alone (K_{11} = 163 M^{-1}). The stepwise constants for 2:1 complex formation are fairly high in both cases, meaning that with small bromide concentrations (< 1 equiv) both species are present in equilibrium (see Figure S33 and S36). Interestingly, when [**R²**·Rb]⁺ complex was titrated with bromide, clear resemblance in the binding behaviour with chloride emerged (Figure 2b) although the total chemical shifts were smaller. This

Table 2. Binding constants (K_{xy})[a] obtained for $[\mathbf{R^1}\cdot M]^+$ and $[\mathbf{R^2}\cdot M]^+$ titrations (M = Rb and Cs) in 4:1 $CDCl_3$/DMSO-d_6 at 303 K.

		$[\mathbf{R^1}\cdot Rb]^+$	$[\mathbf{R^1}\cdot Cs]^+$	$[\mathbf{R^2}\cdot Rb]^+$	$[\mathbf{R^2}\cdot Cs]^+$
Cl^-	K_{11}[b]	77965 ± 36047	22673 ± 9310	95521 ± 44353	50362 ± 25102
	K_{12}[b]	1318 ± 128	1316 ± 173	275 ± 36	445 ± 61
Br^-	K_{11}[b]	-	-	13020 ± 2510	5278 ± 2100
	K_{12}[b]	-	-	85 ± 12	101 ± 41
	K_{11}[c]	965 ± 89	688 ± 82	-	-
	K_{21}[c]	381 ± 147	183 ± 95	-	-
I^-	K_{11}[d]	337 ± 19	253 ± 12	384 ± 38	440 ± 20

[a]log K_{xy}, where x = host, y = guest stoichiometry.[b]1:1 + 1:2 binding model used. [c]1:1 + 2:1 binding model used. [d]1:1 binding model used.

behaviour was modelled with 1:1 + 1:2 binding model resulting in K_{11} = 13020 M^{-1}. Similar 1:1 + 1:2 binding model was also utilized for $[\mathbf{R^2}\cdot Cs]^+ + Br^-$ titration resulting in K_{11} = 5278 M^{-1}. The stepwise binding constants for 1:2 complex formations are very small for both complexes (K_{12} = 85 M^{-1} for $[\mathbf{R^2}\cdot Rb]^+$, and K_{12} = 101 M^{-1} $[\mathbf{R^2}\cdot Cs]^+$), resulting in a very small 1:2 complex concentrations with < 1 equiv of bromide (see Figure S39 and S42). This clear difference in bromide binding behaviour of the cationic complexes of $\mathbf{R^1}$ (unsymmetrical, open conformation) and $\mathbf{R^2}$ (symmetrical, folded) might result from the conformational differences of the receptor scaffolds as observed in the solid-state complexes (see Figures 5 and 6). The folded structure of $\mathbf{R^2}$ in the presence of cation has a suitable binding site for bromide resulting in very strong 1:1 complexation, whereas the more open conformation of $\mathbf{R^1}$ (as seen in the solid-state structure) is unspecific for the bromide anion resulting in different and clearly weaker binding compared to $[\mathbf{R^2}\cdot Rb]^+$ and $[\mathbf{R^2}\cdot Cs]^+$ complexes.

The iodide induced chemical shift differences were modelled with simple 1:1 binding model, resulting in moderate binding constants. For $[\mathbf{R^1}\cdot Rb]^+$ and $[\mathbf{R^1}\cdot Cs]^+$ the binding constants with iodide were K_{11} = 337 and K_{11} = 253 M^{-1}, respectively, and for $[\mathbf{R^2}\cdot Rb]^+$ and $[\mathbf{R^2}\cdot Cs]^+$ 1:1 binding constants were K_{11} = 384 and K_{11} = 440 M^{-1}, respectively This is understandable due to the weak hydrogen bond acceptor character of iodide. Nevertheless, all the obtained binding constants for iodide are higher with the cationic complexes of $\mathbf{R^1}$ and $\mathbf{R^2}$ compared to $\mathbf{R^1}$ and $\mathbf{R^2}$ alone, proving that there is a clear turn-on effect and positive heterotropic cooperativity induced by the cation complexation with the receptors.

Mass spectrometric studies with $\mathbf{R^1}$ and $\mathbf{R^2}$ were performed to get more insight of the selectivity and affinity of the receptors toward the ion pairs. The gas-phase behaviour of $\mathbf{R^1}$ and $\mathbf{R^2}$ with selected ion pairs was studied with complexation and competition experiments. In addition, the topology and kinetic stability of the ion pair complexes with the receptors were studied with collision-induced dissociation (CID) experiments. Complexation experiments with RbCl, RbBr, RbI, CsCl, CsBr, and CsI from samples with 1:3 ratio (receptor : ion pair) showed clearly ion pair binding with both receptors, which was observed on negative polarization as formation of $[\mathbf{R}+CA+A]^-$ complexes ($\mathbf{R}$ = receptor, C = cation, and A = anion). In addition to ion pair complexes, also anion adducts were generally observed, $[\mathbf{R}+2A]^{2-}$ complex being especially abundant (Figure 3). The binding behaviour observed in simple complexation experiments was very similar between $\mathbf{R^1}$ and $\mathbf{R^2}$, and similar complexes were seen with all tested ion pairs, with only the abundance of the observed adducts differing according to the basicity of the anion.

The relative affinities of the receptors toward ion pairs were further studied with competition experiments, where two ion pairs were added to the same sample in excess (1:3:3). The competition pairs were chosen to reveal both the effect of the

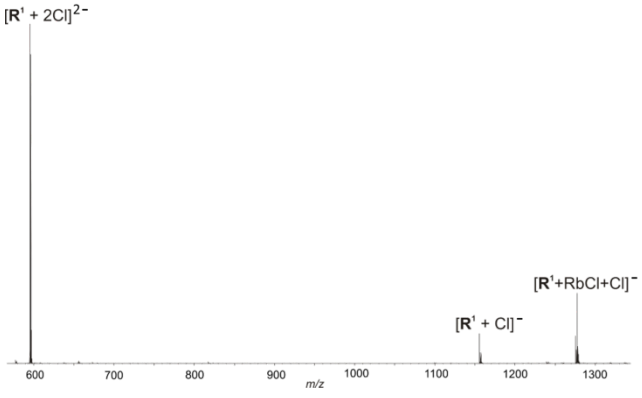

Figure 3. (–)ESI-MS spectrum of $\mathbf{R^1}$ and RbCl (1:3, 20 μM in CH_3CN).

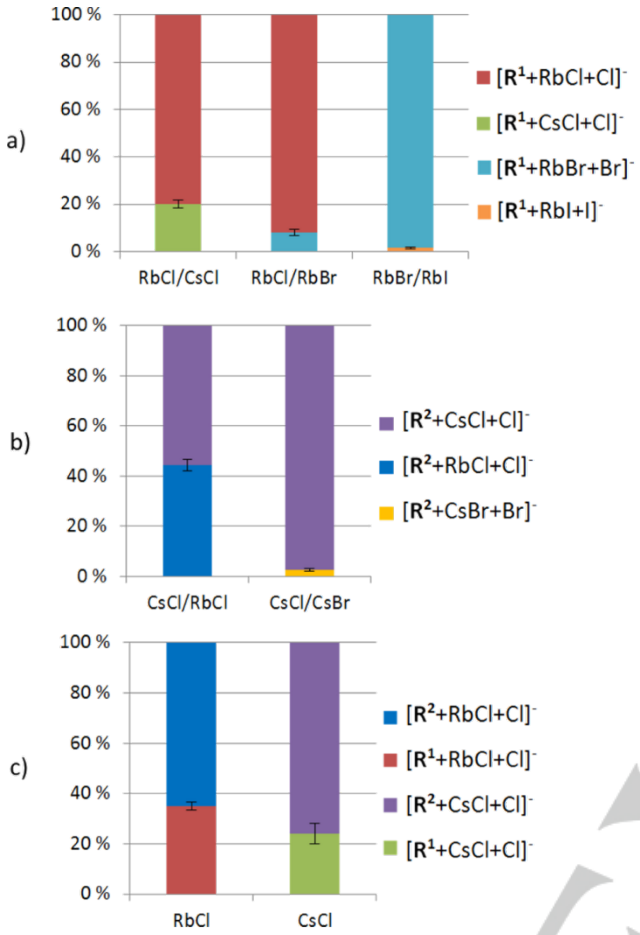

Figure 4. Relative affinites of (a) **R¹** and (b) **R²** towards different ion pairs based on competitive ESI-MS measurements. The **R²** and CsBr/CsI competition result is not shown due the small amount of [**R²**+CsI+I]⁻ ion in experiment (< 1 %). (c) Results of competition experiments between **R¹** and **R²** toward RbCl and CsCl. Both ion pairs favor binding with **R²**.

cation and the anion. Based on competition experiments, both receptors indicated same anion affinity ($Cl^- > Br^- > I^-$) following the basicity of the anions and supporting the results from solution-state experiments. **R¹** showed a clear preference toward rubidium chloride over cesium chloride (Figure 4a), being in accordance with the rubidium selectivity over cesium with DB21C7.[52] Instead, **R²** affinity towards cations was more similar (Figure 4b), and only slight preference for cesium complexation was observed. This is also in accordance with similar solid-state structures of **R²** with rubidium and cesium salts (see Figure 6), and with results showing cesium cation to have a stronger affinity to DB24C8 compared to rubidium in highly polar DMF solution.[53]

Competition experiments were also performed between receptors, and in these experiments receptors were added in 1:1:3 ratio compared to ion pair. Receptor competitions were performed with RbCl and CsCl, both favouring complexation with **R²** rather than **R¹** (Figure 4c). This indicates a stronger affinity of **R²** toward both RbCl and CsCl also in the gas-phase, and supporting the results obtained from ^{1}H NMR titrations. The folded conformation of **R²** seen in the solid-state structures can persist also in the gas-phase, enhancing the ion pair binding ability of **R²**, and explaining the binding preference observed in the competition experiments.

The kinetic stabilities and gas-phase structural features of the complexes were further studied in CID experiments, where both receptors dissociated in a similar pattern. The isolated ion pair complexes [**R**+C+2A]⁻ underwent an elimination of the ion pair in a first dissociation step, and [**R**+A]⁻ was observed as the initial dissociation product. (Figure S45). Peaks corresponding to eliminated free anions [A]⁻ were not observed in CID mass spectra. This implies that one anion is bound to the complex as a contact ion pair rather than two anions being bound to the receptor separately via hydrogen bonding. The elimination of CA was followed by the cleavage of HA, suggesting that the second anion is bound to the receptor through hydrogen bonding, most likely interacting with urea hydrogens. With higher collision energies, a further dissociation of the receptor itself was observed and two consecutive fragmentations from urea side-arms occurred resulting in formation of crown-imidazolidine structure (Figure S45-S47). This further point to, in particular, deprotonation of urea groups and anion hydrogen bonding with urea-hydrogens, although CID as a dissociation method has ergodic nature leading to energy randomization. The obtained dissociation curves were fitted with a sigmoidal model, which allowed the calculation of $CE^{50\%}$, representing roughly the relative energy which is needed for the complex to dissociate to its half intensity (Table S1). When comparing dissociation curves (Figure S48), it is clear that both receptors form more stable complexes with rubidium than cesium salts. Also receptor **R²** forms, generally, more stable complexes compared to **R¹**. The most stable complex according to CID dissociation curves is [**R²**+RbCl+Cl]⁻, although the differences between the anions are negligible. All in all, the mass spectrometry competition and CID data coincides with the solution data.

A series of crystallization experiments were performed and the obtained crystals were studied with single-crystal X-ray crystallography to get more detailed picture of the interactions governing the ion pair binding of **R¹** and **R²**. Crystals with sufficient diffraction quality of only one ion pair complex with **R¹** (**R¹·Rb₂CO₃**) was obtained in spite of numerous attempts. In contrast, seven crystal structures of rubidium and cesium halides and oxyanions were obtained with **R²**. Crystallization experiments with earth-alkaline metal halides were also done resulting in crystal structure **R²·BaCl₂**.

The obtained complexes with **R¹** and **R²** reveal distinctive differences between the receptor conformations in the solid-state. The complex **R¹·Rb₂CO₃** (Figure 5) was obtained by aerial CO_2 fixation in basic organic media (RbF in DMF), phenomenon observed before.[46,54,55] Due to the asymmetric structure of DB21C7 core, in structure **R¹·Rb₂CO₃** the receptor is in "open" conformation, with the receptor arms on opposite sides of the crown ether ring. The rubidium cation is coordinated with all the seven crown ether oxygens, and further coordinative bonds are

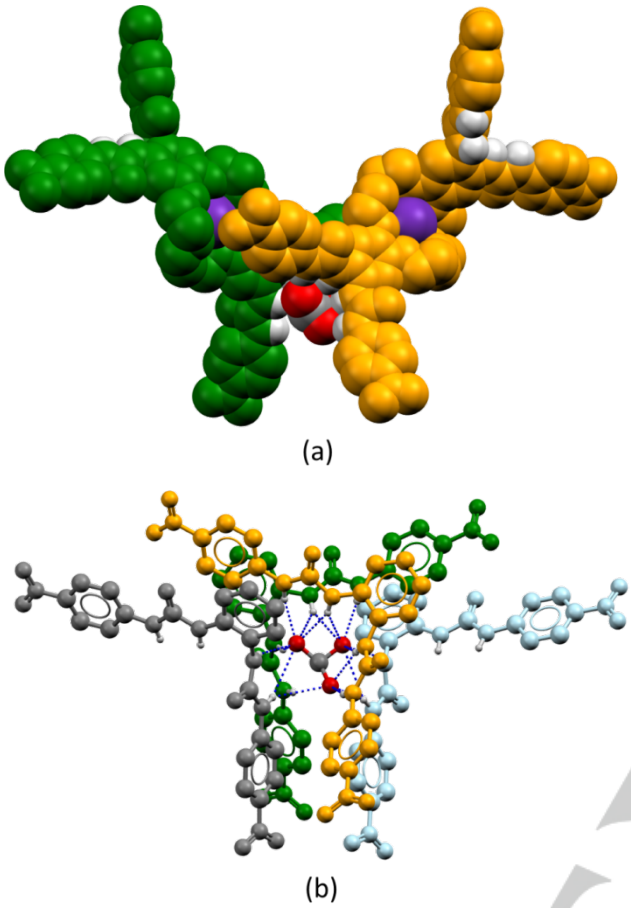

Figure 5. (a) The CPK model of complex **R¹·Rb₂CO₃**, showing two receptor molecules with carbonate anion. Rubidium cations are coordinated by total nine Rb···O bonds, formed with crown ether oxygens, and carbonyl and nitro group oxygens in the adjacent molecules. (b) The carbonate anion is hydrogen bonded with total four **R¹** molecules through urea-group mediated hydrogen bonds. Solvent molecules have been omitted from the figure for clarity.

formed with carbonyl oxygen O2' and nitro group oxygen O8'' in the neighbouring molecules (see Supporting Information for details, Figure S13), resulting in very complex interplay between the cation-complexed receptor and the carbonate anion. The carbonate anion is hydrogen bonded with total four receptor molecules through urea-group mediated hydrogen bonds with N-O distances ranging from 2.854 – 3.112 Å (see Figure 5b and Figure S13d). The dimeric assembly presented in Figure 5a resembles a general ion pair binding motif observed with B18C6 based bis-urea receptor.[46] Possibly due to the asymmetric structure and more flexible conformation of the DB21C7 scaffold, this complex was the only one that crystallized with sufficient crystal quality for single-crystal structure determination. For the symmetric DB24C8 based receptor **R²** single-crystals were easier to obtain, probably because of the more compact structure of the ion pair complex.

In the course of this work crystals of **R²** with different rubidium and cesium halides and oxyanions were obtained [**R²·RbCl** (Figure 6a, Figure S14), **R²·RbI** (Figure S15), **R²·RbCOOCH₃** (Figure S16), **R²·CsCl** (Figure S17), **R²·CsBr** (Figure S18), and **R²·CsCO₃CH₃** (Figure 6b, Figure S19)]. All the obtained alkali metal (Rb and Cs) complexes with **R²** have a folded receptor structure, with the receptor arms having the same orientation, creating a suitable binding site for the anion (Figure 6). The cation is coordinated with all the crown ether oxygens with Rb···O distances being between 2.889 – 3.247 Å (in **R²·RbCl**) and Cs···O distances being between 3.004 – 3.342 Å (in **R²·CsCO₃CH₃**). Similar folded conformation in cesium complex of simple DB24C8 in the solid-state has been observed before.[56] The folding of the receptor opens the crown ether ring, leaving the cation open from the topside for further coordination, and in all the obtained complexes with **R²** there are one to three additional coordinative bonds to the cation formed with either solvent molecules (dichloromethane, methanol, DMF, DMSO) or nitro-group oxygens. In all the crystal structures of **R²** with Rb and Cs, the anion is hydrogen bonded with the urea-groups directed toward the binding pocket. In addition, all the halide complexes have also solvent molecules (methanol, chloroform, dichloromethane) interacting with the anion through -OH and -CH hydrogen bonds. The N···Cl⁻ hydrogen bond lengths in complex **R²·RbCl** vary between 3.220 – 3.551 Å, and in **R²·CsCO₃CH₃** N···O hydrogen bond lengths are between 2.763 – 2.924 Å. The receptor arms that are not involved in the anion binding form either intermolecular hydrogen bonds to the adjacent molecules affecting the packing of the complexes, form intramolecular hydrogen bond between receptor arms enhancing the folding, or interact with solvent molecules. Detailed analysis of the complexes is presented in the Supporting Information.

Crystallization experiments with **R¹** and **R²** and earth-alkaline metals resulted in the solid-state complex **R²·BaCl₂** (Figure 7). Due to the smaller ionic radii of barium (1.40 Å) compared to rubidium (1.68 Å),[57] barium complexation leads to more twisted conformation of the crown ether ring. To optimize the coordination with the crown ether oxygens (Ba···O distances 2.829 – 3.095 Å), the crown ether ring is "closed" from the top, hindering cation coordination from the topside of the receptor. However, this conformation enables solvent molecules (DMF and water) to coordinate with the cation, resulting in three additional coordinative bonds between Ba^{2+} and the solvent molecules. This type of conformation of DB24C8 scaffold has been observed before with Ba^{2+} and K^{+}, which are similar in size.[58,59] Each receptor arm is hydrogen bonded with a different chloride anion, and each anion is hydrogen bonded with a neighboring **R²** molecule (Figure S20) with N···Cl⁻ distances being 3.090 – 3.392 Å.

The obtained solid-state complexes clearly show the structural differences of **R¹** and **R²** in ion pair binding. Because of the asymmetric structure of dibenzo-21-crown-7 scaffold, **R¹** has an open conformation. On the other hand, symmetric structure of dibenzo-24-crown-8 scaffold enables folded conformation of **R²** when complexed with rubidium and cesium cations. The asymmetric structure of **R¹** might also reflect the difficulties in obtaining solid-state complexes with the receptor as opposed to more compact **R²**. When complexed with smaller

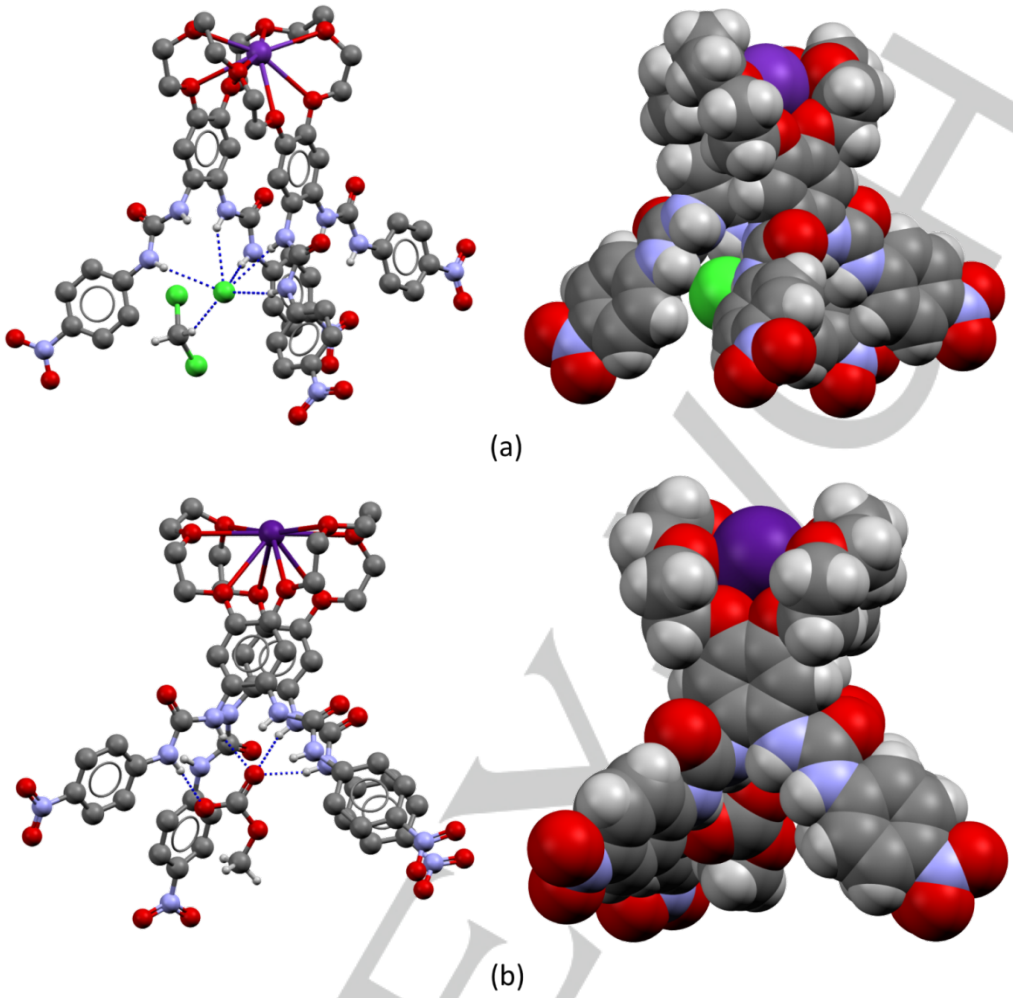

Figure 6. (a) Ball-and-stick and CPK models of complex **R²·RbCl**. Three additional coordinative bonds to Rb^+ are formed by dichloromethane and two nitro-group oxygens of the neighbouring molecule (not shown). The chloride anion is hydrogen bonded with five urea-protons, and a dichloromethane molecule forms an additional C···H hydrogen bond with the chloride. (b) Ball-and-stick and CPK models of complex **R²·CsCO₃CH₃**. The anion is hydrogen bonded with two receptor arms. Two additional coordinative bonds are formed to cesium by nitro-oxygens of the adjacent molecule. All the solvent molecules interacting with the receptor are omitted from the figure.

barium cation, **R²** has more open and twisted conformation to optimize the cation coordination with the crown ether oxygens. Thus the size and the nature of the complexed cation have a clear effect on the solid-state conformation of **R²**. However, the distinctive differences in the solid-state conformations between **R¹** and **R²** can explain the different solution-state behaviour of the receptors, and the gas-phase selectivity of **R²** towards RbCl and CsCl compared to **R¹** as observed in the competition experiments with mass spectrometry.

Finally, theoretical calculations for selected ion pair complexes were performed for two reasons; firstly to visualize the structures of the complexes in solvent (and packing) free environment and secondly to compare the interaction energies. Unfortunately, the optimization of the open structures turned out to be computationally exhaustive, and for that reason only ion pair complexes with folded receptor **R²** were optimized. The obtained crystal structures were used as starting structures and calculations were performed on *ab initio* level of theory (HF/6-31G**).

The geometry optimizations starting from the folded structure of **R²** resulted in rather similar structures with all the ion pairs, in which the cation was bound by the crown moiety and the anion was hydrogen bonded by three urea side-arms with all in all six hydrogen bonds while the fourth sidearm was more distant, likely for steric reasons (see Figure 8 for optimized complex with CsCl. The H···A^- distances of five hydrogen bonds differed on narrow range (2.4 to 2.6 Å for Cl^-, 2.6 to 2.8 Å for Br^- and 2.8 to 3.0 Å for I^-), whereas one of the hydrogen bonds was bit longer (2.9 Å for Cl^-, 3.1 Å for Br^- and 3.4 Å for I^-). There are small differences in hydrogen bonding *in vacuo* compared to

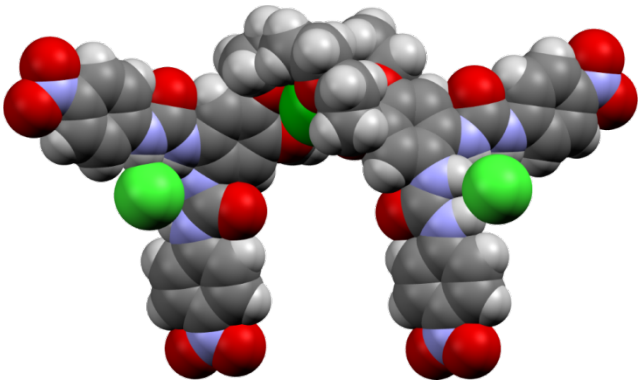

Figure 7. CPK model for complex $\mathbf{R^2}$·$\mathbf{BaCl_2}$. Three additional coordinative bonds with barium are formed to DMF and water molecules (not shown). The chloride anion is further hydrogen bonded by an adjacent $\mathbf{R^2}$ molecule. Only one of the three complexes in the structure is shown. Solvent molecules are omitted for clarity.

crystal structures due to absence of possibility of urea-hydrogens to interact with solvent molecules or neighbouring receptor molecules. The distances between the cation and anion are very similar in all complexes and vary between 8.6 and 9.0 Å (differences arise mainly from differences in ionic radii). The geometry optimization for empty receptor $\mathbf{R^2}$ resulted in a structure with three hydrogen bonds (2.0, 2.1 and 2.3Å), between three urea side-arms (not shown). Total energy of the receptor is ca. 150 kJ mol^{-1} lower without a complexed ion pair, which implies that unfavourable reorganization takes place during the complexation which is then compensated by increased interaction energies in the ion pair complexes. Interaction energies between the receptor and ion pairs increase clearly in order CsI < CsBr < CsCl < RbCl, which supports the experimental results (see Table S2 for interaction energies). Generally, it can be concluded that the experimental observations (NMR, mass spectrometry) concerning relative behaviour of the receptors and their affinities toward ion pairs arise from inherent properties of receptors, and can be justified on molecular level.

Conclusions

In summary, we have synthesized two novel ditopic bis-urea receptors, based on dibenzo-21-crown-7 ($\mathbf{R^1}$) and dibenzo-24-crown-8 scaffolds ($\mathbf{R^2}$). The receptors were obtained in good yields through simple synthetic procedures. The relative ion pair binding affinities toward RbCl, RbBr, RbI, CsCl, CsBr, and CsI were studied in solution with ^{1}H NMR titrations, and in gas-phase with mass spectrometry. Both receptors have similar affinities toward halide anions (chloride, bromide, iodide) in solution, and in the presence of alkali metal (rubidium, cesium) both receptors show clear positive heterotropic cooperativity in anion binding. The rubidium complexes of both receptors have higher halide affinities compared to the corresponding cesium complexes, which probably stems from the smaller size and stronger point charge of the rubidium resulting in stronger electrostatic interactions between the ion pair. However, $\mathbf{R^2}$ shows better selectivity toward RbCl and CsCl compared to $\mathbf{R^1}$ both in solution and in the gas-phase. This is explainable by the conformational differences between the receptors as observed in the obtained crystal structures of ion pair complexes with $\mathbf{R^1}$ and $\mathbf{R^2}$. In the solid-state $\mathbf{R^1}$ has an open conformation due to the asymmetric structure of the central DB21C7 scaffold, whereas $\mathbf{R^2}$ has a compact folded conformation, creating a suitable anion binding site within the receptor. With $\mathbf{R^1}$ the positive heterotropic cooperativity probably results solely from the electrostatic attraction between the cation and anion, whereas with $\mathbf{R^2}$ the stronger anion affinities might result both from electrostatic interactions and from the change in the receptors conformation upon cation coordination, thus representing allosteric cooperativity. The computational studies performed with $\mathbf{R^2}$ revealed selectivity order CsI < CsBr < CsCl < RbCl according to the interaction energies of the ion pair

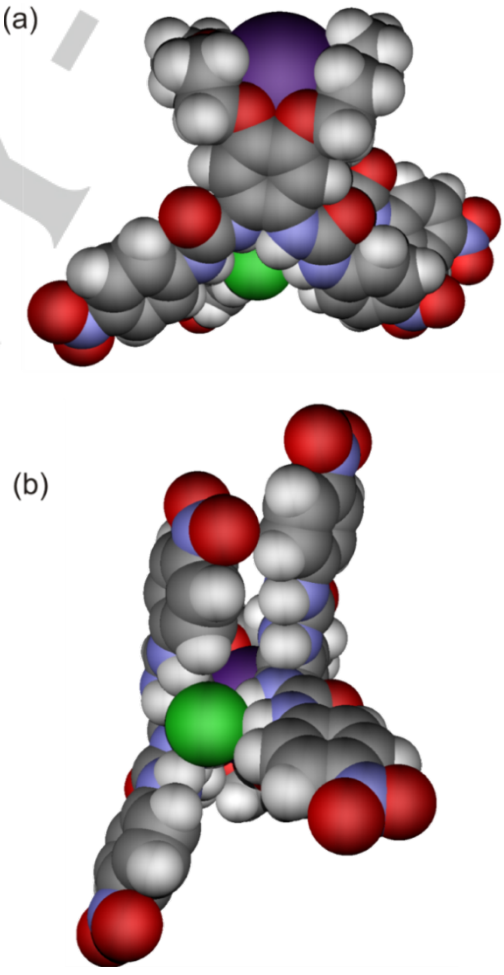

Figure 8. Optimized (HF/6-31G**) lowest energy structure for $\mathbf{R^2}$•**CsCl**. (a) Side-view showing Cs^+ coordination in crown moiety, (b) bottom-view showing hydrogen bonding of Cl^- anion with three side-arms.

complexes, fully supporting the solution and gas-phase results. The molecules studied in this work represent interesting new scaffolds for ditopic receptor systems for studying the cooperative factors affecting the ion pair binding. These receptors could be further developed with different functional groups to gain more selective ion pair receptors effective also in more polar media. The crystal structure $\mathbf{R^2 \cdot BaCl_2}$ shows the tritopic behavior of these receptors exemplifying the versatile nature of these systems.

Acknowledgements

We thank the Academy of Finland (K.R.: Project Nos. 263256 and 265328, EK: 284562 and 278743) and Graduate School of Univ. of Jyväskylä (T.M.) for financial support. Johanna Lind and M. Sc. Esa Haapaniemi are gratefully acknowledged for their help with the MS and NMR experiments. M Sc. Ville Holopainen is acknowledged for his help with the crystallization experiments.

Keywords: ion pair recognition • ditopic receptors • hydrogen bonding • crown ethers • ^{1}H NMR titration • crystallography • mass spectrometry • supramolecular chemistry

[1] S. K. Kim, J. L. Sessler, *Chem. Soc. Rev.* **2010**, *39*, 3784-3809. 10.1039/c002694h

[2] A. J. McConnell, P. D. Beer, *Angew. Chem. Int. Ed.* **2012**, *51*, 5052-5061. 10.1002/anie.201107244

[3] G. Kirkovits, J. Shriver, P. Gale, J. Sessler, *J. Inclusion Phenom. Macrocyclic Chem.* **2001**, *41*, 69-75. 10.1023/A:1014468126351

[4] Z. Sun, F. Pan, Triyanti, M. Albrecht, G. Raabe, *Eur. J. Org. Chem.* **2013**, *2013*, 7922-7932. 10.1002/ejoc.201301032

[5] J. Scheerder, J. P. M. van Duynhoven, J. F. J. Engbersen, D. N. Reinhoudt, *Angew. Chem. Int. Ed.* **1996**, *35*, 1090-1093. 10.1002/anie.199610901

[6] B. Akhuli, P. Ghosh, *Chem. Commun.* **2015**, *51*, 16514-16517. 10.1039/c5cc07291c

[7] J. M. Mahoney, A. M. Beatty, B. D. Smith, *Inorg. Chem.* **2004**, *43*, 7617-7621. 10.1021/ic049066b

[8] J. H. Lee, J. H. Lee, Y. R. Choi, P. Kang, M. Choi, K. Jeong, *J. Org. Chem.* **2014**, *79*, 6403-6409. 10.1021/jo501145z

[9] A. Vargas Jentzsch, D. Emery, J. Mareda, P. Metrangolo, G. Resnati, S. Matile, *Angew. Chem.* **2011**, *123*, 11879-11882. 10.1002/ange.201104966

[10] X. Wang, S. Li, Y. Ao, Q. Wang, Z. Huang, D. Wang, *Org. Biomol. Chem.* **2016**, *14*, 330-334. 10.1039/c5ob02291f

[11] L. A. J. Chrisstoffels, F. de Jong, D. N. Reinhoudt, S. Sivelli, L. Gazzola, A. Casnati, R. Ungaro, *J. Am. Chem. Soc.* **1999**, *121*, 10142-10151. 10.1021/ja991588g

[12] C. C. Tong, R. Quesada, J. L. Sessler, P. A. Gale, *Chem. Commun.* **2008**, 6321-6323. 10.1039/b814988g

[13] K. Brak, E. N. Jacobsen, *Angew. Chem. Int. Ed.* **2013**, *52*, 534-561. 10.1002/anie.201205449

[14] P. Molina, A. Tarraga, M. Alfonso, *Dalton Trans.* **2014**, *43*, 18-29. 10.1039/c3dt52459k

[15] R. Gotor, A. M. Costero, S. Gil, P. Gaviña, K. Rurack, *Eur. J. Org. Chem.* **2014**, *2014*, 4005-4013. 10.1002/ejoc.201402214

[16] Y. Li, Q. Zhao, H. Yang, S. Liu, X. Liu, Y. Zhang, T. Hu, J. Chen, Z. Chang, X. Bu, *Analyst* **2013**, *138*, 5486-5494. 10.1039/c3an00351e

[17] R. Gotor, A. M. Costero, S. Gil, M. Parra, P. Gavina, K. Rurack, *Chem. Commun.* **2013**, *49*, 11056-11058. 10.1039/c3cc45377d

[18] A. P. de Silva, G. D. McClean, S. Pagliari, *Chem. Commun.* **2003**, 2010-2011. 10.1039/b305262a

[19] C. J. Pedersen, *J. Am. Chem. Soc.* **1967**, *89*, 7017-7036. 10.1021/ja01002a035

[20] C. J. Pedersen, *Science* **1988**, *241*, 536-540. 10.1126/science.241.4865.536

[21] G. W. Gokel, W. M. Leevy, M. E. Weber, *Chem. Rev.* **2004**, *104*, 2723-2750. 10.1021/cr020080k

[22] M. T. Reetz, C. M. Niemeyer, K. Harms, *Angew. Chem. Int. Ed.* **1991**, *30*, 1472-1474. 10.1002/anie.199114721

[23] R. Shukla, T. Kida, B. D. Smith, *Org. Lett.* **2000**, *2*, 3099-3102. 10.1021/ol0063104

[24] J. M. Mahoney, A. M. Beatty, B. D. Smith, *J. Am. Chem. Soc.* **2001**, *123*, 5847-5848. 10.1021/ja0156082

[25] D. M. Rudkevich, Z. Brzozka, M. Palys, H. C. Visser, W. Verboom, D. N. Reinhoudt, *Angew. Chem. Int. Ed.* **1994**, *33*, 467-468. 10.1002/anie.199404671

[26] M. Barboiu, G. Vaughan, A. van der. Lee, *Org. Lett.* **2003**, *5*, 3073-3076. 10.1021/ol035096r

[27] P. D. Beer, M. G. B. Drew, R. J. Knubley, M. I. Ogden, *J. Chem. Soc., Dalton Trans.* **1995**, 3117-3123. 10.1039/DT9950003117

[28] J. E. Redman, P. D. Beer, S. W. Dent, M. G.B. Drew, *Chem. Commun.* **1998**, 231-232. 10.1039/A707680K

[29] S. K. Kim, J. L. Sessler, *Acc. Chem. Res.* **2014**, *47*, 2525-2536. 10.1021/ar500157a

[30] G. J. Kirkovits, R. S. Zimmerman, M. T. Huggins, V. M. Lynch, J. L. Sessler, *Eur. J. Org. Chem.* **2002**, *2002*, 3768-3778. 10.1002/1099-0690(200211)2002:22<3768::AID-EJOC3768>3.0.CO;2-R

[31] J. Romanski, P. Piątek, *Chem. Commun.* **2012**, *48*, 11346-11348. 10.1039/c2cc36607j

[32] G. Reeske, M. Schürmann, B. Costisella, K. Jurkschat, *Eur. J. Inorg. Chem.* **2005**, *2005*, 2881-2887. 10.1002/ejic.200500191

[33] P. Beer D., S. W. Dent, *Chem. Commun.* **1998**, 825-826. 10.1039/A800356D

[34] M. K. Chae, J. Lee, N. Kim, K. Jeong, *Tetrahedron Lett.* **2007**, *48*, 6624-6627. 10.1016/j.tetlet.2007.07.115

[35] O. Perraud, V. Robert, A. Martinez, J. Dutasta, *Chem. Eur. J.* **2011**, *17*, 4177-4182. 10.1002/chem.201002116.

[36] J. V. Gavette, J. Lara, L. L. Reling, M. M. Haley, D. W. Johnson, *Chem. Sci.* **2013**, *4*, 585-590. 10.1039/c2sc21501b

[37] P. Piątek, M. Karbarz, J. Romański, *Dalton Trans.* **2014**, *43*, 8515-8522. 10.1039/c4dt00576g

[38] B. Qiao, A. Sengupta, Y. Liu, K. P. McDonald, M. Pink, J. R. Anderson, K. Raghavachari, A. H. Flood, *J. Am. Chem. Soc.* **2015**, *137*, 9746-9757. 10.1021/jacs.5b05839

[39] E. N. W. Howe, M. Bhadbhade, P. Thordarson, *J. Am. Chem. Soc.* **2014**, *136*, 7505-7516. 10.1021/ja503383e

[40] S. Moerkerke, S. Le Gac, F. Topić, K. Rissanen, I. Jabin, *Eur. J. Org. Chem.* **2013**, *2013*, 5315-5322. 10.1002/ejoc.201300639

[41] S. Moerkerke, M. Ménand, I. Jabin, *Chem. Eur. J.* **2010**, *16*, 11712-11719. 10.1002/chem.201001193

[42] J. Eckelmann, V. Saggiomo, F. D. Sonnichsen, U. Luning, *New J. Chem.* **2010**, *34*, 1247-1250. 10.1039/c0nj00160k

[43] T. Nabeshima, T. Saiki, J. Iwabuchi, S. Akine, *J. Am. Chem. Soc.* **2005**, *127*, 5507-5511. 10.1021/ja042882y

[44] V. Valderrey, E. C. Escudero-Adán, P. Ballester, *Angew. Chem. Int. Ed.* **2013**, *52*, 6898-6902. 10.1002/anie.201302524

[45] T. Mäkelä, K. Rissanen, *Dalton Trans.* **2016**. 10.1039/c6dt00414h

[46] T. Mäkelä, E. Kalenius, K. Rissanen, *Inorg. Chem.* **2015**, *54*, 9154-9165. 10.1021/acs.inorgchem.5b01577

[47] T. Mäkelä, M.-E. Minkkinen, K. Rissanen, *Inorg. Chem.* **2016**, *55*, 1339-1346. 10.1021/acs.inorgchem.5b02780

[48] S. Camiolo, P. A. Gale, M. B. Hursthouse, M. E. Light, *Org. Biomol. Chem.* **2003**, *1*, 741-744. 10.1039/B210848H

[49] C. Frassineti, S. Ghelli, P. Gans, A. Sabatini, M. S. Moruzzi, A. Vacca, *Anal. Biochem.* **1995**, *231*, 374-382. 10.1006/abio.1995.9984
[50] P. Thordarson, *Chem. Soc. Rev*. **2011**, *40*, 1305-1323. 10.1039/c0cs00062k
[51] F. Ulatowski, K. Dąbrowa, T. Bałakier, J. Jurczak, *J. Org. Chem.* **2016**, *81*, 1746-1756. 10.1021/acs.joc.5b02909
[52] S. Katsuta, T. Kuwano, Y. Ito, Y. Takeda, *J. Chem. Eng. Data* **2005**, *50*, 1313-1318. 10.1021/je050045l
[53] C. M. Goff, M. A. Matchette, N. Shabestary, S. Khazaeli, *Polyhedron* **1996**, *15*, 3897-3903. 10.1016/0277-5387(96)00018-6
[54] R. Custelcean, L. H. Delmau, B. A. Moyer, J. L. Sessler, W. Cho, D. Gross, G. W. Bates, S. J. Brooks, M. E. Light, P. A. Gale, *Angew. Chem. Int. Ed.* **2005**, *44*, 2537-2542. 10.1002/anie.200462945
[55] I. Ravikumar, P. Ghosh, *Chem. Commun*. **2010**, *46,* 1082–1084. 10.1039/b915661e
[56] J. A. Rusanova, P. J. Squattrito, V. V. Ponomareva, K. V. Domasevitch, V. N. Kokozay, *Z. Naturforsch. B Chem. Sci.* **1999**, *54*, 1129-1132. 10.1515/znb-1999-0907
[57] O. Johnson, *Inorg. Chem.* **1973**, *12*, 780-785. 10.1021/ic50122a015
[58] S. Uwe, Ç Erk, E. Kleinpeter, *Z. Krist.* **2006**, *221*, 231-235. 10.1524/zkri.2006.221.3.231
[59] N. V. Kozhemyakina, J. Nuss, M. Jansen, *Eur. J. Inorg. Chem.* **2009**, *2009*, 3900-3903. 10.1002/ejic.200900542

FULL PAPER

Dibenzo-21-crown-7 and dibenzo-24-crown-8 bis-urea receptors **R**[1] and **R**[2], respectively, have been studied in solution, gas-phase, and solid-state for their ion pair recognition behavior. Both receptors show strong positive heterotropic cooperativity toward chloride when complexed with Rb^+ or Cs^+.

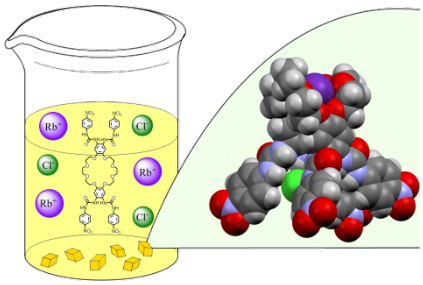

*T. Mäkelä, A. Kiesilä, E. Kalenius & K. Rissanen**

Page No. – Page No.

Ion Pair Complexation with Dibenzo-21-Crown-7 and Dibenzo-24-Crown-8 bis-Urea Receptors

DEPARTMENT OF CHEMISTRY, UNIVERSITY OF JYVÄSKYLÄ
RESEARCH REPORT SERIES

1. Vuolle, Mikko: Electron paramagnetic resonance and molecular orbital study of radical ions generated from (2.2)metacyclophane, pyrene and its hydrogenated compounds by alkali metal reduction and by thallium(III)trifluoroacetate oxidation. (99 pp.) 1976
2. Pasanen, Kaija: Electron paramagnetic resonance study of cation radical generated from various chlorinated biphenyls. (66 pp.) 1977
3. Carbon-13 Workshop, September 6-8, 1977. (91 pp.) 1977
4. Laihia, Katri: On the structure determination of norbornane polyols by NMR spectroscopy. (111 pp.) 1979
5. Nyrönen, Timo: On the EPR, ENDOR and visible absorption spectra of some nitrogen containing heterocyclic compounds in liquid ammonia. (76 pp.) 1978
6. Talvitie, Antti: Structure determination of some sesquiterpenoids by shift reagent NMR. (54 pp.) 1979
7. Häkli, Harri: Structure analysis and molecular dynamics of cyclic compounds by shift reagent NMR. (48 pp.) 1979
8. Pitkänen, Ilkka: Thermodynamics of complexation of 1,2,4-triazole with divalent manganese, cobalt, nickel, copper, zinc, cadmium and lead ions in aqueous sodium perchlorate solutions. (89 pp.) 1980
9. Asunta, Tuula: Preparation and characterization of new organometallic compounds synthesized by using metal vapours. (91 pp.) 1980
10. Sattar, Mohammad Abdus: Analyses of MCPA and its metabolites in soil. (57 pp.) 1980
11. Bibliography 1980. (31 pp.) 1981
12. Knuuttila, Pekka: X-Ray structural studies on some divalent 3d metal compounds of picolinic and isonicotinic acid N-oxides. (77 pp.) 1981
13. Bibliography 1981. (33 pp.) 1982
14. 6^{th} National NMR Symposium, September 9-10, 1982, Abstracts. (49 pp.) 1982
15. Bibliography 1982. (38 pp.) 1983
16. Knuuttila, Hilkka: X-Ray structural studies on some Cu(II), Co(II) and Ni(II) complexes with nicotinic and isonicotinic acid N-oxides. (54 pp.) 1983
17. Symposium on inorganic and analytical chemistry May 18, 1984, Program and Abstracts. (100 pp.) 1984
18. Knuutinen, Juha: On the synthesis, structure verification and gas chromatographic determination of chlorinated catechols and guaiacols occuring in spent bleach liquors of kraft pulp mill. (30 pp.) 1984
19. Bibliography 1983. (47 pp.) 1984
20. Pitkänen, Maija: Addition of BrCl, B_2 and Cl_2 to methyl esters of propenoic and 2-butenoic acid derivatives and ^{13}C NMR studies on methyl esters of saturated aliphatic mono- and dichlorocarboxylic acids. (56 pp.) 1985
21. Bibliography 1984. (39 pp.) 1985
22. Salo, Esa: EPR, ENDOR and TRIPLE spectroscopy of some nitrogen heteroaromatics in liquid ammonia. (111 pp.) 1985

23. Humppi, Tarmo: Synthesis, identification and analysis of dimeric impurities of chlorophenols. (39 pp.) 1985
24. Aho, Martti: The ion exchange and adsorption properties of sphagnum peat under acid conditions. (90 pp.) 1985
25. Bibliography 1985 (61 pp.) 1986
26. Bibliography 1986. (23 pp.) 1987
27. Bibliography 1987. (26 pp.) 1988
28. Paasivirta, Jaakko (Ed.): Structures of organic environmental chemicals. (67 pp.) 1988
29. Paasivirta, Jaakko (Ed.): Chemistry and ecology of organo-element compounds. (93 pp.) 1989
30. Sinkkonen, Seija: Determination of crude oil alkylated dibenzothiophenes in environment. (35 pp.) 1989
31. Kolehmainen, Erkki (Ed.): XII National NMR Symposium Program and Abstracts. (75 pp.) 1989
32. Kuokkanen, Tauno: Chlorocymenes and Chlorocymenenes: Persistent chlorocompounds in spent bleach liquors of kraft pulp mills. (40 pp.) 1989
33. Mäkelä, Reijo: ESR, ENDOR and TRIPLE resonance study on substituted 9,10-anthraquinone radicals in solution. (35 pp.) 1990
34. Veijanen, Anja: An integrated sensory and analytical method for identification of off-flavour compounds. (70 pp.) 1990
35. Kasa, Seppo: EPR, ENDOR and TRIPLE resonance and molecular orbital studies on a substitution reaction of anthracene induced by thallium(III) in two fluorinated carboxylic acids. (114 pp.) 1990
36. Herve, Sirpa: Mussel incubation method for monitoring organochlorine compounds in freshwater recipients of pulp and paper industry. (145 pp.) 1991
37. Pohjola, Pekka: The electron paramagnetic resonance method for characterization of Finnish peat types and iron (III) complexes in the process of peat decomposition. (77 pp.) 1991
38. Paasivirta, Jaakko (Ed.): Organochlorines from pulp mills and other sources. Research methodology studies 1988-91. (120 pp.) 1992
39. Veijanen, Anja (Ed.): VI National Symposium on Mass Spectrometry, May 13-15, 1992, Abstracts. (55 pp.) 1992
40. Rissanen, Kari (Ed.): The 7. National Symposium on Inorganic and Analytical Chemistry, May 22, 1992, Abstracts and Program. (153 pp.) 1992
41. Paasivirta, Jaakko (Ed.): CEOEC'92, Second Finnish-Russian Seminar: Chemistry and Ecology of Organo-Element Compounds. (93 pp.) 1992
42. Koistinen, Jaana: Persistent polychloroaromatic compounds in the environment: structure-specific analyses. (50 pp.) 1993
43. Virkki, Liisa: Structural characterization of chlorolignins by spectroscopic and liquid chromatographic methods and a comparison with humic substances. (62 pp.) 1993
44. Helenius, Vesa: Electronic and vibrational excitations in some

biologically relevant molecules. (30 pp.) 1993

45. Leppä-aho, Jaakko: Thermal behaviour, infrared spectra and x-ray structures of some new rare earth chromates(VI). (64 pp.) 1994
46. Kotila, Sirpa: Synthesis, structure and thermal behavior of solid copper(II) complexes of 2-amino-2- hydroxymethyl-1,3-propanediol. (111 pp.) 1994
47. Mikkonen, Anneli: Retention of molybdenum(VI), vanadium(V) and tungsten(VI) by kaolin and three Finnish mineral soils. (90 pp.) 1995
48. Suontamo, Reijo: Molecular orbital studies of small molecules containing sulfur and selenium. (42 pp.) 1995
49. Hämäläinen, Jouni: Effect of fuel composition on the conversion of fuel-N to nitrogen oxides in the combustion of small single particles. (50 pp.) 1995
50. Nevalainen, Tapio: Polychlorinated diphenyl ethers: synthesis, NMR spectroscopy, structural properties, and estimated toxicity. (76 pp.) 1995
51. Aittola, Jussi-Pekka: Organochloro compounds in the stack emission. (35 pp.) 1995
52. Harju, Timo: Ultrafast polar molecular photophysics of (dibenzylmethine)borondifluoride and 4-aminophthalimide in solution. (61 pp.) 1995
53. Maatela, Paula: Determination of organically bound chlorine in industrial and environmental samples. (83 pp.) 1995
54. Paasivirta, Jaakko (Ed.): CEOEC'95, Third Finnish-Russian Seminar: Chemistry and Ecology of Organo-Element Compounds. (109 pp.) 1995
55. Huuskonen, Juhani: Synthesis and structural studies of some supramolecular compounds. (54 pp.) 1995
56. Palm, Helena: Fate of chlorophenols and their derivatives in sawmill soil and pulp mill recipient environments. (52 pp.) 1995
57. Rantio, Tiina: Chlorohydrocarbons in pulp mill effluents and their fate in the environment. (89 pp.) 1997
58. Ratilainen, Jari: Covalent and non-covalent interactions in molecular recognition. (37 pp.) 1997
59. Kolehmainen, Erkki (Ed.): XIX National NMR Symposium, June 4-6, 1997, Abstracts. (89 pp.) 1997
60. Matilainen, Rose: Development of methods for fertilizer analysis by inductively coupled plasma atomic emission spectrometry. (41 pp.) 1997
61. Koistinen, Jari (Ed.): Spring Meeting on the Division of Synthetic Chemistry, May 15-16, 1997, Program and Abstracts. (36 pp.) 1997
62. Lappalainen, Kari: Monomeric and cyclic bile acid derivatives: syntheses, NMR spectroscopy and molecular recognition properties. (50 pp.) 1997
63. Laitinen, Eira: Molecular dynamics of cyanine dyes and phthalimides in solution: picosecond laser studies. (62 pp.) 1997
64. Eloranta, Jussi: Experimental and theoretical studies on some

quinone and quinol radicals. (40 pp.) 1997

65. Oksanen, Jari: Spectroscopic characterization of some monomeric and aggregated chlorophylls. (43 pp.) 1998
66. Häkkänen, Heikki: Development of a method based on laser-induced plasma spectrometry for rapid spatial analysis of material distributions in paper coatings. (60 pp.) 1998
67. Virtapohja, Janne: Fate of chelating agents used in the pulp and paper industries. (58 pp.) 1998
68. Airola, Karri: X-ray structural studies of supramolecular and organic compounds. (39 pp.) 1998
69. Hyötyläinen, Juha: Transport of lignin–type compounds in the receiving waters of pulp mills. (40 pp.) 1999
70. Ristolainen, Matti: Analysis of the organic material dissolved during totally chlorine-free bleaching. (40 pp.) 1999
71. Eklin, Tero: Development of analytical procedures with industrial samples for atomic emission and atomic absorption spectrometry. (43 pp.) 1999
72. Välisaari, Jouni: Hygiene properties of resol-type phenolic resin laminates. (129 pp.) 1999
73. Hu, Jiwei: Persistent polyhalogenated diphenyl ethers: model compounds syntheses, characterization and molecular orbital studies. (59 pp.) 1999
74. Malkavaara, Petteri: Chemometric adaptations in wood processing chemistry. (56 pp.) 2000
75. Kujala Elena, Laihia Katri, Nieminen Kari (Eds.): NBC 2000, Symposium on Nuclear, Biological and Chemical Threats in the 21st Century. (299 pp.) 2000
76. Rantalainen, Anna-Lea: Semipermeable membrane devices in monitoring persistent organic pollutants in the environment. (58 pp.) 2000
77. Lahtinen, Manu: *In situ* X-ray powder diffraction studies of Pt/C, CuCl/C and Cu_2O/C catalysts at elevated temperatures in various reaction conditions. (92 pp.) 2000
78. Tamminen, Jari: Syntheses, empirical and theoretical characterization, and metal cation complexation of bile acid-based monomers and open/closed dimers. (54 pp.) 2000
79. Vatanen, Virpi: Experimental studies by EPR and theoretical studies by DFT calculations of α-amino-9,10-anthraquinone radical anions and cations in solution. (37 pp.) 2000
80. Kotilainen, Risto: Chemical changes in wood during heating at 150-260 °C. (57 pp.) 2000
81. Nissinen, Maija: X-ray structural studies on weak, non-covalent interactions in supramolecular compounds. (69 pp.) 2001
82. Wegelius, Elina: X-ray structural studies on self-assembled hydrogen-bonded networks and metallosupramolecular complexes. (84 pp.) 2001
83. Paasivirta, Jaakko (Ed.): CEOEC'2001, Fifth Finnish-Russian Seminar: Chemistry and Ecology of Organo-Element Compounds. (163 pp.) 2001
84. Kiljunen, Toni: Theoretical studies on spectroscopy and

atomic dynamics in rare gas solids. (56 pp.) 2001

85. Du, Jin: Derivatives of dextran: synthesis and applications in oncology. (48 pp.) 2001
86. Koivisto, Jari: Structural analysis of selected polychlorinated persistent organic pollutants (POPs) and related compounds. (88 pp.) 2001
87. Feng, Zhinan: Alkaline pulping of non-wood feedstocks and characterization of black liquors. (54 pp.) 2001
88. Halonen, Markku: Lahon havupuun käyttö sulfaattiprosessin raaka-aineena sekä havupuun lahontorjunta. (90 pp.) 2002
89. Falábu, Dezsö: Synthesis, conformational analysis and complexation studies of resorcarene derivatives. (212 pp.) 2001
90. Lehtovuori, Pekka: EMR spectroscopic studies on radicals of ubiquinones Q-*n*, vitamin K_3 and vitamine E in liquid solution. (40 pp.) 2002
91. Perkkalainen, Paula: Polymorphism of sugar alcohols and effect of grinding on thermal behavior on binary sugar alcohol mixtures. (53 pp.) 2002
92. Ihalainen, Janne: Spectroscopic studies on light-harvesting complexes of green plants and purple bacteria. (42 pp.) 2002
93. Kunttu, Henrik, Kiljunen, Toni (Eds.): 4th International Conference on Low Temperature Chemistry. (159 pp.) 2002
94. Väisänen, Ari: Development of methods for toxic element analysis in samples with environmental concern by ICP-AES and ETAAS. (54 pp.) 2002
95. Luostarinen, Minna: Synthesis and characterisation of novel resorcarene derivatives. (200 pp.) 2002
96. Louhelainen, Jarmo: Changes in the chemical composition and physical properties of wood and nonwood black liquors during heating. (68 pp.) 2003
97. Lahtinen, Tanja: Concave hydrocarbon cyclophane π-prismands. (65 pp.) 2003
98. Laihia, Katri (Ed.): NBC 2003, Symposium on Nuclear, Biological and Chemical Threats – A Crisis Management Challenge. (245 pp.) 2003
99. Oasmaa, Anja: Fuel oil quality properties of wood-based pyrolysis liquids. (32 pp.) 2003
100. Virtanen, Elina: Syntheses, structural characterisation, and cation/anion recognition properties of nano-sized bile acid-based host molecules and their precursors. (123 pp.) 2003
101. Nättinen, Kalle: Synthesis and X-ray structural studies of organic and metallo-organic supramolecular systems. (79 pp.) 2003
102. Lampiselkä, Jarkko: Demonstraatio lukion kemian opetuksessa. (285 pp.) 2003
103. Kallioinen, Jani: Photoinduced dynamics of $Ru(dcbpy)_2(NCS)_2$ – in solution and on nanocrystalline titanium dioxide thin films. (47 pp.) 2004
104. Valkonen, Arto (Ed.): VII Synthetic Chemistry Meeting and XXVI Finnish NMR Symposium. (103 pp.) 2004

105. Vaskonen, Kari: Spectroscopic studies on atoms and small molecules isolated in low temperature rare gas matrices. (65 pp.) 2004
106. Lehtovuori, Viivi: Ultrafast light induced dissociation of $Ru(dcbpy)(CO)_2I_2$ in solution. (49 pp.) 2004
107. Saarenketo, Pauli: Structural studies of metal complexing Schiff bases, Schiff base derived *N*-glycosides and cyclophane π-prismands. (95 pp.) 2004
108. Paasivirta, Jaakko (Ed.): CEOEC'2004, Sixth Finnish-Russian Seminar: Chemistry and Ecology of Organo-Element Compounds. (147 pp.) 2004
109. Suontamo, Tuula: Development of a test method for evaluating the cleaning efficiency of hard-surface cleaning agents. (96 pp.) 2004
110. Güneş, Minna: Studies of thiocyanates of silver for nonlinear optics. (48 pp.) 2004
111. Ropponen, Jarmo: Aliphatic polyester dendrimers and dendrons. (81 pp.) 2004
112. Vu, Mân Thi Hong: Alkaline pulping and the subsequent elemental chlorine-free bleaching of bamboo (*Bambusa procera*). (69 pp.) 2004
113. Mansikkamäki, Heidi: Self-assembly of resorcinarenes. (77 pp.) 2006
114. Tuononen, Heikki M.: EPR spectroscopic and quantum chemical studies of some inorganic main group radicals. (79 pp.) 2005
115. Kaski, Saara: Development of methods and applications of laser-induced plasma spectroscopy in vacuum ultraviolet. (44 pp.) 2005
116. Mäkinen, Riika-Mari: Synthesis, crystal structure and thermal decomposition of certain metal thiocyanates and organic thiocyanates. (119 pp.) 2006
117. Ahokas, Jussi: Spectroscopic studies of atoms and small molecules isolated in rare gas solids: photodissociation and thermal reactions. (53 pp.) 2006
118. Busi, Sara: Synthesis, characterization and thermal properties of new quaternary ammonium compounds: new materials for electrolytes, ionic liquids and complexation studies. (102 pp.) 2006
119. Mäntykoski, Keijo: PCBs in processes, products and environment of paper mills using wastepaper as their raw material. (73 pp.) 2006
120. Laamanen, Pirkko-Leena: Simultaneous determination of industrially and environmentally relevant aminopolycarboxylic and hydroxycarboxylic acids by capillary zone electrophoresis. (54 pp.) 2007
121. Salmela, Maria: Description of oxygen-alkali delignification of kraft pulp using analysis of dissolved material. (71 pp.) 2007
122. Lehtovaara, Lauri: Theoretical studies of atomic scale impurities in superfluid ^{4}He. (87 pp.) 2007
123. Rautiainen, J. Mikko: Quantum chemical calculations of structures, bonding, and spectroscopic properties of some sulphur and selenium iodine cations. (71 pp.) 2007
124. Nummelin, Sami: Synthesis, characterization, structural and

retrostructural analysis of self-assembling pore forming dendrimers. (286 pp.) 2008

125. Sopo, Harri: Uranyl(VI) ion complexes of some organic aminobisphenolate ligands: syntheses, structures and extraction studies. (57 pp.) 2008
126. Valkonen, Arto: Structural characteristics and properties of substituted cholanoates and *N*-substituted cholanamides. (80 pp.) 2008
127. Lähde, Anna: Production and surface modification of pharmaceutical nano- and microparticles with the aerosol flow reactor. (43 pp.) 2008
128. Beyeh, Ngong Kodiah: Resorcinarenes and their derivatives: synthesis, characterization and complexation in gas phase and in solution. (75 pp.) 2008
129. Välisaari, Jouni, Lundell, Jan (Eds.): Kemian opetuksen päivät 2008: uusia oppimisympäristöjä ja ongelmalähtöistä opetusta. (118 pp.) 2008
130. Myllyperkiö, Pasi: Ultrafast electron transfer from potential organic and metal containing solar cell sensitizers. (69 pp.) 2009
131. Käkölä, Jaana: Fast chromatographic methods for determining aliphatic carboxylic acids in black liquors. (82 pp.) 2009
132. Koivukorpi, Juha: Bile acid-arene conjugates: from photoswitchability to cancer cell detection. (67 pp.) 2009
133. Tuuttila, Tero: Functional dendritic polyester compounds: synthesis and characterization of small bifunctional dendrimers and dyes. (74 pp.) 2009
134. Salorinne, Kirsi: Tetramethoxy resorcinarene based cation and anion receptors: synthesis, characterization and binding properties. (79 pp.) 2009
135. Rautiainen, Riikka: The use of first-thinning Scots pine (*Pinus sylvestris*) as fiber raw material for the kraft pulp and paper industry. (73 pp.) 2010
136. Ilander, Laura: Uranyl salophens: synthesis and use as ditopic receptors. (199 pp.) 2010
137. Kiviniemi, Tiina: Vibrational dynamics of iodine molecule and its complexes in solid krypton - Towards coherent control of bimolecular reactions? (73 pp.) 2010
138. Ikonen, Satu: Synthesis, characterization and structural properties of various covalent and non-covalent bile acid derivatives of N/O-heterocycles and their precursors. (105 pp.) 2010
139. Siitonen, Anni: Spectroscopic studies of semiconducting single-walled carbon nanotubes. (56 pp.) 2010
140. Raatikainen, Kari: Synthesis and structural studies of piperazine cyclophanes – Supramolecular systems through Halogen and Hydrogen bonding and metal ion coordination. (69 pp.) 2010
141. Leivo, Kimmo: Gelation and gel properties of two- and three-component Pyrene based low molecular weight organogelators. (116 pp.) 2011
142. Martiskainen, Jari: Electronic energy transfer in light-harvesting complexes isolated from *Spinacia oleracea* and from three

photosynthetic green bacteria *Chloroflexus aurantiacus*, *Chlorobium tepidum*, and *Prosthecochloris aestuarii*. (55 pp.) 2011

143. Wichmann, Oula: Syntheses, characterization and structural properties of [O,N,O,X´] aminobisphenolate metal complexes. (101 pp.) 2011
144. Ilander, Aki: Development of ultrasound-assisted digestion methods for the determination of toxic element concentrations in ash samples by ICP-OES. (58 pp.) 2011
145. The Combined XII Spring Meeting of the Division of Synthetic Chemistry and XXXIII Finnish NMR Symposium. Book of Abstracts. (90 pp.) 2011
146. Valto, Piia: Development of fast analysis methods for extractives in papermaking process waters. (73 pp.) 2011
147. Andersin, Jenni: Catalytic activity of palladium-based nanostructures in the conversion of simple olefinic hydro- and chlorohydrocarbons from first principles. (78 pp.) 2011
148. Aumanen, Jukka: Photophysical properties of dansylated poly(propylene amine) dendrimers. (55 pp.) 2011
149. Kärnä, Minna: Ether-functionalized quaternary ammonium ionic liquids – synthesis, characterization and physicochemical properties. (76 pp.) 2011
150. Jurček, Ondřej: Steroid conjugates for applications in pharmacology and biology. (57 pp.) 2011
151. Nauha, Elisa: Crystalline forms of selected Agrochemical actives: design and synthesis of cocrystals. (77 pp.) 2012
152. Ahkola, Heidi: Passive sampling in monitoring of nonylphenol ethoxylates and nonylphenol in aquatic environments. (92 pp.) 2012
153. Helttunen, Kaisa: Exploring the self-assembly of resorcinarenes: from molecular level interactions to mesoscopic structures. (78 pp.) 2012
154. Linnanto, Juha: Light excitation transfer in photosynthesis revealed by quantum chemical calculations and exiton theory. (179 pp.) 2012
155. Roiko-Jokela, Veikko: Digital imaging and infrared measurements of soil adhesion and cleanability of semihard and hard surfaces. (122 pp.) 2012
156. Noponen, Virpi: Amides of bile acids and biologically important small molecules: properties and applications. (85 pp.) 2012
157. Hulkko, Eero: Spectroscopic signatures as a probe of structure and dynamics in condensed-phase systems – studies of iodine and gold ranging from isolated molecules to nanoclusters. (69 pp.) 2012
158. Lappi, Hanna: Production of Hydrocarbon-rich biofuels from extractives-derived materials. (95 pp.) 2012
159. Nykänen, Lauri: Computational studies of Carbon chemistry on transition metal surfaces. (76 pp.) 2012
160. Ahonen, Kari: Solid state studies of pharmaceutically important molecules and their derivatives. (65 pp.) 2012

161. Pakkanen, Hannu: Characterization of organic material dissolved during alkaline pulping of wood and non-wood feedstocks. (76 pp.) 2012
162. Moilanen, Jani: Theoretical and experimental studies of some main group compounds: from closed shell interactions to singlet diradicals and stable radicals. (80 pp.) 2012
163. Himanen, Jatta: Stereoselective synthesis of Oligosaccharides by *De Novo* Saccharide welding. (133 pp.) 2012
164. Bunzen, Hana: Steroidal derivatives of nitrogen containing compounds as potential gelators. (76 pp.) 2013
165. Seppälä, Petri: Structural diversity of copper(II) amino alcohol complexes. Syntheses, structural and magnetic properties of bidentate amino alcohol copper(II) complexes. (67 pp.) 2013
166. Lindgren, Johan: Computational investigations on rotational and vibrational spectroscopies of some diatomics in solid environment. (77 pp.) 2013
167. Giri, Chandan: Sub-component self-assembly of linear and non-linear diamines and diacylhydrazines, formulpyridine and transition metal cations. (145 pp.) 2013
168. Riisiö, Antti: Synthesis, Characterization and Properties of Cu(II)-, Mo(VI)- and U(VI) Complexes With Diaminotetraphenolate Ligands. (51 pp.) 2013
169. Kiljunen, Toni (Ed.): Chemistry and Physics at Low Temperatures. Book of Abstracts. (103 pp.) 2013
170. Hänninen, Mikko: Experimental and Computational Studies of Transition Metal Complexes with Polydentate Amino- and Aminophenolate Ligands: Synthesis, Structure, Reactivity and Magnetic Properties. (66 pp.) 2013
171. Antila, Liisa: Spectroscopic studies of electron transfer reactions at the photoactive electrode of dye-sensitized solar cells. (53 pp.) 2013
172. Kemppainen, Eeva: Mukaiyama-Michael reactions with α-substituted acroleins – a useful tool for the synthesis of the pectenotoxins and other natural product targets. (190 pp.) 2013
173. Virtanen, Suvi: Structural Studies of Dielectric Polymer Nanocomposites. (49 pp.) 2013
174. Yliniemelä-Sipari, Sanna: Understanding The Structural Requirements for Optimal Hydrogen Bond Catalyzed Enolization – A Biomimetic Approach.(160 pp.) 2013
175. Leskinen, Mikko V: Remote β-functionalization of β'-keto esters. (105 pp.) 2014
176. 12th European Conference on Research in Chemistry Education (ECRICE2014). Book of Abstracts. (166 pp.) 2014
177. Peuronen, Anssi: N-Monoalkylated DABCO-Based N-Donors as Versatile Building Blocks in Crystal Engineering and Supramolecular Chemistry. (54 pp.) 2014
178. Perämäki, Siiri: Method development for determination and recovery of rare earth elements from industrial fly ash. (88 pp.) 2014

179. Chernyshev, Alexander, N.: Nitrogen-containing ligands and their platinum(IV) and gold(III) complexes: investigation and basicity and nucleophilicity, luminescence, and aurophilic interactions. (64 pp.) 2014
180. Lehto, Joni: Advanced Biorefinery Concepts Integrated to Chemical Pulping. (142 pp.) 2015
181. Tero, Tiia-Riikka: Tetramethoxy resorcinarenes as platforms for fluorescent and halogen bonding systems. (61 pp.) 2015
182. Löfman, Miika: Bile acid amides as components of microcrystalline organogels. (62 pp.) 2015
183. Selin, Jukka: Adsorption of softwood-derived organic material onto various fillers during papermaking. (169 pp.) 2015
184. Piisola, Antti: Challenges in the stereoselective synthesis of allylic alcohols. (210 pp.) 2015
185. Bonakdarzadeh, Pia: Supramolecular coordination polyhedra based on achiral and chiral pyridyl ligands: design, preparation, and characterization. (65 pp.) 2015
186. Vasko, Petra: Synthesis, characterization, and reactivity of heavier group 13 and 14 metallylenes and metalloid clusters: small molecule activation and more. (66 pp.) 2015
187. Topić, Filip: Structural Studies of Nano-sized Supramolecular Assemblies. (79 pp.) 2015
188. Mustalahti, Satu: Photodynamics Studies of Ligand-Protected Gold Nanoclusters by using Ultrafast Transient Infrared Spectroscopy. (58 pp.) 2015
189. Koivisto, Jaakko: Electronic and vibrational spectroscopic studies of gold-nanoclusters. (63 pp.) 2015
190. Suhonen, Aku: Solid state conformational behavior and interactions of series of aromatis oligoamide foldamers. (68 pp.) 2016
191. Soikkeli, Ville: Hydrometallurgical recovery and leaching studies for selected valuable metals from fly ash samples by ultrasound-assisted extraction followed by ICP-OES determination. (107 pp.) 2016
192. XXXVIII Finnish NMR Symposium. Book of Abstracts. (51 pp.) 2016
193. Mäkelä, Toni: Ion Pair Recognition by Ditopic Crown Ether Based bis-Urea and Uranyl Salophen Receptors. (75 pp.) 2016
194. Lindholm-Lehto, Petra: Occurrence of pharmaceuticals in municipal wastewater treatment plants and receiving surface waters in Central and Southern Finland. (98 pp.) 2016
195. Härkönen, Ville: Computational and Theoretical studies on Lattice Thermal conductivity and Thermal properties of Silicon Clathrates. (89 pp.) 2016
196. Tuokko, Sakari: Understanding selective reduction reactions with heterogeneous Pd and Pt: climbing out of the black box. (85 pp.) 2016
197. Nuora, Piia: Monitapaustutkimus LUMA-Toimintaan liittyvissä oppimisympäristöissä tapahtuvista kemian oppimiskokemuksista. (171 pp.) 2016

198. Kumar, Hemanathan: Novel Concepts on The Recovery of By-Products from Alkaline Pulping. (61 pp.) 2016
199. Arnedo-Sánchez, Leticia: Lanthanide and Transition Metal Complexes as Building Blocks for Supramolecular Functional Materials. (227 pp.) 2016
200. Gell, Lars: Theoretical Investigations of Ligand Protected Silver Nanoclusters. (134 pp.) 2016
201. Vaskuri, Juhani: Oppiennätyksistä opetussuunnitelman perusteisiin - lukion kemian kansallisen opetussuunnitelman kehittyminen Suomessa vuosina 1918-2016. (314 pp.) 2017
202. Lundell Jan, Kiljunen Toni (Eds.): 22nd Horizons in Hydrogen Bond Research. Book of Abstracts. 2017
203. Turunen, Lotta: Design and construction of halogen-bonded capsules and cages. (61 pp.) 2017
204. Hurmalainen, Juha: Experimental and computational studies of unconventional main group compounds: stable radicals and reactive intermediates. (88 pp.) 2017
205. Koivistoinen Juha: Non-linear interactions of femtosecond laser pulses with graphene: photo-oxidation, imaging and photodynamics. (68 pp.) 2017
206. Chen, Chengcong: Combustion behavior of black liquors: droplet swelling and influence of liquor composition. (39 pp.) 2017
207. Mansikkamäki, Akseli: Theoretical and Computational Studies of Magnetic Anisotropy and Exchange Coupling in Molecular Systems. (190 p. + included articles) 2018.
208. Tatikonda, Rajendhraprasad: Multivalent N-donor ligands for the construction of coordination polymers and coordination polymer gels. (62 pp.) 2018
209. Budhathoki, Roshan: Beneficiation, desilication and selective precipitation techniques for phosphorus refining from biomass derived fly ash. (64 pp.) 2018
210. Siitonen, Juha: Synthetic Studies on 1-azabicyclo[5.3.0]decane Alkaloids. (140 pp.) 2018
211. Ullah, Saleem: Advanced Biorefinery Concepts Related to Non-wood Feedstocks. (57 pp.) 2018
212. Ghalibaf, Maryam: Analytical Pyrolysis of Wood and Non-Wood Materials from Integrated Biorefinery Concepts. (106 pp.) 2018

DEPARTMENT OF CHEMISTRY, UNIVERSITY OF JYVÄSKYLÄ
DISSERTATIONS PUBLISHED IN THE JYU DISSERTATIONS RESEARCH SERIES

1. Bulatov, Evgeny: Synthetic and structural studies of covalent and non-covalent interactions of ligands and metal center in platinum(II) complexes containing 2,2′-dipyridylamine or oxime ligands. (58 pp.) 2019. JYU Dissertations 70.
2. Annala, Riia: Conformational Properties and Anion Complexes of Aromatic Oligoamide Foldamers. (80 pp.) 2019. JYU Dissertations 84.
3. Isoaho, Jukka Pekka: Dithionite Bleaching of Thermomechanical Pulp - Chemistry and Optimal Conditions. (73 pp.) 2019. JYU Dissertations 85.
4. Nygrén, Enni: Recovery of rubidium from power plant fly ash. 2019. JYU Dissertations.